Max-Planck Institute for Molecular Genetics

Freie Universität Berlin

Identification and functional characterization of a genetic defect in the kinetochore protein BOD1 associated with autosomal recessive mental retardation and oligomenorrhea

DISSERTATION

Zur Erlangung des akademischen grades

Doctor rerum naturalium

(Dr. rer. nat.)

Vorgelegt von

Sahar Esmaeeli-Nieh

Aus Teheran, Iran

Eingereicht im Fachbereich
Biologie, Chemie, Pharmazie
der
Freien Universität Berlin

Date: August 2010

1. Gutachter: **Prof. Dr. Hans-Hilger Ropers**
Max Planck Institut für molekulare Genetik
Ihnestr. 73, D-14195 Berlin

First Referee: **Prof. Dr. Hans-Hilger Ropers**
Max Planck Institut für molekulare Genetik
Ihnestr. 73, D-14195 Berlin

2. Gutachter: **Prof. Dr. Stephan Sigrist**
Freie Universität
Takustr. 6, D-14195 Berlin

Second Referee: **Prof. Dr. Stephan Sigrist**
Freie Universität
Takustr. 6, D-14195 Berlin

Disputation am: October 25th, 2010

Date of defence: October 25th, 2010

Declaration

I hereby declare that the work presented in this thesis has been conducted independently and without any inappropriate support and that all sources of information, be it experimental or intellectual, are aptly referenced.

I hereby declare that this thesis has not been submitted, either in the same or a different form, to this or any other university for a degree.

Acknowledgments

The PhD work presented in this thesis conducted from December 2006 till August 2010 at the Max-Planck Institute for Molecular Genetics in Berlin in the department of Prof. Dr. Hans-Hilger Ropers, Research group Familial cognitive disorders (Dr. Andreas W. Kuss). This thesis would not have been possible without the help of many people.

I would like to appreciate Professor Dr. Hans Hilger Ropers for his remarkable drive and energy with which he established a well-framed scientific environment. I had a pleasure to be in direct contact with him and benefit his comments, which will help me in building my future scientific carrier.

I owe my most sincere gratitude to Dr. Andreas Walter Kuss, for his invaluable support during the long and arduous journey of PhD from the first days to his critical comments on my thesis.

I am deeply thankful to Prof. Stephan Sigrist for being my second supervisor.

Special thank to Dr. Chandan Goswami for not only training me in cell biology but also for his affable attitude and motivation that he gave me.

In this juncture I thank my former supervisor Professor Dr. Hossein Najmabadi and advisor Dr. Farkhondeh Behjati in Iran for their continued support even during my PhD work.

I thank Professor Dr. Jason Swedlow and Dr. Iain Porter at the University of Dundee for a successful collaboration.

Many thanks to Dr. Lars R. Jensen and Dr. Andreas Tzschach for their comments and profitable discussions. I would like thank, Dr. Nils Rademacher for patiently training me in preparation of primary neurons.

I acknowledge the DAAD - Deutscher Akademischer Austausch Dienst- especially Ms. Eva Synowsky, Ms. Nora Pitsch and Ms. Carola Seeler for providing financial support and creating wonderful orientation atmosphere during the initial months.

Many thank to Benjamin, Raghu, Smita and Masoud who encouraged, helped and supported me at various stages.

I thank to my former and current lab members from the depth of my heart: Lucia, Masoud, Mahdi, Agnes, Johanna, Robert, Georg, Bettina and Marianne.

I would like to thank Susanne Freier not only for her support in the cell culture facility but also for her generous help and support especially during my first year of stay in Berlin.

I would like to thank my Iranian colleagues at the Genetics Research Center, University of social welfare and rehabilitation sciences in Iran, particularly: Ms. Sedigheh Abedini, Ms. Saghar Ghasemi, Ms. Susan Banihashemi.

I run short of words to fully encompass the amount of gratitude me have for my parents and my sister who always motivated and encouraged me even in the deepest of turbulent time, without their support this work wouldn't have been started.

This list will be incomplete without thanking my numerous friends in Dortmund, during the incredible time of attending CDC for learning German, and in Berlin for the wonderful time we spent together, particularly: Benjamin, Pedram, Farzad, Diego, Vered, shirin, Gezel, Yulia, Dana.

And in the end, thanks to Berlin where all this happened!

Sahar Esmaeeli-Nieh
Berlin, August 2010

For my parents

1.Introduction

1.1. Mental retardation

Intellectual disability (ID) or mental retardation (MR), is a major public health issue, affecting more than 1% of children worldwide (Levav and Rutz 2002). Yet the specific causes of ID are often not identified. The definition of ID comprises a significantly reduced ability in learning new skills, understanding new or complex information as well as reduced ability to survive independently with an onset before the age of 18 years (Shabsigh and Rowland 2007). Standardized tests such as the Wechsler Adult Intelligence Scales (WAIS) and the Wechsler Intelligence Scales for Children (WISC) measuring the intelligence quotient (IQ) can quantify the cognitive impairment. These tests are used to diagnose and to assess the severity of ID (Baron 2005) and one speaks of ID if the IQ of an individual is below 70 (Goldenberg and Saugier-Veber 2009). ID is subdivided into several classes with regard to the IQ; the most commonly used classification is profound (IQ<20), severe 20<IQ<35), moderate (35<IQ<50) and mild (50<IQ<70) but numerous studies distinguish only between mild (IQ 70–50) and severe ID (IQ<50) [The american association on intellectual and developmental disabilities:(2010)]. In Western countries, the prevalence of ID is 1.5–2% and in 0.3–0.5% of the cases severe impairment is observed (Leonard and Wen 2002). The vast majority of cases are assumed to be due to defects of single genes or specific genetic causes including cytogenetically visible chromosomal abnormalities like trisomy 21 (see also below).

During the past decade, significant progress has been made in the explanation of genetic factors of severe ID (Ropers 2010). ID can be observed either as part of broader syndromes with additional symptoms affecting other organs (e.g., Down syndrome) or in isolation without further organ involvement. If the brain is the only affected organ, it could be structurally abnormal, such as with lissencephaly, or grossly normal (nonsyndromic ID) (Mochida et al. 2009). Clinical distinction between syndromic and nonsyndromic ID is however often difficult.

The genetic factors involved in the aetiology of ID can be divided into three groups:

i. Large chromosome abnormalities including aneuploidies, large chromosomal deletion/insertions, inversions and translocations. Such cytogenetically visible chromosomal aberrations which can be detected by normal karyotyping using light microscopy (like trisomy 21 in Down Syndrome) account for almost 15% of all cases (Leonard and Wen 2002).

ii. Deletions and duplications, which are too small to be detected by conventional karyotyping. These are detectable with fluorescence in situ hybridization (FISH), Comparative Genomic Hybridization (CGH) and array based CGH (array-CGH). They are often associated with varying degrees of ID in addition to their own characteristic distinguishing features. E.g. Wolf- Hirschhorn syndrome, Cri du Chat syndrome, Williams syndrome, Prader-Willi syndrome, Angelman syndrome, Rubinstein-Taybi syndrome, Miller-Dieker lissencephaly, Smith-Magenis syndrome, Alagille and Di George syndromes.

iii. Coding abnormalities in single genes, single gene disorders have mostly severe phenotype and are far more frequent than generally assumed (Ropers 2010). Moreover, functional considerations from model organisms suggest that most disease-associated gene defects are inherited as recessive traits; therefore, it is likely that many Mendelian disorders have not been identified yet because of lack of consanguineous families in the well-studied Western populations (see section 1.1.2.2.). Identification of single gene defects relies on various strategies; most of them consists two steps, the chromosomal and regional mapping of the relevant defect and mutation screening of positional and functional candidate genes (Ropers 2010).

1.1.1. X-linked forms of ID (XLID)

This form of ID is easily identifiable because of its characteristic inheritance pattern. Although the X-chromosome represents only about 4% of the human genome (Ross et al. 2005), X-chromosomal defects are assumed to account for 8–12% of the ID affecting males (Ropers and Hamel 2005). This fact made the X-chromosome an attractive target for research into the molecular causes of ID. Identification of the vast majority of the genes causing XLID during the past decade became possible after the collection of large cohorts of families by international consortia (Ropers et al. 2003). To date, over 90 genes associated with ID on the X-chromosome have been identified (figure 1-1) (Gecz et al. 2009). So far, the studies of nonsyndromic ID have mostly focused on X-linked recessive forms and 43 genes (http://www.ggc.org/xlmr.htm) cause nonsyndromic ID or 'pure' forms of XLID have been identified, where ID is the only clinical abnormality, and mutations in these genes may account for >50% of such cases. Large-scale mutation screening is now beginning to shed more light on the relative frequency of ID (Ropers 2010).

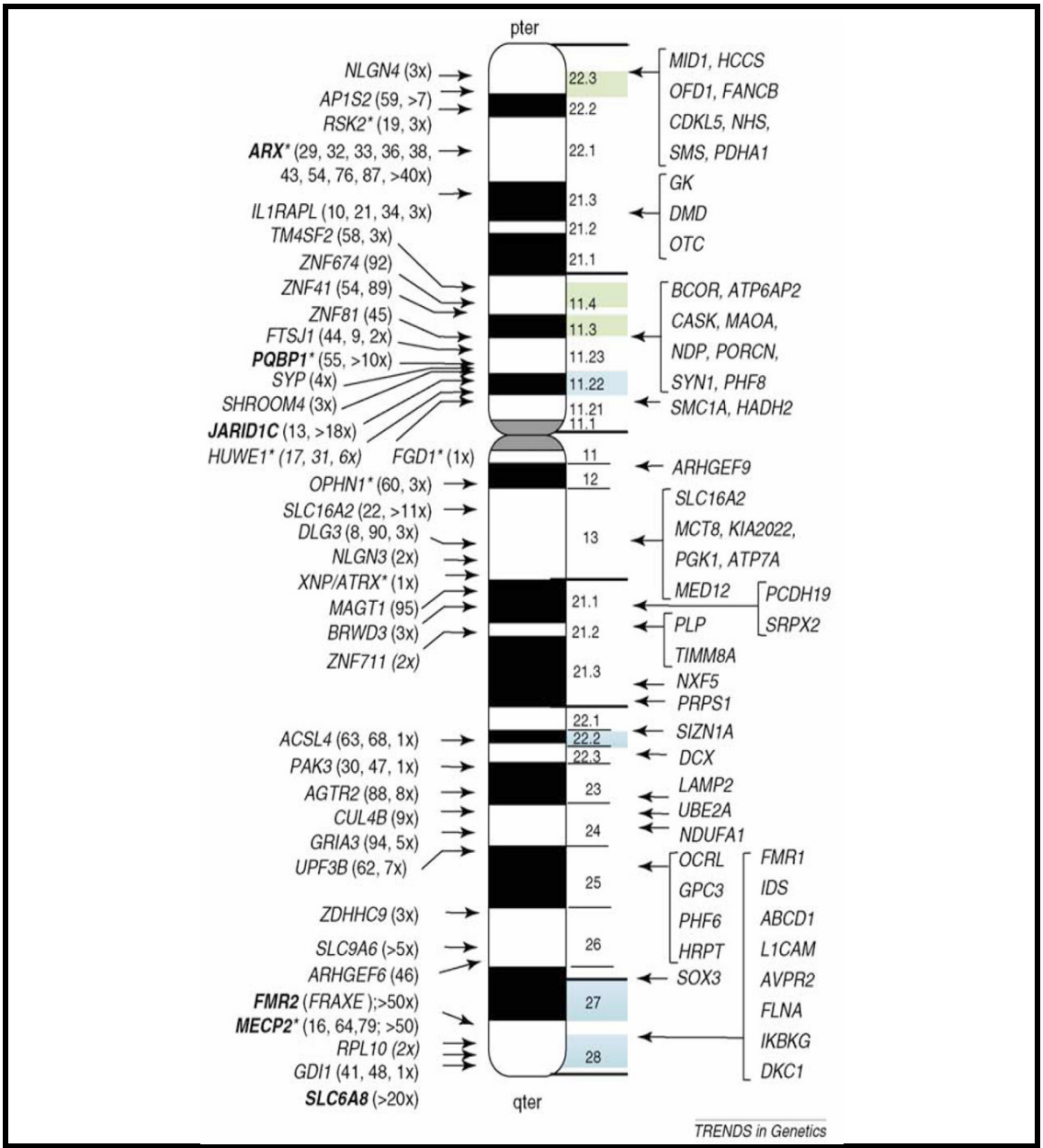

Figure 1-1: Genetic heterogeneity of XLMR. An ideogram of the human X chromosome is shown. The genes with high contribution to NS-XLMR are highlighted in bold. On the left-hand side, a list of genes currently known to be mutated in NS-XLMR patients are shown together with their approximate position and on the right hand side, the position and acronyms of genes currently known to be mutated in syndromic XLMR are shown. The numbers in brackets indicate either the number of unrelated families harboring mutations in that gene (i.e. 3x = three families, as for NLGN4) or the MRX number of the family (i.e. 45 for ZNF81), where a mutation was found. [Image source: (Gecz et al. 2009)].

Fragile X syndrome is the most common heritable form of ID, which may account for 25% of all families with XLID (Ropers 2008). In 1991, cloning of the gene *FMR1* (Fragile X Mental Retardation) revealed, that this syndrome is associated with the expansion of a single trinucleotide gene sequence (CGG) on the X chromosome (Fu et al. 1991; Oberle et al. 1991; Verkerk et al. 1991; Yu et al. 1991), and results in a failure to express the FMR1 protein which is required for normal neural development (Jin and Warren 2000). Four generally accepted conditions of the chromosome region are involved in Fragile X syndrome which relate to the length of the repeated CGG sequence (NFXF 2008):

- "Normal" or "Stable" (6 to ~45 CGG repeats; carriers are not affected by the syndrome)
- "Intermediate" or "Gray Zone Alleles (GZ)" (~45 to ~55, it may be associated with some neurodevelopmental disorders including autism spectrum disorders (ASD) (Loesch et al. 2009) and Parkinson (Loesch et al. 14th International Workshop on Fragile X and X-Linked Mental Retardation 2009)
- "Premutation (PM)" (55-200 CGG repeats; the same phenotype as GZ)
- "Full Mutation" (more than 200 CGG repeats; ~50% of females and all males are affected)

Aside from intellectual disability, prominent characteristics of the Fragile X syndrome include an elongated face, large dysplastic ears, flat feet, and low muscle tone. Behavioural characteristics may include stereotypic movements (e.g., hand-flapping) and atypical social development, particularly shyness, limited eye contact, memory problems, and difficulty with face encoding (MIM #300624). Some individuals with the Fragile X syndrome also meet the diagnostic criteria for autism. While males that carry the full mutation tend to present with severe intellectual disability, the symptoms of females with the full mutation are in the range of minimally affected to severe intellectual disability, which may explain why females are under-diagnosed relative to males (Goldenberg and Saugier-Veber 2009).

ARX mutations rank second with a prevalence of >5% among families with XLID (Gecz et al. 2006; Mandel and Chelly 2004). *CUL4B*, *JARID1C* and *SLC6A8*

mutations are all relatively frequent, each accounting for 2–3% of the families, while defects of all other known XLID genes seem to be significantly less common, in the 1% range or below (Ropers 2008).

1.1.2. Autosomal forms of ID

1.1.2.1. Autosomal dominant ID (ADID)

Families with ARID are seldomly observed because individuals with severe dominant forms of ID rarely reproduce. On the other hand, apparently relevant *de novo* CNVs have been observed in cohorts of patients with 'idiopathic' ID (Poser et al. 2008), and recently screening of genes encoding synaptic proteins has revealed several *de novo* truncating mutations (Hamdan et al. 2009) suggesting that dominant mutations are not very rare.

1.1.2.2. Autosomal recessive ID (ARID)

Epidemiological data and functional considerations suggest that the majority of the gene defects that give rise to disease will be inherited as recessive traits. Thus, autosomal recessive forms of ID (ARID) may be particularly common (Ropers 2008). The strategy of choice for elucidating the molecular defects underlying ARID is homozygosity mapping in large consanguineous families, followed by mutation screening of candidate genes (Bull et al. 1998; Houwen et al. 1994; Lander and Botstein 1987). Recently, this strategy has been employed to identify several gene defects underlying autosomal recessive primary microcephaly and other syndromic forms of ARID (Cox et al. 2006; Hong et al. 2000; Noor et al. 2008; Woods et al. 2006). Moreover, ARID might be relatively common in familial ID even if the pedigree structure is compatible with X-linked inheritance. There is increasing evidence to suggest that there are many loci for nonsyndromic autosomal-recessive ID (NSARID), nevertheless, this form of ID are likely to be under-represented, because in western populations most patients are isolated cases and also the ''nonsyndromic'' nature of the condition makes it difficult to pool multiple pedigrees with the same underlying genetic defects to achieve statistical significance (Ropers 2007). One study suggested at least eight loci for NSARID (Najmabadi et al. 2007). However, so far only six autosomal- recessive genes

have been identified: *PRSS12* (MIM 606709) (Molinari et al. 2002), *CRBN* (MIM 609262) (Higgins et al. 2004), *CC2D1A* (MIM 610055) (Basel-Vanagaite et al. 2006), *GRIK2* (MIM 138244) (Motazacker et al. 2007), *TUSC3* (MIM 601385) (Garshasbi et al. 2008; Molinari et al. 2008). Recently three groups independently identified *TRAPPC9* as a new candidate gene for NSARID which seems to be the most common one, as it is reported in four unrelated families from different parts of the world: Iran, Pakistan, Tunisia and Israel (Mir et al. 2009; Mochida et al. 2009; Philippe et al. 2009). There is recent evidence, however, that NSARID is not quite as heterogeneous as previously suggested (Ropers 2010).

1.2. Function of ID genes

Until recently the function of most ID genes, has remained largely unclear, but currently ongoing studies are shedding more light on the pathogenetic mechanisms underlying disorders of brain development and function. Candidate genes for nonsyndromic ID are involved in many biological processes, which are crucial for the genetic basis of human cognitive function. Many of the causative genes for X-linked ID have been found to function in synapses (Ropers 2006). For instance, Fragile X syndrome caused by the loss of function of the RNA-binding *FMR1* gene product FMRP, is assumed to result from up-regulation of group1 metabotropic glutamate receptor (mGluR) signalling until 2004 (Bear et al. 2004). But many recent studies have shed more light on the role of FMRP at the synapse and in dendritic mRNA transport. For instance, it was shown that enhanced mGluR signalling leads to excessive internalization of AMPA (α-amino- 3-hydroxy-5-methyl-4-isoxazole propionate) receptors (Nakamoto et al. 2007). FMRP interacts with the postsynaptic scaffolding protein Homer which is an integral component of the postsynaptic mGluR signalling complex and is necessary for mGluR-induced long-term depression and translational activation (Ronesi and Huber 2008b), and FMRP controls the stability of mRNA encoding PSD-95, a key molecule regulating synaptic signalling and learning (Zalfa et al. 2007). FMRP also interacts directly with the neuro specific kinesin KIF3C and links this transport molecule with dendritic RNA granules (Davidovic et al. 2007). It was shown that up-

regulation of phosphatase 2A (PP2A) is responsible for rapid FMRP dephosphorylation after immediate group 1 mGluR stimulation (Narayanan et al. 2007), whereas extended mGlu activation results in mTOR-mediated PP2A suppression (Ronesi and Huber 2008a). SYNGAP1, which is associated with ADID, encodes a ras GTPase-activating protein, a component of the NMDA-receptor complex (Hamdan et al. 2009).

The functions of the NSARID genes are less well characterized, but they appear to be quite diverse.

PRSS12, localizes to presynaptic nerve endings of cortical synapses and encodes the neuronal serine protease neurotrypsin (Molinari et al. 2002). This protein specifically cleaves agrin, which is involved in the formation of filopodia on neuronal axons and dendrites (Annies et al. 2006; McCroskery et al. 2006). Agrin cleavage generates an inactivating ligand of the Na^{+}/K^{+-} ATPase at CNS synapses, previously identified as the neuronal receptor for agrin (Hilgenberg et al. 2006). CRBN might regulate mitochondrial energy metabolism (Higgins et al. 2004), recently, a Japanese group identified CRBN as a thalidomide-binding protein and they showed that CRBN has E3 ubiquitin ligase activity (Ito et al. 2010). CC2D1A and TRAPPC9 has been implicated in NF-kappaB signalling (Hu et al. 2005; Nakamura et al. 2008; Ou et al. 2003; Zhao et al. 2010), GRIK2 is a glutamate neurotransmitter receptor (Contractor et al. 2001) and TUSC3 has been shown to be involved in the control of intracellular Mg^{+2} levels (Zhou and Clapham 2009).

As the number of known ID genes increases and their function is explained, pathways are beginning to emerge. For example, several regulators and effectors of Rho GTPases that control the actin cytoskeleton and neurite outgrowth have been implicated in ID (Ramakers 2002). About 25% of the XLMR genes identified are predicted to encode nuclear proteins, including transcriptional regulators and chromatin remodeling proteins (Chiurazzi et al. 2008; Gecz et al. 2009; Ramos and Robert 2005), for example in MECP2, JARID1C, ATRX and PHF8 (Argentaro et al. 2007; Laumonnier et al. 2007; Qi et al. 2010; Villard 2007). ATRX belongs to the SWI2/SNF2 family of chromatin

remodeling proteins; besides the ATPase/helicase domain at its C-terminus, it contains a PHD-like zinc finger at the N-terminus (Argentaro et al. 2007), PHD fingers are common features of chromatin-related proteins (Bienz 2006; Lu et al. 1998; Nagamine et al. 1997). PHF8 belongs to a subfamily of JmjC domain-containing proteins with an amino terminal PHD finger adjacent to the catalytic JmjC domain; PHF8 regulates histone methylation and gene transcription by encoding a novel H4K20me1 and H3K9me1/2 demethylase (Qi et al. 2010). It has been shown that, defects involving kinetochore proteins and other mechanisms interfering with normal chromosome segregation are often found in ID associated with microcephaly (MCPH1-7) (Bond et al. 2005; Jackson et al. 2002; Ritchie et al. 2008; Shen et al. 2005). It is interesting to note that recently it has been shown that cell division defects do not necessarily have to have a macroscopic effect on brain structure in order to cause cognitive dysfunction (Garshasbi et al. 2006).

1.3. Aim of this study

This project is part of a large-scale study into the molecular causes of ARID by studying consanguineous families with at least two affected, clinically well-characterized individuals, which have been and are still being recruited in Iran.

My work focuses on the identification and functional characterization of the specific disease-causing mutation in a large consanguineous Iranian family with two branches and four female patients where ID is accompanied by oligomenorrhea and a genomic locus had been identified before by autozygosity mapping on chromosome 5q.

2. Patients, Materials and Methods

2.1. Patients

A seven-generation family with autosomal recessive mental retardation was ascertained from a remote region in central Iran, through collaboration with the Genetics research center of the University of Social Welfare and Rehabilitation Sciences, Tehran, Iran. Approval for this study was obtained from the appropriate review boards in both Germany and Iran. After obtaining written informed consent from the parents, the patients and unaffected relatives were examined in a standardized way using a questionnaire (see appendix 1) and photographs were taken to document physical findings. The clinical geneticists examined the mental status of all the affected individuals by sophisticated tests such as a modified version of the Wechsler Intelligence test. The pedigree of family M-193 is shown in figure 2-1.

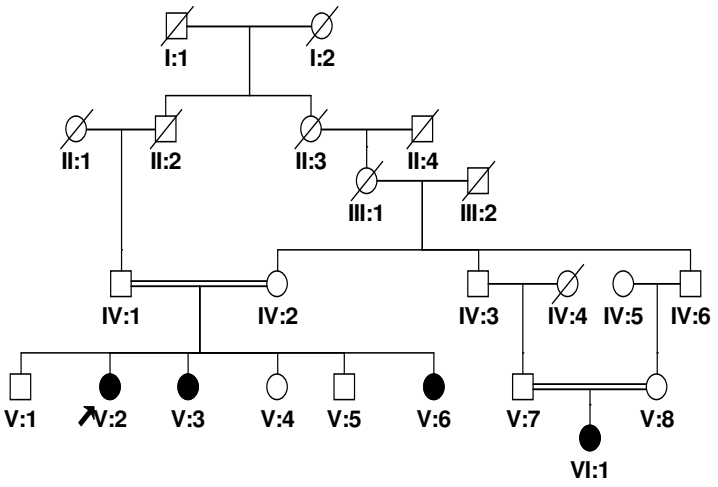

Figure 2-1: Pedigree of family M-193

The three affected females of the left branch (V:2; V:3; V:6) suffered from moderate MR (IQ 50-55), short stature and obesity (table 2-1). However, also the mother (152 cm), the father (172 cm) and the healthy adult siblings (V:1=160 cm; V:4=152 cm; V:5=170 cm) were short. Obesity was also

observed in the mother (BMI 37.2) and the healthy eldest brother (V:1; BMI 37.9). The three patients in this branch had either primary (V:3) or secondary (V:2; V:6) oligomenorrhoea of unknown cause. Endocrinological tests and ultrasound investigations of the ovaries revealed no abnormalities.

The patient in the right branch of the family (VI:1) suffered from mild mental retardation (IQ 70). On examination at the age of 13 years, she had short stature and was mildly obese (BMI 25.6). Head circumferences in all patients were within the normal range Brain MRI scans were performed in all four patients and revealed no morphological abnormalities.

Table 2-1: Clinical description of family M-193

	V:2	V:3	V:6	VI:1
Age	30y	27y	19y	13y
IQ*	50-55	50-55	50-55	70
OFC**	54 cm (25-50th cent.)	57 cm (75th cent.)	55 cm (50th cent.)	53 cm (50th cent.)
Height	156 cm (3rd cent.)	152 cm (<3rd cent.)	151 cm (<3rd cent.)	137 cm (<3rd cent.)
Weight	94 kg (>>97th cent.)	93 kg (>>97th cent.)	71 kg (90th cent.)	48 kg (50th cent.)
BMI***	38.6	40.3	31.1	25.6

* IQ: intelligence quotient

** OFC: occipitofrontal circumference;

*** BMI: body mass index

After obtaining written consent, blood samples for DNA preparation were collected from the parents and all children of both branches and genomic DNA was extracted using a standard salting out method. For the index patient, standard 450 G-band karyotyping was performed in order to exclude

cytogenetically visible chromosomal aberrations and Fragile X testing was carried out by PCR and Southern blot analysis. Filter-dried blood of the proband was screened by tandem mass spectrometry to exclude disorders of the amino acid, fatty acid (e.g. phenylketonuria) or organic acid metabolism (Chace et al. 2003; Wilcken et al. 2003). EBV immortalized lymphoblastoid cell lines (LCL) were established for patient V:2, V:3 and V:6 In addition biopsies were obtained and fibroblast cultures (FB) established from patients V:2 and V:6.

2.2. Materials

2.2.1. General reagents

Table 2-2: Chemicals

Chemical	**Supplier**
[α-32P]dCTP	Amersham Biosciences
Acrylamide (Molecular biology grade)	Sigma
Agarose	Invitrogen
Ammonium persulfate	Sigma
Ampicillin	Sigma
Aqua ad inectabilia	Baxter
B27-Supplement minus AO	GIBCO
Betaine	Sigma
Bromophenol Blue	Sigma
BSA	Sigma
Chloroform	Merck

Chloroform	Sigma
Complete, Mini Protease Inhibitor Cocktail Tablets	Roche
Cycloheximide (CHX)	Sigma
DAPI	Serva
Diethylpyrocarbonate (DEPC)	Aldrich
DMEM (Dulbecco´s Modified Eagle Medium)	Cambrex
DMSO	Sigma
dNTPs	Roth
EDTA	Merck
Ethanol	Merck
Ethidiumbromide	Serva
Fetal calfserum (FCS)	Biochrom
First strand buffer 5x	Merk
Formaldehyde-37.0% (v/v)	FlukaBiochemika
Formamide	FlukaBiochemika
Glycerol	Roth
Glycin	Merck
HEPES	Calbiochem
Isopropanol	Merck
Hydrogen Chloride	Merck
Kanamycin	Invitrogen
L-Glutamine (200 mM/ml)	Cambrex

Laminin	Sigma
Lipofectamine 2000 transfectionreagent	Invitrogen
Magnesium chloride	Merck
Methanol	Merck
Milk powder	Protifar
Neurobasalmedium	Invitrogen
Northern blot hybridization buffer	Ambion
OptiMEM	Invitrogen
Penicillin-Streptomycin (10000 U/ml Pen., 10 mg/ml Strep.)	Cambrex
PFA (Paraformaldehyde)	Merck
Phenol	Sigma
Polyethylenglycol (PEG)	Merck
Poly-D-Lysin	Sigma
Poly-L-Lysine aqueous solution (0.1 w/v)	Sigma
Polyfect	Qiagen
Ponceau S dye	Invitrogen
Potassium Chloride	Sigma
Quantum333 for fibroblasts	PAA
RPMI 1640	Cambrex
RNA - human adult brain	BD Bioscience
RNA - human fetal brain	BD Bioscience
RNA- human adult Temporal lobe	BioChain

RNA- human fetal Temporal lobe	BioChain
RNA- human Hippocampus	BioChain
RNA-human Ovary	BioChain
SDS	Roth
Sodium Acetate	Sigma-Aldrich
Sodium Chloride	Roth
SodiumHydroxide	Merck
SodiumHydroxide	Sigma
Sodium perchlorate	Merck
Sodium triphosphate	Merck
TEMED	Gibco BRL
Triton X100	Invitrogen
TRIzol reagent	Gibco BRL
Trypsin EDTA (500 mg/ml Trypsin, 200 mg/ml EDTA)	Cambrex
Tween 20	Invitrogen
Whatman paper	Sigma
β-mercaptoethanol	Whatman

2.2.2. Buffers and Media

Table 2-3: Buffers and Media

Buffer/Medium	Composition
APS 10%	10% w/v APS in water, aliquoted and stored at –20°C
Blocking buffer	5% milk powder in PBST
DEPC H_2O	0.1% DEPC was stirred overnight in water and autoclaved afterwards.
DNA re-suspension buffer	0,4M Tris-HCl PH=8, 0.06M NaEDTA, 0,15M NaCl
DNA-Loading buffer	15% Ficoll, 0,25% Bromphenolblue in double distilledH_2O
Ethidium bromide	10 mg/ml EtBr in double distilled H_2O
Fibroblast primary cells	Quantum333, 15% FCS, 100 U/ml Penicillin + 100 µg/ml Streptomycin, 20% conditioned medium with 1ng/ml bFGF
First strand buffer 5x	250 mMTris-HCl (pH 8.3 at room temperature), 375 mMKCl, 15 mM $MgCl_2$
HaCat cell media	From Cambrex + 10% FCS + 100 U/ml Penicillin + 100 µg/ml Streptomycin + 2 mM L-Glutamine
Laemmli protein loading buffer (5X)	Aqueous solution containing 62.5 mMTrisHCl (pH 6.8), 5% beta-mercaptoethanol (v/v), 50% Glycerol (v/v), 2% SDS (w/v), 0.1% (w/v) Bromophenol Blue.
Lymphoblastoid cell lines	RPMI-1640 containing 10.0% (v/v) FBS; 100 U/ml Penicillin; 68.6 µM Streptomycin; 2.00 mM L-Glu.
MOPS 10 x	0,4 M MOPS; 0,1 M NaAc; 10 mM EDTA pH 7,0
Northern blot running buffer	2.2 M formaldehyde, 1x MOPS in DEPC H_2O

Primary cortical neuron media	Neurobasal medium, B27supplemement, 1,25µl L-Glutamin
Primary fibroblast media	500ml Q333media+ 10 % FCS, 100 U/ml Penicillin/Streptomycin, 10 ng/ml bFGF
Northern blot sample buffer	50% formamid, 2.2M formaldehyde, 1x MOPS, 40 µg/ml Ethidium Bromide
Northern blot wash buffer	2x SSC / 0.1% SDS
PBS 1 x buffer	137 mMNaCl; 2,7 mMKCl; 10,1 mM Na2HPO4; 1,8 mM KH_2PO_4
PBST buffer	1 x PBS; 1:1000 Tween 20
Ponceau Red solution	2% (w/v) Ponceau S dye, 5% (v/v) Acetic acid
SDS-PAGE running buffer (1X)	196mM glycine, 0.1% SDS, 50mM Tris-HCl (pH 8.3)
Western blot Separating gel buffer	1,5 M Tris-HCl, 0,4 % SDS pH 8,8
SSC 10x	3M NaCl, 0,3M Na-citrate in double distilledH_2O, adjust pH 7 with 1M HCl
Stacking gel buffer	0,5 M Tris-HCl, 0,4 % SDS pH 6,8
Stripping buffer	1% SDS, 20 mM TRIS/HCl (pH 6.8), 1% (v/v) β-mercaptoethanol
TAE buffer 50 x	50 mM EDTA, 5,71% v/v acetic acid, 2M Tris-HCl
TBE buffer	0.1 M Tris, 0.1 M boric acid, 2 mM EDTA
TBS	20 mMTris, 150 mMNaCl
TBST buffer	20 mMTris, 150 mMNaCl. 0.1% (w/v) Tween-20
TE	10 mMTris-HClpH 7,5; 1 mM EDTA

WB Transfer buffer 1x	0.1% SDS, 20% (v/v) MeOH, 48mM TRIS7/HCl, 39mMGlycine
Western Blot Blotting buffer 5x	29,11g Tris; 14,65g Glycin; 18,75 ml SDS in 1L double distilledH_2O

2.2.3. Instruments

Table 2-4: Instruments

Instrument	Manufacturer
B 5050 E incubator	Heraeus
Capillary Sequencer ABI 377	Applied Biosystems
Centrifuge 5810R	Eppendorf
Centrifuge Rotanta 46R/Rotina 4R	Hettich-Zentrifugen
Centrifuge Rotina 48R	Hettich-Zentrifugen
Clean bench Herasafe	Heraeus
CO_2 water jacketed incubator	Forma Scientific
Concentrator 5301	Eppendorf
Control environment incubator shaker	New Brunswick Scientific
cytospin^R cytocentrifuge	Shandon
E.A.S.Y. 440K Gel Documentation System	Herolab
Electrophoresis power supply 2	Heathkit
Fluorescent light microscope	Zeiss
Geiger Counter, Series 900 mini-monitor	Artisan Electronics Corp.
Hamilton syringe	Hamilton

Horizontal gel apparatus Horizon® 11.14 and 20.25	Life technologies
HyperCassetteBioMAX (Northern blot)	Amersham
Inverted light microscope, Eclipse TS100	Nikon
L8-70M ultracentrifuge	Beckmann
Laminar flow hood, CA/REV 6 Cleanbench	Clean Air
Mini-Gel apparatus	Bio-Rad
Multichannel pipette	Rainin
Phase lock gel light	Eppendorf
pH-meter	Knick
Pipett boy	Integra biosciences
Pipettes	Gilson
Power Pac 300 electrophoresis power supply	Bio-Rad
PTC-225 Tetrad and Dyad thermal cycler	Bio-Rad
REAX 2000 vortexer	Heidolph
RnaseZapWipes	Ambion
Rotating mini hybridization oven	Appligene
Rotors TLA120.1, TLS-55, SW40	Beckmann
Scanner, Expression 1680 Pro	Epson
sonicator	Bandelin sanopuls
Sorvall RC-5B refrigerated super speed centrifuge	Du Pont instrument
SPD 111V Speed Vac	Savant
SpectrophotometerNanoDrop ND-1000	PEQLAB

Steri-cycle CO_2 incubator 371	Thermo Electron Corp.
Stereoscop	ZeissStemi SV11
Table centrifuge 5415C	Eppendorf
ThermoForma 758 Ultrafreezer	Thermo Electron Corp.
Thermomixer 5436	Eppendorf
TL100 ultracentrifuge	Beckmann
UV stratalinker 1800	Stratagene
UV trasilluminator	UVPinc
Western blot cassette (HyperCassette)	Amersham
Western blot Trans Blot SD	Bio-Rad
X-ray film developing machine, Curix 60	Agfa
Zeiss LSM510 confocal microscope	Zeiss

2.2.4. Consumables (Disposable materials)

Table 2-5: Consumables (disposable materials)

Name	**Supplier**
Adhesive PCR film	Abgene
Biomax MS X-ray film (sensitive)	Kodak
Cell culture flask (75 & 100 cm^2)	TTP
Chromatography paper	Whatman
Disposable reaction tube 14 ml	Greiner BioOne

Disposable reaction tube 30 ml	Sarstedt
Falcon tube	Greiner BioOne
Glass coverslip	Menzel-Gläser
Hybond-XL (Northern blot membrane)	Amersham
Immobilon-P transfer membrane (Western blot membrane)	Millipore
MS Photographic film	Kodak
MS X-ray film	Kodak
Parafilm	Pechiney Plastic Packaging
Pasteur pipette	Roth
PCR plate (96 well)	Abgene
Pipette tip (0.1 – 10, 1-20, 20 – 200 & 1000 µl)	Biozyme
Reaction tube (1.5 & 2 ml)	Eppendorf
Scalpel	Aesculap
Serological pipette (2, 5, 10 & 25 ml)	Corning
Superfrost Plus glass slide	Menzel-Gläser

2.2.5. Kits and markers

Table 2-6: Kits and Markers

Name	**Supplier**
0.24-9.5 Kb RNA ladder	Invitrogen

1 kb DNA ladder	Roth
BigDyeTerminatormix	Applied Biosystems
Bio-X-ACT (Bioline) PCR Kit	Bioline
DC protein assay kit	BIO-RAD
Dithiothreitol (DTT)	Invitrogen
DynabeadsOligo (dT)25 kit	DYNAL Biotech
ECL kit	Amersham Biosciences
FastPlasmid Mini kit	Qiagen
GeneChip® Human Mapping 10K Array and Assay Kit	Affymetrix
Hyper Ladder I	Bioline
Hyper ladder IV	Bioline
Maxiprep Kit	Qiagen
Micro Spin G-250 column	Amersham
MiniElute PCR purification kit	Qiagen
MiniprepKit	Qiagen
Oligo(dT)12-18 primer	Invitrogen
Oligo(dT)20 primer	Invitrogen
Pinpointcell surface protein isolation kit	Pierce
Plasmidminiprep	Qiagen
Plasmidmaxiprep	Qiagen
pUC Mix marker, 8	Fermentas
QIAquick Gel Extraction Kit	QIAGEN

QuickChange site-directed mutagenesis kit	Stratagene
Quick Ligase (T4 DNA ligase)	New England Biolabs (NEB)
Random Primers	Promega
SDS-PAGE protein marker - High range	Sigma
Taq PCR core kit	Qiagen, Bioline
TOPO TA Cloning kit for sequencing	Invitrogen

2.2.6. Plasmids

Table 2-7: Plasmids	
Plasmid	**Supplier**
pEGFPN1	Clontech
pmCherryC1	Clontech

2.2.7. Antibodies

Table 2-8: Antibodies				
Primary antibody	**Type**	**Raised in**	**Supplier**	**Dilution (Immunoflorescence staining)**
NCL- Emerin	Monoclonal	Mouse	Novocastra	1:80
Lamin A/C	Monoclonal	Mouse	Mckeon	1:500
LAP2 ß	Polyclonal	Rabbit	Received from FU, Berlin (Dr. Otto)	1:300

LUMA	Polyclonal	Rabbit	Received from MDC, Berlin (Dr. Bengtsson)	1:700
Gama-tubulin		Mouse	Received from MPIMG, Berlin (Dr. Gowsami)	1:500
Alpha-tubulin		Mouse	Received from MPIMG, Berlin (Dr. Gowsami)	1:500
YL (viral tubluin)		Rat	Received from MPIMG, Berlin (Dr. Gowsami)	1:300
BOD1	Polyclonal	Rabbit	Received from University of Dundee, Scotland (Dr. Porter)	1:250 (IF); 1:50 (western blot)
SET1A		Goat	Received from Herman B Wells Center for Pediatric Research, USA (Prof. Skalnik)	1:250
SET1B		Rabbit	Received from Herman B Wells Center for Pediatric Research, USA (Prof. Skalnik)	1:250
MAP2kinase	Monoclonal	Mouse	Received from MPIMG, Berlin(Dr. Kalscheuer)	1:500
PDS95	Monoclonal	Mouse	Received from MPIMG, Berlin(Dr. Kalscheuer)	1:200
NR2B	Monoclonal	Mouse	Received from MPIMG, Berlin(Dr. Kalscheuer)	1:200
Anti-beta-Tubulin III	Monoclonal	Mouse	Zigma	1:1000
Anti-beta-Actin	Monoclonal	Mouse	Zigma	1:1000
Bassoon	Monoclonal	Mouse	Synapticsystems	1:200
ProSAP2/shank3		Antiguinea pig	Received from MPIMG, Berlin (Dr. Gowsami)	1:200

LaminB	Polyclonal	Goat	SantaCruz biotechnology	1:200
H3K9me2	Monoclonal	Mouse	Abcam	1:400

2.2.8. Enzymes

Table 2-9: Enzymes

Enzymes	**Supplier**
BamHI	New England Biolabs (NEB)
BglII restriction enzyme (10 U/µl)	New England Biolabs (NEB)
DNA polymerase 1, Klenow fragment	USB
EcoRI restriction enzyme	New England Biolabs (NEB)
Proteinase K	Fermentas
KpnI restriction enzyme	New England Biolabs (NEB)
RQ Rnase-FreeDNase	Promega
RNAsin	Promega
SuperScript III Reverse Transcriptase	Invitrogen
T4 DNA ligase	Promega

2.2.9. Software

Table 2-10: Software

Name	Application and Source
Allegro	Parametric linkage analysis http://www.decode.com/software/allegro
Alohomora	Conversion Tool http://gmc.mdc-berlin.de/alohomora/
Beadstudio	http://www.illumina.com/
CodonCode	sequence assembly, contig editing and mutation detection. http://www.codoncode.com/
Cyrilic2.1.3	To draw pedigrees
GeneHunter	Parametric and non-parametric linkage analysis http://www.broad.mit.edu/ftp/distribution/software/genehunter/
GRR	Pedigree based relationship evaluation http://www.sph.umich.edu/csg/abecasis/GRR/
Haplopainter	Visualization of haplotypes created by GeneHunter or Merlin http://haplopainter.sourceforge.net/html/ManualIndex.htm
Merlin	Non-parametric linkage analysis http://www.sph.umich.edu/csg/abecasis/Merlin/download
PedCheck	Finding mendelian errors and unlikely genotypes http://watson.hgen.pitt.edu/register
GraphPad Prism 4.03	Data flow static analysis tool
SDS 2.1.1.	To analyse qRT-PCR data

ZeissLSMimage examiner	Provided with Zeiss laser scanning microscope

2.2.10. Bioinformatic databases and web-based tools

Table 2-11: Bioinformatic databases and tools

Database	Type	Internet Address
DAVID	Functional Annotation Bioinformatics Microarray Analysis	http://david.abcc.ncifcrf.gov/
European Bioinformatics Institute, Hinxton, UK and The Wellcome Trust Sanger Institute, Hinxton, UK	Ensembl	http://www.ensembl.org
ExPaSy	Proteomics Server	http://www.expasy.org/
GenBank	Genome database	http://www.ncbi.nlm.nih.gov/Genbank/
Genome Bioinformatics Group, University of California, Santa Cruz, CA, USA	Genome Browser, Blat Search, PCR	http://genome.ucsc.edu/
National Center for Biotechnology Information, Bethesda, MD, USA	PubMed, UniGene, Nucleotide, Blast Search	http://www.ncbi.nlm.nih.gov/
Online Mendelian Inheritance in Man (OMIM)	Database of human genesand genetic disorders	http://www.ncbi.nlm.nih.gov/Omim
Panther	Protein ANalysisTHrough Evolutionary	http://www.pantherdb.org/

	Relationships	
POSMED	Positional cloning gene ranking	http://omicspace.riken.jp/PosMed/
Primer3	Primer design	http://frodo.wi.mit.edu/cgi-bin/primer3/primer3_www.cgi
Webcutter	DNA restriction map	http://rna.lundberg.gu.se/cutter2/

2.3. Methods

Figure 2-2 shows the strategy that was used in order to discover the putatively disease causing mutation in the affected individuals. Subsequently each method is described separately.

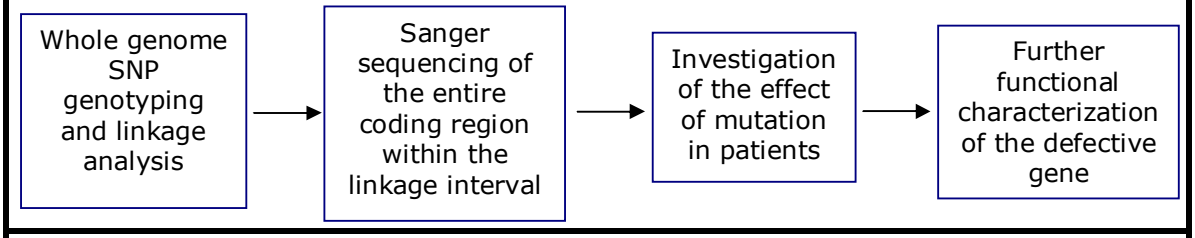

Figure 2-2: Approach for the identification of putative disease causing mutations

2.3.1. SNP genotyping

Pogress in SNP discovery and genotyping provide the opportunity to use them as a useful linkage analysis tool in order to investigate the genetic causes of human diseases (Collins et al. 1997; Matiseet al. 2003). In this study, after preparing appropriate DNA concentrations and quality control (by analyzing the DNA on an agarose gel), whole genome SNP Genotyping was performed using the AffymetrixGeneChip® Human Mapping 10k Array (Xba142). This is a high-throughput genotyping platform (Figure 2-3), which uses a one-primer assay to genotype 10,000, SNPs per individual on a single oligonucleotide array. This

approach uses restriction digestion to fractionate the genome, followed by amplification of a specific fractionated subset of the genome. The resulting reduction in genome complexity enables allele-specific hybridization to the array. The arrays are scanned using GeneChip® Operating Software (GCOS). The resulting image file, the .dat file, is then displayed and a grid is applied to the image. Following the application of the grid a .cel file is automatically generated. The .cel file contains the average image data and is the data file required for analysis of the array data in GeneChip® DNA Analysis Software (GDAS). Following the generation of the .cel files, GDAS can be immediately used to generate genotyping calls (10K GeneChip® Mapping Assay Manual).

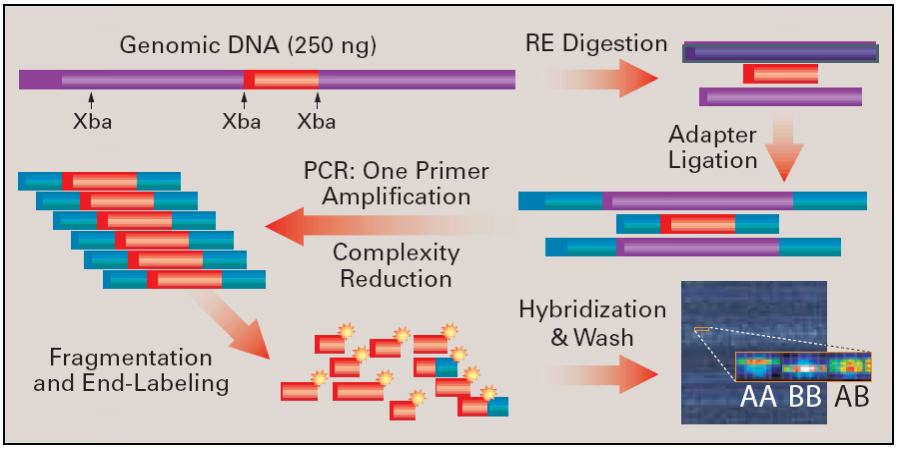

Figure 2-3: GeneChip ® mapping assay overview (Image source: http://www-microarrays.u-strasbg.fr/base.php?page=affySNPsE.php).

2.3.2. Linkage analysis

The human genome contains 20-30 thousand genes. Therefore, finding the particular gene or genes responsible for any given human disease has always been a tricky task.

"Linkage analysis" serves as a way of disease gene-hunting and genetic testing. Genetic linkage explains a condition where two chromosomal locations

(two loci, two genes, two polymorphisms) are very close to each other and where there is no historical (ancestral) recombination event between these locations. This lack of crossing-over has the effect that one of the locations (which is e.g. a gene implicated in a disease) during meiosis drags along the other (e.g. a harmless polymorphic Mendelian character i.e. a genetic marker). Thus persons carrying a gene defect tend to have a certain allele value at a linked marker position. Linkage, and linkage disequilibrium are two key concepts in this issue; Two genetic loci are linked if they are transmitted together from parent to offspring more often than expected under independent inheritance; They are in linkage disequilibrium if, across the population as a whole, they are found together on the same haplotype more often than expected. In general, two loci in linkage disequilibrium will also be linked, but the reverse is not necessarily true (Dawn Teare and Barrett 2005).

To establish linkage, informative meioses are necessary. Meiosis is informative when a gamete is recombinant for a certain pair of markers. The ratio of such meioses is the recombination fraction (θ). This value is varying between 0 and 0.5. The null hypothesis represents no linkage between disease and marker locus (θ=0.5), and the alternative hypothesis assumes linkage exists (θ<0.5).

$$\theta = \text{Recombination fraction} = \frac{\text{Recombinant meioses}}{\text{Recombinant M.} + \text{Nonrecombinant M.}}$$

The probability of linkage is the proportion between the overall likelihood given linkage and the likelihood given no linkage:

$$\text{Odds of linkage} = \frac{\text{Likelihood if recombination fraction } \theta=\theta_1}{\text{Likelihood if recombination fraction } \theta=0.5}$$

Linkage is usually reported as a logarithm of the odds (LOD) score. This score was first proposed by Morton (Morton 1955). Large positive scores are evidence for linkage (or cosegregation), and negative scores are evidence against linkage. The ultimate objective of the analysis is to estimate the

recombination fraction between individual markers and the disease locus (two-point) or position of the disease locus relative to a fixed map of markers where the location of each marker is assumed to be known (multipoint). The best (maximum likelihood) estimate of θ or position is that which maximises the LOD score function i.e. yields the maximum LOD score. All LOD scores at θ = 0.5 are zero because they are then measuring the ratio of two identical probabilities, and log (1) = 0.

If these calculations are carried out under the assumption of a specific mode of inheritance (e.g. dominant or recessive) for the trait locus, linkage analysis is referred to as parametric. In contrast, nonparametric linkage analysis does not need a genetic model and is supported by shared chromosomal segments in affected individuals. In this study both approaches were used.

$$LOD(\theta)=\log_{10}\left(\frac{Like(\theta)}{Like(\theta=1/2)}\right)$$

2.3.2.1. Data conversion

The ALOHOMORA software (Ruschendorf and Nurnberg 2005) were used to convert AffymetrixGeneChip® Human Mapping 10K Array SNP genotype data together with pedigree and SNP allele frequency data into input files suitable for downstream software such as GRR, PedCheck, Allegro, GeneHunter and Merlin.

2.3.2.2. Examination of pedigree data for consistency with genotypes

Prior to linkage analysis, elimination of all Mendelian inconsistencies in the pedigree data is essential. Errors at this stage can be due to sample mix-up, non-paternity or wrongly called genotypes. The PedCheck program (O'Connell and Weeks 1998) was implemented in order to detect Mendelian errors.

The GRR software was applied in order to verify relationships between individuals in a given pedigree, sample duplications and switches. GRR offers a convenient way to identify individuals with patterns of allele sharing that are inconsistent with their specified relationship by coloring code and plotting the mean-variance statistics. Relationships whose mean-variance does not fit to the assumed category can be considered as falsely classified.

2.3.2.2. Data formatting for linkage analysis

Pedigree information was prepared in a tab-delimited text file that contains SNP IDs in one column followed by the genotype for each sample in a tab-delimited separate column, having the following column structures:

Family ID Sample ID Father ID Mother ID Sex Affection

The pedigree file must have the name "pedfile.pro" and must be located in the samefolder as the genotype file.

The next requirement concerns the genotyping data file which has to have a header line describing the columns. The first column contains the SNP name and all other columns contain genotypes. The columns are tab-delimited, having the following column structures:

SNP_Name sample1 sample2 sample3 sample4

The genotypes must be coded A or AA for homozygotes for the first allele, B or BB forhomozygotes for the second allele and AB for heterozygotes. The sample IDs in thecolumns header are either identical with the sample ID in the "pedfile.pro".

The preferred genetic map and the marker allele frequencies for the appropriate ethnicity have to be prepared. For our analysis we used the Caucasian population allele frequencies provided by Affymetrix and genetic marker map information provided by decode.

2.3.2.3. Parametric and non-parametric linkage analysis

For Parametric linkage analysis the Allegro V1.2 (Gudbjartsson et al. 2000) and GeneHunter V2.1 (Kruglyak et al. 1996) soft wares were applied and non-parametric linkage analysis was performed, using GeneHunter and Merlin (Abecasis et al. 2002).

Allegro, GeneHunter and Merlin use the Lander-Green algorithm and have a pedigree size restriction per analysis (2n-f<16: where "f" and "n" are the number of founders and non-founders respectively). With this algorithm, increasing the number of individuals and markers will respectively increase the calculation time exponentially and linearly while missing data have only a modest effect on calculation time.

2.3.2.4. Graphical haplotype reconstruction

For easy visualization of the complex haplotype information that resulted from the analysis of genome-wide high-density SNP marker panels, the software Haplopainter V.027b (Thiele and Nurnberg 2005) was used. It is a pedigree-drawing application, which has been developed to facilitate gene mapping in Mendelian diseases in terms of fast and reliable definition of the smallest critical interval harboring the underlying gene defect.

2.3.3. Mutation screening

2.3.3.1. Isolation of the genomic DNA from lymphoblastoeid cell pellet:

EBV-transformed lymphoblast (LCL) and fibroblast (FB) cell lines from patients were established (see Appendix A). Pellets containing 10^8 cells from these cell lines were frozen at -80°C and used for RNA or protein isolation. Information about the medium that was used to culture LCL and FB cells is given in Table 2-3.

2.3.3.2. DNA Extraction

DNA extraction from LCL cells was performed according to the following protocol:

Preparebuffer A:

Buffer A	For 100 ml
0.4 M Tris-HCL-buffer (pH=8)	40 ml from 1 M stock
0.06 M Na-EDTA-buffer	12 ml from 0,5 M stock
0.15 M NaCl solution	15 ml from 1 M stock
	33 ml aqua dest.

After autoclavation add 5 ml 20% -SDS (Sodiumdodecylsulfat)

1. Transport the cell pellets on ice from the freezer room to the lab
2. Add 20 ml from solution A (see above) on ice to each sample: (First add 1 ml, then add the rest of 19ml)
3. Vortex, until suspension appears homogenous
4. Put the falcon tubes into the rack at room temperature
5. Add 30 µl RNase A (10mg/ml)
6. Incubate for 60min at 37°C
7. Add 5 ml sodiumperchlorate (Natriumperchlorat)
8. Shake it by inverting the tube 10-15 times (not more) manually
9. Add 20 ml cold chloroform under the hood
10. Shake it by inverting the tube10-15 times manually
11. Centrifuge for 10 min at 4000 U/min
12. Take away the upper phase with a glass pipette and the pipette boy [If the upper phase is very cloudy (a lot of protein debris) repeat the chloroform extraction]
13. Transport in a new and labelled Falcon tube
14. Add a volume of ice-cold ethanol (100%) [e.g.: at 25 ml sample volume add 25 ml ethanol]

15. Take up the DNA with an expendable diluting loop [The DNA falls out by inverting the tube several times]
16. Transport the DNA in an eppendorf tube with 1ml cold ethanol (70%)
17. Spin it for 1 min at 7500 U/min
18. Pipette off the ethanol
19. Add 500 µl of new ethanol (70%)
20. Centrifuge for 1 min at 7500 U/min
21. Remove the ethanol
22. Leave it open in the Thermomixer at 50°C, until the DNA pellet is dry
23. Add 500 µl Tris-EDTA (TE) buffer
24. Leave it over night to resolve at room temperature

2.3.3.3. Polymerase Chain Reaction (PCR)

PCR was used for the amplification of genomic DNA as template for Sanger sequencing. Each PCR reaction was prepared according to the conditions shown in Table 2-12 and Table 2-13, using Taq PCR core kit.

Table 2-12: Touch down PCR thermal cycle

	Temp	**Time**	**Cycle number**
Initial denaturation	94°C	2 min	1x
Denaturation	94°C	30 sec	
Annealing	65°C >> 55°C*	30 sec	20x
Extension	72°C	30 sec**	
Denaturation	94°C	30 sec	
Annealing	55°C	30 sec	30x
Extension	72°C	30 sec**	
Final extension	72°C	10 min	1x

	4°C	unlimited	

*Annealing temperature was reduced 0.5°C after each cycle

** 1 min extension time was considered for each 1000 bp

Table 2-13: Alternative PCR conditions for some reactions

	Temperature	**Time**	**Cycle number**
Initial denaturation	96°C	3 min	1x
Denaturation	95°C	30 sec	
Annealing	primer sequence-dependent	45 sec	30x
Extension	72°C	30 sec	
Final extension	72°C	5 min	1x
	4°C	unlimited	

The primers used for sequencing of *BOD1* are listed in Table S1, Appendix B.

2.3.3.4. Agarose gel electrophoresis:

The specificity and the amount of PCR products were checked by agarose gel electrophoresis before further analysis.

The gel composition was 0.7-1.6% agarose (Invitrogen) in TBE buffer supplemented with 0.5 µg/ml Ethidium-bromide. At least 0.2 volumes of gel loading buffer containing 0.25% Bromophenol blue, 0.25% xylenecyanol FF, and 30% glycerol was added to the nucleic acid solutions before loading into the wells. HyperLadder I, IV, V were used as size markers. Gels were run at 80-120 V for 30-60 min. Nucleic acids were visualized and pictures taken using the E.A.S.Y Win32 gel documentation system.

2.3.3.5. Sequencing

The original PCR products were sequenced in both directions using the ABI 377 DNA sequencer.

The labelling reactions were carried out using the composition and amounts of reagents shown in Table 2-14.

Table 2-14: PCR reaction mix for sequencing reaction	
Name	**Amount**
DNA (PCR Product)	2ng/100bp
BigDye Terminator mix (V3,1)	2µl
5X Buffer	2µl
Primer (10pmol)	1µl
H_2O	Add to 10µl

Subsequently, sequencing reactions were performed based on the program shown in Table 2-15.

Table 2-15: PCR conditions for sequencing reaction			
	Temperature	**Time**	**Cycle number**
Initial denaturation	96°C	1 min	1x
Denaturation	96°C	30 sec	
Annealing	50 °C	15 sec	25x
Extension	60°C	4 min	
	4°C	unlimited	

DNA precipitation and purifications were done based on the following protocol:

1. Add 1µl 2%SDS and incubate in 98°C for 10 seconds
2. Add 25 µl 100% EtOH to each reaction and mix thoroughly by inverting

3. Spin at 4000 rpm in the cool room for 60
4. Carefully discard the supernatant by inverting the tubes on a paper towel
5. Add 150 µl 70% EtOH and invert the tubes without disturbing the pellets
6. Spin at 4000 rpm in the cool room for 30 min
7. Carefully discard the supernatant by inverting the tubes on the paper towel
8. Repeat the washing step
9. Dry the pellet by putting the plate headfirst onto a paper towel and centrifuge just up to 4000 rpm and then stop
10. Put an adhesive film on the plate, enwrap it with Aluminum foil (if its necessary)
11. Base calling after putting samples in the sequencing machine.

Sequence data were assembled and analysed using the CodonCode aligner 3.0.3 beta 5 software.

2.3.4. Methods related to nucleic acids

2.3.4.1. RNA extraction from cell-lines using TRIzol

Total RNA from FB and LCL cells was isolated by using the TRIzol reagent RNA extraction protocol:

1. Suspend cell pellet (5 x 10^7 cells) with 10 ml TRIzol reagent in a 30 ml RNase free tube.
2. Homogenize the suspension by shaking vigorously for several seconds. Incubate the sample 30 min at room temperature (20-30 ºC) so that it can completely dissolve.
3. Add 0.2 ml chloroform for each 1 ml of initial TRIzol (2 ml chloroform for 10 ml Trizol). Shake for 15 seconds and incubate for additional 2-3 min at room temp.
4. Centrifuge the samples for 20 min at 5000 RPM at 4°C.
5. Transfer the aqueous phase to a fresh tube or make aliquots of 550 µl to an eppendorf.
6. Add 0.5 volume of isopropanol per 1 ml of TRIzol reagent used for initial homogenization (5 ml or 550 µl) to the aqueous phase, mix well by vortexing and keep at room temperature for 5-10 min.

7. Centrifuge the samples for 10 min at 8000 RPM at 4ºC (12000 g for microfuge).
8. Remove the supernatant and add 10 ml filter sterilized 70% ethanol (500 µl for microtube) and mix well.
9. Centrifuge the samples for 5 min at 5000 RPM at 4ºC (7500 g for microfuge).
10. Take off the supernatant and dry the pellet at room temp. Avoid completely drying the pellets, as this will decrease the solubility of the RNA.
11. Dissolve the RNA in 500 µl of sterile DEPC water and put it on ice for 10 min following by transferring the sample to 65ºC for 5 min.
12. Measure the RNA concentration by Nanodrop ND-1000 Spectrophotometer and check the quality on Agarosegel.
13. Keep the RNA in the freezer (-20 or -80°C) until further use.

2.3.4.2. RNA extraction from Mouse/Rat tissue

Total RNA from the mouse or rat whole brain and mouse ovaries was extracted by using the following protocol:

1. Homogenize 50-100 mg tissue (10^7) cells in 1ml TRIzol and incubate 5 min at room temperature
2. Add 0.2 ml CHCL3 per ml TRIzol and mix vigorously. Incubate 3 min at room temperature
3. Centrifuge the samples for 50 min at 12000 g
4. Transfer upper aqueous phase into new tube and precipitate RNA by adding 0.5 ml isopropyl alcohol per ml TRIzol. Incubate 10 min at room temperature
5. Carefully remove supernatant and wash pellet once with 1 ml 75% EtOH per ml TRIzol
6. Centrifuge for 10 min at 7500g at 4ºC and remove supernatant
7. Air-dry pellet for 5-10 min at room temperature. Dissolve RNA in 50 µl DEPC water and incubate for 5 min at 65ºC.
8. Proceed in the same way as described for RNA extraction from cell culture (Section 2.3.4.1, steps 12 & 13)

2.3.4.3. RNA extraction from whole blood

The PAXgene blood RNA system was used, following the PAXgene Blood RNA kit handbook.

2.3.4.4. DNase treatment of RNA

Prior to making cDNA, RNA was treated with DNase to remove any DNA contamination based on the protocol in Table 2-16.

Table 2-16: DNase treatment of extracted RNA from cell line using DNase 1 digestion (Promega kit)

RNA	2µl (~4µg)
10x buffer	1µl
Dnase1 (Rnase free Dnase)	4 µl (100/µgRNA)
Water (Nuclease free)	3 µl (to the volume of 10 µl)
30 min at 37° C	
Dnase stop solution	1 µl (contains Mg++ ion chelator)
10 min at 65° C (inactivation in presence of Dnase stop slution)	

2.3.4.5. Two step RT-PCR

At first, cDNA was synthesized with SuperScriptIII® reverse transcriptase kit (Invitrogen) together with random hexamers, based on the listed in Table 2-17 and Table 2-2

Table 2-17: cDNA synthesis from total RNA	
Prepare reaction mix as follows:	
Total RNA	5 µg
Random primers (Promega)	2 µl
DNTPs (10mM, Roche)	1 µl
Water up to 21 µl	12 µl
Heat- shok at 65° C	5 min
Ice	At least 1 min
5x first strand buffer (invitrogen)	6 µl
0.1M DTT (invitrogen)	1 µl
Rnasin (Promega)	1 µl
SS III-RT (invitrogen)	1 µl

After preparing the samples cDNA synthesis was performed in a PCR machine using the following settings (Table 2-18).

Table 2-18: cDNA synthesis from total RNA	
Temperature	Time
25 °C	5 min
50 °C	60 min
75 °C	15 min

The success of cDNA synthesis was checked using primers for HUWE1, a control gene located on chromosome X with exon spanning primers

CAAGTGAGGAAAAGGGCAAA (exon64) and GTTCATGAGCTGCCCCAGT (exon65) which give rise to a 568bp amplicon.

After successful cDNA preparation, a 35 cycle PCR using flanking primers for *BOD1* to amplify all the possible splice variants was performed, using the primers listed in Table 2-19.

Table 2-19: Sequence of primers in human/ mouse / rat

	Forward Sequence	**Reverse Sequence**
Human	CATCGTGGAGCAGCTCAAG	GCACTCTTATGTAACCGAATC
Mouse	AGCTCATCGCTCTCATAGTGG	AGCTCATCGCTCTCATAGTGG
Rat	ATGCAAAGGTCGTTGGTGAC	AAAGGTTCGTTCAGGACAGC

Table 2-20 and Table 2-21 show the PCR reaction conditions and profile, which were used for the amplification of cDNA from human/mouse/rat.

Table 2-20: PCR reaction for amplification of *BOD1* cDNA (Bioline kit)

Sample reaction Mix	**Amount**
DNA	1
Primer Forward (10pico mol)	1
Primer Reverse (10pico mol)	1
BIOXACT Longmix	13
dH_2O	10

Table 2-21: PCR thermal cycle for amplification of *BOD1* cDNA			
Cycle step	**Temp**	**Time**	**Cycle number**
Initial denaturation	96°C	3 min	1x
Denaturation	96°C	30 sec	
Annealing	57 °C	30 sec	34x
Extension	72°C	90 sec	
Final extension	72°C	10 min	1x

2.3.4.6. Isoform Specific RT-PCR

Each of the splice variants was verified by individual exon junction primers shown in Table 2-22.

Table 2-22: Exonjuction primers			
Forward Sequence	**Reverse sequence**	**Exon juction location**	**Specific for isofom**
GGTTCAGTCAGGGATGTTGG	CAAAAGGTGTCTGGCGTATTC	2,3 and 3,4	1+2+3+4
TGGACACCAAGCCAGCTTAC	AAAAGGTGTCTGGCGTATTTG	1,2 and 2,4	1+2+4
AAGGTCAGGGATGTTGGAAG	CAAAAGGTGTCTGGCGTATTC	1,3 and 3,4	1+3+4
CCAAGAATACGCCAGACACC	TCCCCTTTCAATCTGGTCAC	1,4 and 4	1+4

PCR conditions are shown in Table 2-21 (extension period of 30 sec and 25 cycles was used).

RT-PCR products from full length RT-PCR as well as isoform specific RT-PCR were separated and visualized by agarose gel electrophoresis as described in 2.3.3.4. (DNA marker HyperLadder IV was used).

2.3.4.7. Gel extraction

To confirm the splice variants, each isoform was cut out from the gel and eluted by using MiniElute gel extraction kit for 70bp-4kbp segments following the Qiagen protocol.

2.3.4.8. Northern blot analysis

DEPC treated water:

Treatment with DEPC is the most common method to remove RNases from solutions. 1 ml of 0.1 % DEPC was added to 2000 ml double distilled water, mixed thoroughly, and let set at room temperature for 1 hr. Then residual DEPC was destroyed and the water was sterilized by autoclaving and cooled to room temperature prior to use.

Poly-A RNA extraction:

Poly-A+ RNAs were obtained from 100 µg total RNA by using Dynabeads oligo-dT25.

Membrane preparation:

Before loading the samples, the 1% agarose gel was run at 60 V for 10 min at room temprature. The gel was prepared with Northern blot running buffer at a voltage of 60 V for 10 min at room temperature was applied to a 1% agarose gel, which was prepared with Northern blot running buffer (Table 2-3).

The RNA was mixed with northern blot sample buffer (Table 2-3), denatured (65°C, 5 min) and kept on ice before loading onto the gel. Electrophoresis was performed for ~16 hr at 50 V/~30 mA.

The gel was afterwards soaked in DEPC H_2O for 20 min in order to remove formaldehyde before it was photographed using a UV sensitive ruler (0 cm of the ruler placed beside loading wells) in order to permit following band localization.

Then, the gel was soaked in 10x SSC for 20 min.

The blotting setup for transferring RNA onto the Hybond-XL membrane was prepared as shown in figure 2-4:

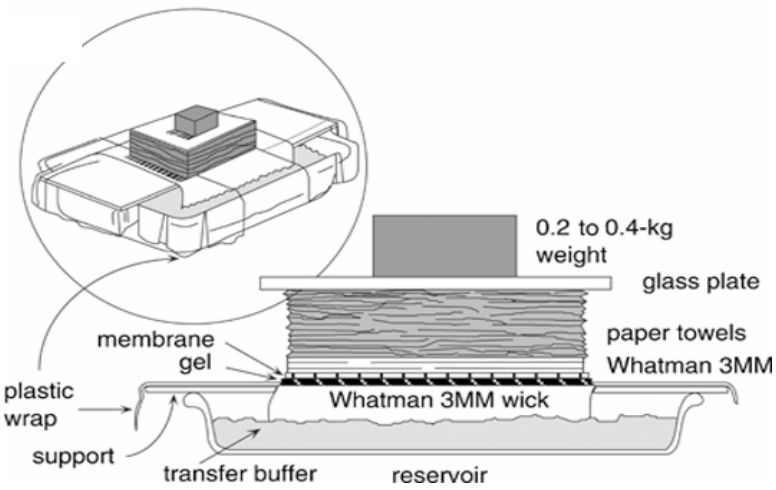

Figure 2-4: Northern blot setup. The whatman paper upon which the gel is placed has to be soaked in and dip into the 10x SSC (Image source: http://www.currentprotocols.com/protocol/et0802).

The transfer was performed overnight at room temperature.

Using a needle, the well positions were marked on the membrane. The membrane was then soaked in 10x SSC (Table 2-3) for 2 min and dried on paper tissue with the RNA side facing away from the tissue. Subsequently, the RNA was cross-linked to the membrane using 2 times auto-crosslink setting (1200 micro-joules in 25 sec) of a UV Strata-linker 1800 machine (Table 2-3).

The blot was then sealed and stored at –20°C for hybridization.

Probe Preparation

A specific probe for 5'UTR region of *BOD1* was designed and alignment for the specificity of the probe was checked by BLAST alignment (Sense: CTCTGCTGTATCAGAGGGGG and Antisense: CCCCCTCTGATACAGCAGAG)

Membrane pre-hybridization

Prior to probe hybridization, the membrane was incubated at 37°C with 50 ml hybridization buffer (Table 2-23) in a falcon tube for 1 hr and the kinase was inactivated at 95 ºC.

Table 2-23: hybridization buffer

Name	Amount
BOD1 antisense oligo	10 µl
32 gamma-ATP	3 µl
T4 kinase	1 µl
10x PNK buffer	2 µl
dH_2O	12 µl

Probe purification:

To remove unincorporated nucleotides, a G250 microspin column was used. First, the tube solution was homogenized by vortexing. Then, after breaking the bottom of the tube it was centrifuged for 1 min with 740g and 70 µl of the flow-through were added to the labeled probe. The rest of the flow-through was discarded and the entire volume of the probe was loaded on the column and centrifuged for 2 min at 740g. The flow-through was used for hybridization.

Hybridization:

Prior to hybridization, the purified probe was denatured at 95°C for 2 min and subsequently added directly to the membrane with hybridization solution (without touching the membrane) and incubated with the membrane overnight at 37°C in a rotating glass tube.

Washing and imaging:

500 ml wash buffer (Table 2-3) was pre-warmed at 42°C. The hybridization solution was discarded and the hybridization tube was filled with 100 ml of wash buffer and rotated at 42°C for 30 min. Subsequently, the washing solution was discarded and the process was repeated three more times each for 20 min. For imaging, the membrane was sealed in plastic foil and exposed to sensitive Biomax X-ray film in a HyperCassette and incubated overnight at -80°C and developed using a Curix 60 X-ray film-developing machine.

2.3.4.9. Whole genome expression profiling:

cRNA amplification:

RNA amplification is one of the standard methods to prepare RNA samples for analysis by expression microarray techniques. The Illumina® TotalPrep RNA Amplification Kit, manufactured by Ambion, Inc. was used for generating biotinylated, amplified RNA for direct hybridization with IlluminaSentrix® arrays.

The procedure consists of reverse transcription with an oligo (dT) primer bearing a T7 promoter using Array-Script™, a reverse transcriptase (RT) engineered to produce higher yields of first-strand cDNA than wild type enzymes. ArrayScript catalyzes the synthesis of virtually full-length cDNA, which is the best way to ensure production of reproducible microarray samples. The cDNA then undergoes second strand synthesis and clean-up to become a template for in vitro transcription with T7 RNA Polymerase. To maximize cRNA yield, Ambion's proprietary MEGAscript® in vitro transcription (IVT) technology along with biotin UTP (provided in the kit) is used to generate hundreds to thousands of biotinylated, antisense RNA copies of each mRNA in a sample. Reverse transcription to synthesize first-strand cDNA is primed with the T7 oligo(dT) primer for synthesis of cDNA containing a T7 promoter sequence. Second-strand cDNA synthesis converts the single-stranded cDNA into a double-stranded DNA (dsDNA) template for transcription. The reaction employs DNA Polymerase and RNase H to simultaneously degrade the RNA and synthesize second strand cDNA. cDNA purification removes RNA, primers,

enzymes, and salts that would inhibit in vitro transcription. In vitro transcription to synthesize cRNA generates multiple copies of biotinylated cRNA from the double-stranded cDNA templates; this is the amplification and labelling step. cRNA purification removes unincorporated NTPs, salts, enzymes, and inorganic phosphate. After purification, the cRNA is ready for use with Illumina's direct hybridization array kits.

While as little as 50 ng total RNA can theoretically be used to produce enough material for further hybridizations, we used 500 ng of total RNA per reaction.

6-Sample BeadChip Hybridisation

Upon the completion of the cRNA amplification, RNA samples were quantified using Nanodrop ND-1000 Spectrophotometer. 1.5 µg of cRNA sample was hybridized to the BeadChip in a multiple step procedure according to the manufacturer's instructions; the chips were dried and scanned on the BeadArray reader.

Expression Data Analysis

For the analysis of expression data the BeadStudio software package included in the Illumina® Gene Expression System (table 2-10) was applied, which is a tool for analyzing gene expression data from scanned microarray images collected from the IlluminaBeadArray Reader.

We did differential analysis by comparing all the patients as a group against all the controls as another group; we also analyzed each patient separately against the group of controls.

Normalization aims to cleanse the data by mathematically factoring out systematic errors among experimental groups so that their values can be compared. In the case of microarray experiments, systematic variation can result from variation in hybridization temperature, sample concentration, formamide concentration, etc. Normalization is a process by which two or more populations of gene expression values from two or more samples are adjusted for easier comparison. BeadStudio provide different methods of

normalization, for our experiments the "Rank- Invariant Method" was used. (BeadStudio User Guide more information about bead studio software). Genes with differentiation scores smaller than -13 in patients as compared to controls were used for further *in silico* analysis.

Functional gene classification

The results from array based gene expression analysis were interpreted using two different web based classification tools: DAVID (http://david.abcc.ncifcrf.gov/home.jsp) and Panther (http://www.pantherdb.org/).

DAVID (Dennis et al. 2003; Huang da et al. 2009)**:** Groups genes based on functional similarity of large lists of genes derived from high throughput studies. The functional classification tool generates a gene-to-gene similarity matrix based shared functional annotation using over 75,000 terms from 14 functional annotation sources. The DAVID clustering algorithm classifies highly related genes into functionally related groups. Tools are provided to further explore each functional gene cluster including listing of the "consensus terms" shared by the genes in the cluster, display of enriched terms, and heat map visualization of gene-to-term relationships. A global view of cluster-to-cluster relationships is provided using fuzzy heat map visualization. Summary information provided by the functional classification tool is linked to DAVID Functional Annotation Tools and to external databases allowing further detailed exploration of gene and term information.

PNATHER (Thomas et al. 2003; Thomas et al. 2006)**:** Multiple gene lists can be mapped to PANTHER molecular function and biological process categories, as well as to biological pathways. Its pathway visualization tool displays experimental results on detailed diagrams of the relationships between genes/proteins in known pathways.

2.3.4.10. Real time PCR

Quantitative Real-time PCR was performed by using the same exon junction primers used in the isoform specific RT-PCR (Table 2-22). SYBR green was

used to monitor DNA synthesis. SYBR green is a dye that binds to double-stranded (ds) DNA but not to single-stranded (ss) DNA and is frequently used in real-time PCR reactions. When it is bound to ds-DNA, it fluoresces very brightly (much more brightly than ethidium bromide). Moreover SYBR green is used because the ratio of fluorescence in the presence of ds-DNA to the fluorescence in the presence of ss-DNA is much higher than the ratio for ethidium bromide. Direct detection of PCR product is monitored by measuring the increase in fluorescence caused by the binding of SYBR Green dye to ds-DNA.

For calculating the results of quantification assays, one can use either absolute or relative quantification. In this study we used absolute quantification to quantify unknown samples by interpolating their quantity from a standard curve. To construct a standard curve four-fold dilutions of a total RNA preparation from control cDNA were used and the units diluted values were 1, 0.5, 0.25, 0.125. Negative controls or NTC (no template control) were used to verify amplification quality and to check if primers and Taq polymerase/SYBR green PCR mixes are not contaminated; the method also allows determining if the primers can form primer-dimer artifacts.

Normalization is necessary to improve the reliability of the experiment by including an invariant endogenous control (e.g. a house keeping gene) in the assay to correct for sample to sample variations and errors in sample quantification (Bustin 2002; Pfaffl 2001), therefore standard curves were generated for both the target and the endogenous reference (in this study GAPDH). For each experimental sample, the amount of target and endogenous reference is determined from the appropriate standard curve. Then, the target amount is divided by the endogenous reference amount to obtain a normalized target value.

As shown in Table 2-24, the reaction was carried out in 30 µl volumes. The SYBR Green PCR Master Mix is supplied in a 2X concentration and contains SYBR Green I Dye, AmpliTaq Gold DNA Polymerase, dNTPs with dUTP, Passive Reference, and optimized buffer components (Applied biosystem guide).

Table 2-24: Reactions protocol			
Reagent	**Volume**	**Water**	**Add to each reaction**
Primer Forward (10pmol)	1 µl	1.5 µl	2.5 µl
Primer Reverse (10pmol)	1 µl	1.5 µl	2.5 µl
SYBR Green master mix	15 µl	-	15 µl
Master Mix			20 µl
cDNA	0.5 µl (20 µg)	9.5 µl	10 µl

ABI PRISM 7900 HT Sequence Detection System using a 96-well format was used.

Cycling parameters are shown in Table 2-25.

Table 2-25: PCR thermal cycle for qRT-PCR			
Cycle step	**Temp**	**Time**	**Cycle number**
Initial denaturation	95°C	1 min	1x
Denaturation	95°C	15 sec	40
Annealing	55 °C	1 min	

Amplification plot and quantity values were obtained with the Sequence Detection Software (SDS 2.1, PE Applied Biosystems). All the reactions for the target genes were performed in triplicate.

The output data were analysed using the SDS 2.1 software, and T-test and standard deviation calculated with GraphPad Prism 4.

2.3.4.11. Nonsense Mediated Decay (NMD) mRNA analysis

To test NMD in the patients, fibroblast cell cultures from two patients and three controls were prepared, each was subdivided into two sister 75 cm^2 flasks with a cell density of 10^6 cells/mm^2. At different time points one flask was treated with cycloheximide (CHX) (a translation elongation inhibitor) at a concentration of 500µg/ml and the other one remained untreated (added 500µg/ml DMSO). After 6.5 hr of incubation, fibroblasts were harvested with trypsin and after RNA isolation qRT-PCR was carried out by using SYBR green and isoform specific primers, GAPDH used for normalization of all the samples. The results were plotted by using GraphPad Prism 4. Standard deviations were calculated and T-test analyses were performed using the same software.

To interpret the results, the CHX treated cells were compared with the untreated cells from the sister flask; In case of NMD, an increase in the level of RNA expression was observed in the cells treated with CHX compared to untreated cells.

2.3.4.12. Cloning of pmCherryC1 constructs and mutagenesis

Restriction enzyme digestion

pmCherry-BOD1 wild type construct was prepared by cut/paste method; BOD1 was cut from pEGFP-N1-BOD1 wild type construct (Porter et al 2007) and ligated into pmCherry-C1 vector .

For restriction digestion, approximately 1000 µg pEGFP-N1-BOD1 was used in 20 µl restriction digestion mixtures. The restriction-digestion mixture contained specific restriction buffer (NEB I) and BSA at a concentration of 1X and autoclaved double distilled H_2O. Restriction enzymes (EcoRI and KpnI) were added at the ratio of 1 U/µg to the DNA. The reaction mixture was incubated at 37°C for 80 min.

Figure 2-5 shows the pmCherry-C1 vector with its detailed multiple cloning site and pEGFP-N1-BOD1.

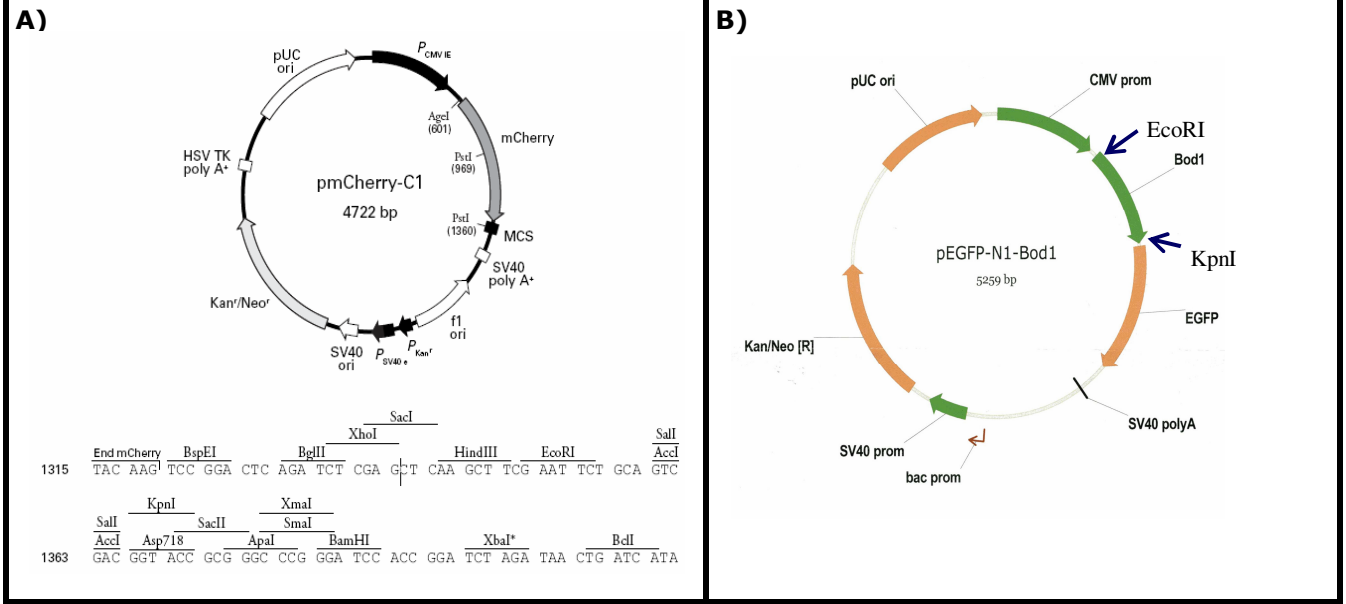

Figure 2-5: Vectors used for cloning *BOD1* cDNA. A)pmCherryC1 vector **B)**PEGFP-N1-BOD1 construct

Ligation of dsDNA

For ligation, restriction enzyme digested insert and vector dsDNA were first checked on an agarose gel. The bands were excised from the gel and dsDNA was purified by using Qiagen kit as described in 2.3.4.7

Ligation was performed by using a quick ligation kit (New England Biolabs) the purified insert and vector dsDNA were mixed with autoclaved double distilled H_2O and ligation buffer so that the concentration of ligation buffer in the final solution was1xSubsequently. T4-DNA ligase was added to the reaction mixture. The mixture was incubated 3 min at room temperature. For a better efficiency of ligation, insert and vector in the ligation mixture were maintained at a higher molar ratio (at least 10:1 for insert to vector). This enhances the probability of ligation reaction.

Competent *E.coli* cell preparation

A single colony of bacterial cells was incubated in 3 ml of Luria-Bertani (LB) broth and grown over night. 1 ml of this culture was added to 10ml of LB liquid medium and incubated at 37°C to make a broth culture. The cells were grown until an OD 0.4-0.5 was reached at 60 nm (measured by Spectrophotometry). The cells were incubated for 1 min on ice and centrifuged at 300 rpm for 5 min at 4°C. The pellet was resuspended in 3 ml of ice-cold $CaCl_2$ (10 mM) solution and incubated for 3 min on ice. The suspension was further centrifuged for 5 min at 4°C. Finally the pellet was resuspended in ice-cold $CaCl_2$ (10 mM) solution supplemented with 10% glycerol, distributed in tubes and stored at -80°C.

LB medium: 10 g BactoTryptone, 5 g Bacto Yeast extract, 10 g NaCl dissolved in 1 liter of double distilled water and autoclaved at 121°C and 15 lbs for 20 min.

Transformation of *E.coli*

200 ng of Plasmid DNA were incubated with 100 µl of chemically competent cells (DH5α,Top10) for 30 min on ice. The mixture was then heat shocked at 42°C for 90 sec and chilled on ice for 2 min. The cells were subsequently incubated for 1 hr in 700 µl LB medium with vigorous shaking at 37°C. Afterwards, cells were plated onto LB Agar plates containing kanamycin (50 µg/ml) and incubated overnight at 37°C.

Plasmid DNA isolation

Single bacterial colonies carrying the plasmid of interest were grown overnight at 37°C with vigorous shaking in 5 ml LB medium containing kanamycin (50 µg/ml). The next day, plasmids were prepared using the Miniprep Kit (Qiagen) according to the manufacturer's instructions.

When larger amounts of DNA were required, 5 ml of LB/kanamycin were inoculated with a single colony, and incubated for 8 hr. Of this culture 0.5 ml

were used to inoculate 100 ml of LB with specific antibiotic, which was incubated overnight at 37°C with vigorous shaking. The Next day, plasmid DNA was prepared using Maxiprep Kit (Qiagene) or if highly purified plasmid was needed, CsCl purification was performed.

To verify whether the obtained plasmids contained the expected fragments, the constructs were digested with corresponding restriction enzymes and checked on agarose gels. Additionally clones carrying inserts of the right size were sequenced using vector primers (Forward: ATGGACGAGCTGTACAAGTCCGGAC and Reverse: TAAAGCAAGTAAAACCTCTACAAATG).

2.3.4.12.1. Mutagenesis

Stop mutations were generated in the pmCherry-BOD1 construct using the QuikChange Site-Directed Mutagenesis Kit (Stratagene) based on the manufacturers instructions using the following forward and reverse primers: CGATGAACAAAAACCAGTTGtGAAATGGTCTGAGGCAGAG and CTCTGCCTCAGACCATTTCAcAACTGGTTTTTGTTCATCG respectively. The change was confirmed by Sanger sequencing.

2.3.4.12.2. Deletion constructs

For cloning BOD1-deletion constructs in cherry vector (Figure 2-6), pmCherry-BOD1-wt was used as a template.

In the case of C-terminal deletions, the site directed mutagenesis kit and the oligos which are listed in Table 2-26, were used to generate a stop codon at an appropriate site and subsequently it was proceeded as explained in section 2.3.4.12.1.

In the case of N-terminal deletions, the following primers as shown in table 2-26 were used. The forward primers contain a TCAAGCTTCGAATTC sequence and the reverse primer contains a CGACCGTGC GGTACC sequence at the 5'-end in which the first nine base pairs are responsible for facilitation of the directional cloning and the last six base pairs are recognition site for EcoRI and

KpnI, respectively. After amplification, the sequences were digested, ligated and verified as explained in section 2-3-4-12.

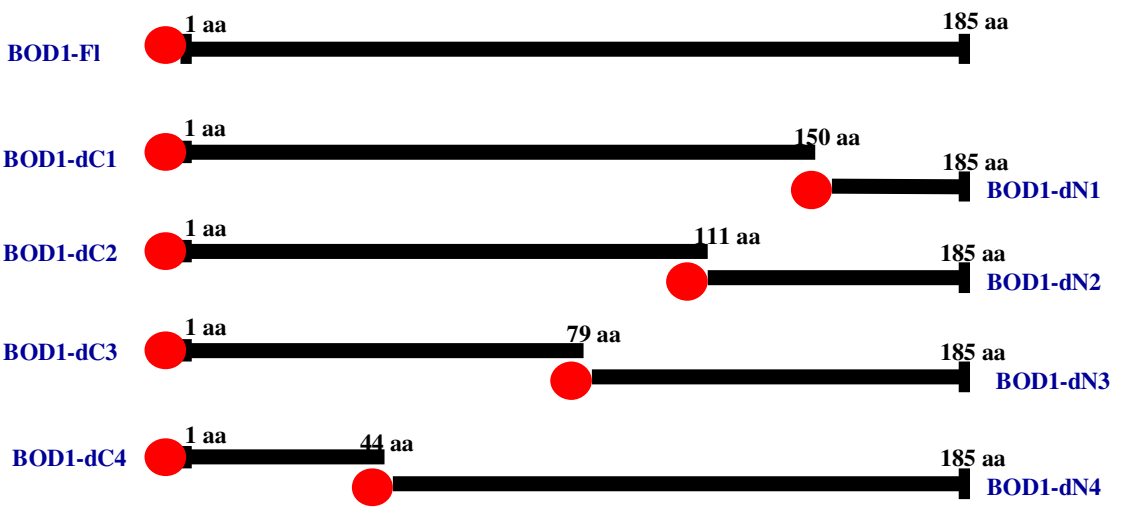

Figure 2-6: BOD1 deletion constructs length. Position of cherry tag indicated with red circle.

Table 2-26: Primers used for constructing deletion constructs

Name	Sequences
AK_SE_pmcherryBOD1_C1F	CCACATCTTCAGGCCACAAATAtAACGAGCAATTCATGAGTTCCTGG
AK_SE_pmcherryBOD1_C1R	CCAGGAACTCATGAATTGCTCGTTaTATTTGTGGCCTGAAGATGTGG
AK_SE_pmcherryBOD1_C3F	CTGCCTGGCCGACGTGGACACCtAGCCAGCTTACCAAAACCTGAGG
AK_SE_pmcherryBOD1_C3R	CCTCAGGTTTTGGTAAGCTGGCTaGGTGTCCACGTCGGCCAGGCAG
AK_SE_pmcherryBOD1_C4F	CCCATCAACCCGGCCTCGtaGCCTCCCGGCGACCCGCAGCTCATCG
AK_SE_pmcherryBOD1_C4R	CGATGAGCTGCGGGTCGCCGGGAGGCtaCGAGGCCGGGTTGATGGG
AK_SE_cheryBOD1_EcorI_N1F	TCAAGCTTC GAATTC CGAGCAATTCATGAGTTCCTGGC
AK_SE_cheryBOD1_KpnI_N1R	CGACCGTGC GGTACC TTAGGAAGTGTCCTGAGATGGAGCTG

AK_SE_cheryBOD1_EcorI_N2F	TCAAGCTTC GAATTC CGAAATGGTCTGAGGCAGAGTGTG
AK_SE_cheryBOD1_EcorI_N3F	TCAAGCTTC GAATTC CCAGCTTACCAAAACCTGAGGCAG
AK_SE_cheryBOD1_EcorI_N4F	TCAAGCTTC GAATTC CCTCCCGGCGACCCGCAGCTCATC

2.3.5. Biochemical methods

2.3.5.1. Western blotting

Cell lysate prepration

- Prepare cell lysation buffer (Table 2-27)

Table 2-27: Cell lysation buffer

Component	Amount for 150 ml
0,1M DTT	1,5 ml
0,01% bromophenol blue	1,5 ml
10% Glycerol	17,25 ml
60mM Tris, pH6,8	9 ml
2% SDS	30 ml
Water	90,75 ml

- Apply 3µl lysate buffer per 20.000 cells (Total volume should be at least 100 µl to enable sonicating).
- Sonicate: 10-15 bursts with the sonicator (Bandelin sanopuls, Pro.No: 519.00002687.033) (20-30 Amplitude)
- Denature at 95°C for 2 min, afterwards vortex and spin down.

Separation of denatured proteins by SDS-PAGE

SDS poly-acrylamide gel electrophoresis (SDS-PAGE) was carried out with 10% acrylamide gels on a Bio-Rad mini-apparatus (Table 2-4). The method is called SDS-PAGE because sodium dodecyl sulfate (SDS), a strong anionic detergent, is used to denature the proteins. To separate the denatured proteins according to their molecular weight, a discontinuous poly-acrylamide gel consisting of a stacking gel on top of a separating gel was used (see Table 2-28 for gel composition). The method applied here followed the most commonly used system, the so called Laemmli method (Laemmli 1970).

Table 2-28: SDS gel composition

Component	**10 ml of 10% separating gel**	**5 ml stacking gel**
H_2O	4.1	3.075
1.5 M Tris-HCl, pH 8.8	2.5	---
0.5 M Tris-HCl, pH 6.8	---	1.25
20% (w/v) SDS	0.05	0.025
Acrylamide/Bis-acrylamide (30%/0.8% w/v)	3.3	0.67
10% (w/v) APS*	0.05	0.025
TEMED*	0.005	0.005

* APS and TEMED were added just prior to pouring the gels.

Protocol:

- Denature protein samples fully by first adding Laemmli protein loading buffer in 1:4 v/v (from a 5x stock of Laemmli protein loading buffer) and subsequently heating the mixture at 95°C for 5 min.

- Prepare SDS-PAGE cassettes by using a pair of clean glass plate (10 cm wide and 7 cm high) separated by a pair of spacer (0.75 mm thickness for thin gel or 1.5 mm thickness for thick gel).
- Fill up approximately 5 cm of the cassettes with liquid separating gel mixture and allow polymerizing within the cassettes.
- Add a thin layer of water slowly to the top of separating gel layer to make the top layer of separating gel smooth.
- Pour stacking gel mixture on the top of the separating gel and insert a 15-well comb within.
- After polymerization of the stacking gel, remove combs slowly without disturbing the wells.
- Insert cassettes into the electrophoresis chamber vertically, and fill with electrophoresis running buffer.
- Load 50-75 µg denatured protein samples into the wells
- Connect the apparatus to a constant current source (150 V) for electrophoresis (migration of the proteins in the gel can be judged by visually monitoring the migration of the tracking dyes, e.g. Bromophenol blue, added to the protein-loading buffer).
- When the dye front comes close to the end of the gel, stop the electrophoresis.

Membrane preparation

Membrane preparation was performed according to the following protocol:

- Incubate unfixed gels shortly in a transfer buffer.
- Soak Whatman filter paper and nitrocellulose membranes in the same transfer buffer.
- Place the gel on the membrane.
- Place two layers (3 sheets each) of Whatman filter papers (8.5 x 5.6 cm) on both sides of the gel-membrane combination to make the transfer set.
- Remove air bubbles from the whole transfer-set by rolling a glass rod over it.

- Place this combination on a transfer unit in such a way that the gel is connected to the cathode while the membrane is connected to the anode.
- Connect the apparatus to a power supply and perform the electro-transfer at a constant current of 50 mAmp (for a single gel) for 2 hr.
- Confirm transfer of proteins from the gel onto membrane by staining the membranes with Ponceau Red dye solution.
- Block the membrane with 5% non-fat milk dissolved in TBST (Tween 0.1%) buffer.
- Incubate with primary antibody in TBST buffer for 1 hr.
- 3X wash with TBST buffer for 5 min / shaking.
- Incubate with secondary antibody in TBST buffer for 1 hr.
- 3X wash with TBST buffer for 5 min / shaking.
- Develop signals, according to the procedures by using PerkinElmer kit (western Lightning Chemiluminescence Reagent, NL100)
- Expose the film and develop it.

Re-using membranes

In order to probe different proteins, previously probed membranes were stripped by incubating the membrane in the stripping buffer (Table 2-3) for 30 min at 50°C. They were then washed with PBST, 3 times (10 min each time) at room temperature before blocking with 5% non-fat milk powder dissolved in TBST buffer for 30 min at room temperature and reprobing with a different primary antibody.

2.3.6. Methods related to Cell biology:

2.3.6.1. Cell preparation

2.3.6.1.1. HaCaT cells

HaCaT cells (nontumorigenic human keratinocytes) were cultured in DMEM medium with 10% FCS, glutamine, antibiotic and maintained in a humidified atmosphere that contained 5% CO2 at 37°C.

2.3.6.1.2. Fibroblast cells

Cells obtained from anterior part of the patients' thigh using appropriate biopsy punchers (www.biopypunch.com). Then the cells were cultured in Quantum333 with 15% FCS, 100 U/ml Penicillin + 100 µg/ml Streptomycin, 20% conditioned medium with 1ng/ml bFGF.

2.3.6.1.3. Mouse Primary corticoneuronal cells preparation and transfection

The cortex was extracted from mouse embryonic brain at an age of E14.5 (it is expected to obtain 2-3 million cells per mouse brain).

The following procedure was applied:

Preparation of plates:

One day before killing the mother, it is needed to prepare plates according to the following procedures:

- Sterilize cover slips with ethanol and bunsen burner and place them in the tissue culture wells
- Coat plates with poly-D-Lysine/Laminin (Poly-D-Lysine Promotes adhesion and prevents the aggregation of cells. Laminin as extra cellular matrix protein helps in elongation of Neurites). Dilute poly-D-lysine 1:500 and laminin 1:50 in PBS then add 1 ml to each well in multi-well plates (12-well). Incubate for 30 min at room temperature or over night at 4°C
- Wash 2X with PBS, 1 ml per well
- Add 2 ml neurobasal medium to each well and incubate it at 37°C, 8% CO2

Killing donor female:

The pregnant mother was killed by neck fracture. The abdominal skin was then sterilized with 70% EtOH and lifted with surgical tweezers. Then a V-shaped gash was created with curved scissors. The abdominal membrane was then opened carefully with a sharp scissor and the embryos carefully removed from the womb and placed in a sterile Petri dish containing PBS for transportation.

Preparation of embryos and isolation of neuronal cells:

The preparation was carried out on a sterile flow bench according to the following procedure:

- Sterilize all instruments through successive bathing in EtOH, PBS-1, PBS-2 and DMEM (sterilization and equilibration)
- Wash the embryos briefly with PBS and transfer in a dry fresh Petri dish
- Separate the head with scissors and put it into a sterile culture dish
- Open skull with two curved forceps and take out the brain
- Add approximately 1-2 ml DMEM to brain with disposable pipette so that brain floats in the medium
- Separate brain stem from brain lobes under a stereoscope, then with fine tweezers, bend the cerebral membrane and remove cortex
- Precisely separate the cortex from the hippocampus (the cortex located above hippocampus like a hat)
- Transfer the cortex halves in a chilled DMEM-Tube on ice
- Do the same for all the embryos

Preparation of single cells from isolated embryonic cortex:

The following protocol was applied:

- Remove the EDTA then add 5 ml trypsin to the cells and incubate for 7 min in 37°C / 5%CO2 incubator and swirl once in between (keep the time exactly)
- Stop trypsin activity by adding stop medium (DMEM+10%FCS) and centrifuge at 200 g (Multifuge 3SR, Rotor 6645=1000 rpm) for 3 min
- Wash off the FCS two times, and centrifuge after each time at 200 g for 3 min
- Suck off DMEM gently and add 2 ml neurobasal media and smash the cells into small pieces by three steps of absorption and discharging through a narrowed pasteur pipette to achieve a suspension of individual cells:

  1- Six times with 1000 µl pipette

2 & 3- Subsequent a bit finer and finest pipette, each three times (prior to start one should narrow the lumen of the glass pipette with a bunsen burner into two different degrees of finer and finest)

Warning: This step requires experience. It is the critical moment that determines the vitality of the cells.

- Dilute the Cells by adding 28 ml neurobasal medium (in total 30ml)
- Count the cells with cell counter
- Remove 1 ml out of 2 ml old medium in each well, then seed the cells in 12-well plates with the density of $1.5x10^5$ cells per cm^2
- Incubate the cells in the incubator at 37°C / 8 % CO2
- After approximately 1 hr, exchange the first medium in order to remove unwanted foreign cells and slow growing cells.

Use the cells at the earliest from the 4^{th} (better is the 7^{th}) day after seeding. Overall, the crops are viable over several weeks. The First change of medium is after day 3-4 and the following media changes will be every 7^{th} day.

Note: It is important that the preparation of neurons is carried out at the earliest possible stage of embryonic brain development, namely before the start of proliferation and differentiation of glial cells. This date in the mouse embryo is the day 14.5^{th}. An earlier date would be problematic because removal of the cerebral membrane almost is impossible and cell yield drops dramatically. A very clean preparation of neurons is important to get a higher number of pure neurons at the end.

2.3.6.2. Transfection

Transient transfection of HaCat cells:

Cells were cultured at a cell density of 1.5 x $10^5/mm^2$ in 12-well plates, one day before transfection. Cells were then transfeced by pEGFP-BOD1 (wt) or pEGFP-N1 vector (Control) or different deletion-cherry constructs. A solution-A (containing 0.125 µg of plasmid DNA and 100 µl OptiMEM), and a solution-B (with 2 µl lipofectamine and 100 µl OptiMEM) were prepared and kept for 5 min

at room temperature. Subsequently, solutions were mixed and incubated at room temperature for 20 min. Meanwhile, cell culture medium was replaced by transfection medium (antibiotic free culture medium). Afterwards the transfection mixture was slowly added to the cells which then were incubated at 37°C in a humidified incubator with 5% CO2 for 2 hr. Then the medium was refreshed (by the normal medium as explained in section 2.3.6.1.1 for HaCat cells) and cells were incubated for another 14 hrs. Afterwards, cells were fixed with PFA 4%.

Transfecection of primary fibroblast cells

Cells were transfeceted using Polyfect. Cells were plated at a density of 5 x $10^4/cm^2$ in 12-well plates. Tranfection mixture was prepared (0.3 µg BOD1-cherry-del constructs, 10 µl polyfect, 100 µl OptiMEM) and incubated at room temperature for 10 min. At about 75-80% of confluency of the cells were transfected. After 24 hr, the cells were fixed with PFA 4%.

Transient transfection of murine primray cortical neurons

1 ml of medium was removed and transfection mixture (the same as HaCaT cells but 0.1 µg DNA) added to the cells at days 7 and 8 (after preparation). On both days cells were fixed with PFA 4% at two time points (6 and 8 hr). Thus BOD1-GFP was not overexpressed all over the cell and at the same time it was not expressed at a level too low to distinguish between specific and non-specific expression.

2.3.6.3. Fixation of LCL cells

LCL cells are cultured in suspension and they don't have the ability to attach to a surface, therefore a cytospin centrifuge (Shandon) was used to deposit the cells onto a slide for further analysis by microscope.

The following protocol was used:

Prepare a flask of 10^5 cells/ml in the appropriate medium.

- Prepare slides mounted with paper pad and cuvette in the metal holder (Shandon cytospin hand book)
- Load 250 µl of the suspension in each cuvette
- Spin at 300 rpm for 5 min
- Extract the slide, paper and cuvette without disarranging
- Carefully detach the cuvette and the paper without damaging the fresh cytospin

  Warning: it is important to hold the glass slide and the cuvette firmly together when extracting from metal holder

- Mark the area around the cytocentrifuged cells with dry point or permanent marker
- Proceed with fixation and staining of the cells (see below).

2.3.6.4. Immunocytochemistry

To visualize a specific antigen or protein in cells (HaCat, Fibroblats or primary neuron) by binding a specific antibody, immunoflorescence staining was carried out:

- Fix the Cells (different time point, depending on the type of the cells or purpose of experiment, each mentioned above) with 4% PFA for 10 min
- Wash 3 times with PBST 0.2% (tween in PBS) each for 10 min
- Permeabilize the cells with 0.2% Triton X-100 (in PBS) for 5 min
- Wash 3 times with PBST 0.2% (tween in PBS) each for 10 min
- Block with 4% BSA (in PBST) for 1 hr at room temperature
- Incubate overnight with different antibodies, (Table 2-8 shows primary antibodies, providers and concentrations used for immunoflorescence staining)
- Incubate the cells with the related secondary antibody (1:1000 dilution) for 1 hour and add DAPI for the last 10 min
- Take images by confocal laser-scanning microscope (LSM510) with a 40x or 63x objective and analyse with the Zeiss LSM image examiner software.

3. Results

3.1. Linkage analysis results

To perform linkage analysis and autozygosity mapping the Human SNPs 10K Array Version 2 (Affymetrix) was used for genotyping all patients from family M-193 as well as their parents and healthy siblings. For data analysis we employed the Alohomora software package (v.30) and performed multipoint linkage analysis using the Allegro software (Gudbjartsson et al. 2005) based on the assumption of autosomal recessive pattern of inheritance and disease allele frequency of 0.001. This analysis yielded a single significant peak (LOD score of 4.4) between SNP markers rs50364 and rs2036563 on chromosome 5q (5q35.1-35.2) (figures 3-1 and 3-2).

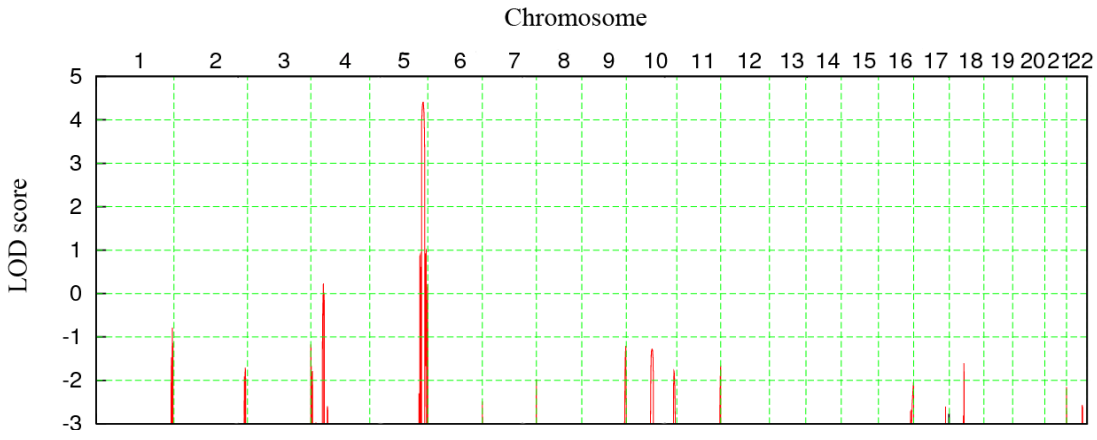

Table 3-1: linkage analysis for family M-193. Whole genome parametric (Allegro Software) multipoint linkage analysis revealed a single interval with a LOD score of 4.4 on chromosome 5q35.

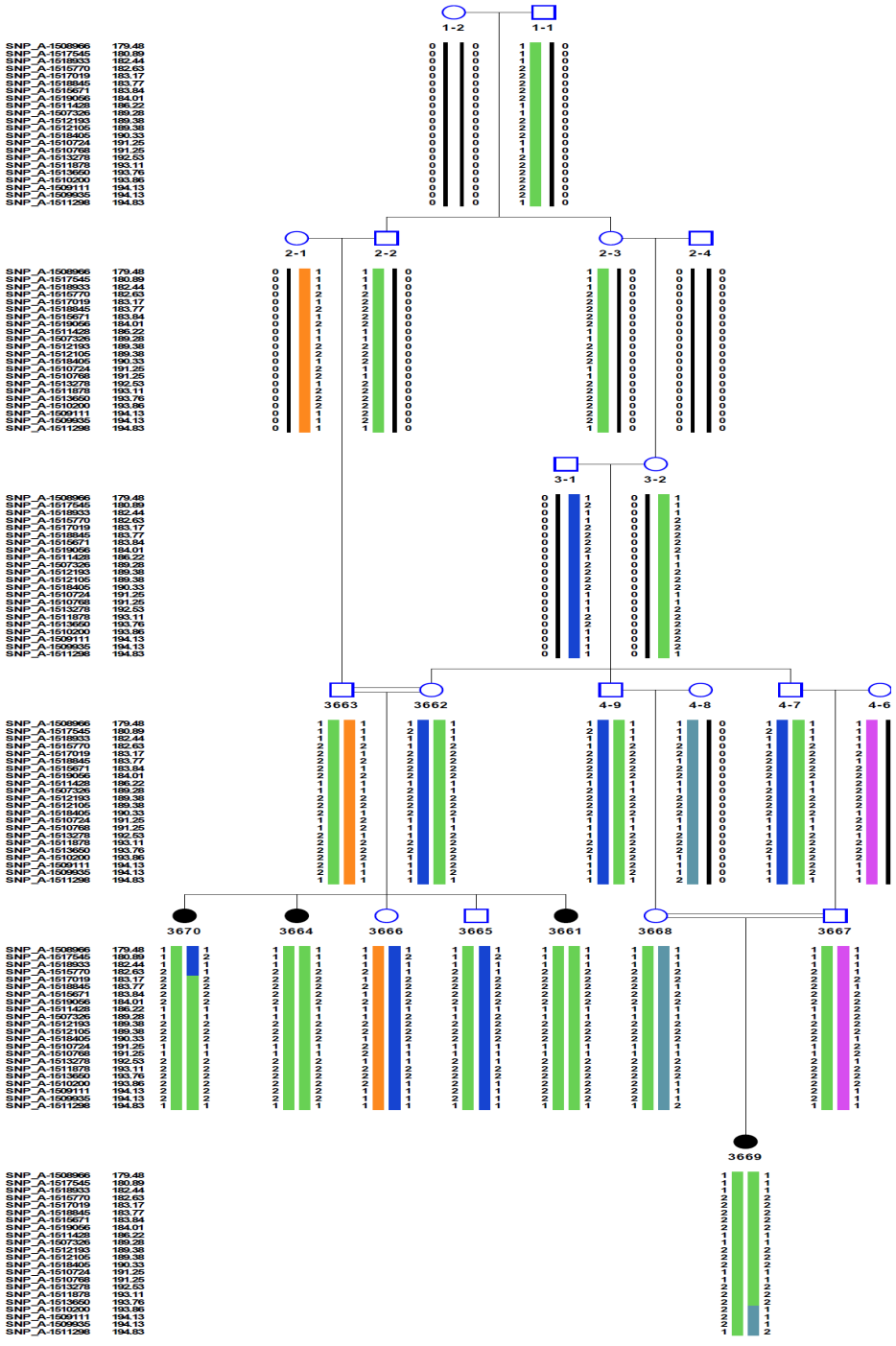

Figure 3-2: Haplotyping results for families M-193. Haplotype between SNP markers rs50364 and rs2036563 on chromosome 5q.

3.2. Nonsense mutation in *BOD1*

The linkage interval encompasses 4.33 MB and includes 28 reference sequence genes (figure 3-3)

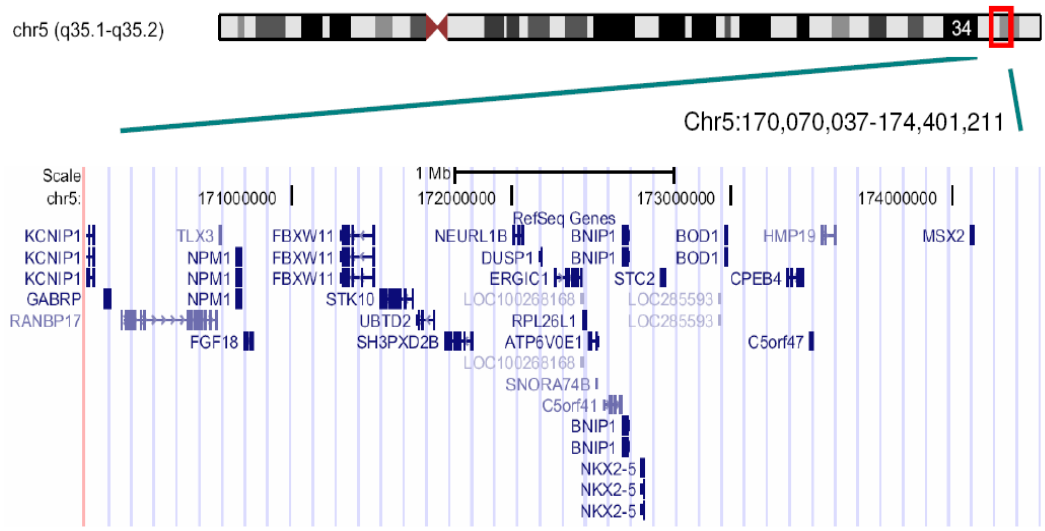

Figure 3-3: The genes contained in the identified linkage interval in family M-193.

For mutation screening the coding regions of all the genes within the interval were sequenced. The results revealed a point mutation (*c. 334 C>T*) in exon 2 of a gene called *BOD1* (Biorientation Defective 1). In addition to this mutation I could find some other polymorphic changes in the interval, which are shown in Table 3-2. Also I found a heterozygote insertion in the second exon of the *MSX2* gene, which narrows down the interval about 300 Kbp.

Table 3-2: detected changes within the interval	
Gene	**Results**
MSX2	dbSNP rs4242182 dbSNP rs2381939 dbSNP rs14459 dbSNP rs2890848 dbSNP 126 rs2890849 exon2d insA
DUSP1	dbSNP rs2431663
	dbSNP rs11363866
STK10	dbSNP 126 rs2306961
BOD1	c.334 C>T
RNBP17	dbSNP rs6555936

BOD1 contains 4 exons and the identified mutation (*c.334 C>T*) is located in exon 2, leading to a premature stop codon in the messenger RNA (R112X). This change co-segregated with the disease (figure 3-4, A and B) and was not found in 380 Iranian and 340 German control chromosomes. BOD1 is conserved throughout metazoans (Figure 3-5), which indicates the importance of this gene and its product.

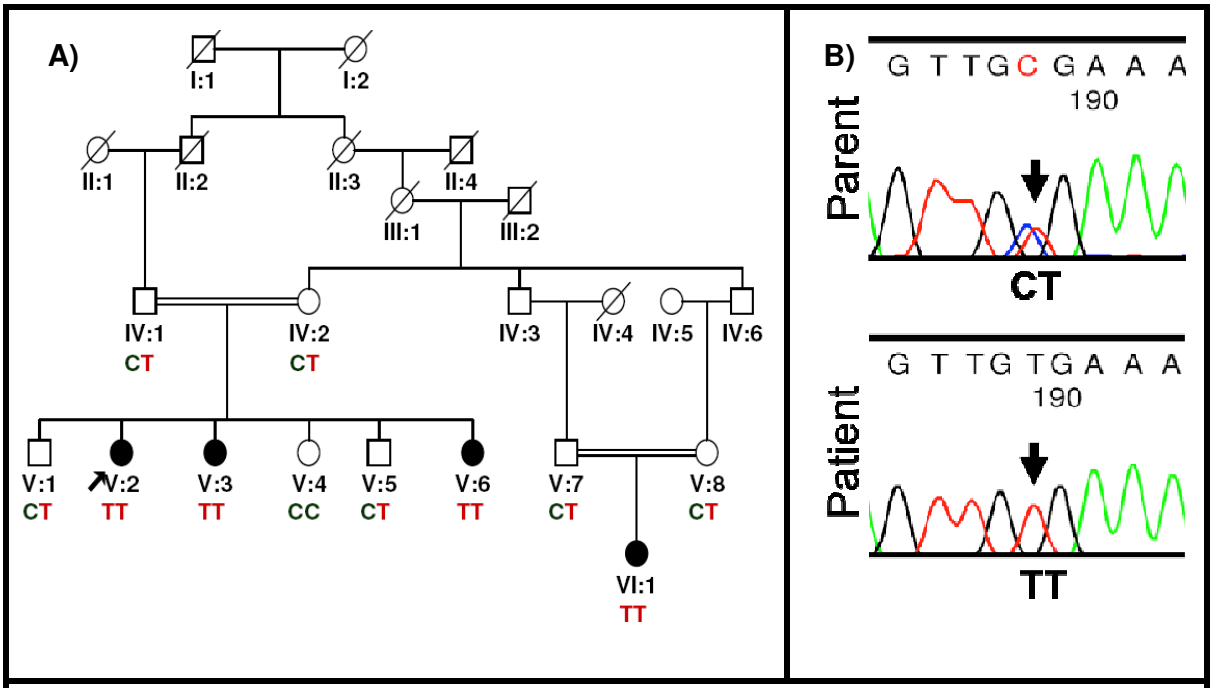

Figure 3-4 A) Family pedigree and segregation of the mutation within the family. Filled symbols represent affected individuals. **B)** Sequence chromatograms from one patient (V:2) and one parent (IV:1) are shown.

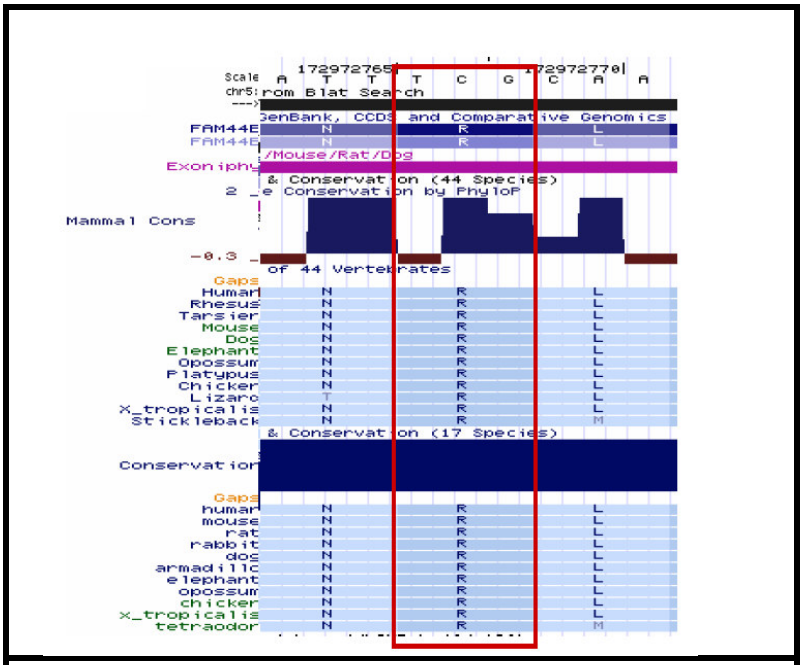

Figure 3-5: p. R112X changes a conserved arginine codon into a stop codon.

3.3. Effect of BOD1 Mutation in patient cells

3.3.1. Transcript study

3.3.1.1. Loss of *BOD1* expression in patient cells

To investigate the effect of the *c.334 C>T* mutation in patient cells by RT-PCR experiments, I designed flanking primers specific for the 3' and 5' UTR of *BOD1* (position of the primers are shown in figure 3-6).

Total RNA was isolated from lymphoblastoid cell lines (LCL) of patients V:2, V:3 and V:6; and fibroblast (FB) cultures of patients V:2 and V:3 as well as LCL cells and FB cells from five and three controls respectively. The RNA was treated with DNase (because the use of flanking primers can otherwise lead to amplification of *BOD1P* a pseudogene of *BOD1*).

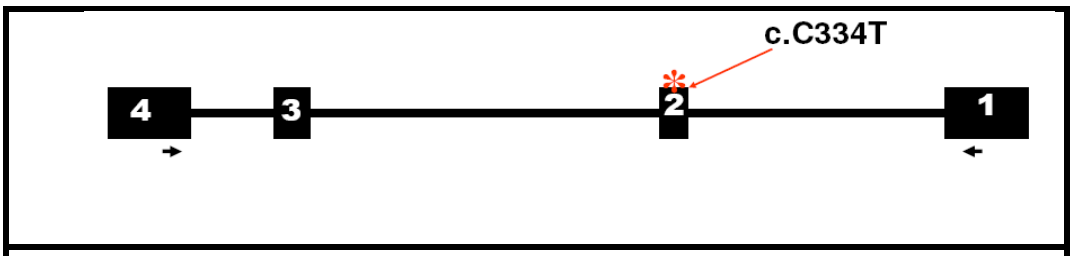

Figure 3-6: Schematic representation of *BOD1*. Exons are represented by numbered boxes. The position of c.C334T is marked by an asterisk and flanking primers are indicated as arrows.

Database investigations showed two splice variants of *BOD1*, both containing the second exon. Thus by using flanking primers, I expected to observe reduction in expression level of both isoforms, the results of RT-PCR as shown in figure 3-7, however led to the amplification of four transcripts represented by four bands on the agarose gel. This finding was confirmed in experiments with several other cell lines (HeLa, HEK 293T, HaCaT, LNCaP, NR2A, SHSY). Sequencing each band revealed two unreported isoforms in addition to the two reported ones. Both new splice variants are not containing the second exon. The results were confirmed by isoform specific RT-PCR and Northern blotting

using a specific probe for *BOD1*. As shown in figure 3-8, a different pattern of RNA expression between patients and controls in both FB and LCL cells was observed; the expression of splice variants containing exons: 1+2+3+4 and 1+2+4 are reduced in patients while the expression levels of the splice variants containing exons 1+3+4 and 1+4 seem slightly increased.

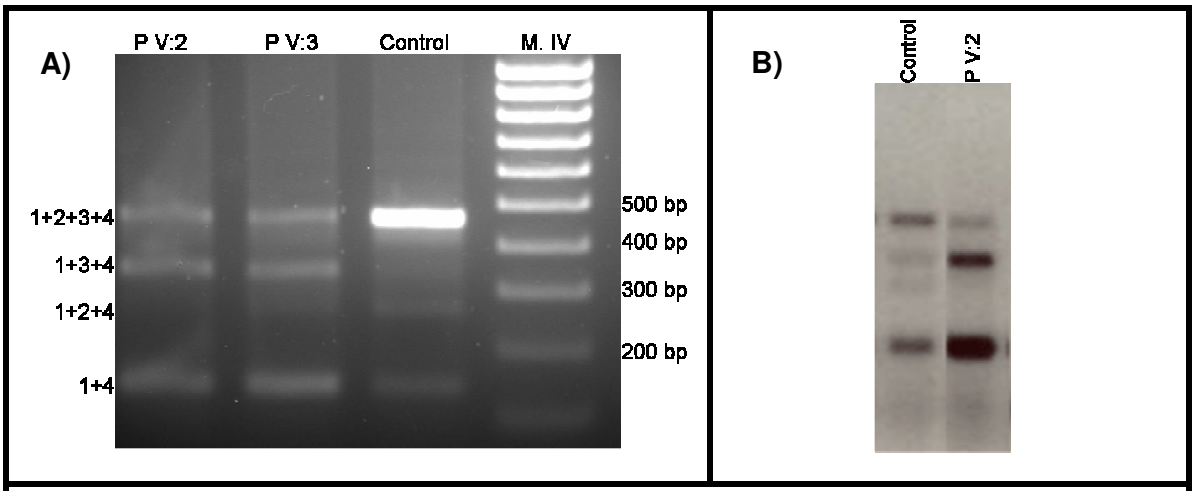

Figure 3-7: Reduction in expression of the main transcript of *BOD1* in patients. Shown are the results from semi-quantitative RT-PCR on FB cells using flanking primers in patients and controls. In addition to two reported *BOD1* isoforms (1+2+3+4 and 1+2+4) two new splice variants including exons:1+3+4 & exons:1+4 were observed. M. IV: DNA hyper ladder IV (Bioline). **A)** RT-PCR in FB cells. **B)** RT-PCR in LCL cells.

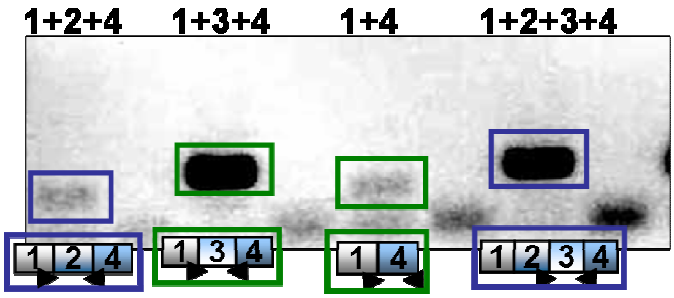

Figure 3-8: Confirmation of splice variants by isoform specific RT-PCR. Numbers indicate different exon combinations in splice variants. The splice variants which were previously reported are shown in the blue boxes. The two so far unreported isoforms are shown in green boxes. The positions of the used exon junction primers are indicatedby arrow heads.

3.3.1.2. Expression of *BOD1* splice variants in the Brain

With regard to the ID phenotype of the patients, it is important to know if and how the *BOD1* splice variants are expressed in the brain. I therefore made cDNA from commercially available RNA of different brain regions from both adult and fetal stages and performed qRT-PCRs, using isoform specific primers. As shown in figure 3-9, all the splice variants are present throughout the brain at both investigated developmental stages. This indicates that all *BOD1* isoforms might play a role in brain function and/or development.

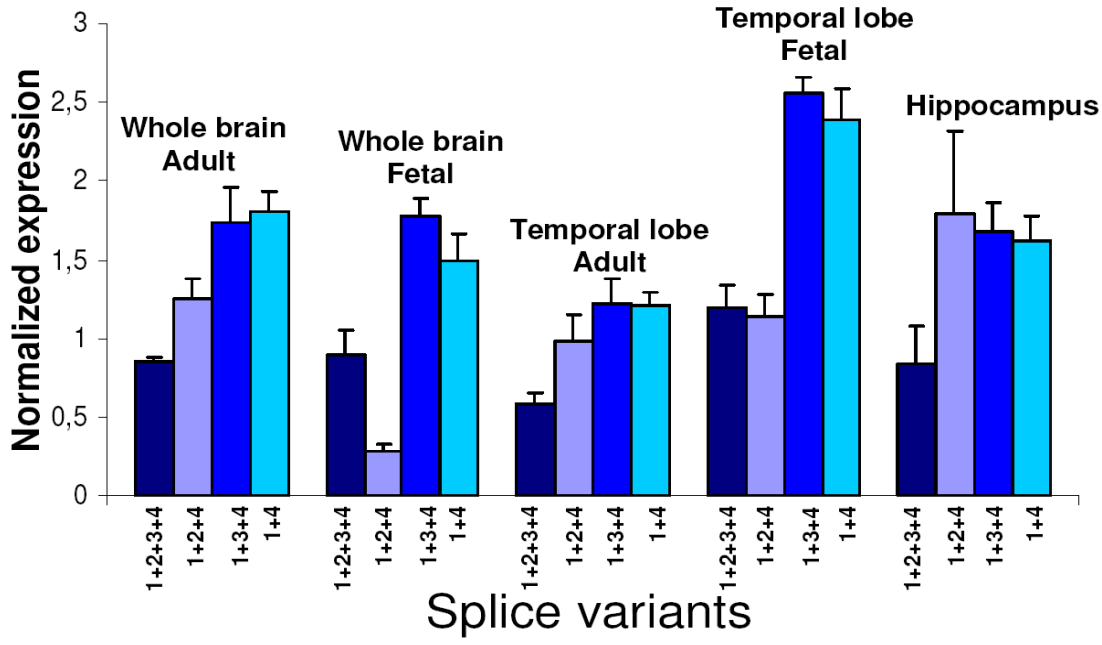

Figure 3-9: All *BOD1* splice variants are expressed in different brain regions at adult and fetal stages. qRT-PCR was twice performed in triplicates, using isoform specific primers. Columns represent *BOD1* expression relative to *GAPDH* expression. Error bars represent the standard deviation (SD).

3.3.1.3. Quantification of residual *BOD1* expression in patient cells

To exactly quantify the different expression patterns of *BOD1* isoforms between patients and controls, I first investigated the expression levels of the full

transcript of *BOD1* in FB and LCL cells from healthy individuals and the results showed a high discrepancy in expression pattern of *BOD1* in LCL cells but a more stable and therefore more reliable pattern was observed in FB cells (see figure S1 in appendix C). Therefore, to study the expression levels of *BOD1* splice variants in the patients, I chose FB cells to perform qRT-PCRs for all four splice variants, using isoform specific primers. As shown in figure 3-10, this revealed the loss of all *BOD1* isoforms, even the two that do not contain the mutated exon2.

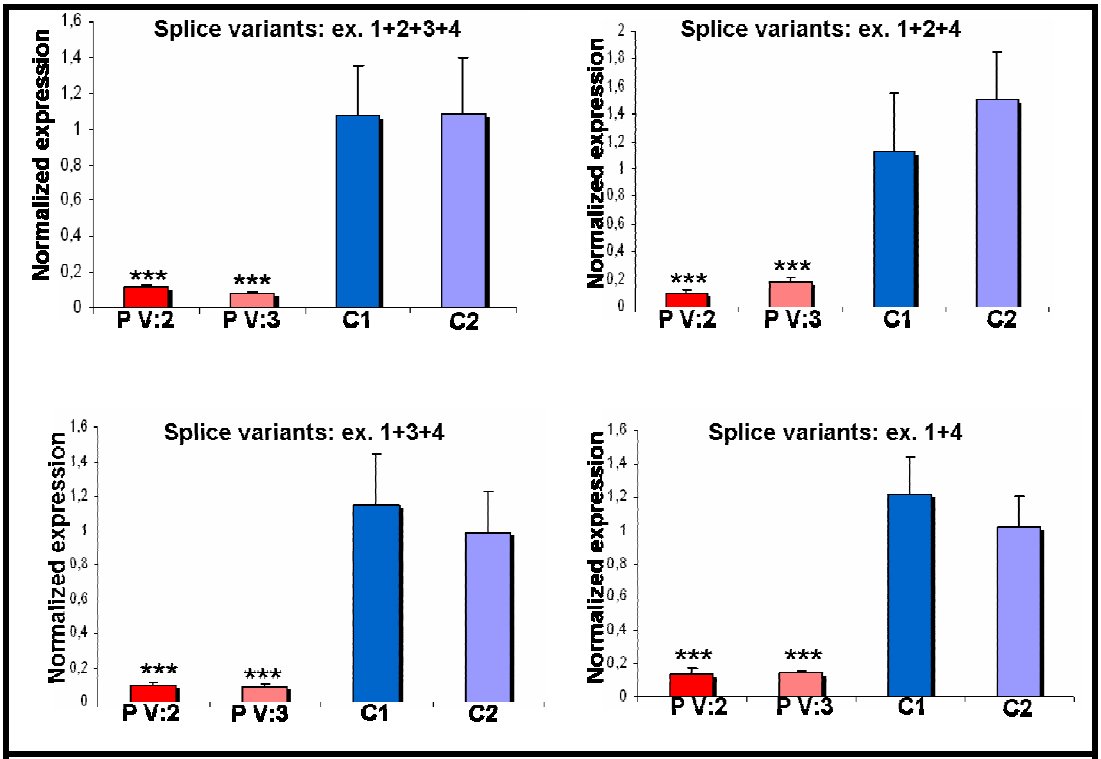

Figure 3-10: Expression of all four splice variants in patients is strongly reduced as compared to controls. qRT-PCR was performed on patient and control FB cells. The experiments were performed twice with independent cells and each time in triplicate. Expression of all the splice variants is reduced in patients compared with controls. One representative result is shown. ***: p< 0.001 (student's t-test). Error bars represent the SD.

3.3.2. Loss of expression of *BOD1* splice variants in patients is only partly due to Nonsense Mediated mRNA Decay (NMD)

mRNA isoforms that harbor a premature termination codon (PTC) are predicted to be degraded through the nonsense-mediated mRNA decay (NMD) pathway. I therefore expected to see a reduction in the expression levels of splice variants containing the nonsense mutation, as each transcript is scanned for PTCs independently (Maquat and Gong 2009). Interestingly I observed reduced levels of RNA expression not only in the splice variants containing mutated exon2, but also in the splice variants without the stop mutation. To determine whether the observed reduction in expression of the transcripts was due to NMD, I treated patient and control FB cells with cycloheximide (CHX) prior to RNA preparation and performed isoform specific RT-PCR. NMD is a translation dependent mechanism and CHX is an inhibitor of protein biosynthesis in eukaryotic organisms, therefore CHX allows to investigate NMD (Dang et al. 2009) (see section 4.2). As shown in figure 3-11, the mRNA levels of all the isoforms except one were restored by CHX treatment, which suggests that in these cases the mutation could indeed lead to NMD. However, as in our patient cell lines even isoforms without the mutation-containing exon 2 is absent, one could speculate that there might also be an alternative mechanism of mRNA degradation, which is triggered by the presence of the mutation in the pre-mRNA prior to splicing. In this context it is even more intriguing that CHX treatment did not restore mRNA levels for Isoform containing exons 1+2+4 even though it contains the mutated exon.

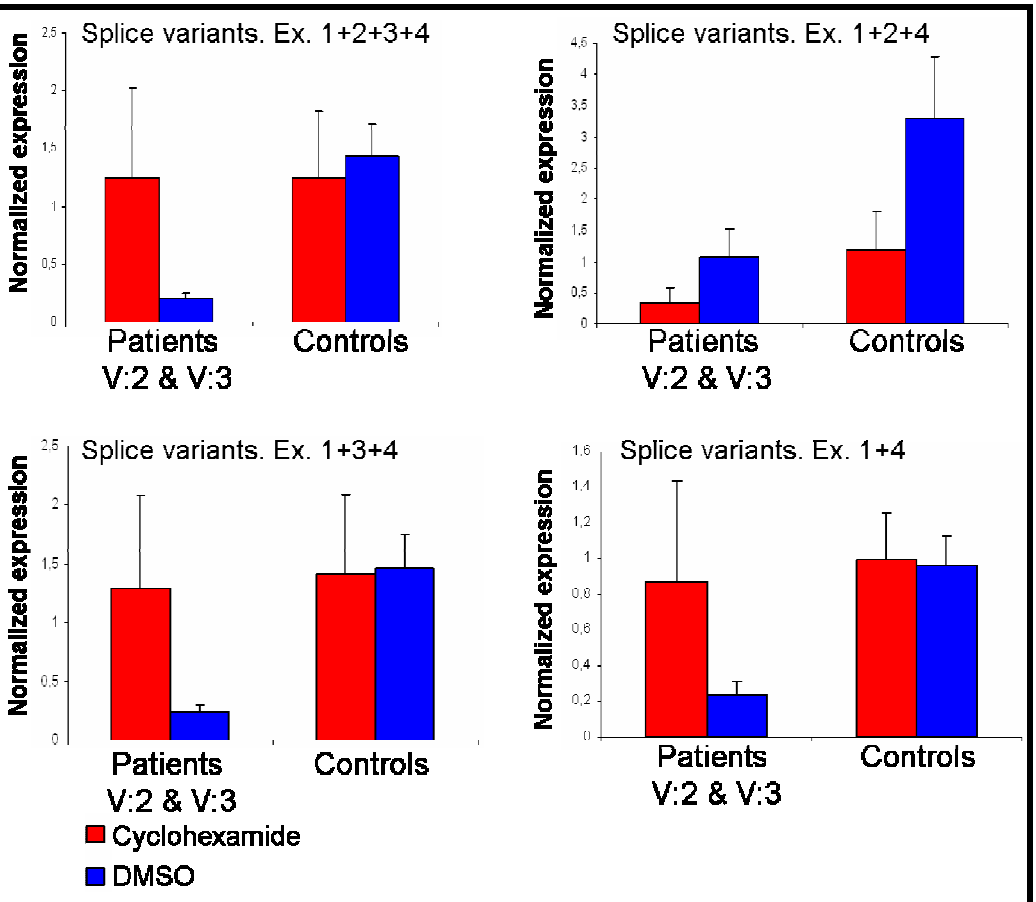

Figure 3-11: NMD analysis in patient FB cells. The experiments were performed twice with independent cells and each time in triplicate. The shown results here are from pooled patientand control samples. Loss of expression of *BOD1* splice variants seems to be due to nonsense mediated decay, as it could be abrogated by cycloheximide treatment of the cells. DMSO: Dimethylsulfoxide. Error bars represent the SD.

3.3.3. Loss of BOD1 protein from patient FB cells and LCL cells

To confirm the loss of expression of BOD1 in patients, western blots were carried out, using a rabbit polyclonal antibody raised against recombinant GST-BOD1 (Porter et al 2007), which on immunoblots stains a band corresponding

to a 22-KD protein. Alpha-tubulin was used as internal control. The result from a western blot experiment in FB cells is shown in figure 3-12. The absence of the BOD1 main isoform in both FB and LCL cells was confirmed.

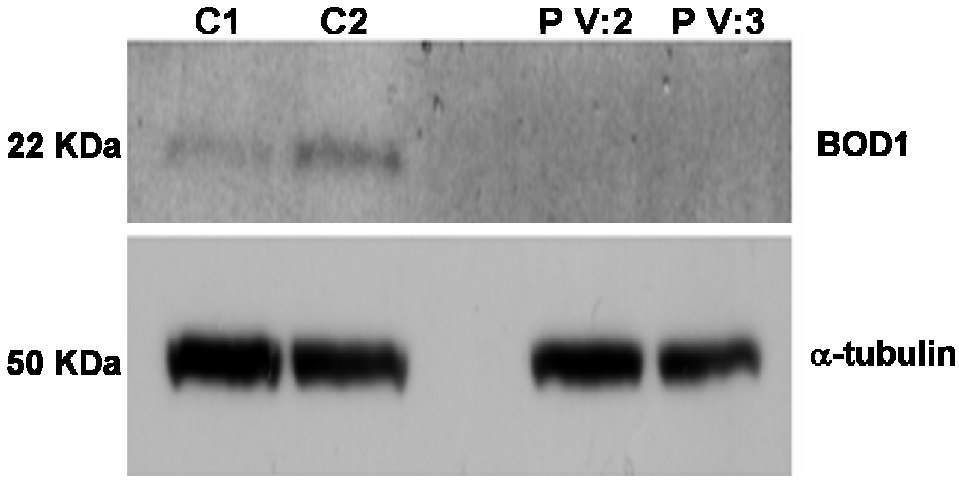

Figure 3-12: BOD1 protein is absent in patients. Results form a Western blot experiment using protein extracts from FB cells and a BOD1 polyclonal antibody are shown. The BOD1 antibody recognizes a 22KDa protein, matching the full-length BOD1 protein. While BOD1 is present in both controls, it is completely absent from patient cells. Alpha tubulin was used as internal control. (Experiment performed by Dr. Iain Porter, Division of Gene Regulation and Expression, University of Dundee).

3.3.4. Study of BOD1 in mitosis of patient FB and LCL cells

In 2007 BOD1 was demonstrated to be required for proper chromosome biorientation in human HeLa cells (Porter et al. 2007). The same group could show that siRNA depletion of BOD1 leads to a loss of proper phosphorylation of the kinesin MCAK, which prevents the resolution of syntelic attachments. Moreover, they could identify a role for BOD1 in the regulation of Plk1 kinase during G2 phase and mitosis (unpublished data). Plk1 is a promiscuous kinase localizing to many structures throughout mitosis (Takaki et al. 2008). Given the dramatic phenotypes seen during mitosis in HeLa cells depleted of BOD1 we wanted to determine if there were similar defects in patient cells.

3.3.4.1. Chromosome biorientation defect in patient LCL cells

BOD1 is a protein that promotes chromosome biorientation by unleashing chromosomes from improperly oriented microtubule attachments (Porter, McClelland et al. 2007). Thus initially we examined any increased number of chromosome biorientation defects in the patient cells as compared to controls by performing immunofluorescence staining on LCL cells. As shown in figure 3-13, we could observe that the metaphase plate in the patient LCL cells is completely distorted and chromosomes are mostly disoriented and pulled towards one of the poles in about 10% of the patient LCL cells.

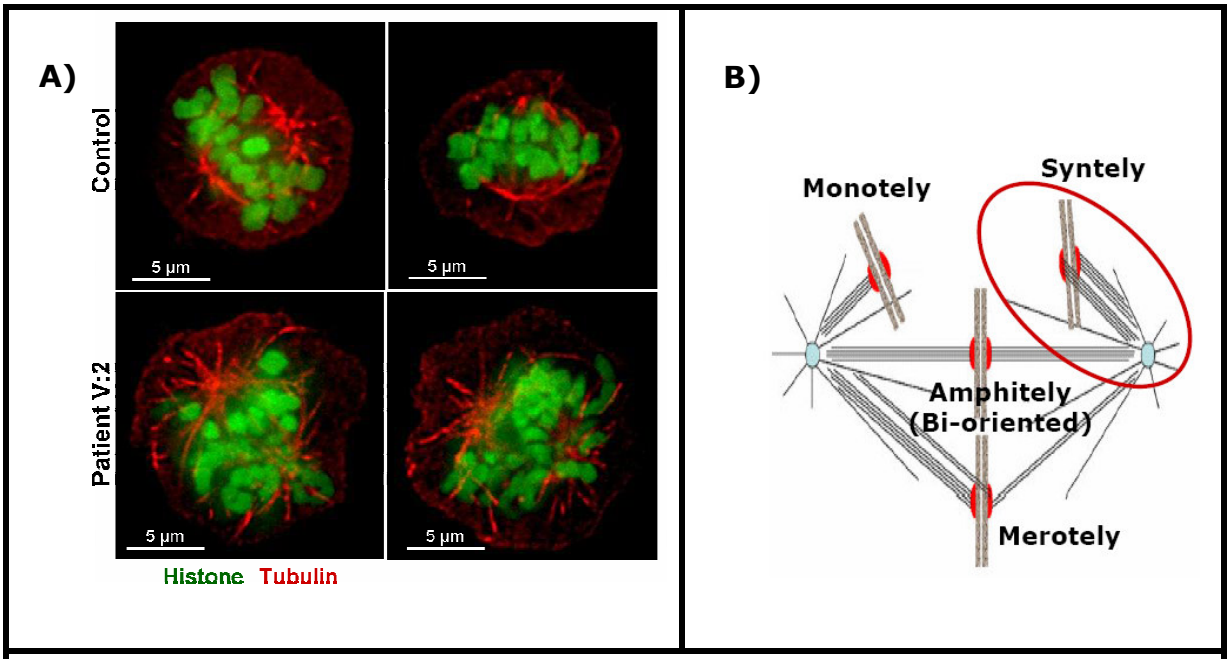

Figure 3-13: A) Distorted metaphase plate observed in patient LCL cells. Chromosomes were stained with a Histone antibody (green) and microtubules were stained with a gamma-tubulin antibody (red). While chromosomes are normally located exactly between two spindle poles during mitosis (control panels), in patient cells, the metaphase plate is distorted and chromosomes are mostly pulled towards one of the poles (patient panels). Scale bar is 5µm. (Experiment performed by Dr. Iain Porter, Division of Gene Regulation and Expression, University of Dundee). **B) Schematic representation of normal (amphitely) and possible faulty chromosome arrangements in the metaphase plate.** The observed patient phenotype is syntelic (red circle) [figure B : (Compton 2007)].

3.3.4.2. Investigation of patient FB cells

Before investigating patient FB cells, we first used an antibody against P4HB Prolyl 4 hydroxylase subunit beta (which is required for collagen synthesis) as a FB cells specific marker to verify the FB-nature of the cells. As shown in figure 3-14, Positive staining of the FB cells with this antibody was observed.

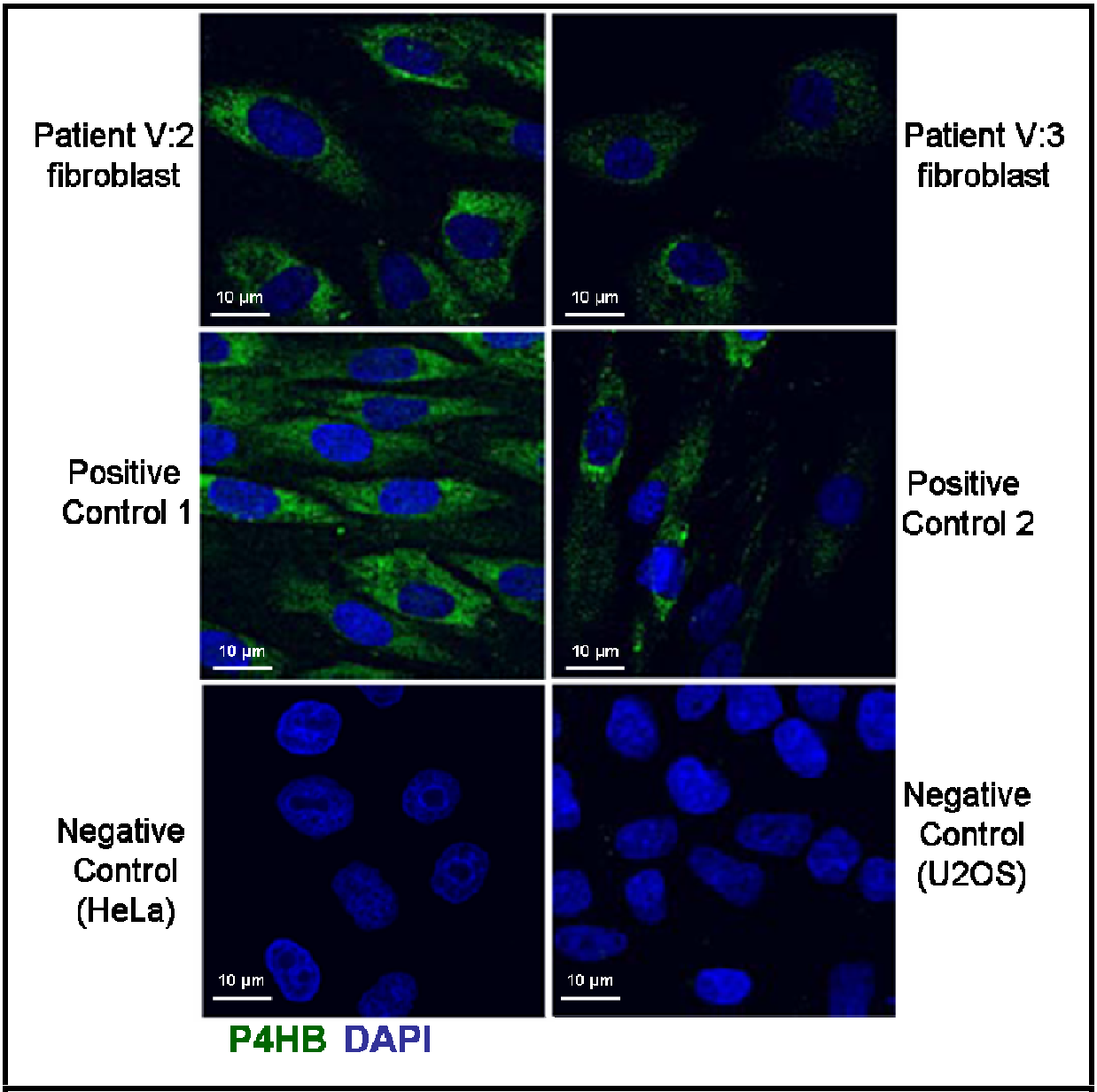

Figure 3-14: Positive staining of FB cells with fibroblast specific marker polyl-4-Hydroxylase (P4HB). Indirect immunoflorescence confocal images are shown. FB specific P4HB staining: green; DAPI staining (DNA): blue. P4HB can be detected clearly in the control FB cells and in patient V:3 it is also expressed, albeit at lower levels than in the cells from patient V:2. HeLa and U2OS cells are negative for P4HB.Scale bar is 10 µm. (Experiment performed by Dr. Iain Porter, Division of Gene Regulation and Expression, University of Dundee).

3.3.4.2.1. Patient FB cells go through mitosis at an accelerated rate

We examined the mitotic timings of patient FB and LCL cells using DIC timelapse microscopy, measuring the time from nuclear envelope breakdown (NEB) to anaphase onset (figure 3-15A). NEB was defined as the time when a clear delineation of the nuclear envelope was no longer visible. It is important to note that cells were seeded into microwell imaging chambers and were all imaged at the same time so they were under identical conditions. We have performed the imaging at 5 min and 4 min intervals, the data we have presented here come from 4 min intervals but the observation s with 5 min intervals were very similar. Surprisingly, the cumulative mitotic timings shown in figure 3-15B demonstrate that the patient cells progress through mitosis with 50% of the cells completing mitosis in 20 min compared to 30 min for the control cells. We examined the LCL cells in the same way, confirming that the patient cells, with no detectable BOD1, proceed through mitosis 10 min more quickly than controls (figure 3-15C).

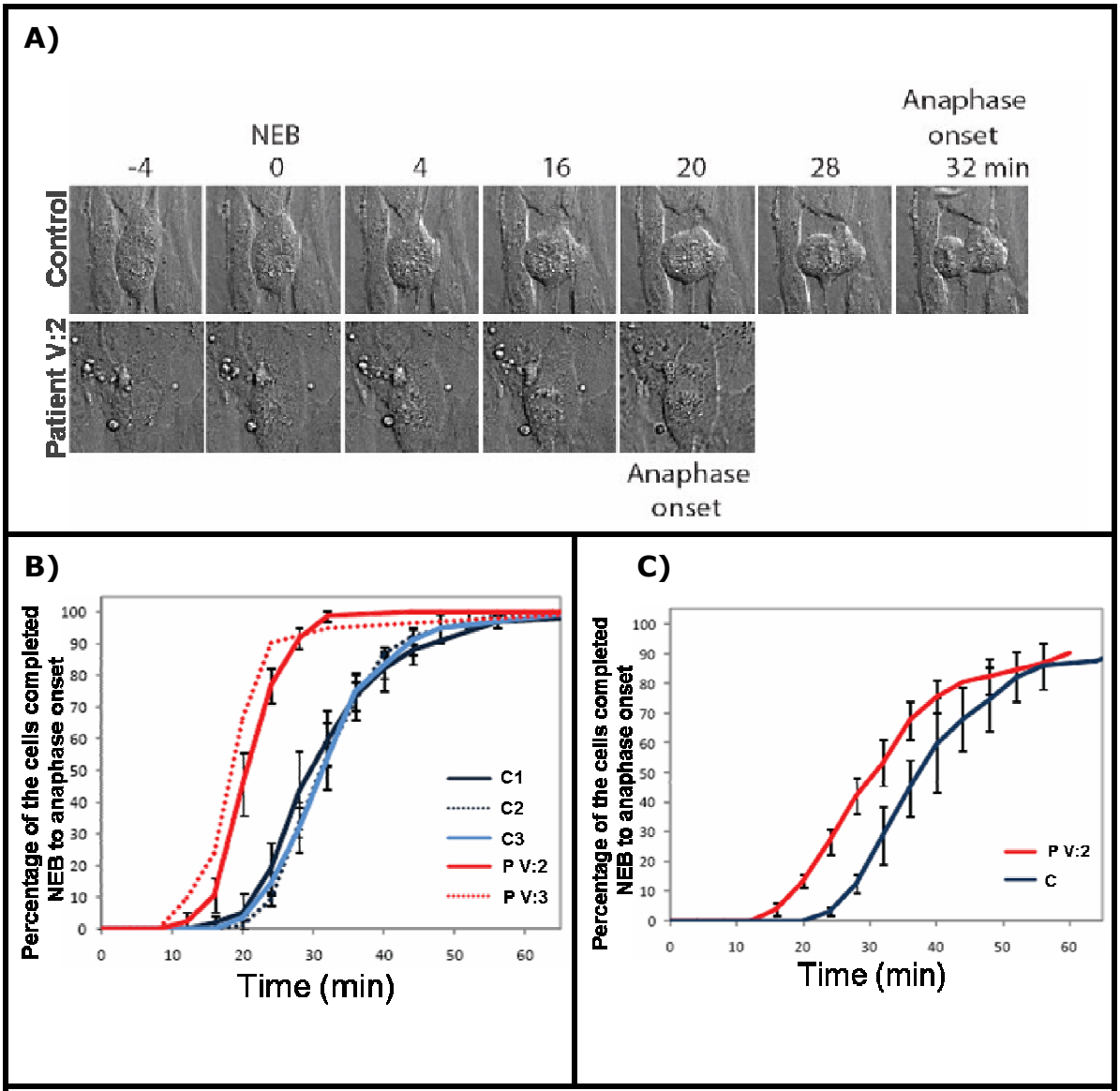

Figure 3-15: BOD1 can regulate mitotic timing. A) Live cell microscopy using DIC timelapse microscopy in FB cells from control and patient. Measuring the time between nuclear envelope breakdown (t= 0) and anaphase onset (t=32 in control and t=20 in patient). **B)** Mitotic profile in FB cells. **C)** Mitotic profile in LCL cells.

In both FB and LCL cells, the patient cells go through mitosis 10 min more quickly than the controls. Error bars represent Standard Error of the Mean (SEM). (Experiments performed by Dr. Iain Porter, Division of Gene Regulation and Expression, University of Dundee).

Investigation of the mitotic profile of FB cells (figure 3-16) demonstrated no significant increases in prometaphase cells, which would have been indicative

of alignment defects. However, there was a slight reduction in the numbers of metaphase cells and an increase in cytokinetic cells, in line with the live cell microscopy findings, suggesting that patient cells were progressing through metaphase and into anaphase at a higher rate.

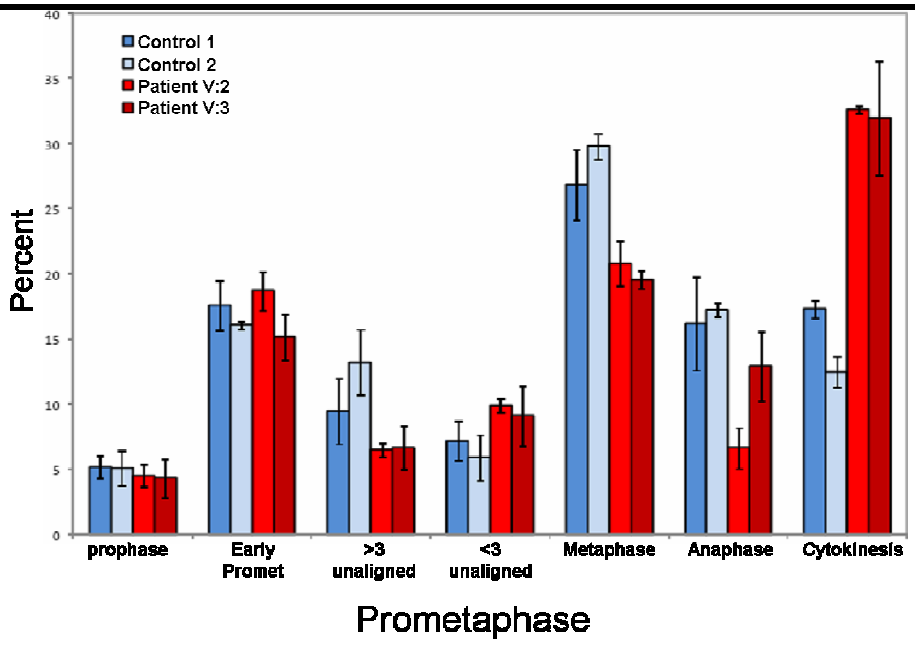

Figure 3-16: Changes in the cell cycle behaviour of patients. Mitotic profile of primary FB cells in patients and controls FB cells. Patient cells were progressing through metaphase and into anaphase at a higher rate. Error bars represent SEM. (Experiment performed by Dr. Iain Porter, Division of Gene Regulation and Expression, University of Dundee).

3.3.4.2.2. Patient FB cells show mislocalisation of Plk1 but increased tolerance to Plk1 inhibitor

It was demonstrated that BOD1 has a critical role in modulating the function of Plk1, a protein which functions at the centrosome and kinetochore during entry from G2 to mitosis (Takaki et al. 2008), and it is required for proper Plk1 function during G2 and mitotic entry. Following depletion of HeLa cells with *BOD1*siRNA, Plk1 is partially delocalized from centrosomes and kinetochores during mitosis (Porter et al, unpublished data). We therefore next sought to

ascertain if the level of Plk1 is reduced at kinetochores and centrosomes in the patient cells. Quantitative immunofluorescence of FB cells revealed that patient cells had reduced levels of Plk1 at kinetochores but elevated levels at centrosomes similar to the effect seen in HeLa cells treated with *BOD1*siRNA (Figure 3-17). This indicates that the primary defect observed in *BOD1* depleted HeLa cells remains true for the patient FB cells.

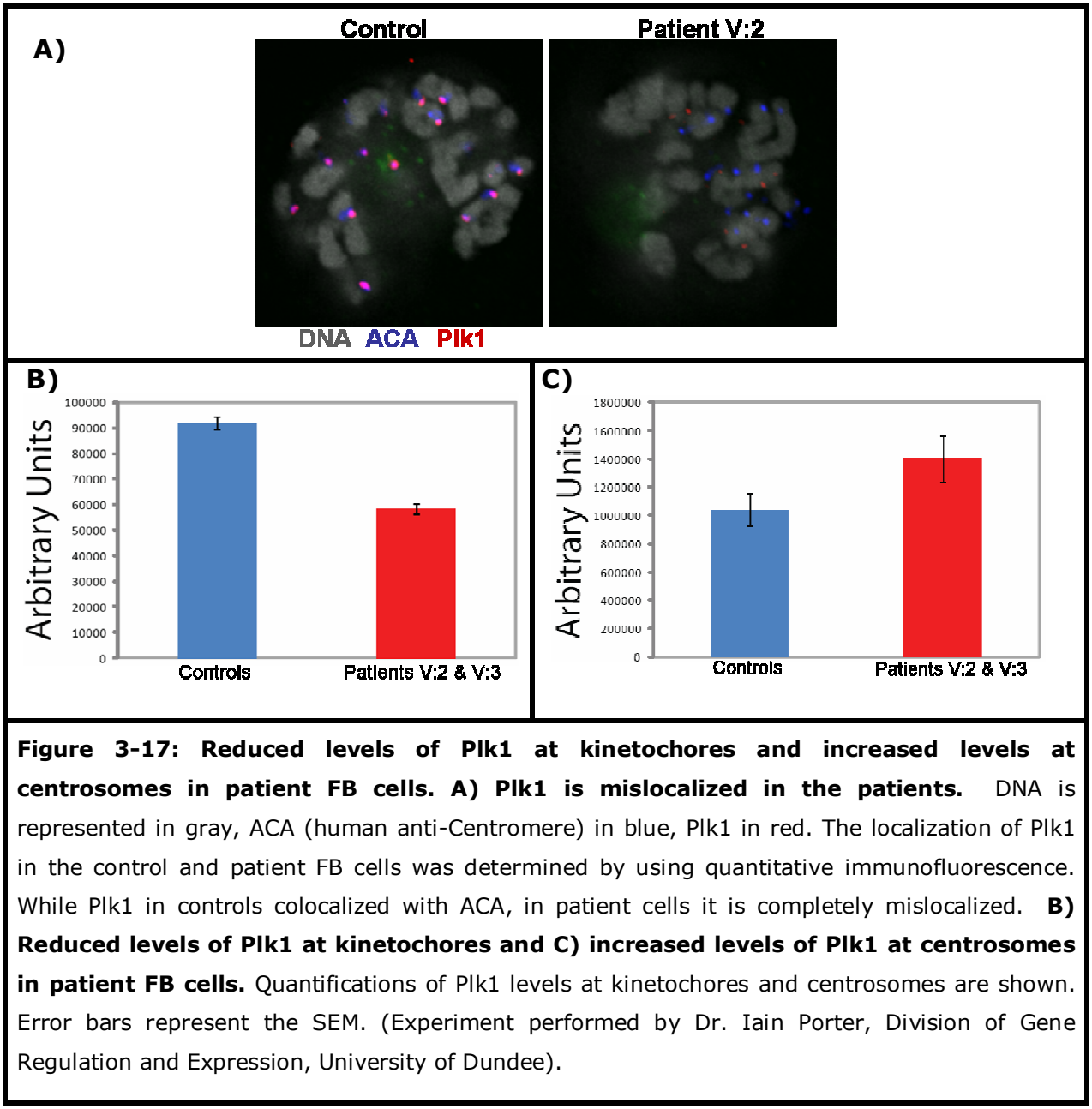

Figure 3-17: Reduced levels of Plk1 at kinetochores and increased levels at centrosomes in patient FB cells. A) Plk1 is mislocalized in the patients. DNA is represented in gray, ACA (human anti-Centromere) in blue, Plk1 in red. The localization of Plk1 in the control and patient FB cells was determined by using quantitative immunofluorescence. While Plk1 in controls colocalized with ACA, in patient cells it is completely mislocalized. **B) Reduced levels of Plk1 at kinetochores and C) increased levels of Plk1 at centrosomes in patient FB cells.** Quantifications of Plk1 levels at kinetochores and centrosomes are shown. Error bars represent the SEM. (Experiment performed by Dr. Iain Porter, Division of Gene Regulation and Expression, University of Dundee).

To understand how patient FB cells with no detectable BOD1 could progress through mitosis with reduced Plk1 levels and proliferate with no detectable problems we performed an experiment and asked what sensitivity cells had to the Plk1 inhibitor (BI 2536). Therefore we arrested the cells overnight with RO-3306, then released them into media containing increasing concentrations of the Plk1 inhibitor (BI 2536). After 1 hr the cells were fixed and their mitotic profiles determined. Inhibition of Plk1 classically inhibits the formation of bi-polar spindles resulting in the majority of cells displaying monopolar spindles (Lenart et al. 2007; Sunkel and Glover 1988). Surprisingly it appears that the patient cells are less sensitive to BI 2536, forming fewer monopolar spindles than control cells at any given concentration of the inhibitor and still managing to form metaphase plates at 200 nM BI 2536 where control cells could not (figure 3-18). In addition, in 12.5 nM BI 2536, 10 to 15% of control and patients cells could proceed to anaphase and beyond, although the control cells had five fold more segregation errors than the patient cells. This suggests that the patient cells must have adapted to the loss of proper Plk1 function. they might have somehow upregulated Plk1 function, allowing the cells to proceed through mitosis more quickly preventing the prometaphase type arrest seen in the BOD1 depleted HeLa cells.

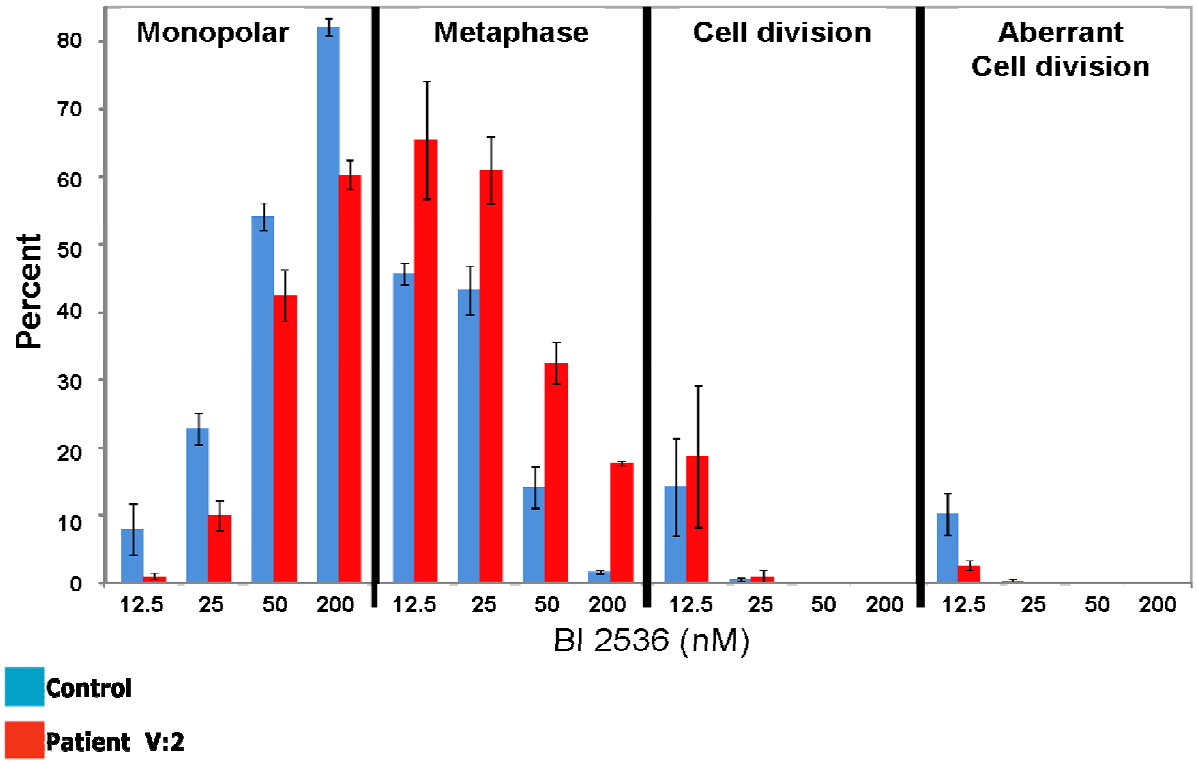

Figure 3-18: Patient cells have adapted to the loss of proper Plk1 function. Graph shown how FB cells respond to the Plk1 inhibitor (BI 2536). No patient cells were arrested at prophase and even at the highest concentration of the drug, where control cells can not form metaphase plates the patient cells manage in approximately 15% of cases. The patient cells appear to be more resistant to the Plk1 inhibitor. Error bars represent the SEM. (Experiment performed by Dr. Iain Porter, Division of Gene Regulation and Expression, University of Dundee).

3.3.5. Investigation of BOD1 function in non-dividing cells

It is shown that BOD1-GFP localizes to the centrosomes throughout the cell cycle, and mutations in a number of other proteins which are located at the centrosomes, such as MCPH1 and ASPM, are reported (Buchman et al. 2010; Kaindl et al. 2009), but usually in patients with a mutation in one of the Autosomal recessive primary microcephaly (MCPH) genes, ID is accompanied with microcephaly (Passemard et al. 2009), but the patients in this study don't display microcephaly or other features detectable by MRI. Thus to find out the

function of BOD1 during interphase and to find additional evidence concerning its involvement in human cognition, we tried to characterize the function of this protein during interphase. These investigations involved the study of patient cells as well as overexpression of BOD1 in HaCaT cells.

3.3.5.1. Investigation of BOD1 in patient cells

3.3.5.1.1. Nuclear organization defects

Difference in nucleus size and shape:

Endogenous staining of patient LCL cells by BOD1 direct antibody (figure S2 appendix D), revealed some evidence for nuclear defects in the patients. Nonetheless LCL cells grow in suspension and prior to investigation of these cells I fixed them on the cover slip using a cytospin protocol, which could be damaging for the cells, thus LCL cells are not a proper model for these kinds of study and I resorted to FB cells for the further investigation of BOD1.

Examination of patient FB cells demonstrated a difference in nucleus size and shape between patients and controls. As shown in figure 3-19, nuclei in control FB cells are ovally shaped (as they should be) and they are in the same size range but the patient's nuclei tend to be more spherical and they have different sizes.

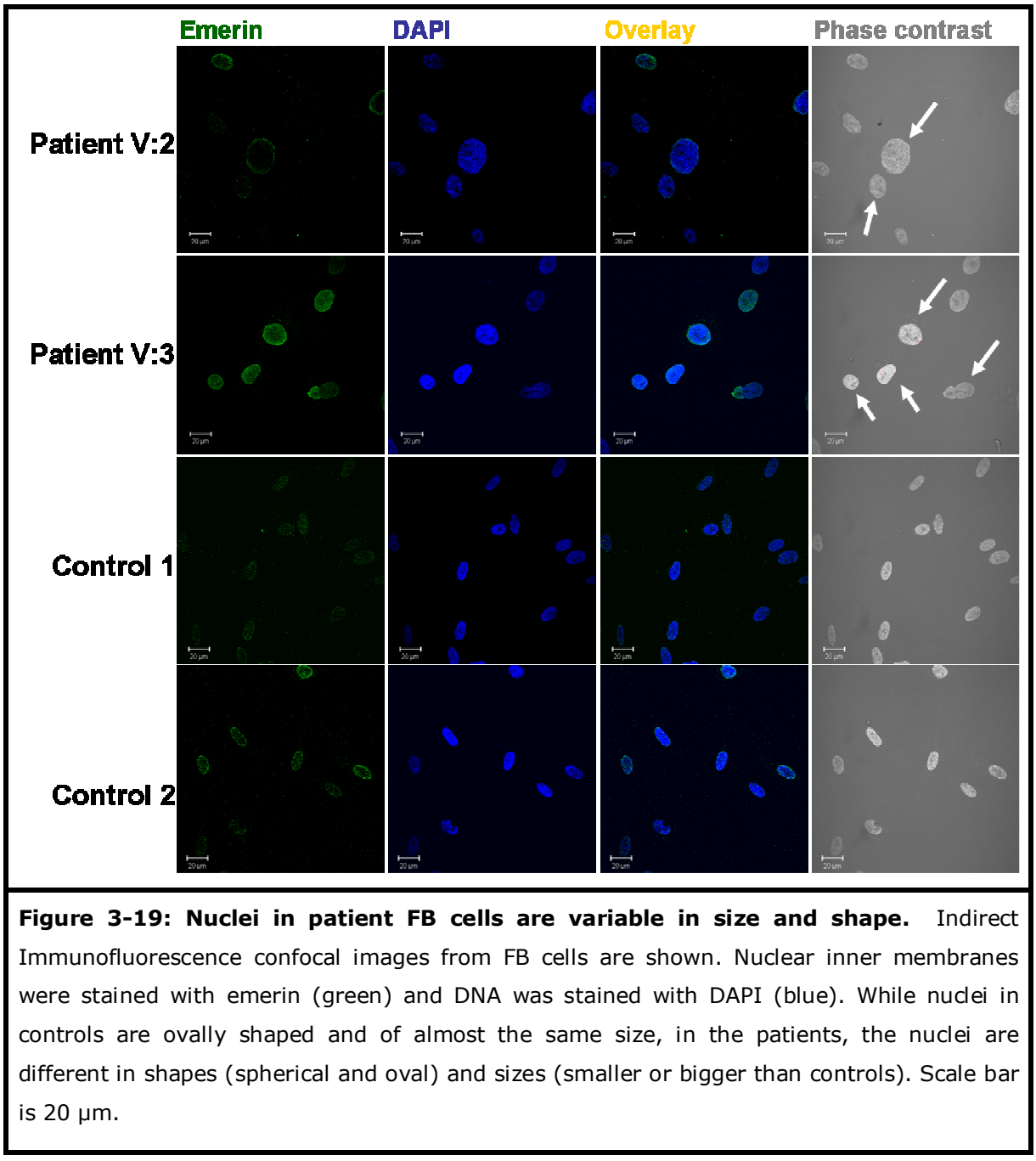

Figure 3-19: Nuclei in patient FB cells are variable in size and shape. Indirect Immunofluorescence confocal images from FB cells are shown. Nuclear inner membranes were stained with emerin (green) and DNA was stained with DAPI (blue). While nuclei in controls are ovally shaped and of almost the same size, in the patients, the nuclei are different in shapes (spherical and oval) and sizes (smaller or bigger than controls). Scale bar is 20 µm.

Difference in nuclear size is not a result of G1 or G2 checkpoint accumulation:

The interphase consists of three distinct phases: G1, S and G2. G1 is an intermediate phase occupying the time between the end of cell division in mitosis and the beginning of DNA replication during S (synthesis) phase.

During this time, the cell grows in preparation for DNA replication which will take
place in S phase. During this phase of the cell cycle DNA packaged into chromosomes is replicated. G2 phase is the final subphase and very similar to G1, it follows successful completion of DNA synthesis and chromosomal replication during the S phase, G2 prepares the cell for mitosis (M phase) and is the final chance of the cell to grow before it splits into two independent cells during mitosis. The main difference between G1 and G2 is, in G2 nuclear size and DNA material is twice that of G1.

To ensure that the observed differences in nuclear size and shape of FB cells between patients and controls are not caused by defects in G1 or G2 check points and therefore accumulation of the cells in one of these stages, but due to the absence of BOD1 function in patients, I analysed the FB cells from patients and controls by propidium iodide (PI) staining followed by FACScaning. PI stains DNA and it was used to analyze cellular DNA content. Together with FACScan it allows to distinguish between cells in G1 and G2 phase based on the DNA content and cell size: in G2 cell size and DNA content are doubled as compared to G1. As shown in figure 3-20 there is no difference in the number of FB cells in G1 or G2 between patients and controls (see all the numbers in Table S2, Appnedix E), suggesting that the observed differences in nuclear size are not due to a defect in G1/S/G2 check points.

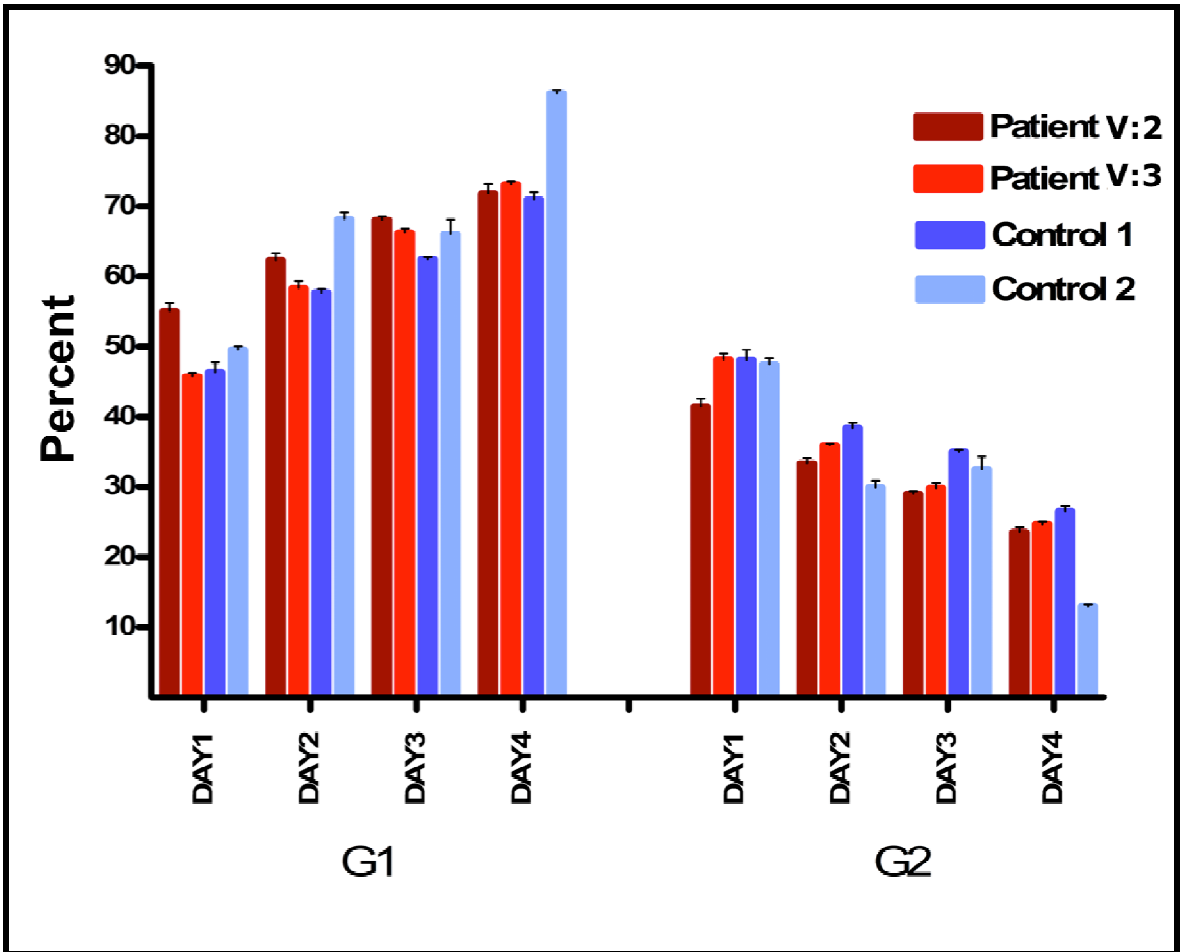

Figure 3-20: G1 andG2 checkpoints are not affected by loss of BOD1 inpatient FB cells. Shown is the Percentage of cells calculated from 5000 cells harvested on four subsequent days (each time in triplicate) analysed by FACScan. There is no accumulation in G1 or G2 phases of patients. Error bars represent SEM.

Nuclear size measurement:

It seems that there is no accumulation of the patient cells in G1 or G2. Thus, to investigate the observed phenotype in the patients' nuclei, FB cells of two different patients and two different controls were grown on cover slips under the same conditions and fixed with PFA 4%, then 200 nuclei were photographed. The nucleus diameter was then measured by Zeiss image examiner software. Length, width, area and circumference of at least 150 cells were measured in each fraction and the diameters of these cells were averaged (see all the numbers in Table S3 & S4, Appendix F & G). An example of how

the measurement was performed is shown in figure 3-21A. The nucleus surface area (S) and the whole nucleus volume (V) were calculated by the following equations:

S = πr2 and V = 4/3 πr3 (S = area, V = volume, r = radius, π≈3.14).

The results are shown in figure 3-21 B and C.

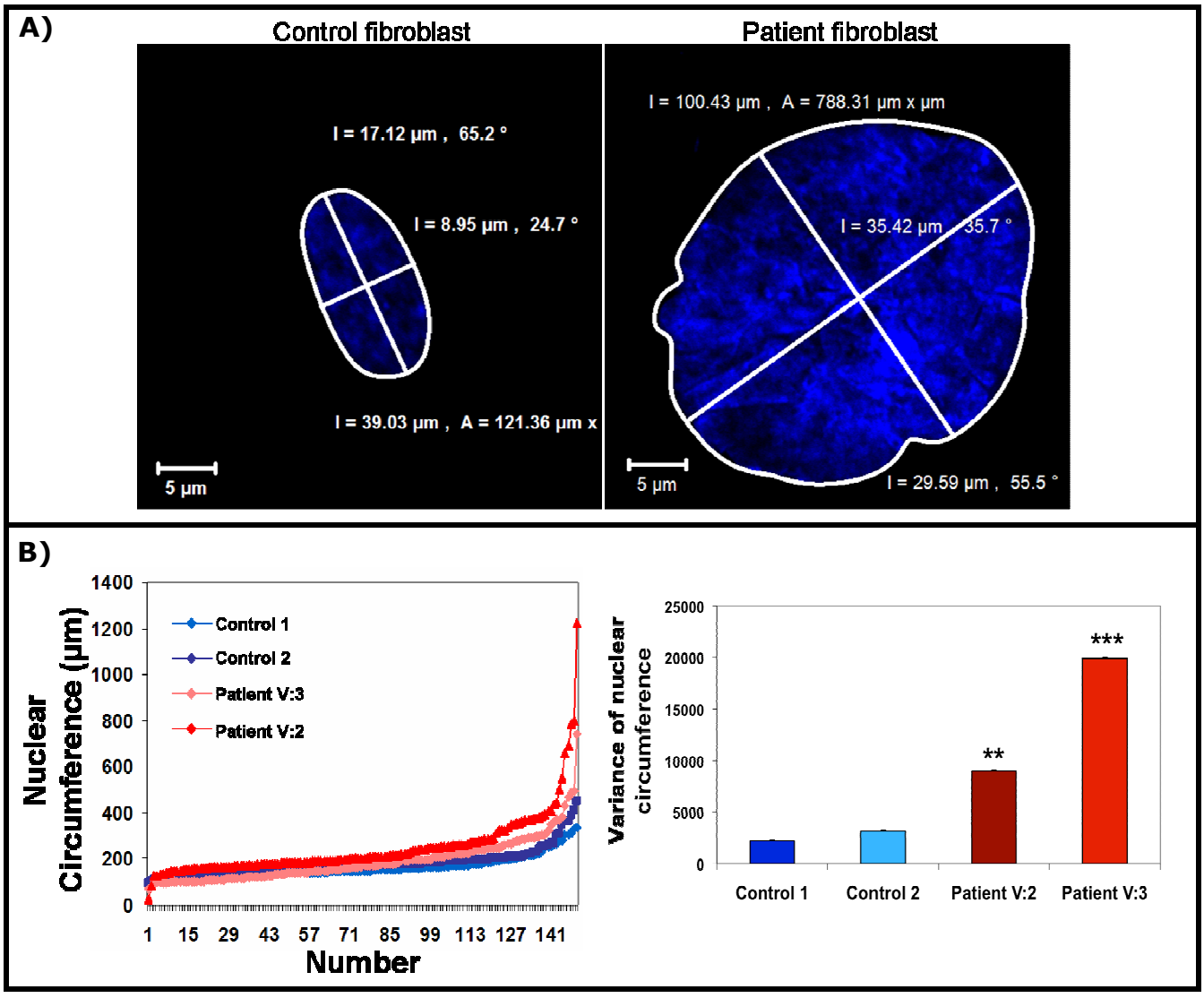

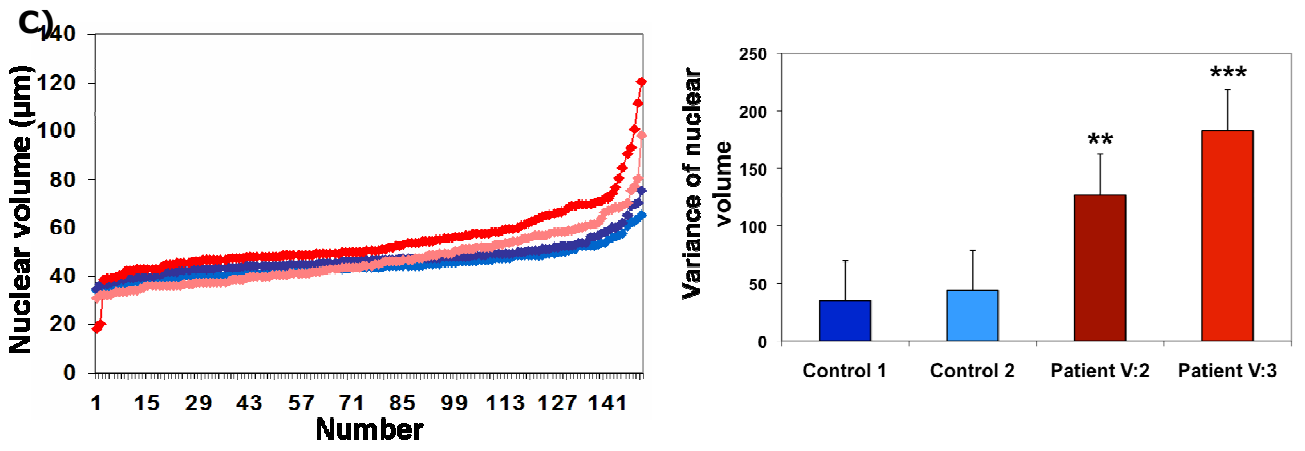

Figure 3-21: Nuclei from patient FB cells are variable in size and shape. A) Illustration of how the length, width, area and circumference were measured in 150 FB cells from patients and controls by Zeiss image examiner software. The cells were photographed using the LSM510META confocal microscope at 63× magnification and zoom scan of 3.5. **B & C)** The graphs on the left show that all the measured nuclei in controls are similar in circumferences and volume, so both curves corresponding to controls are overlapping but the curves corresponding to patient FB cells are not only diverging from the controls but also from each other. The graphs on the right show the variance of 150 FB cells. The difference in variability between patients and controls is significant, ***: $p<10^{-45}$ and **: $p<10^{-32}$ (F-test). Error bars represent SD.

The nucleus increases in size from the time of its formation, immediately following nuclear envelope assembly, to when it reaches its final size in interphase. Indeed it corresponds to the karyoplasmic ratio (Gregory, 2005), which suggests the existence of a mechanism that links nuclear and cellular volumes; for instance the ratio of nuclear to cellular volume ration in both, budding and fission yeasts, remains constant throughout the cell cycle, even as cell volume increases (Jorgensen et al. 2007; Neumann and Nurse 2007). While the mechanisms that control nuclear volume remain unclear, the existence of a karyoplasmic ratio suggests that the ratio between nuclear and cytoplasmic volumes is crucial for cell integrity. Nuclear size is important for cell function. Moreover, it has been found there is a strong correlation between nuclear size, RNA transcription levels and cell size (Schmidt and Schibler

1995). Furthermore, the volume of the nucleus might be important for both retaining nuclear compartments, for example the nucleolus, and the activity of enzymes which are sensitive to macromolecular crowding such as DNA polymerase (Miyoshi and Sugimoto 2008). As to the sensitivity of the self-organization to the concentration of the individual components, the regulation of nuclear volume might have an important role in enabling this process (Webster et al. 2009).

3.3.5.1.2. Staining with different nuclear markers

For further investigation of the observed structural defect in patient FB cells nuclei, I stained them with different nuclear markers for envelope and matrix respectively.

Nuclear envelope staining:

An antibody against Emerin (an integral inner-nuclear-envelope protein) was used to stain the nuclear envelope. As shown in figure 3-22A, control nuclei are ovally shaped and have an intact nuclear membrane. In patient FB cells, however, an unusual number of nuclear invaginations was observed. To quantify this phenotype, 300 nuclei from cells of two separate patients and controls were counted and the percentage of defective nuclei is shown in figure 3-22B.

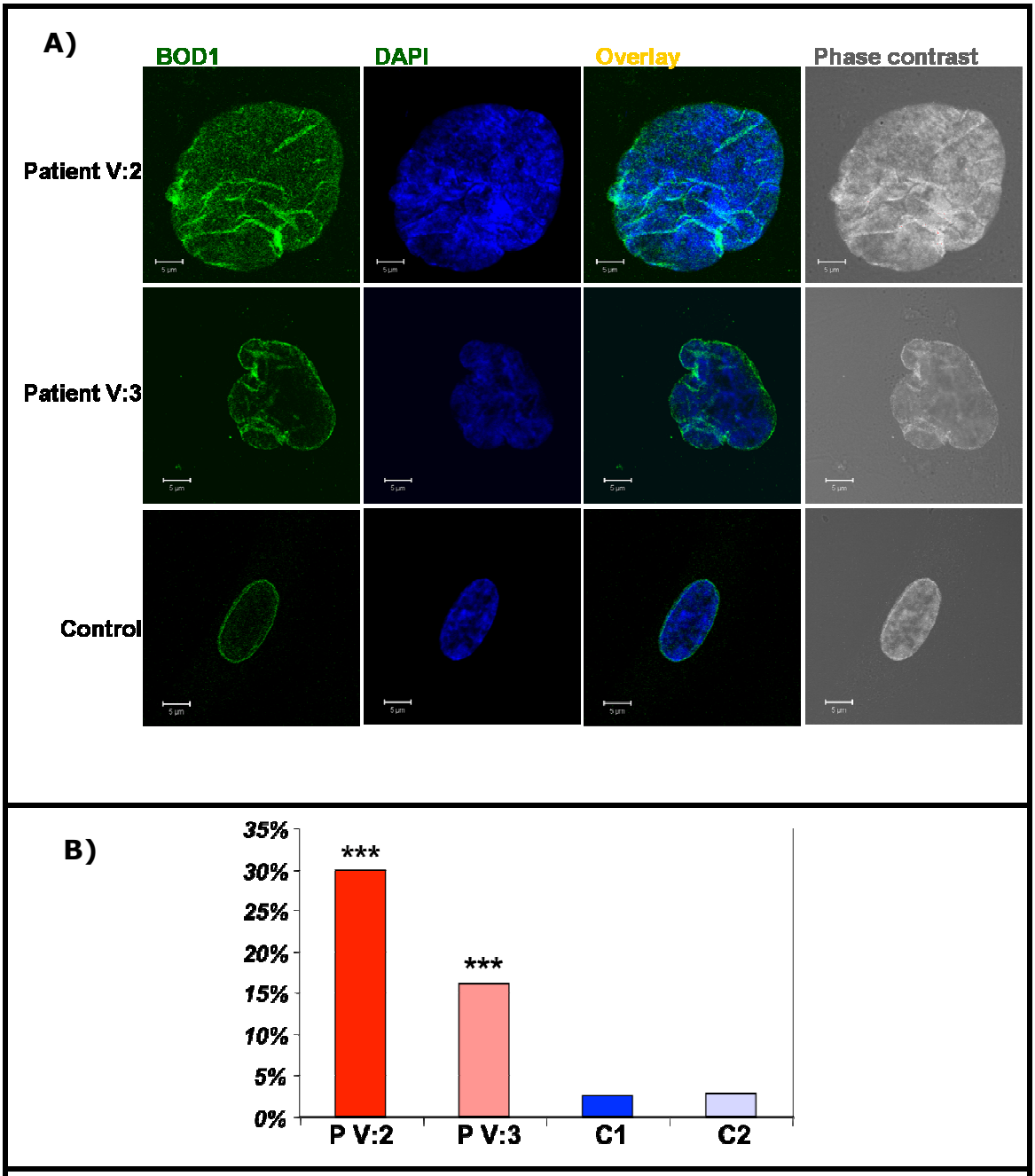

Figure 3-22: Nuclear invagination in patient FB cell nuclei. A) Indirect confocal immunoflorescence images are shown. Nuclear inner membranes were stained with emerin (green) and DNA was stained with DAPI (blue). The nuclear envelope in patients is invaginated whereas in controls it was intact. **B)** Quantification of nuclear invagination. 300 nuclei were counted from two the patient and control cell lines respectively by fluorescence microscopy. ***: p< 0. 1 (Student's t-test). Scale bar is 5 µm.

Nuclear Matrix staining:

Indirect immunoflorescence staining of the nuclear matrix by laminA/C in the nuclear matrix revealed nuclear matrix defects (shown in figure 3-23) in the patients.

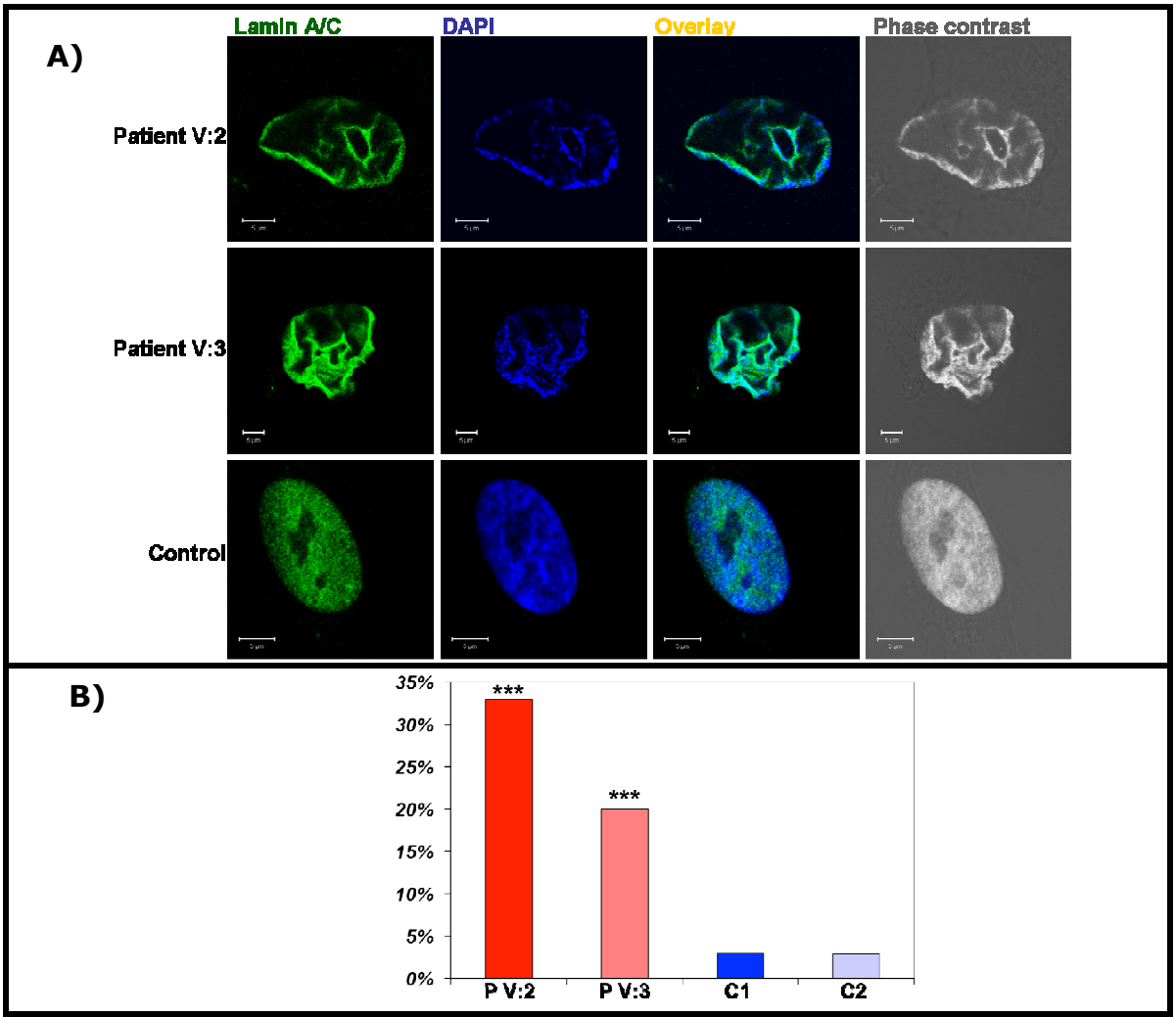

Figure 3-23: Nuclear Matrix defects in patient FB cells. A) Indirect confocal immunoflorescence images are shown. The Nuclear matrix was stained with Lamin A/C (green) and DNA was stained with DAPI (blue). Nuclear matrix is distributed uniquely in controls but it aggregated together in patients. Scale bar is 5μm. **B)** Quantification of nuclear matrix defects. 300 nuclei were counted from each of the patients and controls by fluorescence microscopy and the defects in nuclear matrix was observed in similar percentage as defects in the nuclear envelope. ***: p< 0. 1 (Student's t-test). Scale bar is 5 μm.

3.3.5.1.3. Cytoskeletal defects

Primary Cilia formation in patient FB cells is delayed:

Increasing numbers of proteins which localise to centrosomes and are involved in centrosome function are being associated with ID in humans. Defects in centrosomal proteins such as ASPM and MCPH1 are associated with microcephaly (Buchman et al. 2010) but the proteins associated with Bardet-Biedl Syndrome (BBS) cause ID without microcephaly. BBS is a highly pleiotropic syndrome, with a wide range of clinical features including visual loss, obesity and decreased functionality of the gonads. There are currently around 12 proteins associated with BBS, all are constituent parts of the BBsome complex and are involved in intraflagellar transport required for cilia formation and maintenance (Nachury et al. 2007). Cilia are conserved microtubule-based organelles which develop from basal bodies (a centrosome-derived structure) and stick out from the cell surface (Nigg and Raff 2009), this organelle is present on mammalian neurons and glia cells and is essential for a number of cellular functions and in involved in a number of signalling pathways (Fliegauf et al. 2007; Nigg and Raff 2009). Primary cilia are produced in many types and defects in cilia production are associated with a number of syndromes whose symptoms include ID (Sharma et al. 2008). We therefore were interested to see if BOD1 was also involved in cilia formation and/or maintenance.

When staining for cilia using an antibody specific for acetylated tubulin we could see very little difference in the number of cilia present in asynchronously growing FB cells (figure 3-24 A). We then wanted to look at how quickly and how asymmetrically cilia were produced in the cells; to do this we arrested the cells overnight with a CDK1 inhibitor called RO3306 which blocks the cells at the G2/M boundary (Vassilev et al. 2006). We then released the cells for 3 hours and counted how many cilia were produced between the daughter cells. When we looked at the rate of production of cilia in control and patients FB cells we could see that 3 hr after release from a G2/M block 28 % of control cells had produced cilia in at least one of the daughter cells whereas only 8%

of patient cells (figure 3-24 B) had produced around 3 fold fewer cilia although production does still appear to be asymmetric.

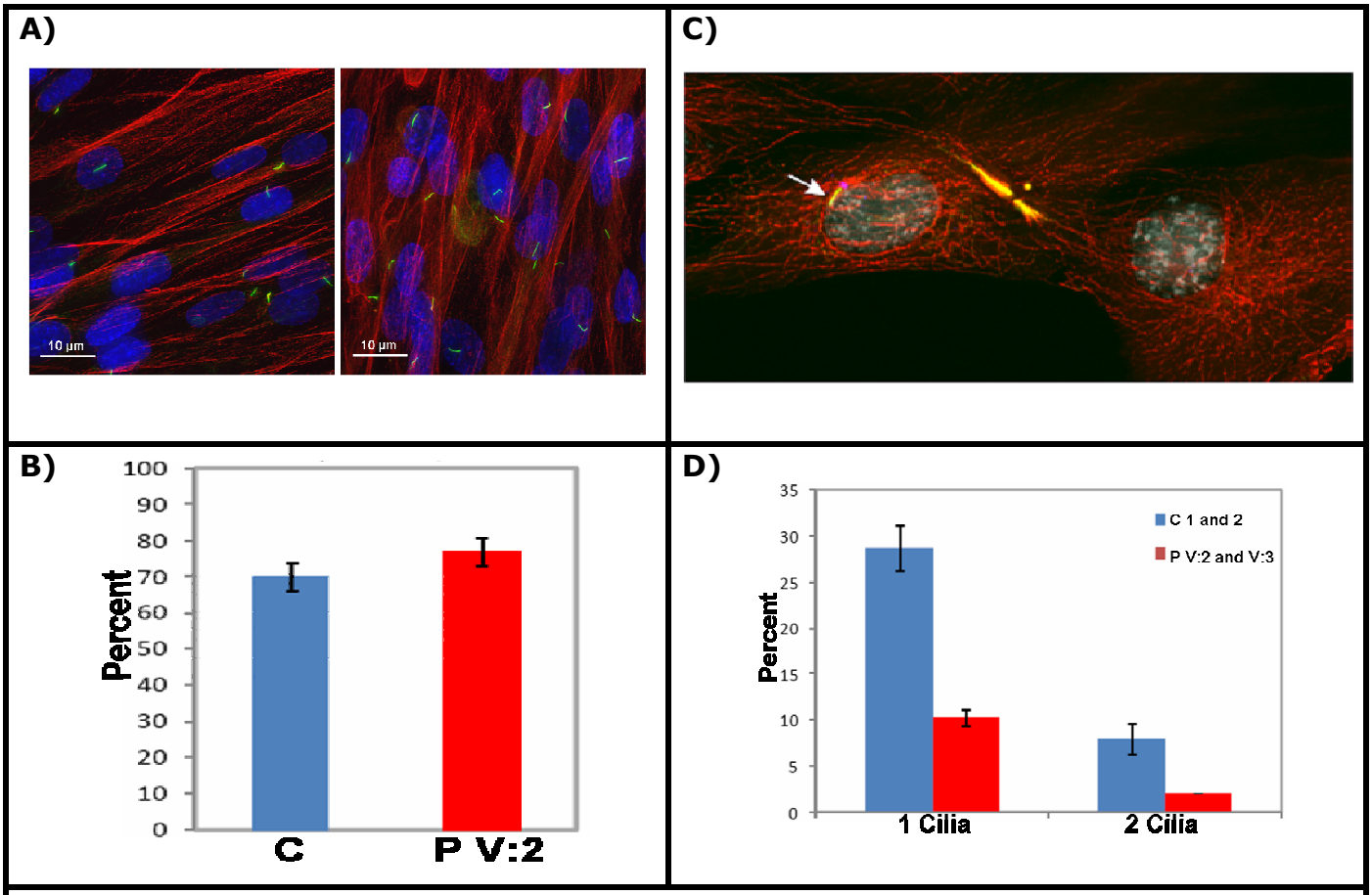

Figure 3-24: cilia production in asynchronously growing FB cells. A) Representative images of primary cilia in control and patient FB cells. Tubulin is stained in red, acetylated tubulin in green and DNA in blue. **B)** The percentage of asynchronously growing FB cells containing primary cilia from pooled patients and controls are plotted. There appears to be very little difference between the control and patient cells. Error bars represent the SEM. **C)** Representative image of sister FB cells 3 hr after release from the CDK1 inhibitor (RO 3306). The Arrow indicates forming primary cilia in a single sister cell. Tubulin is stained in red, acetylated tubulin in green and DNA in grey. **D)** Percentage of FB cells displaying primary cilia in one or both sister cells 3 hr after release from RO 3006 are plotted. After 3 hr the patient cells had produced around 3 fold fewer cilia as compared to controls, even though production does still appear to be asymmetric. Error bars represent the SEM. (Experiment performed by Dr. Iain Porter, Division of Gene Regulation and Expression, University of Dundee).

Tubulin morphology defects:

Given the centrosomal localization of BOD1 (Porter et al. 2007), the morphology and orientation of microtubules were checked (Burakov et al. 2003; Moynihan et al. 2009). To do this, I fixed the cells on three consecutive days to study their movements at different stages of confluence. As shown in figure 3-25, patient cells did not show proper contact inhibition: They were growing on top of each other and were depolarized. Moreover patient FB cells were accumulating in some parts of the culture dish whereas other parts remained empty.

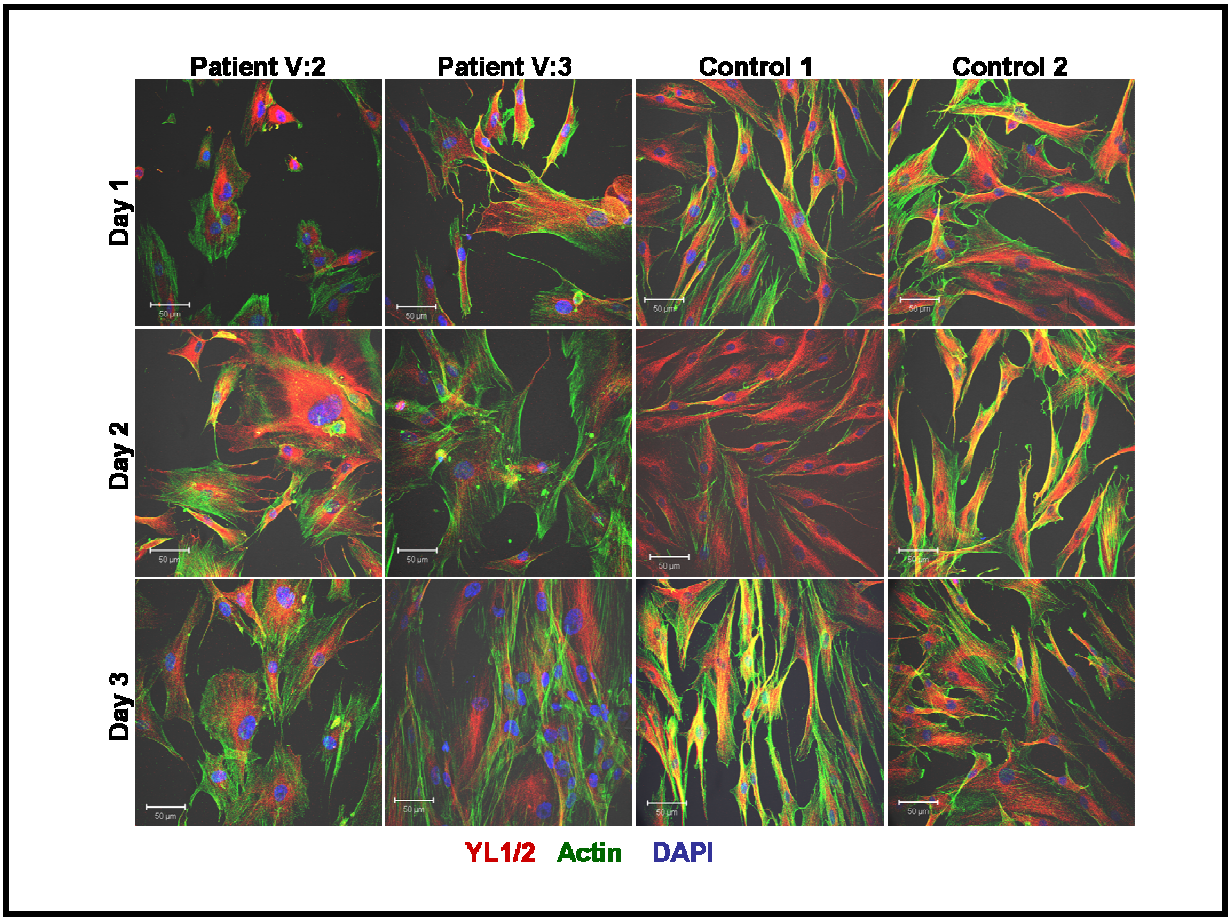

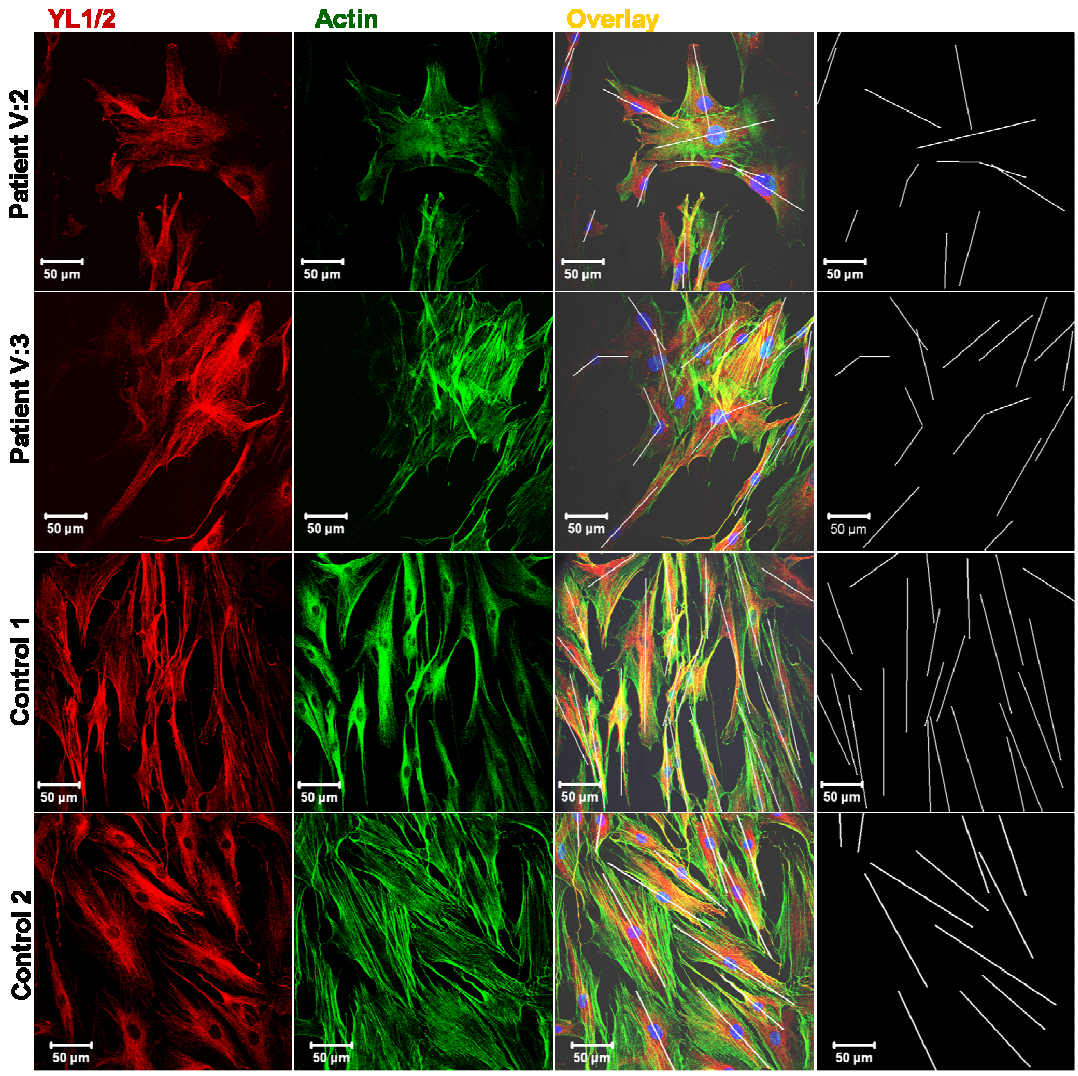

Figure 3-25: Depolarization of tubulin in patient cells. Confocal indirect images from patient and control FB cells are shown. Tyrosinated tubulin was stained with YL1/2(red), cytoskeleton was stained with actin (green) and DNA was stained with DAPI (blue). **A)** The images were taken on three successive days and from 10 different fields per culture. Multiple pointed microtubules and disoriented cells in patients are shown, so patient cells are growing either on the top of each other or sparsely. Scale bar is 50 µm. **B)** Comparison of the orientation of the cells in the patients and controls are shown. White lines recapitulate the orientation of the cells. Patient cells are disorientated. Scale bar is 50 µm.

To check if the observed difference in the morphology of the patient FB cells is either due to the differences in cell density or to some technical issues. The

cells from both patients and controls were allowed to reach full confluence (to rule out the possibility of different polarization due to different cell density) and subsequently the cells were stained with tyrosinated tubulin and then they were imaged. It is important to note that, to rule out the technical errors, the experiment was performed in a different laboratory (University of Dundee). The tubulin profile is shown in figure 3-26. Disorganized tubulin morphology is observed in patient cells (which could in turn lead to different polarization of the cells).

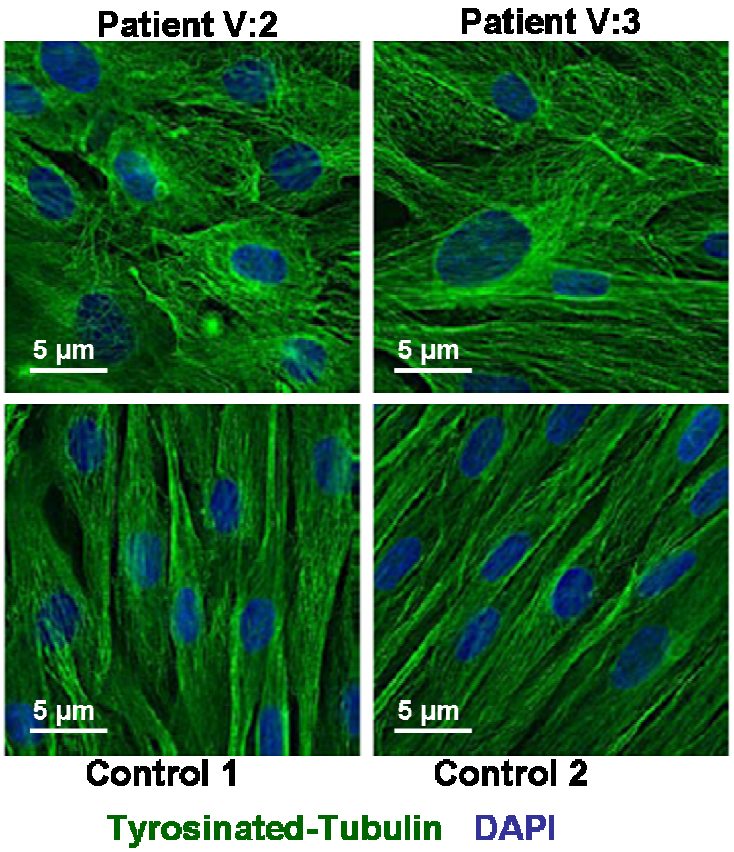

Figure 3-26: Morphology of fully confluent FB cells from patients and controls. Shown are indirect confocal images. Cells were stained with tyrosinated tubulin (green) and DAPI. The Disoriented cells and multiple pointed microtubules in patients are shown. (Experiment performed by Dr. Iain Porter, Division of Gene Regulation and Expression, University of Dundee).

3.3.5.2. Investigation of BOD1 in HaCat cells

Due to limited access to the patients and a lack of any post-mortem material as, we wanted to establish a system for functional studies in cellular models, particularly with respect to a role of BOD1-wt during interphase. Therefore I overexpressed BOD1 tagged with GFP or cherry in HaCat cells.

3.3.5.2.1. Overexpression of BOD1 leads to change in nuclear morphology

Overexpression of BOD1-GFP in HaCat cells, interestingly, leads to a side effect in the nucleus morphology of the transfected cells compared to untransfected ones. GFP was used as a control to certify that this observation is not because of a negative effect of GFP but due to the overexpression of BOD1. Also the expression level is reduced to the lowest possible level to ensure that this observation is not an artifact. As shown in Figure, the nuclear shape is deformed in transfected cells with BOD1-GFP whereas no changes were observed in transfected cells with only GFP.

It is important to note that overexpression does not always lead to a negative side effect, however it sometimes (specially in case of nuclear proteins) could displace the endogenous protein or its interacting partner (Pegoraro et al. 2009). Nonetheless, as far as it is known, BOD1 doesn't form a complex (Porter et al. 2007) and also a high-throughput protein interaction screening to detect the cellular interaction partners [Method source: (Poser et al. 2008; Selbach and Mann 2006)] of this protein pointed to no candidate (Experiments performed by group of Anthony A Hyman from Max Planck institute for molecular cell Biology and genetics in Dresden and Matthias Mann from Max Planck institute of biochemistry in Munich). Therefore the side effect out of overexpresssion of BOD1 might be due to the delocalization of this protein itself.

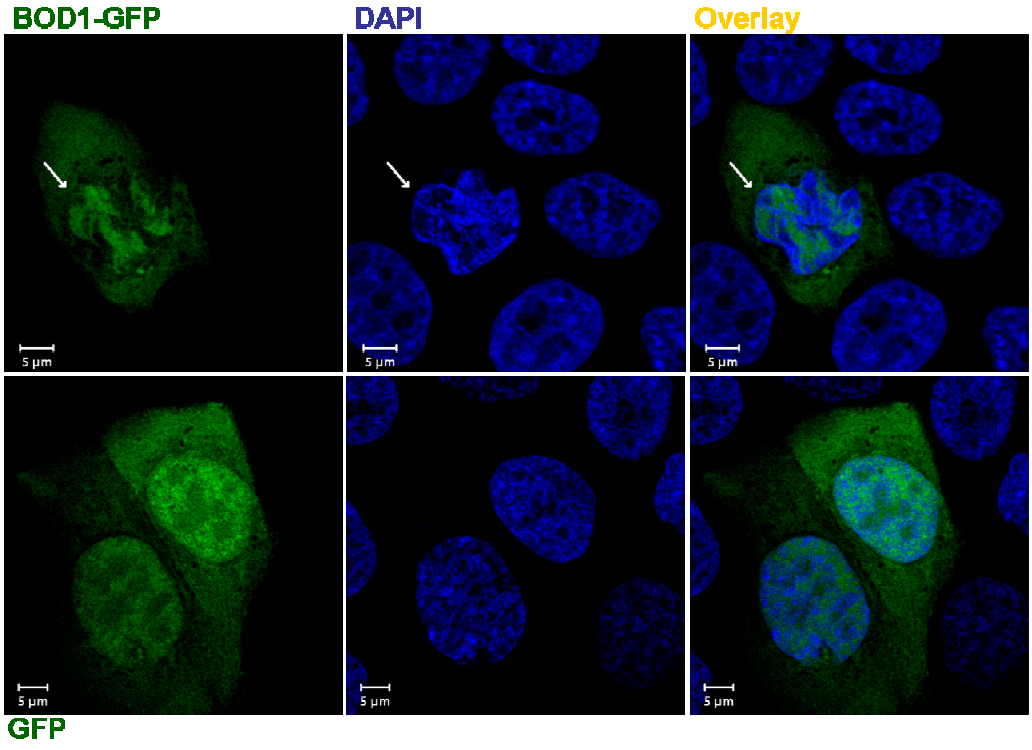

Figure 3-27: Overexpression of BOD1-GFP leads to nuclear morphology defects. Confocal images are shown. Arrow indicates the deformed nucleus in the transfected cells with BOD1-GFP.

3.3.5.2.2. Overexpression of BOD1 leads to change in chromatin organization

BOD1 is a centrosomal protein, and aberrations in centrosomal proteins, in addition to mitotic defects, are expected to reflect defects in the formation or maintenance of cilia (as shown in section 3.3.5.1.3), as well as nuclear chromatin remodelling.

To follow up the observation regarding changes in the nuclear morphology (section 3.3.5.2.1.), we investigated the localization of BOD1-GFP in the nucleus during interphase. Interestingly (as shown in figure 3-28) BOD1 and chromatin are not colocalizing and when the signal intensity is high for BOD1 it is low for DNA and vice versa. This was not observed in transfected cells with GFP, which confirms that the result seems indeed to reflect the true localization of BOD1.

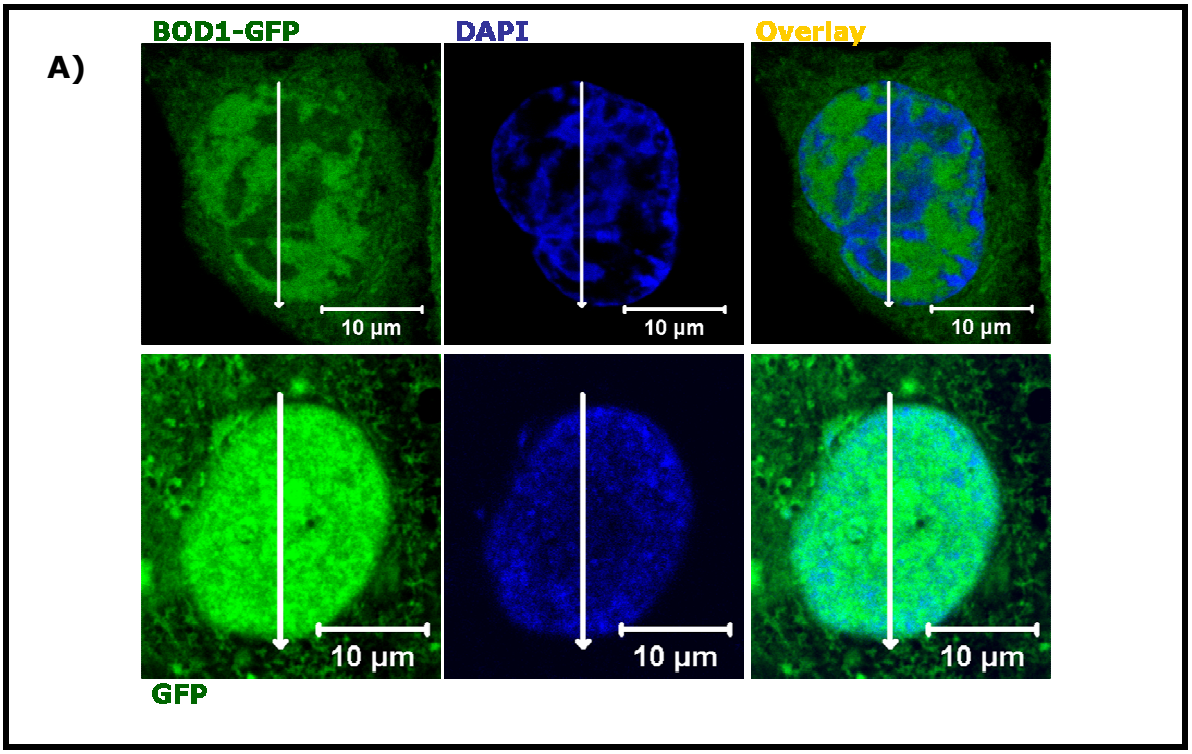

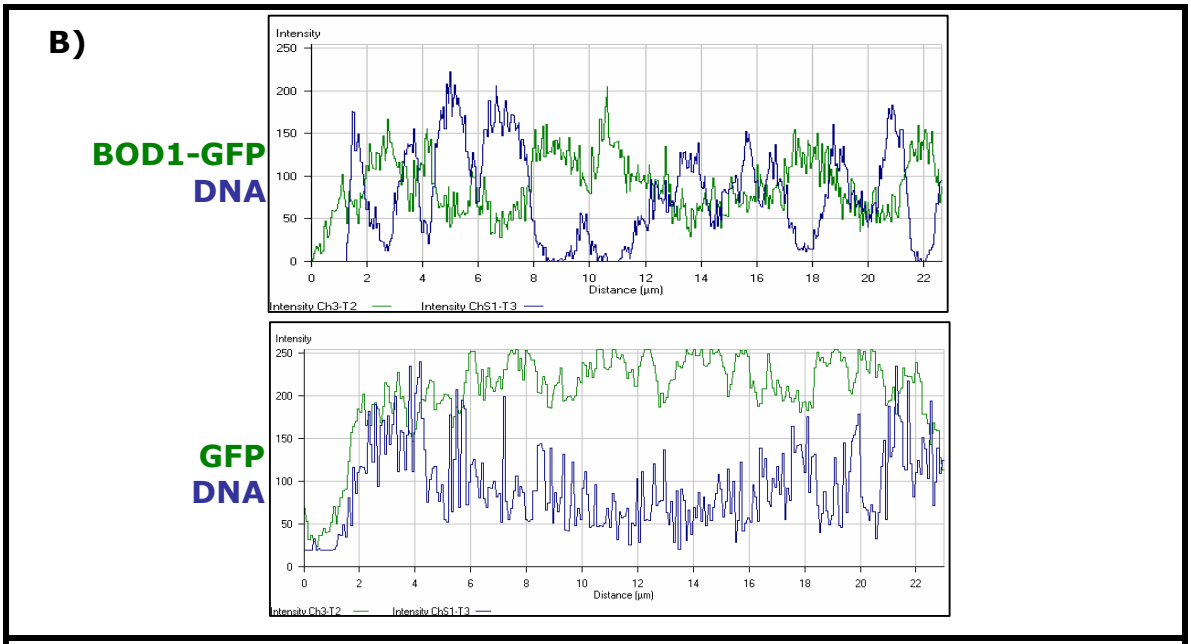

Figure 3-28: BOD1-GFP does not colocalize with DNA. A) Confocal images of HaCat cells expressing BOD1-GFP or GFP are shown. The overlay shows that BOD-GFP and DNA are not colocalizing, which is also illustrated in the intensity diagrams shown in **B)** The diagrams represent the staining profiles along the white arrows in A). The profiles were generated using the LSM510 software. This indicates that other than GFP, BOD1-GFP is going to the interchromatin space and doesn't colocalize with chromatin.

3.3.5.2.3. Overexpression of BOD1 leads to nuclear envelope defect

A higher percentage of nuclear membrane invagination (nuclear membrane defect) (Johnson et al. 2003) in the patient cells on one hand and the nuclear shape defect in HaCat cells as a result of overexpression of the BOD1 on the other hand, were observed. Nonetheless, it is known that the nuclear shape alters either due to changes in the nuclear lamina (in many cases) or by forces that act from the cytoplasm (in some cases). In either case, it is still not fully clear how nuclear shape affects function, although two main hypotheses exist. The first hypothesis suggests that changes in nuclear shape alter the rigidity of the nucleus; this could be beneficial for cells that need to squeeze through tight spaces, but deleterious to cells that are under mechanical forces; The second hypothesis proposes that changes in nuclear shape lead to changes in chromatin organization thereby can affect gene expression. Thus this defect

might have different influence on various cell types. Numerous diseases, e.g. aging, are associated with alterations in nuclear shape (Webster et al. 2009). To investigate how BOD1 affects nuclear morphology, it is needed to clarify which nuclear compartments precisely are defective, and as to the importance of nuclear membrane in nuclear morphology and chromatin organization (D. J. Anderson and Hetzer 2008; D. J. Anderson et al. 2009; Ma et al. 2007; Peric-Hupkes et al. 2010), investigation of nuclear membrane by emerin were carried out. The cells were transfected with BOD1-GFP and GFP and after 2 hr transfection and 14 hr posttransfection, they were fixed and indirect immunoflorescence stainings were performed by using an Emerin antibody (inner nuclear membrane marker). As shown in figure 3-29, the nuclear membrane in cells transfected with BOD1 is completely distorted whereas there is no defect in the non-transfected cells or those transfected only with GFP.

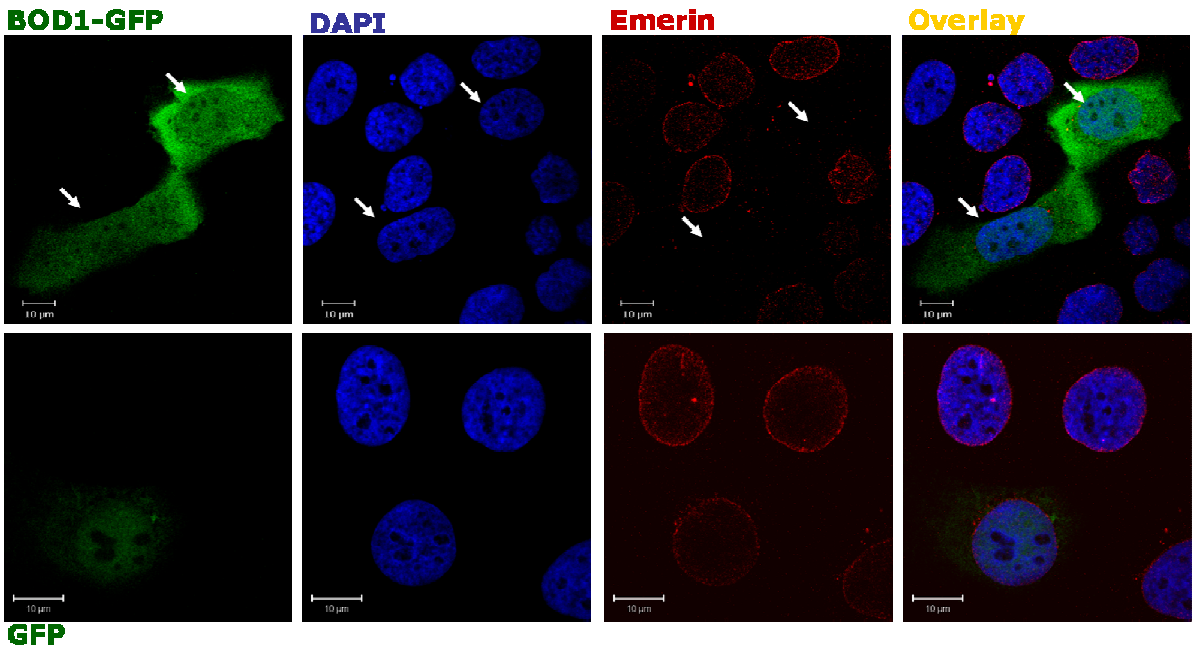

Figure 3-29: Over-expressed BOD1-GFP leads to Nuclear envelope defect. Shown are representative confocal indirect immunoflorescence images of HaCat cells transfected with BOD1-GFP and GFP (green). The innernuclear membrane was stained with emerin (red) and DNA was stained with DAPI (blue). Loss of emerin staining is shown in transfected cells with BOD1-GFP: Arrows indicate the nuclear envelope defect in transfected cells with overexpressed BOD1-GFP. Scale bar is 10 µm.

3.3.5.2.4. Overexpression of BOD1 leads to nuclear matrix defect

To investigate the nuclear matrix and due to the importance of lamins in nuclear organization (Peric-Hupkes et al. 2010), lamins A/C are the most reasonable candidates to investigate in this context.

The nuclear lamina is made up predominantly of intermediate filaments called lamins, of which there are two main types: type A and type B, according to homology in sequence, biochemical properties and cellular localisation during the cell cycle (Dechat et al. 2008; Fisher et al. 1986; McKeon et al. 1986). The Lamina form dimers through their rod domain and interact with integral proteins of the inner nuclear membrane such as: MAN1, lamina-associated polypeptide-1 (LAP1), SUN protein, lamina-associated polypeptide-2b (LAP-2b), lamin B receptor (LBR), emerin, and a nesprin-1 isoform (Dauer and Worman 2009). Lamins underlie the inner nuclear membrane and interact with portions of the chromatin. In mammals, there are two major A-type lamins, lamin A and lamin C, which are generated by differential splicing and alternative polyadenylation from one gene, the LMNA gene. There are also two major B-type lamins, lamin B1 and lamin B2, each encoded by its own gene. Besides providing mechanical support, the nuclear lamina regulates important cellular events such as DNA replication and cell division. Additionally, it participates in chromatin organization and it anchors the nuclear pore complexes embedded in the nuclear envelope (Dechat et al. 2008). Lamin A architecture depends on many elements, potentially including actin, actin-binding proteins, spectrins, nesprins, nuclear titin, LEM-domain proteins, nuclear myosin motors, etc. (Gruenbaum et al. 2005).

Thus, when there is a defect in the nuclear membrane accompanied by a chromatin organization defect, one can expect to observe a defect in Lamin A/C organization. As shown in figure 3-30, overexpression of BOD1 leads to a defect in nuclear matrix organization and therefore causes aggregation or collapsing the lamin A network but this defect was not observed in non-transfected cells or cells transfected only with GFP.

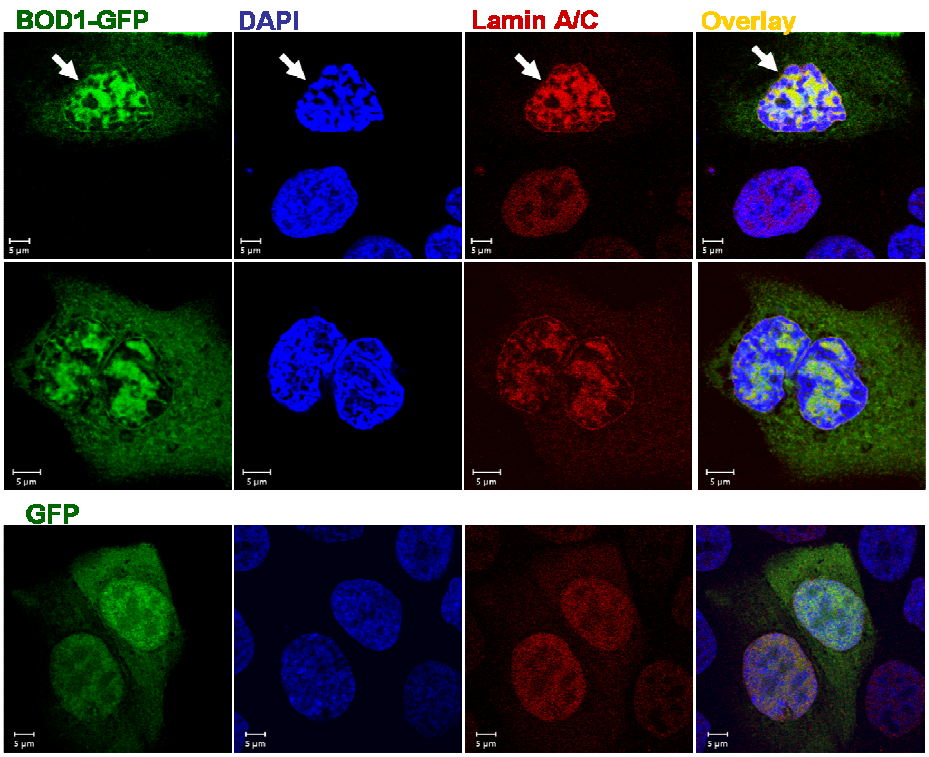

Figure 3-30: Overexpression of BOD1 leads to a defect in lamina organization. Confocal indirect immunoflorescence images of HaCaT cells transfected with BOD1-GFP or GFP are shown. Nuclear matrix was stained with Lamin A/C (red) and DNA was stained with DAPI (blue) to show the localization of Lamin A/C in cells transfected with BOD1-GFP. Overexpression of BOD1 causes the lamin A network to aggregate or collapse. There is still a thin but distinct "rim" stain for both BOD1 and lamin A, suggesting that BOD1 might colocalize with lamin A near the inner membrane and this interaction may be less disrupted by overexpression of BOD1. Scale bar is 5 µm.

3.3.5.2.5. Overexpression of BOD1 demostrated tubulin organization defect

It has been described before that centrosomes are controlling microtubule network emanation (Moynihan et al. 2009). Given the centrosomal localization of BOD1 (Porter et al. 2007), polymerization of microtubules was studied by overexpression of BOD1-GFP in HaCat cells and staining of the cells by

tyrosinated tubulin, which often used for the study of tubulin organization. Defects in tubulin polymerization were observed in transftected cells with BOD1-GFP but not with GFP alone (figure 3-31). The arrow in the figure indicates microtubule-organizing center (MTOC). MTOCs have two main functions: The organization of eukaryotic flagella and cilia and the organization of the Mitotic and Meiotic spindle apparatus separating the chromosomes during cell division, which are in line with the findings in the patient FB cells where some defects in cilia production and depolarization of the patient cells were observed (section 3.3.5.1.3).

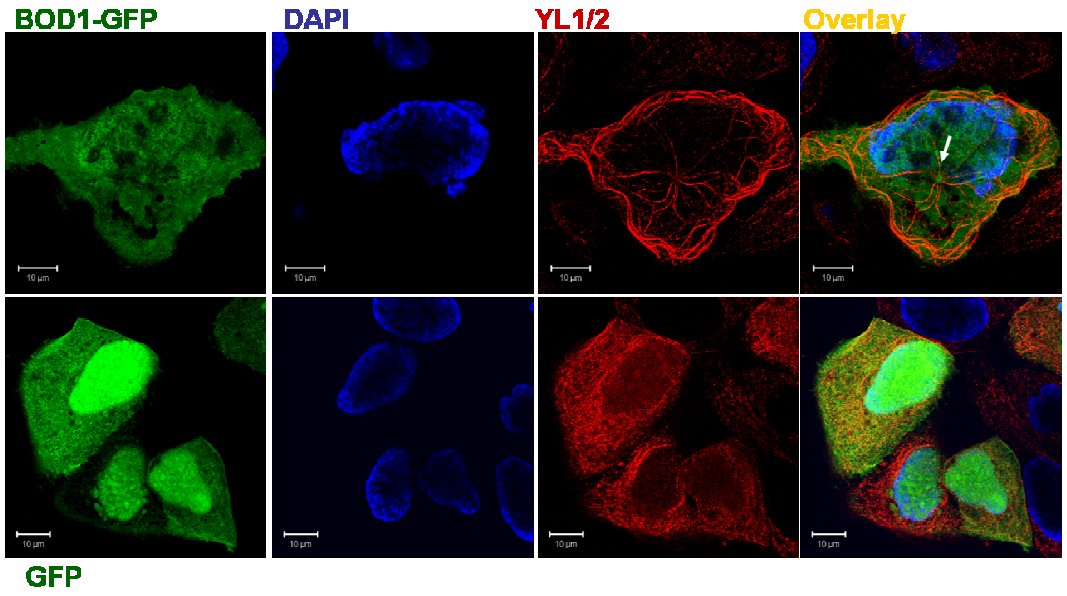

Figure 3-31: Overexpression of BOD1-GFP leads to tubulin organization defect. Confocal indirect immunoflorescence images are shown. Tyrosinated tubulin was stained with YL1/2(red). Overexpression of BOD1-GFP leads to delocalization of microtubule-organizing center (MTOC) to the surface which shown with arrow. Scale bar is 10 µm.

3.3.5.2.6. Characterization of BOD1 nuclear localization signal

Based on the observations up to here, there is some preliminary evidence as to a role of BOD1 in the maintenance of nuclear structure, moreover a previous

study on BOD1 (Porter et al. 2007) suggested that this protein first localizes to the nucleus and then moves to the cytoplasm. Thus, I wanted to localize the Nuclear Localization Signal (NLS) in this protein by generating several BOD1 deletion constructs and transfecting them into FB cells. BOD1 is a very small protein, and BOD1-Cherry can be easily diffuse in or out of the nucleus, therefore the red colour out of cherry expression always is visible in both cytoplasm and nucleus but with different intensity. To find out the expression pattern of BOD1 from the different constructs, the transfected cells were imaged stochastically by LSM510 confocal microscope and subsequently and the expression intensity for each construct was calculated (as shown in figure 3-32 A) (all the individual values are shown in Table S5, appendix H). The NLS is suggested to be located on the N-terminus of BOD1 (figure 3-32 A & B).

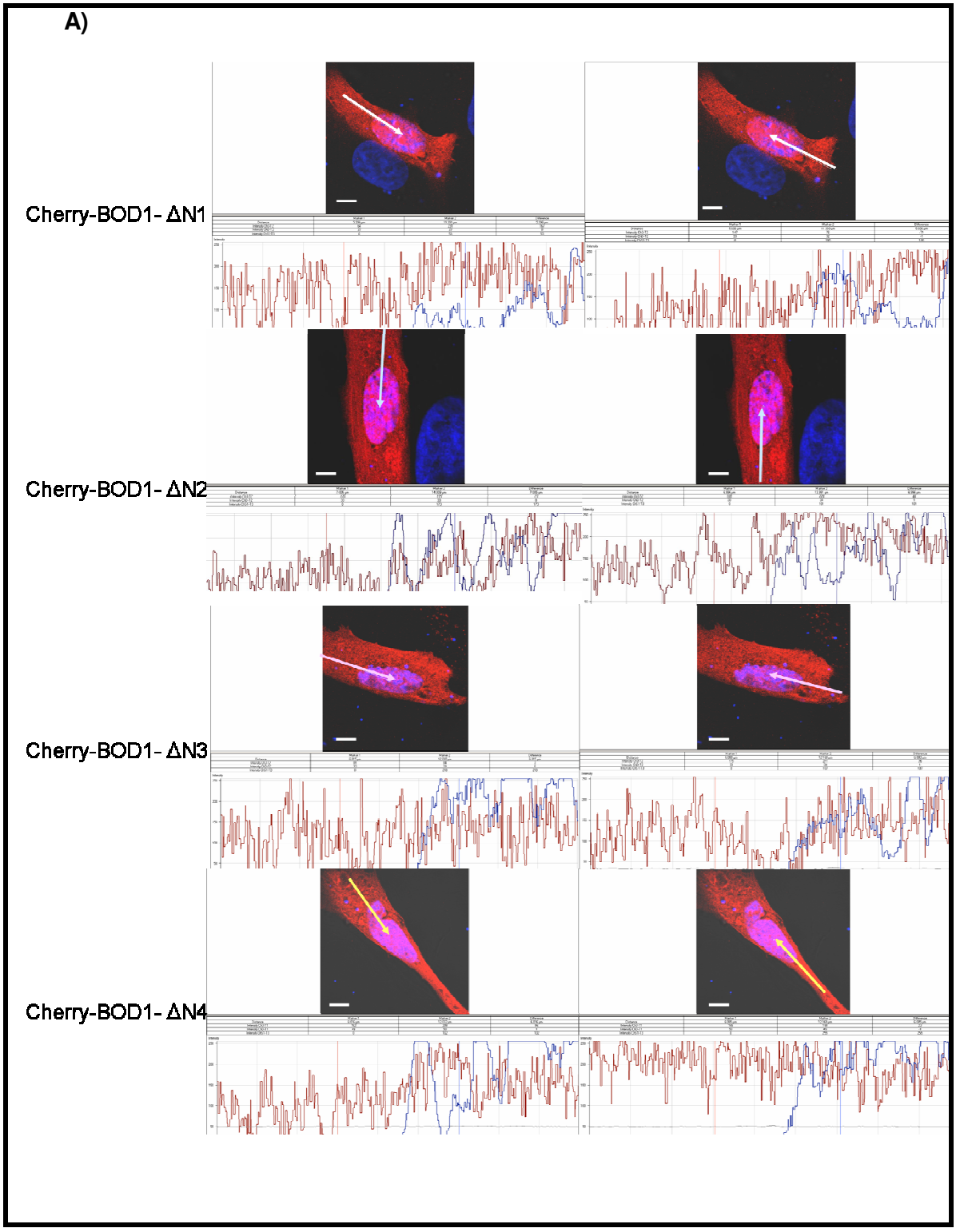
A)
Cherry-BOD1- ΔN1
Cherry-BOD1- ΔN2
Cherry-BOD1- ΔN3
Cherry-BOD1- ΔN4

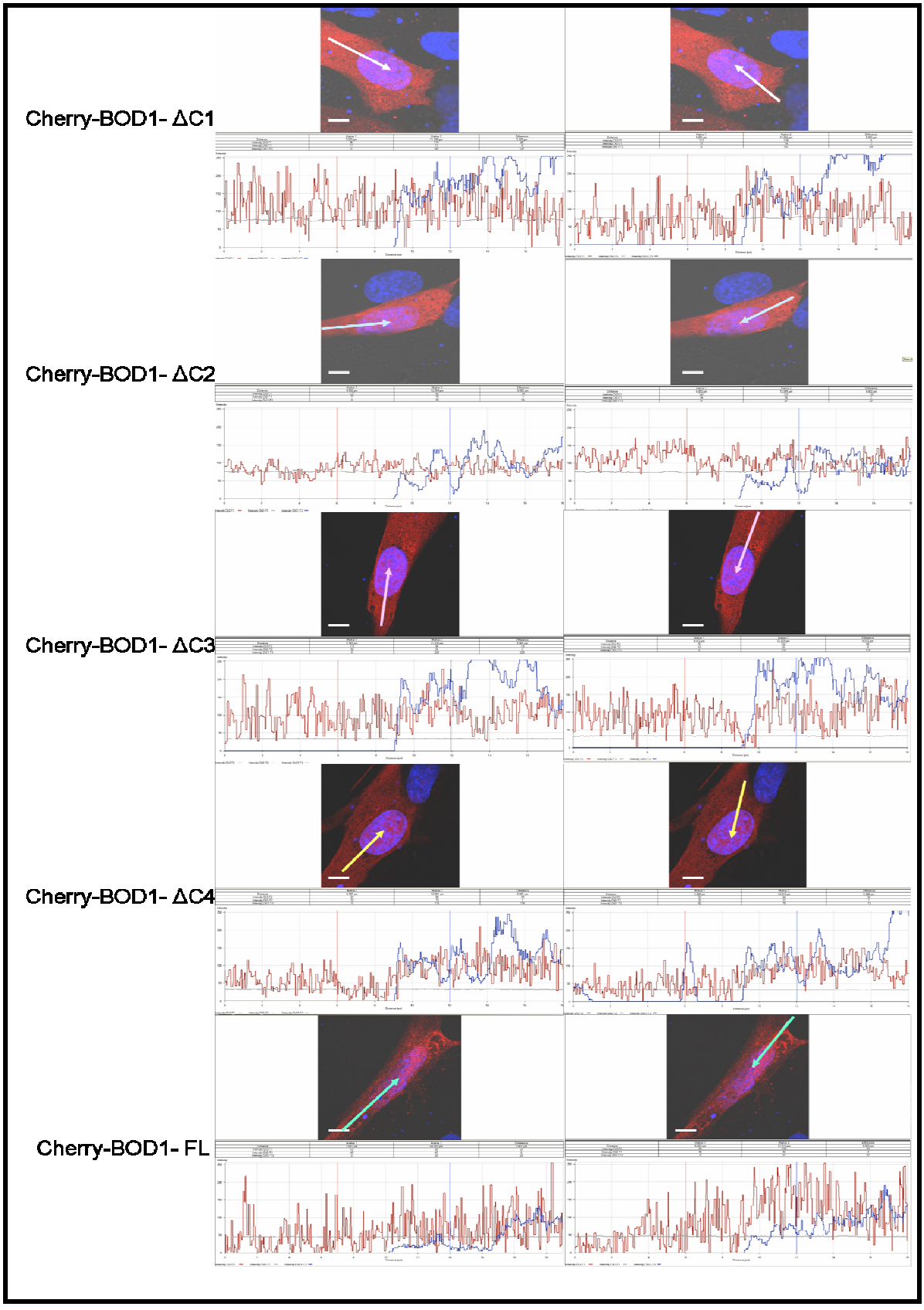
Cherry-BOD1- ΔC1
Cherry-BOD1- ΔC2
Cherry-BOD1- ΔC3
Cherry-BOD1- ΔC4
Cherry-BOD1- FL

B)

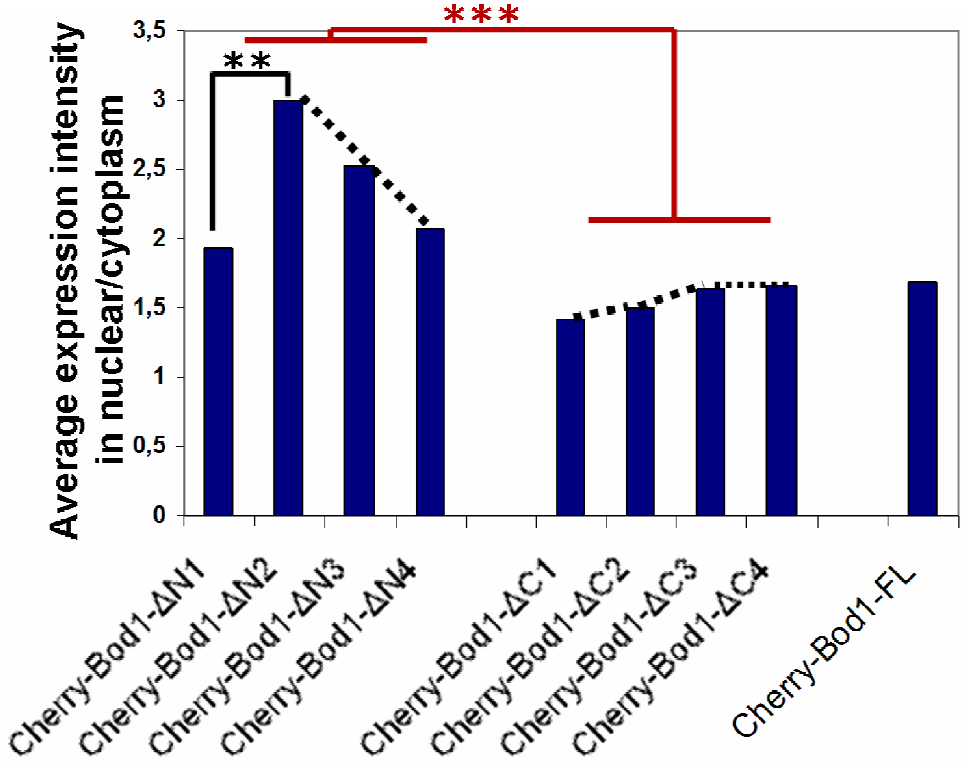

C)

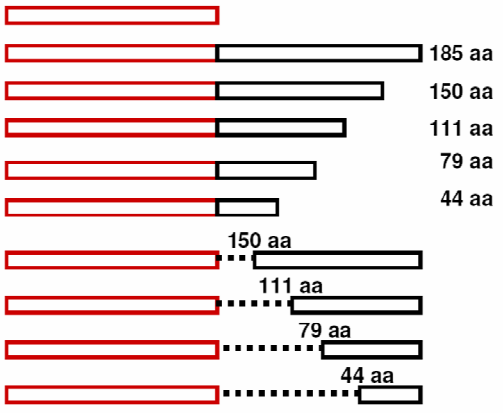

Name	N/C value
Cherry	
Cherry-Bod1-FL	1.69
Cherry-Bod1-ΔC1	1.42
Cherry-Bod1-ΔC2	1.49
Cherry-Bod1-ΔC3	1.63
Cherry-Bod1-ΔC4	1.66
Cherry-Bod1-ΔN4	2.07
Cherry-Bod1-ΔN3	2.53
Cherry-Bod1-ΔN2	3.00
Cherry-Bod1-ΔN1	1.93

Figure 3-32: Nuclear Localization Signal might be located on N-terminus of BOD1. A) Expression intensity of each construct per cell was measured. I drew two lines on each cell from opposite directions, so each line covers 50% length in the cytoplasm and 50% length it covers at least half of the nucleus; Each line gives two values, one equivalent to the expression intensity in the cytoplasm and another one in the nucleus. I did the same for 10 cells per construct. The results were calculated from the average number of division of the "N/C values" (nuclear intensity/cytoplasmic intensity). Here one example of how the measurments were performed are shown. Scale bar is 5 µm. **B)** The average values from all nine constructs were plotted. The value of 1 means no enrichment and equal distribution in both nucleus and cytoplasm, value of more than 1 means positive enrichment in nucleus; the higher value means higher enrichment in nucleus. *** $p<0.005$ and **$P<0.05$. **C)** The schematic represents the results from measurenment of expression intensiy in nuclear and cytplasm or the "N/C values". Suggesting NLS is located in N-terminus of BOD1, around amino acids number 111 to 141. N stands for Nucleus and C for Cytoplasm.

3.3.5.3. Illumina gene expression profiling

It is known that control of transcription is mediated by three main mechanisms:

1- Transcription factors (Hochedlinger and Plath 2009; Welstead et al. 2008).
2- Posttranslational modification of Histones or DNA methylation (Huangfu et al. 2008; Mikkelsen et al. 2008; Shi et al. 2008).
3- Higher-chromatin organization (Dekker 2008; Fraser and Bickmore 2007).

Almost nothing is known about the mechanism of the latter, but probably the nuclear membrane is one of the major players (Peric-Hupkes et al. 2010). As my confocal microscopy observations suggested that BOD1 might be involved in chromatin organization and thereby a defect in BOD1 might influence gene expression I set out to check the difference in expression pattern between patients and controls. Whole genome expression profiling (using IlluminaSentrix® Human-6 Expression BeadChip version2) was performed in order to compare the expression levels of ~48,000 known and unknown genes in LCL cells between patient V:3 and six separate controls. Since the patient and controls were not sex-matched all the known genes on x-chromosome

were removed from the output list of the experiment (using Microsoft office access software) prior to further procedures, leaving ~46,000 genes of which, 88 were down-regulated and 607 were up-regulated in the patient with differential scores ≤±13 (corresponding to a P-value of ≤0.05). Subsequently the DAVID functional annotation database (Dennis et al. 2003; Huang da et al. 2009) was used for classification of the biological processes from these down- and up-regulated genes. The down-regulated genes did not seem to participate in any particular pathway, however interestingly some of the up-regulated genes were found to be involved in pathways related to chromatin organization and regulation of gene expression, suggesting that BOD1 participates in these pathways as well. A summary of the functional clustering of the up-regulated genes is shown in Table 3-2 (see Table S6, Appendix I for the full list of the proteins). Interestingly, the extent of up-regulation was particularly high among genes that are critical in cognition such as: *ARHGEF5* (Regulation of immature dendritic cell migration), *DPYSL4* (neurogenesis), *AGRN* (synapse organization and biogenesis), *PITPNM1* (brain development) and *ATN1* (central nervous system development), *KIF13B* (Neuronal polarity) and *SETBP1* (generates severe form of mental retardation).

Table 3-2: Functional annotation clustering for Up-regulated genes in patient (DAVID annotation tool)

Enrichment score. 2.37	**Count**	**P_Value**	**Enrichment score**
Nucleus	181	2.6E-5	8.75
Gene expression	117	5.8E-2	2.34
DNA metabolic process	45	5.8E-5	1.91
Transcription	65	3.3E-2	1.65
Gene expression	117	5.8E-2	1.65
Regulation of gene expression	88	9.4E-2	1.65
Chromatin organization and biogenesis	21	6.8E-3	1.63
Chromatin modification	13	1.0E-3	1.63
Chromatin regulator	9	3.2E-2	1.63
Establishment and/or maintenance of chromatin architecture	15	5.5E-2	1.63
DNA packaging	15	6.2E-2	1.63

Consequently, I picked some of the up-regulated genes randomly to verify the expression profiling data by performing qRT-PCR (Primers shows in Table S7, Appendix J) on LCL cells from patients and controls (figure 3-33).

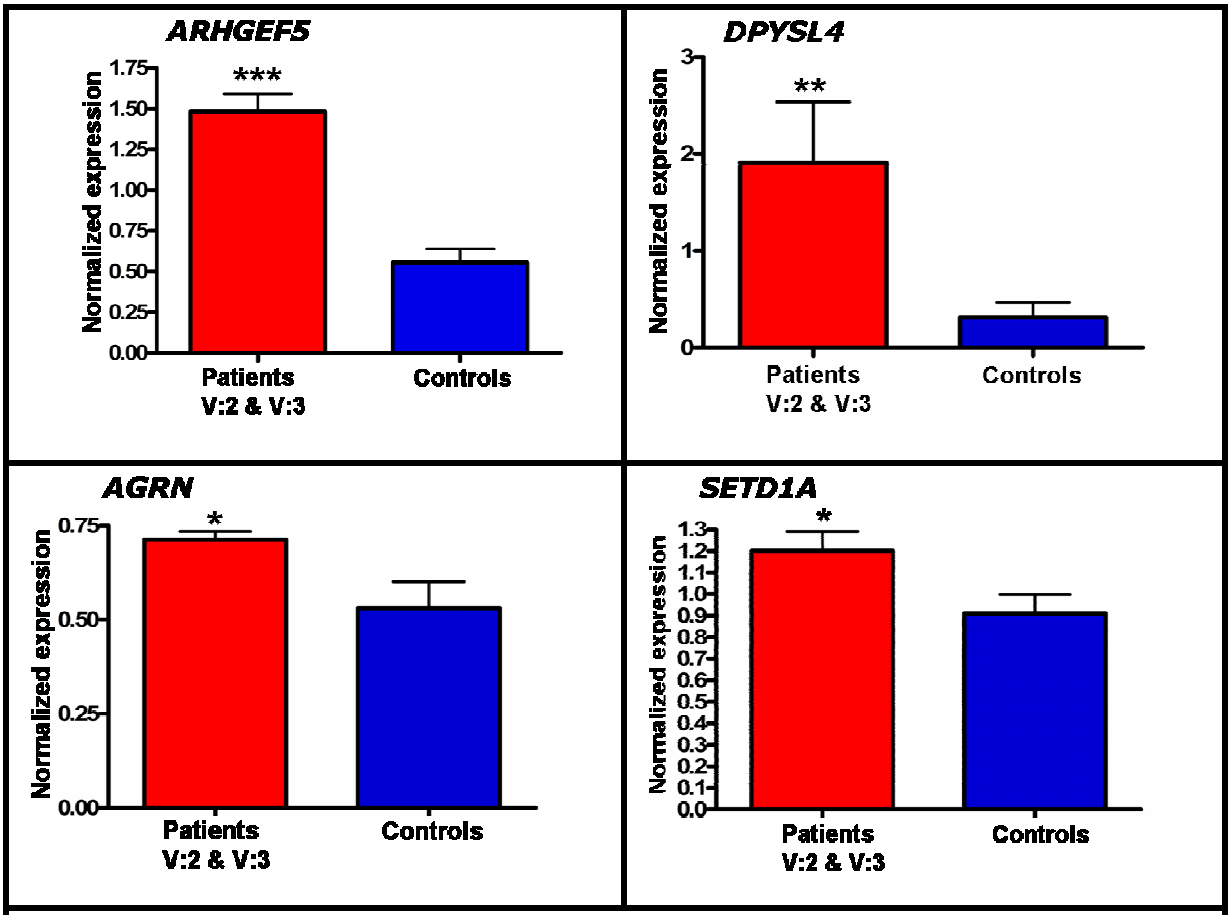

Figure 3-33: Verification of the whole genome expression profiling data using qRT-PCR. The experiments were performed in triplicate. The results shown here are from pools of two different patients and three different controls. The chip data were verified, as increased expression of all four candidate genes in patients were observed. ***:P<0.0001, **: P<0.01 and *: P<0.05 (Student's t-test). Error bars represent the SEM.

3.3.6. BOD1 might localize in the synapse

To find out whether BOD1 has a function beyond its involvement in the cell cycle with respect to the ID phenotype of the patients, neurons are a particularly interesting study object. For these studies I chose to use mouse. To find the localization of BOD1 in neuronal cells, I transfected primary

neuronal cells with BOD1-GFP or GFP and subsequently stained them with different pre/post-synaptic markers. The staining with presynaptic markers worked much better than post-synaptic ones, because at the stage where the cells were transfected (one week after preparation), postsynaptic structures are not yet fully formed, hence staining with PSD95, a post synaptic density protein, didn't work properly.

The results are shown in figure 3-34, BOD1 is co-localized with Bassoon and NR2B. Bassoon is a 420 kDa protein and localizes at presynaptic nerve terminals and NR2B is a subunit of NMD receptor. BOD1 is not expressed in all the synapses, which it might be an explanation for the mild to moderate phenotype of ID as a result of mutation in *BOD1*.

I have repeated the experiment with an independent mouse and the results were reproducible.

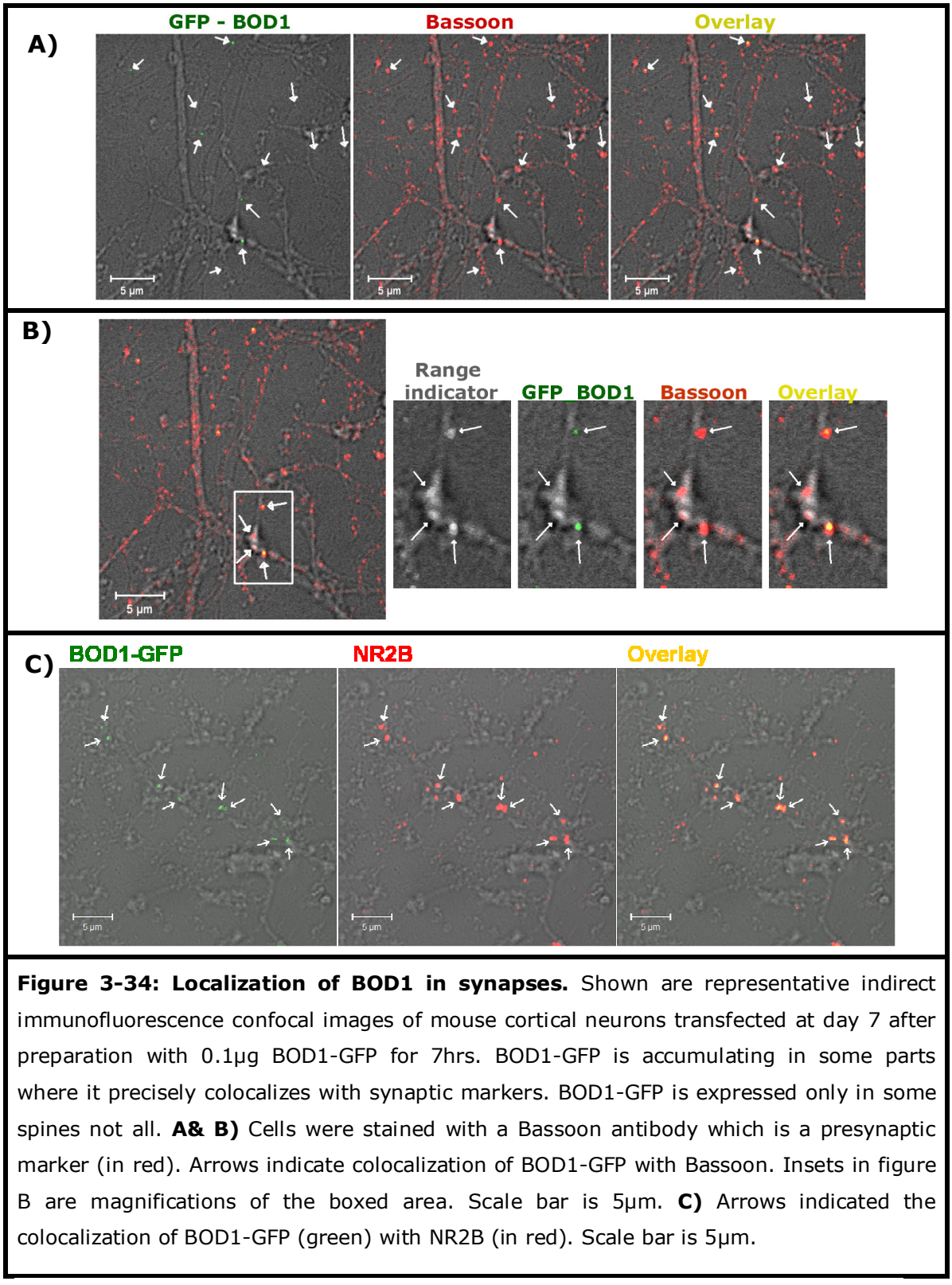

Figure 3-34: Localization of BOD1 in synapses. Shown are representative indirect immunofluorescence confocal images of mouse cortical neurons transfected at day 7 after preparation with 0.1µg BOD1-GFP for 7hrs. BOD1-GFP is accumulating in some parts where it precisely colocalizes with synaptic markers. BOD1-GFP is expressed only in some spines not all. **A& B)** Cells were stained with a Bassoon antibody which is a presynaptic marker (in red). Arrows indicate colocalization of BOD1-GFP with Bassoon. Insets in figure B are magnifications of the boxed area. Scale bar is 5µm. **C)** Arrows indicated the colocalization of BOD1-GFP (green) with NR2B (in red). Scale bar is 5µm.

The shown in figure 3-35 is staining with Bassoon and ProSAP/Shank3 which is a postsynaptic marker. As shown in this figure BOD1 does not always colocalize with all the synaptic markers. As it colocalizes with Bassoon but doesn't colocalize with ProSAP/Shank3 which serves as another control.

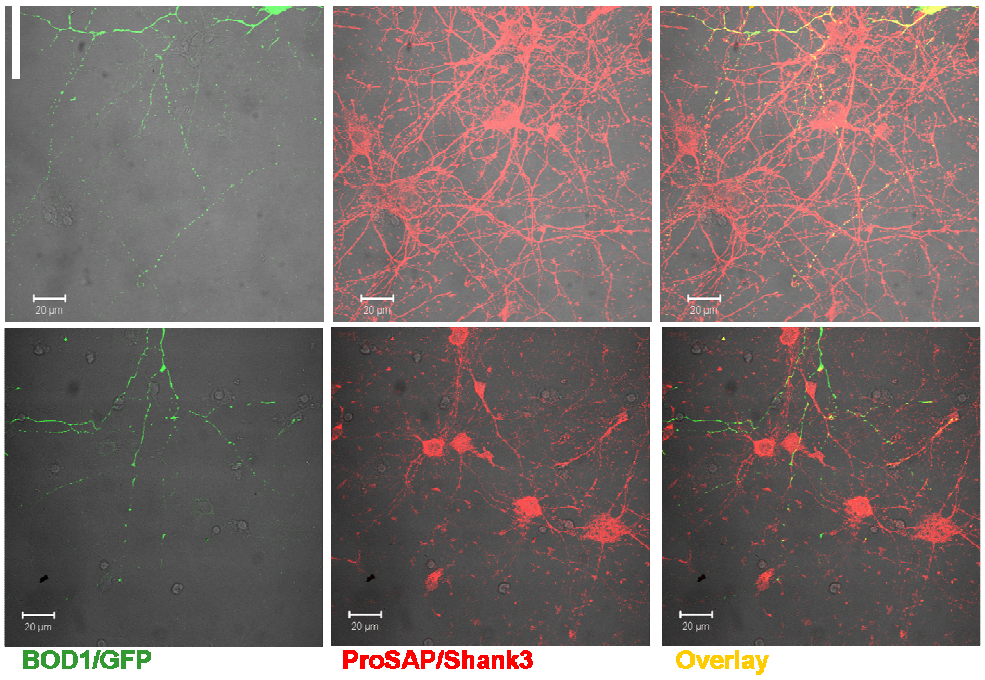

Figure 3-35: BOD1 is not colocalized with all the synaptic markers. Shown are indirect immunofluorescence confocal images of mouse cortical neuron transfected at day 8th after cells preparation by 0.1µg BOD1-GFP for 7hrs. BOD1 is colocolized with Bassoon but does not colocolized with ProSAP2/Shank3. Scale bar is 20 µm.

Expression of GFP compared to BOD1-GFP in primary neuronal cells is shown in figure 3-36. GFP is not colocalized with bassoon and it has ubiquitous distribution throughout the cell while BOD1-GFP is not ubiquitously expressed throughout the cell and some accumulations of green colour always colocalize with bassoon.

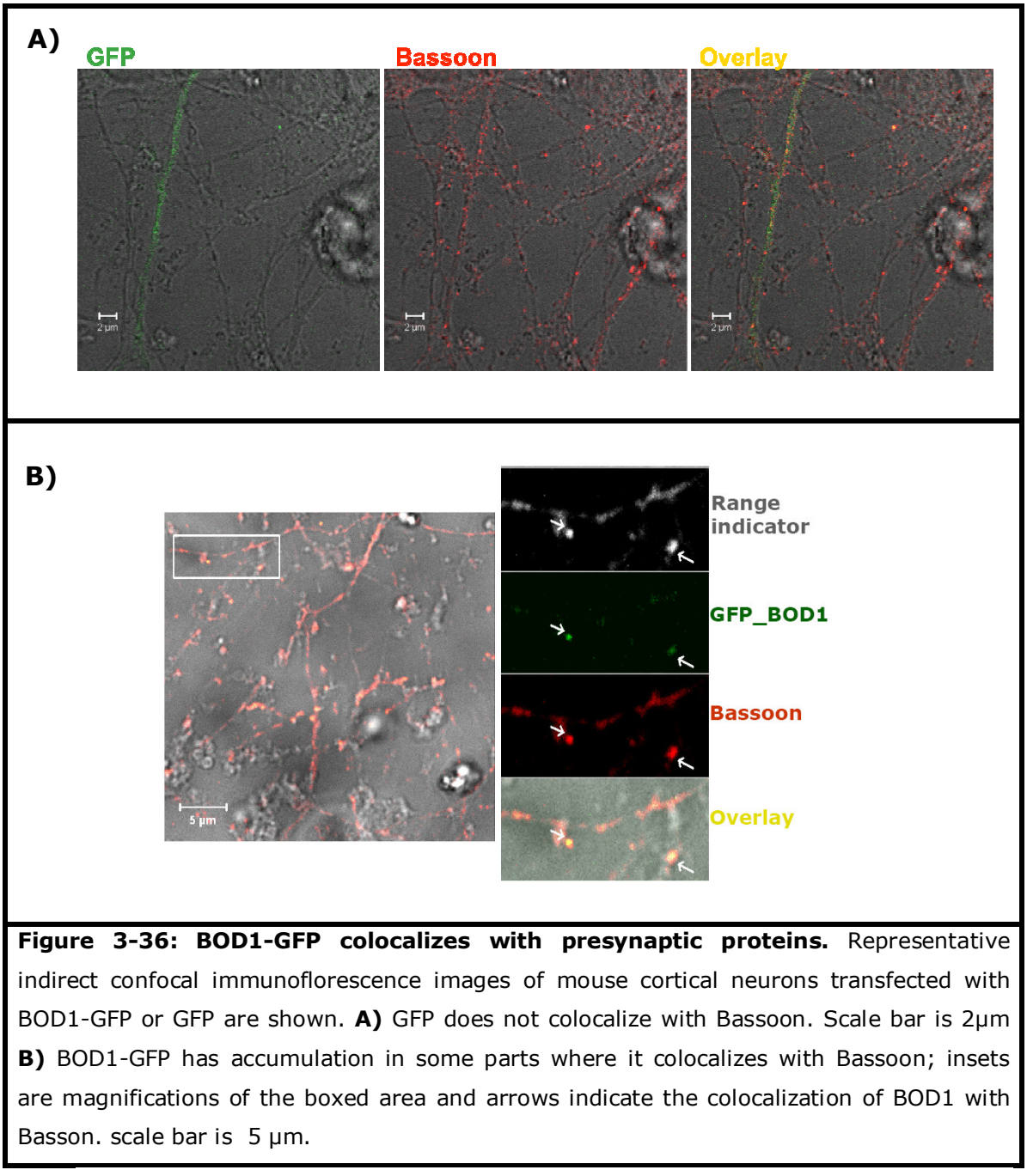

Figure 3-36: BOD1-GFP colocalizes with presynaptic proteins. Representative indirect confocal immunoflorescence images of mouse cortical neurons transfected with BOD1-GFP or GFP are shown. **A)** GFP does not colocalize with Bassoon. Scale bar is 2µm **B)** BOD1-GFP has accumulation in some parts where it colocalizes with Bassoon; insets are magnifications of the boxed area and arrows indicate the colocalization of BOD1 with Basson. scale bar is 5 µm.

4. Discussion

The basis for this PhD thesis is a *BOD1* nonsense mutation I found in a large consanguineous Iranian family where a genomic autosomal recessive intellectual disability (ARID) locus on chromosome 5q35.2 had already been identified by linkage analysis. All four affected patients in both family branches are females and are affected by mild ID as well as obesity and oligomenorrhea. In this study, we investigated the genotypic and phenotypic correlation to interpret the two major phenotypes, ID and oligomenorrhea in the patients.

Oligomenorrhea is characterized by infrequent uterine bleeding episodes with intervals of more than 35 days, the duration of such events may vary. This condition can be caused by eating disorders, however, obesity was not only observed in the patients but also in an unaffected sibling as well as the mother. Therefore it cannot be concluded that the patients' mutation is the cause for obesity. Furthermore oligomenorrhea cannot be a result of obesity in this family as the obese mother has six children. On the other hand, several researchers hypothesize that an as-yet unrecognized neuroendocrine phenomenon may be involved, and therefore the menstrual irregularities may be related to the biological underpinnings of these disorders, rather than a result of nutritional deficiencies (Greydanus and McAnarney 1982; Nichols et al. 2007). Hence endocrinological tests to check for possible hormonal deficiency and ultrasound investigations to check for structural defects in ovaries were carried out, but no abnormalities could be detected. Therefore neither obesity nor hormonal deficiency can be considered as the cause for oligomenorrhea in the patients. This suggests that the observed genetic defect most likely is involved in the etiology of this feature as well as for the ID observed in the patients.

4.1. Biorientation Defective 1 (BOD1)

BOD1 or FAM44B (family with sequence similarity 44 member B) is one of three related proteins that constitute the Fam44 protein family. These proteins are encoded by genes on three different chromosomal loci (4p16.1, 5q35.2,

and 18q21.31 for Fam44A, FAM44B, and Fam44C, respectively), suggesting that the three genes have arisen from a gene duplication event. Figure 4-1A shows that Fam44A is approximately twice as large as the other family members because of a large C-terminal extension, which does not appear to relate to any other known protein. FAM44A is very similar to BOD1 at the N terminus except that it contains a long string of proline residues at the extreme N terminus. BOD1 and Fam44C are rigorously similar (the cDNA of FAM44B is very similar to FAM44C on the genomic level). FAM44 protein family is highly conserved through metazoans as shown in figure 4-1B.

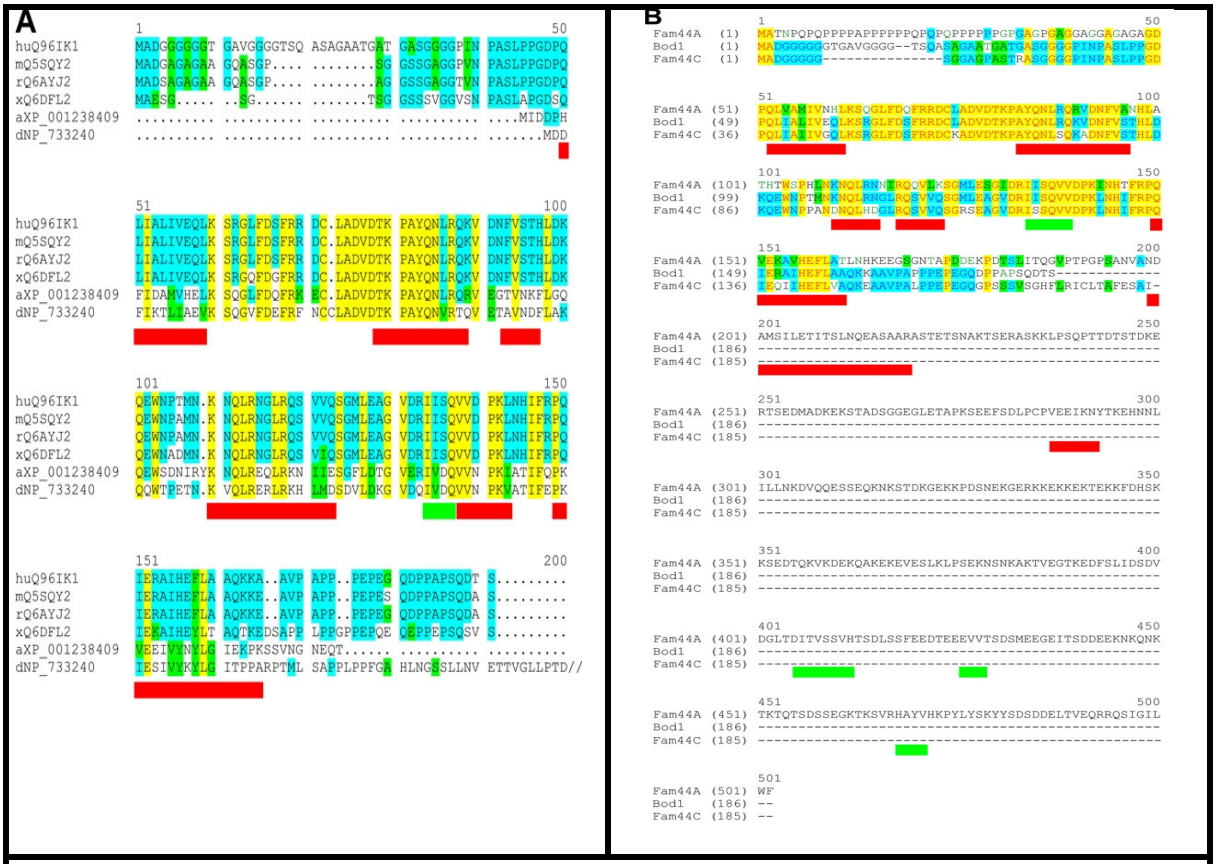

Figure 4-1: Fam44 protein family sequence alignment. Identical amino acids are coloured in yellow, amino acids shared by two or more sequences are coloured blue, and weakly similar amino acids are shaded green. Red and green bars below alignments indicate positions of predicted helices and β sheets, respectively (Porter et al. 2007). **A.** Alignment of conserved *BOD1* sequences. Human (hu Q96IK1), mouse (m Q5SQY2), rat (rQ6AYJ2), Xenopus (xQ6DFL2), Anopheles (aXP_001238409), and Drosophila (dNP_733240) sequences are shown. **B.** Alignment of human FAM44 family members. *BOD1* has orthologues in mouse, rat, Xenopus, Drosophila and Anopheles. [Image source: (Porter et al. 2007)].

According to Stanford source data (http://smd.stanford.edu/cgi-bin/source/sourceSearch), *BOD1* is expressed in 36 different tissues including blood, brain, uterus, placenta, cervix and ovary (http://www.ncbi.nlm.nih.gov/UniGene; UniGene Hs.425091). Based on the Allen brain atlas mouse project (http://www.brain-map.org), *bod1* is mainly expressed in cerebellum (cerebellar cortex and cerebral cortex) and Hippocampus (figure 4-2); the cerebellum is responsible for motor control as

well as several types of motor learning. The hippocampus is closely associated with the cerebellar cortex and plays an important role in long-term memory. Taken together, these findings strongly support an involvement of *BOD1* in higher brain functions.

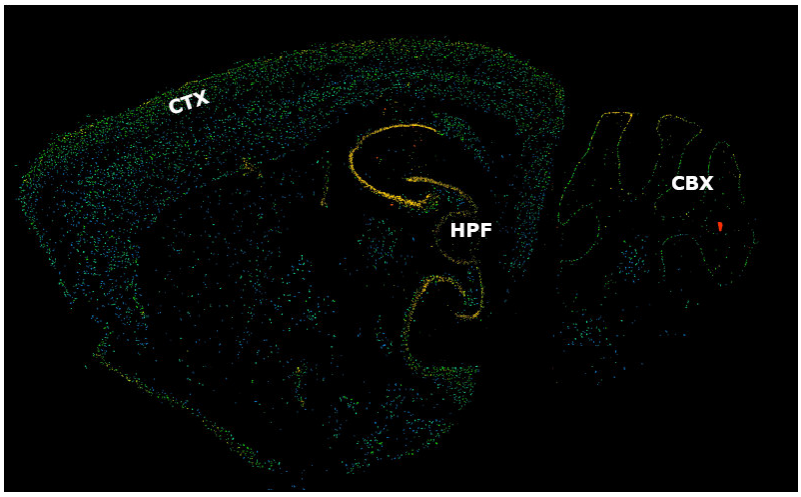

Figure 4-2: Expression analysis of RIKEN cDNA 2310022M17 gene (*bod1*). In sagittal section of brain from a Mus musculus male (strain C57BL/6J) at age of 55days. In the mouse brain *bod1* is mostly expressed in the cerebral cortex (CBX) and hippocampus (HPF: hippocampal formation). It is also found in the cerbellar cortex (CTX)(image source: http://www.brain-map.org).

The length of the full transcript of *BOD1* is 185 bp and the gene product has a molecular weight of 19196 Da.

4.1.1. BOD1 is required for the correction of syntelic attachment

The Spindle is a microtubule-based structure, which is responsible for chromosome segregation during mitosis. Spindle microtubules attach to chromosomes through unique structures called kinetochores, which are located adjacent to the centromeric heterochromatin. Sister kinetochores on each chromosome are attached to micro- tubules from opposite poles of the spindle, which ensures sister chromatids to segregate faithfully, and that they move to

opposite daughter cells when these dissociate during anaphase: The segregation of sister chromatids to opposite spindle poles during anaphase is dependent on the prior capture of sister kinetochores by microtubules extending from opposite spindle poles (bi-orientation). The mechanism of establishing and maintaining the proper bi-oriented attachment of chromosomes to spindle microtubules is complex, thus inappropriate attachment frequently occurs (Compton 2007).

Accurate chromosome segregation is required for cell and organism viability. Errors are irreversible and cause aneuploidy. Improper attachments are frequently made during early stages of spindle assembly, as shown in figure 4-3 (Compton 2007). Syntely arises if chromosome orientation favours the capture of centrosomal microtubule with the same charge (e.g. plus ends) from the same pole or when microtubules of sister kinetochores are pulled toward the same pole through pole-focusing mechanisms pull. The frequency of syntely in unperturbed cells at present is unknown, partly because syntelic attachments are difficult to visualize in living cells. Monotely occurs when one kinetochore forms microtubule attachments before its sister (Rieder and Salmon 1998). Merotely is fairly common in early mitosis and, if it remains uncorrected, leads to lagging chromatids at anaphase that are easily detected in the spindle midzone subsequent to migration of all other chromatids toward poles and results in incorrect chromosome bi-orientation (Cimini and Degrassi 2005).

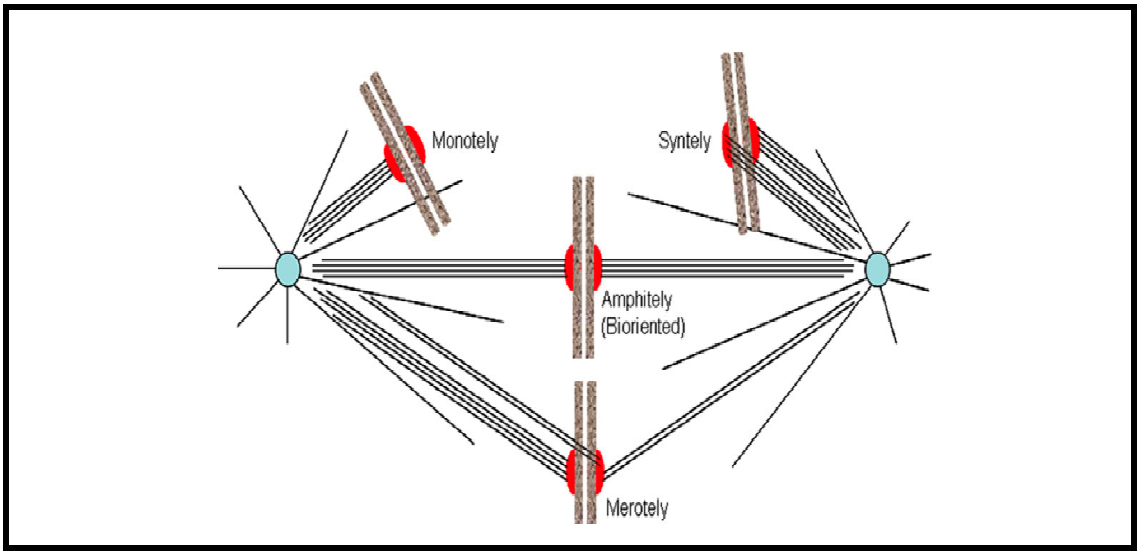

Figure 4-3: Normal and abnormal microtubule attachments to chromosomes. In mammalian cells, multiple microtubules attach to each kinetochore (red). Precise chromosome segregation requires sister kinetochores on chromosomes to attach to microtubules from opposite spindle poles, leading to biorientation or amphitely. Incorrect orientations can be amphitelic (normal bipolar attachment of sister centromeres to opposite poles); merotelic (abnormal attachment of one kinetochore) to both poles or syntelic (abnormal attachment of both sister kinetochores to one pole) [Image source: (Compton 2007)].

The combined proteomic analysis of Xenopus in vitro-assembled chromosomes with RNAi and live-cell imaging in HeLa cells revealed BOD1 as a novel protein required for proper chromosome biorientation. BOD1 exists in two forms, one that is most likely a monomeric, unbound form and one in a complex of ~490 kDa. BOD1-GFP localizes to the centrosome throughout the cell cycle and to kinetochores only during mitotis. Centrosomes function as a microtubule organizing center (MTOC), in which γ-tubulin provides a microtubule anchoring machinery by forming a γ-tubulin ring complex (γ-TuRC) (Shimada and Komatsu 2009). They are responsible for the attachment of chromosomes to the mitotic and meiotic spindles and are essential for chromosome segregation (Hemerly et al. 2009). The centrosome performs most of its function via the kinetochore, which contains a variety of proteins with functions ranging from establishing a centromeric nucleosome structure to checkpoint control.

Figure 4-4 shows Immunoflorescence imaging of BOD1 (Porter et al., 2007). Depletion of *BOD1* by siRNA in HeLa cells causes elongated mitotic spindles with severe biorientation defects. *BOD1*-depleted cells formed syntelic attachments that could oscillate and generate enough force to separate sister kinetochores suggesting that microtubule–kinetochore interactions were intact. Indeed releasing cells from a monastrol block, which increases the frequency of syntelic attachments, further increased the number of cells displaying bi-orientation defects (Porter et al. 2007). Syntelic attachment must be re-oriented to be converted to proper bi-orientation. This re-orientation is facilitated by Aurora B–MCAK (mitotic centromere-associated kinesin) interaction (Dewar et al. 2004; Hauf et al. 2003; Lampson et al. 2004; Tanaka

et al. 2002). MCAK and Aurora B kinase (Ipl1 in budding yeast) both co-localized to the centrosome. Aurora B kinase functions in the attachment of the mitotic spindle to the centromere and localizes to microtubules near kinetochores, over-expression of this enzyme creates aneuploid cells [Review: (Liu and Lampson 2009)]. MCAK belongs to the KinI subfamily of kinesin-related proteins, in hamster it is shown that MCAK is an ATPase that catalytically depolymerizes microtubules. It is proposed that up to 14 MCAK dimers assemble at the end of a microtubule to form an ATP-hydrolyzing complex that processively depolymerizes the microtubule (Hunter et al. 2003). Aurora B kinase controls the centromere localization and catalytic activity of the microtubule depolymerase MCAK, which may help to correct improper chromosome attachments (Gorbsky 2004).

Detailed examination of mal-oriented chromosomes in *BOD1* depleted cells revealed a high incidence of syntelic attachments which demonstrated was due, at least in part, to the failure of the Aurora B kinase to phosphorylate MCAK, in fact *BOD1* depletion did not affect the activity or localization of Aurora B, but caused mislocalisation of the microtubule depolymerase MCAK and inability to properly phosphorylate the kinesin MCAK. BOD1 is not required for the spindle assembly checkpoint but appears to be required either for the efficient detection or removal of syntelic attachments (Porter et al. 2007). Thus, it plays a critical role in defining and monitoring the proper attachment of microtubules to the kinetochore.

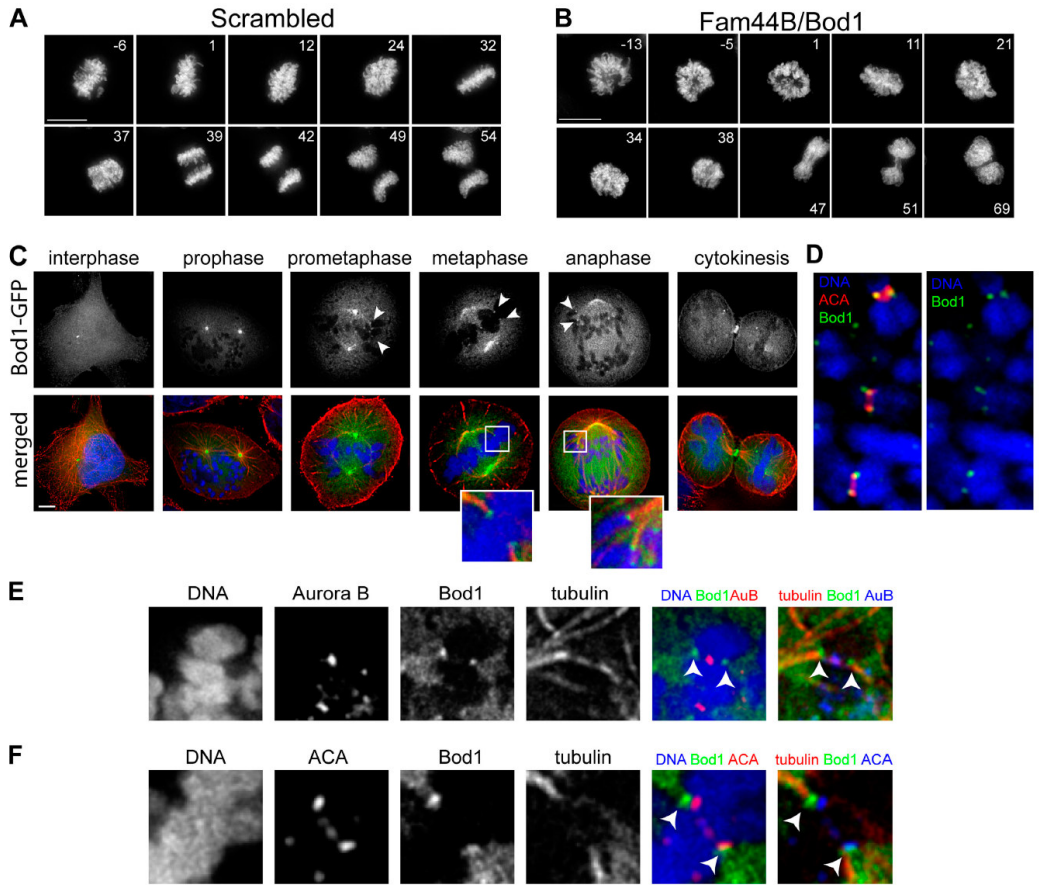

Figure 4-4: BOD1 is localizing to centrosomes and kinetochores. A and B. Selected maximum intensity projections from time-lapse images of HeLa cells show gene-specific mitotic phenotypes. Cells were transfected with the pU6YH plasmid expressing scrambled shRNA (A) or shRNA targeting Bod1 (B). Images were taken 60 hr after transfection over a period of 60–120 min. Numbers indicate time (minutes) from the establishment of a metaphase plate. **C.** HeLa cells transfected with Bod1-GFP were fixed after 48h with PFA. (top) Localization of Bod1-GFP at various points in the cell cycle. (bottom) A merged image with microtubules (red), chromosomes (blue), and Bod1-GFP (green). Arrowheads indicate concentrations of Bod1-GFP at microtubule ends. Insets are magnified images of boxed areas. **D.** Chromosome spreads of nocodazole-arrested HeLa cells stained for endogenous Bod1 (green), ACA (red), and DNA (blue). **E** and **F.** The localization of Bod1-GFP was determined with respect to Aurora B (E) and ACA (F). Kinetochore localization of Bod1-GFP is indicated by arrowheads. [Image source: (Porter et al. 2007)].

4.1.2. Depletion of BOD1 leads to delocalization of Sgo1 and premature chromosome separation

In mammalian cells Shugoshin (Sgo1), Japanese for guardian spirit, is known to be a protector of centromeric cohesin during meiotic divisions. In flies, the localization of Sgo1 to centromeres depends on the action of INCENP and Aurora B; In contrast, the release of Sgo1 has been shown to depend on the POLO kinase (Plk1) (Clarke et al. 2005). Studies in Xenopus and humans also elucidated the role of Budding unhibited by benzidazoles 1 or Bub1 (a spindle-checkpoint kinase that helps direct PP2A to centromeres), in maintaining Sgo1 protection at the centromere by neutralizing Plk1-mediated chromosomal removal of Sgo1 (Kitajima et al. 2005; Tang et al. 2004; Tang et al. 2006). The separation in meiosis I (homologs separate from one another) is unique as centromeric cohesin (cohesion between sister chromatids) is maintained through the first division in a Sgo1-dependent manner, and only at the second meiotic division is all cohesin lost and sister chromatids allowed to separate (Kitajima et al. 2004). Evidence suggests that indeed the centromeric protection of cohesion is secondarily derived from the role of Sgo1 in establishing correct bipolar spindle attachments (Kawashima et al. 2007; Vanoosthuyse et al. 2007). A summary of all the suggested pathways which are involving in Sgo1 function in cohesion protection shows in figure 4-5.

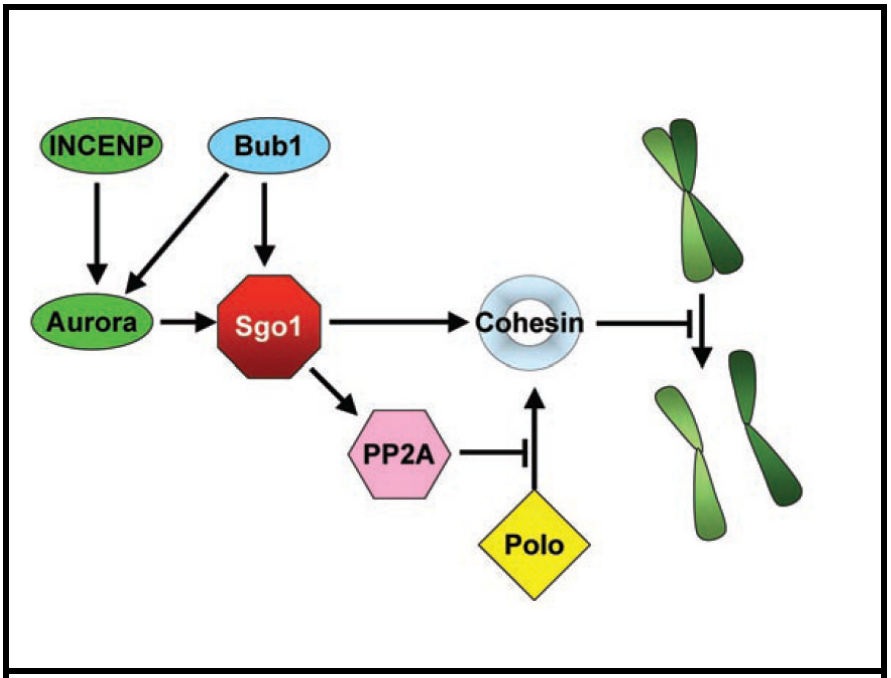

Figure 4-5: A model representing multiple pathways for Sgo1 action in cohesion protection. A pair of sister chromatids is shown in green. [Image source: (Macy et al. 2009)]

It is shown that Depletion of *BOD1* with siRNA results in premature sister chromatid separation like in *Sgo1* depleted cells (figure 4-6). Also depletion of BOD1 leads to delocalization of Sgo1 from centromeres. However, no direct interaction between Sgo1 and BOD1 has been found; Bod1-GFP consistently localises to the outer kinetochores, whereas Sgo1 is located largely at the inner-centromere (Porter et al. unpublished).

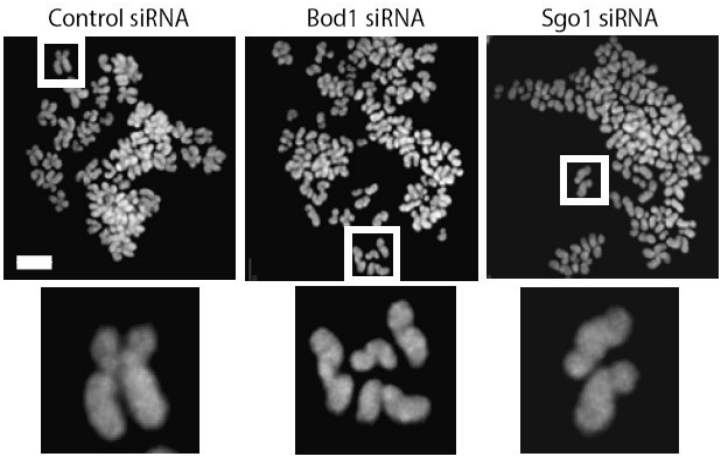

Figure 4-6: Depletion of *BOD1* leads to premature sister chromatid separation. Chromosome spreads of HeLa cells transfected with control *BOD1* or *Sgo1* siRNA is shown. In control cells typical bivalent sister chromatids joined at the primary constriction however in both BOD1 and Sgo1 depleted cells sister chromatids were separated [Image source: (Porter et al. unpublished)].

4.1.3. BOD1 is a regulator of the G2/M kinase Plk1

Sgo1 has previously been implicated in the localization of Plk1 kinase to kinetochores during mitosis (Powells et al., 2007) and Plk1 and Sgo1 have reciprocal requirements of each other for their proper localization. Depletion of BOD1 from HeLa cells results in loss of both Plk1 and Sgo1 variants from both kinetochores and centrosomes, suggesting BOD1 is upstream of both Plk1 and the Sgo1. Polo-like kinases (Plk) have emerged as key regulators of mitotic and meiotic divisions in all model organisms where they have been analyzed to date. The Plk family comprises four related serine/threonine kinases with different subcellular localization and functions in mammals (van de Weerdt and Medema 2006). Mammalian Plk1 and its counterparts in other organisms (Cdc5 in budding yeast, Plo1 in fission yeast, Polo in Drosophila, Plk-1 in nematdes, and Plx1 in Xenopus) are most important regulators of cell proliferation within the Plk family. Plk1 localizes to many structures throughout mitosis, from

centrosomes in G2, to kinetochores in prophase - metaphase and then the spindle midzone and midbody after anaphase onset. Plk1 is a promiscuous kinase and it controls a number of processes throughout the cell cycle in vertebrate cells by phosphorylating different substrates (figure 4-7) (Petronczki et al. 2008; van de Weerdt and Medema 2006). In the absence of Plk1 animal cells fail to establish a bipolar spindle and to attach kinetochores properly to the microtubules. Instead, cells assemble a monopolar spindle that is surrounded by a characteristic circular arrangement of chromosomes (figure 4-7). As a consequence, cells get trapped in mitosis by the activation of the spindle assembly checkpoint, which monitors the correct attachment of chromosomes to the mitotic spindle (Takaki et al. 2008). The localization and function of Plk1 is, in many cases, dependent on its ability to phosphorylate target substrates to which it can subsequently bind via its PBD domain (Kang et al. 2006). Plk1 is activated by phosphorylation of T210 in G2 by Aurora A in conjunction with Bora (Macurek et al., 2008; Seki et al., 2008). BOD1 is the regulator of Plk1 kinase during G2 and mitosis.

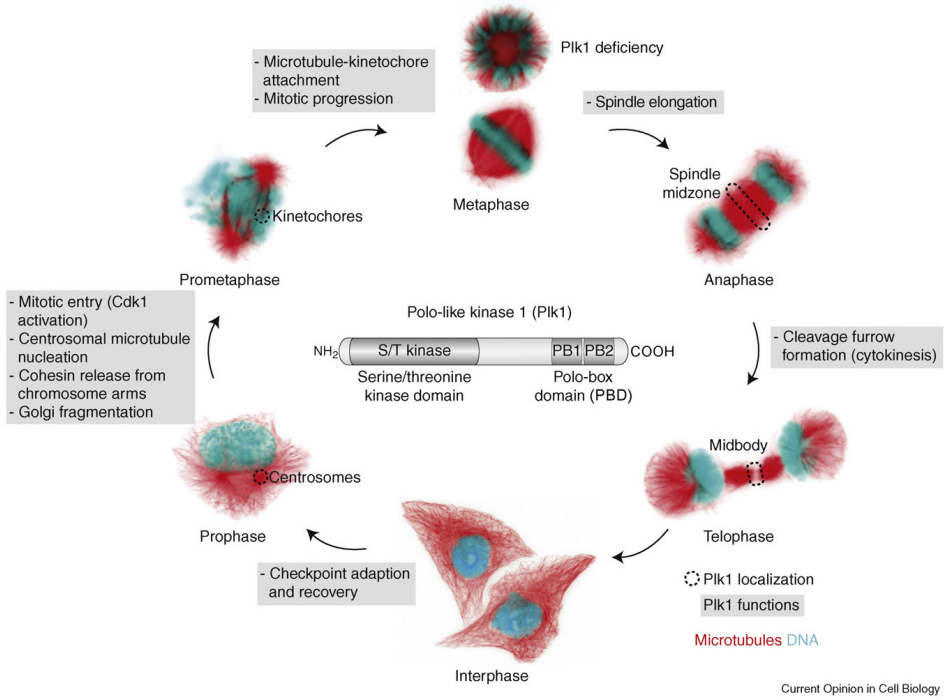

Figure 4-7: Localization and functions of Polo-like kinase 1 (Plk1) during the vertebrate cell cycle. The grey boxes at each stage of the cell cycle demonstrate the functions of Plk1 at the corresponding stage, which are illustrated by immunofluorescence images of cultured human cells (microtubules are shown in red, DNA in cyan). Localization of Plk1 to subcellular structures is indicated by dashed objects. In the center of the figure, the domain structure of Plk1 is shown. The PBD is responsible for the subcellular targeting of Plk1 [Image source: (Takaki et al. 2008)].

4.2. Effect of the mutation

To investigate the effect of the mutation in patients, I amplified all possible splice variants of this gene from RNA obtained from patient LCL and FB cells by RT-PCR (using flanking primers). Interestingly, in this experiment I could identify a total of four splice variants, from which two were not yet reported and I confirmed these results by sequencing as well as isoform-specific RT-PCR. The two previously reported splice variants contain both the second exon, and two previously unreported splice variants do not contain the second exon with the mutation.

All of these I could also amplify in RNA extracted from different cell lines belonging to different tissues. e.g. HeLa cells (human epithelial cells from a fatal cervical carcinoma) , Hek293 cells (human embryonic kidney cell cultures), IMR cells (human lung FB), SH-SY5Y cells (human neuroblastoma cells), LnCap (androgen-sensitive human prostate adenocarcinoma cells).

An Alignment of all four splice variants is shown in figure 4-8, the common region in all four transcript is the first exon and translated amino acid out of this part:

- In the transcript contains exons 1+2+4, which is actually reported in database, skipping of the third exon shifted the position of the original terminal codon (located at the end of the 3rd exon, whole exon 4 is 3'UTR), a bit further into beginning of exon 4; so it adds eight amino acid after the second exon which do not exist in the full transcript.
- In the case of the transcript contains exons 1+3+4, the stop codon is located in the beginning of the third exon and it stops after production of six amino acid, nevertheless this transcript is the shortest splice variant.
- The transcript contains exons 1+4, stops after translation of 20 amino acids from the fourth exon.

Figure 4-8: Alignment of all four *BOD1* splice variants. Yellow represents the common region between all splice variants. Green shows the common region between the full transcript and the new splice variant containing exons 1+2+4. The nonsense mutation is indicated by the red box.

Isoform specific qRT-PCR (using exon junction primers), however, showed a loss of expression of all four isoforms in patient cells. This was surprising, as only mRNA isoforms that harbor a premature termination codon (PTC) were expected to be degraded through the nonsense-mediated mRNA decay (NMD) pathway; because each transcript is scanned for PTCs independently. What is more, to promote NMD, the distance between the PTC and the subsequent exon-exon junction should be at least 50-55 nucleotides (Le Hir et al. 2000) yet this distance in the patients is only 29 nucleotides which also argued against an involvement of NMD.

Therefore I investigated whether NMD was at all responsible for the loss of expression of all isoforms.

NMD is a post-transcriptional quality-control machinery in eukaryotic gene expression (see also figure 4-9) that degrades transcripts containing premature

termination codons (PTCs) located upstream of the final exon-exon junction (Buhler et al. 2006).

As NMD is a translation dependent mechanism, translation blocking inhibits degradation of the mRNA.

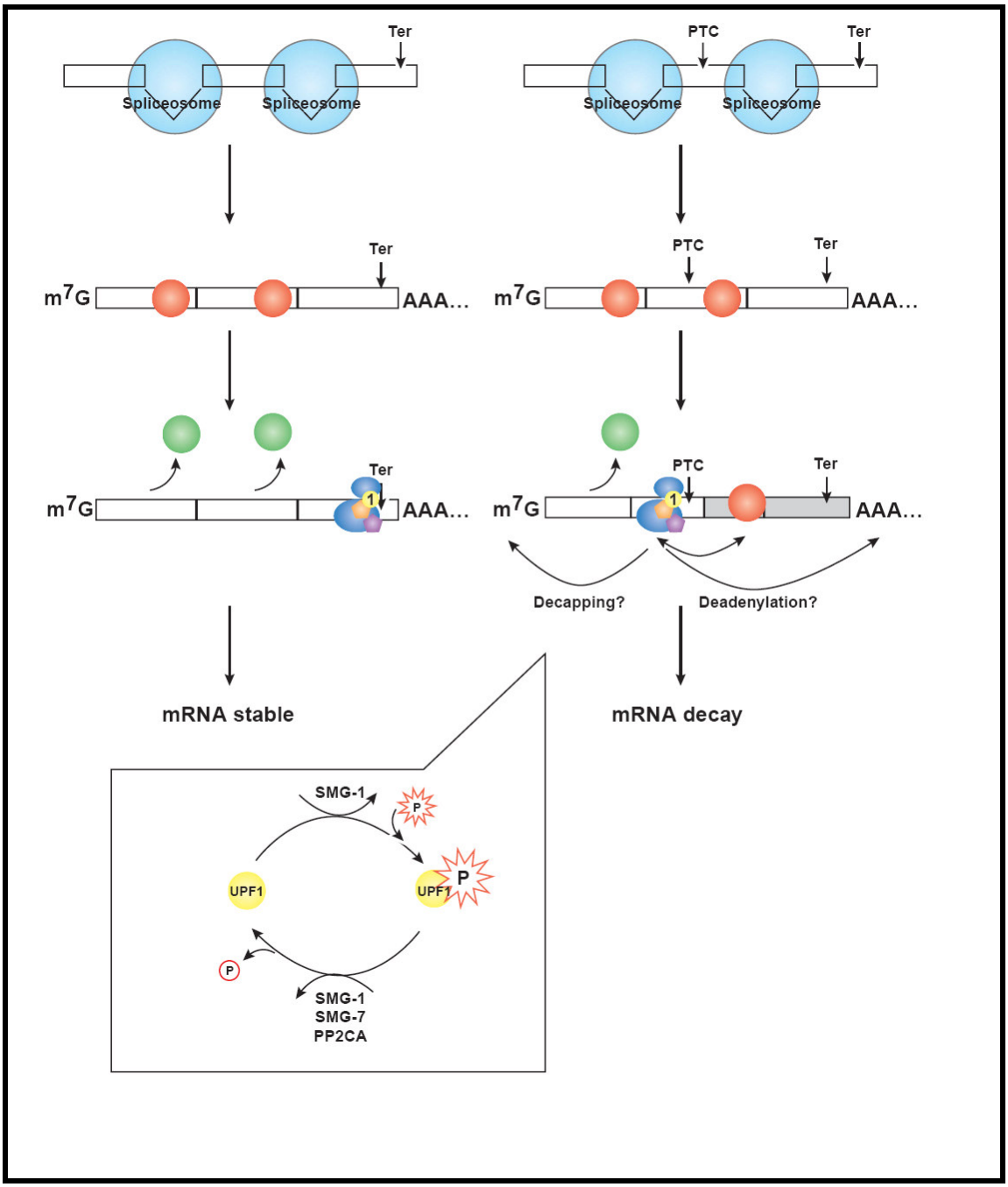

Figure 4-9: Mechanism of how NMD eliminates mRNAs containing premature termination codons. During splicing in the nucleus, a protein complex which is called exon junction complex (EJC), deposited 5′ of exon-exon junctions. Upon transport through the nuclear pore, the EJC (red) is remodeled, several proteins are released and others persist and accompany the mRNP into the polysomes. During translation of a PTCfree mRNA (left), the EJCs (green) are stripped off the mRNA by the translating ribosome (blue). If the translating ribosome encounters a PTC upstream of at least one EJC (right), it doesn't reach the EJC which subsequently triggers NMD (Holbrook et al. 2004). EJC components include eIF4AIII, Y14, MAGOH (mago-nashi homologue), Barentz (BTZ) and many other proteins (Maquat and Gong 2009). The inset shows the essential phosphorylation cycle of UPF1, this cycle is necessary for NMD to occur and is mediated through SMG factors: on post-spliced mRNAs during recognition of PTC, if an EJC exists downstream, it forms a surveillance complex termed "SURF", SMG-1 phosphorylates Up-frame shift protein 1 (UPF1) (demonstrated in yellow) (the step that is a rate-limiting for NMD) (Yamashita et al. 2009) and then a complex consisting of SMG-5, SMG-7 and the catalytic subunit of protein phosphatase 2A (PP2CA) dephosphorylates UPF1. RNA degraded either by 5'-to-3' and 3'-to-5' exonucleases or deadenylases and decapping enzyme (Muhlemann and Lykke-Andersen 2010). [Image source: (Holbrook et al. 2004)]

I thus used cycloheximide (CHX) to block NMD and found that CHX-treatment of patient cells could rescue the mRNA expression of all isoforms, even the ones without the mutation (splice variants containing exons 1+3+4 and 1+4) which could be due to some sort of regulatory process that acts inappropriately when seeing the low level of protein from the defective allele, but interestingly the splice variant containing exons 1+2+4 which actually harbors the mutation was not rescued. In sum, this result suggests there might be a different mechanism other than NMD involved and further investigation is needed to explain the mechanism underlying the observed pattern.

We next performed an Immunoblot analysis on lysates of patient FB and LCL cells and controls, using a rabbit polyclonal antibody raised against full length BOD1 (Porter et al. 2007). In line with the previously observed absence of functional *BOD1* transcripts, this revealed loss of detectable levels of BOD1 in

the patients. Thus we conclude that the complete loss of BOD1 is responsible for the phenotypes observed in the affected individuals from this family.

Therefore we next investigated the basic cell biology of BOD1 in further detail to get some more indication as to how lack of BOD1 in patients may induce the patient phenotype (ID and Oligomenorrhea).

4.2.1. Correlating genotype to phenotype in patients

As only limited patient material is available and the generation of a mouse knockout for functional investigations is not an ideal option, since only one *bod1* isoform is present in both mouse and rat (figure 4-10). We performed cell biological studies of BOD1 in HeLa cells by siRNA knockdown (see section 4.1) and tried to recapitulate any findings in FB cells obtained from patients.

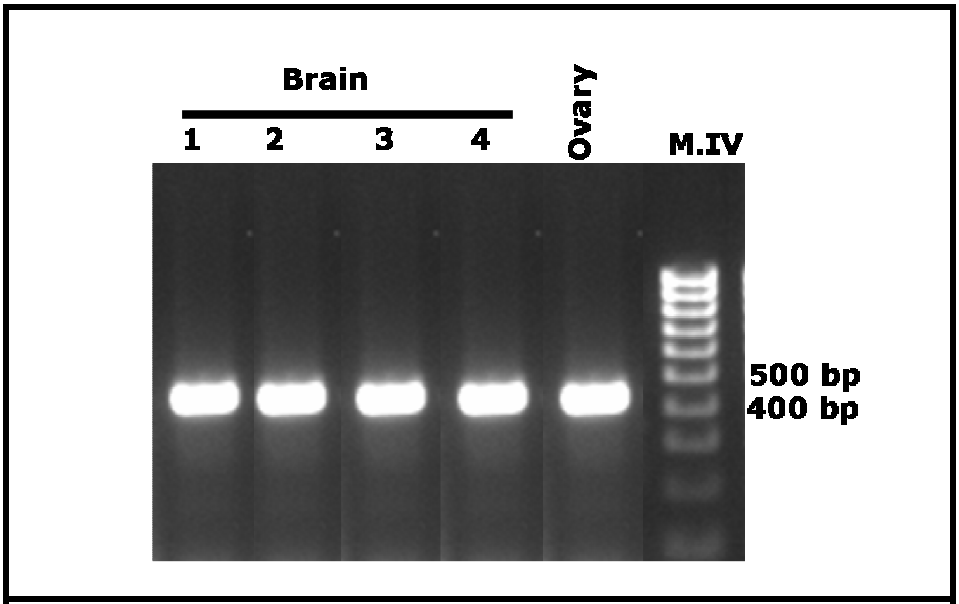

Figure 4-10: *bod1* in mice has only one transcript. The result from RT-PCR of mouse brains and ovaries are shown. RNA was extracted from whole brain of four mice as well as from the pooled ovaries of all four mice. RT-PCR with *bod1* specific primers shows only one transcript in mouse brain and ovary. DNA ladder marker IV (M.IV) was used as size standard.

4.2.1.1. BOD1 might raise the apoptotic rate

In collaboration with colleagues from the University of Dundee we found that loss of BOD1 protein leads to a biorientation defect in about 10% of the patient cells and changes in the mitotic index. Interestingly, karyotyping of the patients' blood didn't demonstrate any aneuploidy and based on findings in *BOD1* depleted HeLa cells, we assume that patients are loosing the aneuploid cells through apoptosis. However, a small increase in the rate of apoptosis might not be so important in many human tissues but it might be more crucial for cognition and even though MRI scans displayed no abnormalities, structural defects beyond the resolution of this method might still be considered a not unlikely cause for the cognitive dysfunction in our patients.

4.2.1.2. BOD1 is involved in regulation of Plk1, which is important in asymmetric cell division

BOD1 is involved in the regulation of Plk1 kinase (see section 4.1.3). Interestingly and also consistent with the live cell imaging data, which revealed that patients cells go through mitosis more quickly (see section 3.3.4.2.1), the small reduction in the metaphase and an increase in the cytokinetic was observed, suggesting the patient cells were progressing through metaphase and into anaphase at a higher rate [Plk1 is important for the speed of mitosis (Takaki et al. 2008)]. Also we shown that in FB cells which do not contain BOD1, Plk1 no longer localizes fully to kinetochores and localization to centrosomes is aberrant. Hence, in agreement with all previous findings (see section 4.1.3), BOD1 in the patient cells acts as a regulator of the G2/M kinase Plk1 and they entered into mitosis at an accelerated rate.

Moreover, Plk1 play a role in spindle formation and in the absence of Plk1 animal cells are unable to establish a bipolar spindle and to properly attach kinetochores to the microtubules (Takaki et al. 2008) and another evidence on the mal-functionality of Plk1 in patients due to loss of BOD1 is formation of the polypolar spindles in the patient FB cells which were absent in controls.

With regard to the oligomenorrhea phenotype of our patients we assume that since lack of BOD1 has an influence on mitosis it may also lead to a defect in meiosis which in turn causes the phenotype. Indeed evidence for an involvement of meiosis defects in the cause of oligomenorrhea has been observed before in a case of mosaic chromosome structural rearrangement which leads to dicentric chromosomes and subsequently segregation errors during meiosis and therefore oligomenorrhea (Laml et al. 2002; Northup et al. 2007).

In addition, our hypothesis is corroborated by the fact that all four isoforms are expressed in ovaries, which I could show by RT-PCR experiments on commercially available RNA from human ovaries (see figure S3, appendix K).

FB cells lacking BOD1 proceed through mitosis at an accelerated rate and they are less sensitive to Plk1 inhibitors. This suggests there is an adaptation response that allows cell proliferation and development in the absence of BOD1 and proper Plk1 function, but ultimately leads to ID. Developmental defects due to misregulation of Plk1 may arise for a number of reasons. During neurogenesis and development of the neural tube orientation of the cleavage plane is known to be important for determining cells fate (Wilcock et al. 2007). Accelerated advancement into anaphase, which occurs in the patients FB cells, may well interfere with the correct positioning of the cleavage plane and therefore generation of the correct proportions of neurons and progenitors. Plk1 is also known to be required for proper formation of the cleavage plane and furrow ingression by interacting with and regulating RhoA (Burkard et al. 2007; Petronczki et al. 2007). This may also interfere with proper orientation of cell division and cell fate. Rho proteins have, in themselves, also been implicated in ID, regulating proper spine formation [for a review see (Ramakers 2002)] so Plk1 may be involved in their regulation in a wider context. Plk1 has also recently been shown to regulate asymmetric recruitment of PON and Numb to the cortex of mitotic neural progenitor cells in Drosophila, promoting differentiation (Wang et al., 2007), further implicating Plk1's requirement during development.

4.2.1.3. Primary Cilia formation is delayed in patient FB cells

Given the centrosomal localization of BOD1 and role of centrosome in microtubule initiation and organization as well as cilia formation (Moynihan et al. 2009; Nigg and Raff 2009), we investigated patient FB cells. We could observe some preliminary evidence for disorientation of microtubules in the patients. Looking into cilia formation in the FB cells of patients and controls (3 hr after release from a G2/M block) revealed 28% of control FB cells had produced cilia in at least one of the daughter cells whereas only 8% of patient cells had. So the production rates of cilia in patient cells were 3 fold lower than in controls.

Primary cilia are produced in many types, provide a number of cellular functions and are in involved in a number of signaling pathways (Fliegauf et al. 2007; Nigg and Raff 2009). Interestingly, cilia production, and asynchronicity of cilia production between daughter cells, is also thought to be important during development (C. T. Anderson and Stearns 2009) and defects in cilia production are also associated with a number of syndromes whose symptoms include ID (Sharma et al. 2008). Asymmetric inheritance of mother and daughter centrosomes has recently been shown to be required for proper development of the neocortex (Wang et al. 2007) and asymmetric growth of cilia has also been demonstrated to have an important role in development (C. T. Anderson and Stearns 2009) with signaling molecules such as PDGFRα and inversin preferentially localizing to cilia emanating from the mother centriole, and asymmetric response to Sonic hedgehog homolog (Shh). In the context of a developing embryo this could also cause developmental defects.

4.2.1.4. BOD1 might regulate certain downstream target genes through contributions to the epigenetic control of chromatin structure and gene expression

It is shown that BOD1-GFP localizes to the centrosome throughout the cell cycle and to kinetochores during mitosis (Porter et al. 2007). Neuronal cells, however, are postmitotic. Therefore, to find an explanation for the cognitive

dysfunction beyond a putatively deficient involvement of BOD1 during brain development, we investigated this protein in the interphase of patient cells.

In LCL cells from patients I thus could observe some evidence for a nuclear structural defect in the patients' LCL cells. However, LCL cells grow in suspension and before any kinds of structural study one has to fix them on a cover slip by centrifuging, which might be damaging. I therefore selected patient FB cells for further investigation. To investigate FB cells, first I performed DAPI staining and studied the cells in patients and controls using confocal microscopy; the first observed striking phenotype was a difference in nucleus morphology and size between patients and controls; Nuclei in patient cells had a tendency to be more spherical than ovally shaped (as they should be) and they varied more strongly in size. To determine if these differences are statistically significant, I measured the width, length, nucleus circumference and volume of 150 nuclei from two patients and two controls, using the Zeiss image examiner software. This showed that the differences in both variability in nucleus circumference and size between patients and controls were significantly meaningful (F-test). Nonetheless to check that if the observed differences are due to the normal variations between FB cells, I also calculated the F-test within the patient and control duos respectively, the results pointed to no significant P-value. Beside these findings I employed FACScan to verify that the observed differences actually are not due to some checkpoint defect during interphase: no differences in G1 and G2 of two different patients and controls were observed (see section 3.3.5.1.1) which confirmed that the observed difference between patients and control is not owing to accumulation of the cells in G1 or G2.

Study of the patients FB cells with different nuclear markers corresponding to different nuclear compartments revealed some defects in nuclear envelope and matrix of about 20-30% of patients and 2-4% of controls FB cells.

4.2.1.4.1. Nuclear structural defect in overexpression studies

All of the upper observations suggested BOD1 might be involved in nuclear organization. Overexpression of BOD1-GFP in HaCat cells points to the same direction as well. So, it seems that during interphase BOD1 localizes to the interchromatin space (IC) and it doesn't overlap with chromatin.

Recent studies showed that changes in the chromosome territory (CTs) can influence on development and gene expression pattern through influencing IC (CT-IC model) (Cremer and Cremer 2001). On the other hand, it was found that lamins are major contributors in structural organization of nucleus and chromatin (Dechat et al. 2008; Mattout-Drubezki and Gruenbaum 2003; Schirmer and Foisner 2007). Therefore the reasonable candidates to investigate this observesion further [see reviews: (Montes de Oca et al. 2009; Wagner and Krohne 2007)], were Lamin A/C and Emerin (a lamin-binding protein which contains LEM domain, based on some evidence lamins interact with chromatin and DNA through these kinds of protein (Shumaker et al. 1998). Using antibodies against these proteins in HaCat cells overexpressing BOD1-GFP we observed some defects in both nuclear matrix and envelope. These results suggested that BOD1 might be influencing gene expression through changes in the chromatin structure (one of the three main mechanisms that are involved in control of transcription (see section 3.3.5.3).

Previous studies suggested that BOD1 first localizes to the nucleus and then moves to the cytoplasm (Porter et al. 2007). Taken together with the observations mentioned before this prompted me to try to localize the Nuclear Localization Signal (NLS) in BOD1 by generating several C-terminus and N-terminus deletion constructs and transfecting them into FB cells. My results suggest that a NLS is located around 111-141 AA from the N-terminus of BOD1, which is in line with a cNLS mapper (Kosugi et al. 2008; Kosugi et al. 2009b; Kosugi et al. 2009a) prediction that localizes the NLS region of BOD1 within 137-166 AA from the N-teminus (figure 4-11).

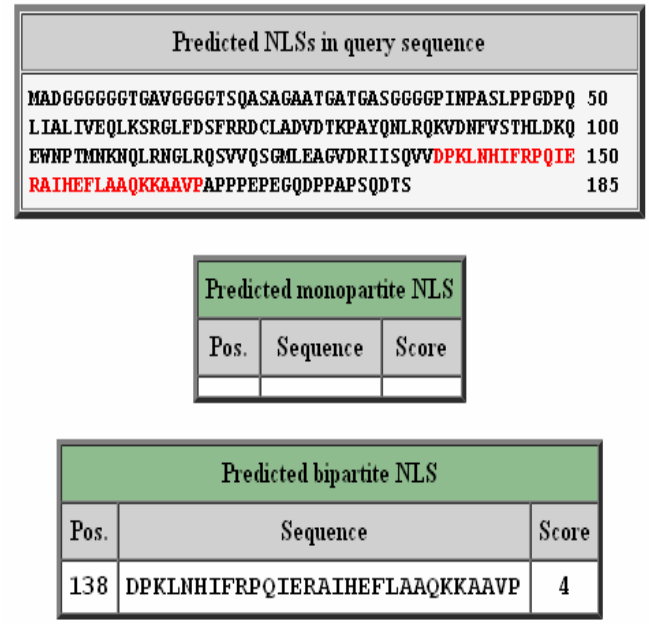

Figure 4-11: BOD1 NLS is predicted to lie between amino acid 137 and 168. Prediction was performed by cNLS Mapper software (http://nls-mapper.iab.keio.ac.jp/cgi-bin/NLS_Mapper_form.cgi) with a cut-off score of 4.

However confirmation of the results is needed; for instance by using a GFP tagged exclusively cytosolic protein. Adding the sequence of 137-168 AA to this construct (e.g. X-GFP) should then lead to a nuclear localization.

4.2.1.4.2. Whole genome expression profiling points to some important genes in cognition

Overexpression studies suggested that BOD1 may be involved in the regulation of gene expression. Thus, *BOD1* mutations may give rise to ID trough influencing down stream target genes which are important in human cognition. To shed more light on this issue, whole genome expression profiling on LCL cells was carried out. As shown in table 3-2, most of up-regulated pathways in the patient compared to six different controls are involved in chromatin organization and gene regulation. Some of the up-regulated genes play crucial roles in cognitive impairment; for several of those genes which where chosen

randomly, the up-regulation was confirmed by qRT-PCR. Highly significant up-regulation was observed for several genes that are known to play a role in brain development and function as shown in table 4-1.

Table 4-1: Up-regulated genes which are important in cognitive impairment.

Gene names and function	Differential scores*
ARHGEF5 (Regulation of immature dendritic cell migration)	+345.32
DPYSL4 (Neurogenesis)	+345.32
SETBP1 (Defects cause a severe form of mental retardation)	+104.73
KIF13B (Neuronal polarity)	+96.69
AGRN (Synapse organization and biogenesis)	+49.57
PITPNM1 (Brain development)	+32.30
ATN1 (Central nervous system development)	+24.6

* To identify the differential changes in the levels of transcripts, it was necessary to compare the gene expression values between two groups: patients and controls and conduct a t-test to identify the significant changes. The differential score of 13 corresponds to a p-value of 0.05 and a positive score represents up-regulation.

Taken together, the observations concerning nuclear localization of BOD1 suggest, that loss of BOD1 leads to nuclear structural defects which as a consequence might change the chromatin organization and regulation of certain downstream target genes which play more essential roles human cognition. To precisely find how BOD1 is involved in generating this defect, follow up studies are needed.

4.2.1.4.3. Evidence for localization of BOD1 in synapses

In another possible scenario for an involvement of BOD1 in higher brain functions the protein could have an entirely different localization and function in non-dividing neuronal cells. It is e.g. reported that some of the kinetochore proteins in addition to a mitotic role, are involved in postmitotic neurons; such as ZWINT-1 which is a kinetochore protein and has an additional role in presynaptic events that are regulated by RAB3 and SNAP25 (van Vlijmen et al.

2008). Or SGT1, which is required for the mitotic activity of kinetochores but is also detected in cortex, hippocampus, and cerebellum and shows a reduced in density of SGT1-immunopositive neurons were observed in Alzheimer cerebral cortex (Spiechowicz et al. 2006).

Since we do not have access to brain samples from patients, I checked the expression levels of all four isoforms in commercially available RNA from different brain regions and selected brain parts with crucial involvement in memory and learning. These qRT-PCR experiments revealed that all four splice variants are expressed at significant levels in all the tested samples at both adult and fetal stages. Therefore it was reasonable to look for localization of this protein in neuronal cells.

Dendritic spines are small protrusions on the surface of neuronal dendrites that form the postsynaptic component of the excitatory synapse and play important roles in learning and memory, and alterations in dendritic spines are found in many types of ID and other neurological disorders (Calabrese et al., 2006). Such investigations were performed on primary neurons isolated from the cortex of mouse embryos (E14.5), expressing BOD1-GFP in these cells. Indirect confocal immunoflorescence imaging yielded convincing evidence for colocalization of BOD1 with some of the presynaptic markers tested (Bassoon and NR2B) which was not observed in control cells that only expressed GFP. These results provide compelling preliminary evidence for a synaptic localization of BOD1, thus expanding the functional spectrum of BOD1. This also shows that there might be a direct involvement of BOD1 in cognitive processes which could be impaired by a loss of BOD1 and account for the mild to moderate ID phenotype in the patients. However, further investigations, for instance focusing on a putative role of BOD1 in neuronal plasticity, will be needed to support this hypothesis.

4.3. Summary

The schematic shown in figure 4-12, summarizes my PhD Project and shown all the speculated links between BOD1 and patients phenotype.

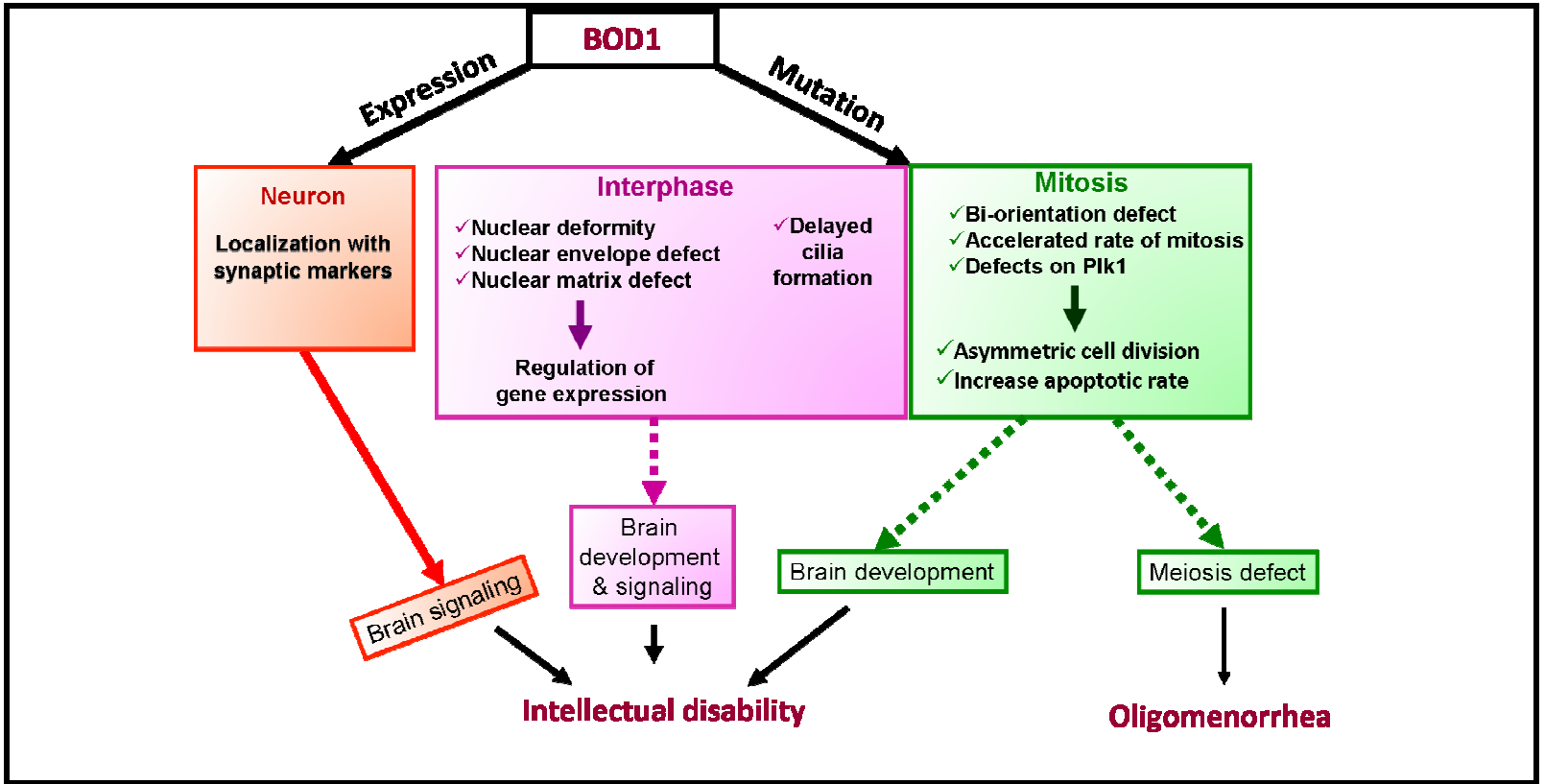

Figure 4-12: Model represents the recommended phenotypic-genotypic correlation. On the right side, all the suggested defects during mitosis and interphase that caused by the mutation in patients are shown and on the left side a suggested link to ID based on the expression of BOD1 in primary neuronal cells is shown.

5. References

1. Abecasis, G. R., et al. (2002), 'Merlin--rapid analysis of dense genetic maps using sparse gene flow trees', *Nat Genet,* 30 (1), 97-101.

2. Anderson, C. T. and Stearns, T. (2009), 'Centriole age underlies asynchronous primary cilium growth in mammalian cells', *Curr Biol,* 19 (17), 1498-502.

3. Anderson, D. J. and Hetzer, M. W. (2008), 'Reshaping of the endoplasmic reticulum limits the rate for nuclear envelope formation', *J Cell Biol,* 182 (5), 911-24.

4. Anderson, D. J., et al. (2009), 'Recruitment of functionally distinct membrane proteins to chromatin mediates nuclear envelope formation in vivo', *J Cell Biol,* 186 (2), 183-91.

5. Annies, M., et al. (2006), 'Clustering transmembrane-agrin induces filopodia-like processes on axons and dendrites', *Mol Cell Neurosci,* 31 (3), 515-24.

6. Anonymous (2010), 'The american association on intellectual and developmental disabilities', *Intellect Dev Disabil,* 48 (3), 239-41.

7. Argentaro, A., et al. (2007), 'Structural consequences of disease-causing mutations in the ATRX-DNMT3-DNMT3L (ADD) domain of the chromatin-associated protein ATRX', *Proc Natl Acad Sci U S A,* 104 (29), 11939-44.

8. Baron, I. S. (2005), 'Test review: Wechsler Intelligence Scale for Children-Fourth Edition (WISC-IV)', *Child Neuropsychol,* 11 (5), 471-5.

9. Basel-Vanagaite, L., et al. (2006), 'The CC2D1A, a member of a new gene family with C2 domains, is involved in autosomal recessive non-syndromic mental retardation', *J Med Genet,* 43 (3), 203-10.

10. Bear, M. F., Huber, K. M., and Warren, S. T. (2004), 'The mGluR theory of fragile X mental retardation', *Trends Neurosci,* 27 (7), 370-7.

11. Bienz, M. (2006), 'The PHD finger, a nuclear protein-interaction domain', *Trends Biochem Sci,* 31 (1), 35-40.

12. Bond, J., et al. (2005), 'A centrosomal mechanism involving CDK5RAP2 and CENPJ controls brain size', *Nat Genet,* 37 (4), 353-5.

13. Buchman, J. J., et al. (2010), 'Cdk5rap2 interacts with pericentrin to maintain the neural progenitor pool in the developing neocortex', *Neuron,* 66 (3), 386-402.

14. Buhler, M., et al. (2006), 'EJC-independent degradation of nonsense immunoglobulin-mu mRNA depends on 3' UTR length', *Nat Struct Mol Biol,* 13 (5), 462-4.

15. Bull, L. N., et al. (1998), 'A gene encoding a P-type ATPase mutated in two forms of hereditary cholestasis', *Nat Genet,* 18 (3), 219-24.

16. Burakov, A., et al. (2003), 'Centrosome positioning in interphase cells', *J Cell Biol,* 162 (6), 963-9.

17. Burkard, M. E., et al. (2007), 'Chemical genetics reveals the requirement for Polo-like kinase 1 activity in positioning RhoA and triggering cytokinesis in human cells', *Proc Natl Acad Sci U S A,* 104 (11), 4383-8.

18. Bustin, S. A. (2002), 'Quantification of mRNA using real-time reverse transcription PCR (RT-PCR): trends and problems', *J Mol Endocrinol,* 29 (1), 23-39.

19. Chiurazzi, P., et al. (2008), 'XLMR genes: update 2007', *Eur J Hum Genet,* 16 (4), 422-34.

20. Cimini, D. and Degrassi, F. (2005), 'Aneuploidy: a matter of bad connections', *Trends Cell Biol,* 15 (8), 442-51.

21. Clarke, A. S., et al. (2005), 'POLO kinase regulates the Drosophila centromere cohesion protein MEI-S332', *Dev Cell,* 8 (1), 53-64.

22. Compton, D. A. (2007), 'Chromosome orientation', *J Cell Biol,* 179 (2), 179-81.

23. Contractor, A., Swanson, G., and Heinemann, S. F. (2001), 'Kainate receptors are involved in short- and long-term plasticity at mossy fiber synapses in the hippocampus', *Neuron,* 29 (1), 209-16.

24. Cox, J., et al. (2006), 'What primary microcephaly can tell us about brain growth', *Trends Mol Med,* 12 (8), 358-66.

25. Cremer, T. and Cremer, C. (2001), 'Chromosome territories, nuclear architecture and gene regulation in mammalian cells', *Nat Rev Genet,* 2 (4), 292-301.

26. Dang, Y., et al. (2009), 'Inhibition of nonsense-mediated mRNA decay by the natural product pateamine A through eukaryotic initiation factor 4AIII', *J Biol Chem,* 284 (35), 23613-21.

27. Dauer, W. T. and Worman, H. J. (2009), 'The nuclear envelope as a signaling node in development and disease', *Dev Cell,* 17 (5), 626-38.

28. Davidovic, L., et al. (2007), 'The fragile X mental retardation protein is a molecular adaptor between the neurospecific KIF3C kinesin and dendritic RNA granules', *Hum Mol Genet,* 16 (24), 3047-58.

29. Dawn Teare, M. and Barrett, J. H. (2005), 'Genetic linkage studies', *Lancet,* 366 (9490), 1036-44.

30. Dechat, T., et al. (2008), 'Nuclear lamins: major factors in the structural organization and function of the nucleus and chromatin', *Genes Dev,* 22 (7), 832-53.

31. Dekker, J. (2008), 'Gene regulation in the third dimension', *Science,* 319 (5871), 1793-4.

32. Dennis, G., Jr., et al. (2003), 'DAVID: Database for Annotation, Visualization, and Integrated Discovery', *Genome Biol,* 4 (5), P3.

33. Dewar, H., et al. (2004), 'Tension between two kinetochores suffices for their bi-orientation on the mitotic spindle', *Nature,* 428 (6978), 93-7.

34. Fisher, D. Z., Chaudhary, N., and Blobel, G. (1986), 'cDNA sequencing of nuclear lamins A and C reveals primary and secondary structural homology to intermediate filament proteins', *Proc Natl Acad Sci U S A,* 83 (17), 6450-4.

35. Fliegauf, M., Benzing, T., and Omran, H. (2007), 'When cilia go bad: cilia defects and ciliopathies', *Nat Rev Mol Cell Biol,* 8 (11), 880-93.

36. Fraser, P. and Bickmore, W. (2007), 'Nuclear organization of the genome and the potential for gene regulation', *Nature,* 447 (7143), 413-7.

37. Fu, Y. H., et al. (1991), 'Variation of the CGG repeat at the fragile X site results in genetic instability: resolution of the Sherman paradox', *Cell,* 67 (6), 1047-58.

38. Garshasbi, M., et al. (2008), 'A defect in the TUSC3 gene is associated with autosomal recessive mental retardation', *Am J Hum Genet,* 82 (5), 1158-64.

39. --- (2006), 'SNP array-based homozygosity mapping reveals MCPH1 deletion in family with autosomal recessive mental retardation and mild microcephaly', *Hum Genet,* 118 (6), 708-15.

40. Gecz, J., Cloosterman, D., and Partington, M. (2006), 'ARX: a gene for all seasons', *Curr Opin Genet Dev,* 16 (3), 308-16.

41. Gecz, J., Shoubridge, C., and Corbett, M. (2009), 'The genetic landscape of intellectual disability arising from chromosome X', *Trends Genet,* 25 (7), 308-16.

42. Goldenberg, A. and Saugier-Veber, P. (2009), '[Genetics of mental retardation.]', *Pathol Biol (Paris)*.

43. Gorbsky, G. J. (2004), 'Mitosis: MCAK under the aura of Aurora B', *Curr Biol,* 14 (9), R346-8.

44. Greydanus, D. E. and McAnarney, E. R. (1982), 'Menstruation and its disorders in adolescence', *Curr Probl Pediatr,* 12 (10), 1-61.

45. Gruenbaum, Y., et al. (2005), 'The nuclear lamina comes of age', *Nat Rev Mol Cell Biol,* 6 (1), 21-31.

46. Gudbjartsson, D. F., et al. (2000), 'Allegro, a new computer program for multipoint linkage analysis', *Nat Genet,* 25 (1), 12-3.

47. Hamdan, F. F., et al. (2009), 'Mutations in SYNGAP1 in autosomal nonsyndromic mental retardation', *N Engl J Med,* 360 (6), 599-605.

48. Hauf, S., et al. (2003), 'The small molecule Hesperadin reveals a role for Aurora B in correcting kinetochore-microtubule attachment and in maintaining the spindle assembly checkpoint', *J Cell Biol,* 161 (2), 281-94.

49. Hemerly, A. S., et al. (2009), 'Orc1 controls centriole and centrosome copy number in human cells', *Science,* 323 (5915), 789-93.

50. Higgins, J. J., et al. (2004), 'A mutation in a novel ATP-dependent Lon protease gene in a kindred with mild mental retardation', *Neurology,* 63 (10), 1927-31.

51. Hilgenberg, L. G., et al. (2006), 'Alpha3Na+/K+-ATPase is a neuronal receptor for agrin', *Cell,* 125 (2), 359-69.

52. Hochedlinger, K. and Plath, K. (2009), 'Epigenetic reprogramming and induced pluripotency', *Development,* 136 (4), 509-23.

53. Holbrook, J. A., et al. (2004), 'Nonsense-mediated decay approaches the clinic', *Nat Genet,* 36 (8), 801-8.

54. Hong, S. E., et al. (2000), 'Autosomal recessive lissencephaly with cerebellar hypoplasia is associated with human RELN mutations', *Nat Genet,* 26 (1), 93-6.

55. Houwen, R. H., et al. (1994), 'Genome screening by searching for shared segments: mapping a gene for benign recurrent intrahepatic cholestasis', *Nat Genet,* 8 (4), 380-6.

56. Hu, W. H., et al. (2005), 'NIBP, a novel NIK and IKK(beta)-binding protein that enhances NF-(kappa)B activation', *J Biol Chem,* 280 (32), 29233-41.

57. Huang da, W., Sherman, B. T., and Lempicki, R. A. (2009), 'Systematic and integrative analysis of large gene lists using DAVID bioinformatics resources', *Nat Protoc,* 4 (1), 44-57.

58. Huangfu, D., et al. (2008), 'Induction of pluripotent stem cells by defined factors is greatly improved by small-molecule compounds', *Nat Biotechnol,* 26 (7), 795-7.

59. Hunter, A. W., et al. (2003), 'The kinesin-related protein MCAK is a microtubule depolymerase that forms an ATP-hydrolyzing complex at microtubule ends', *Mol Cell,* 11 (2), 445-57.

60. Ito, T., et al. (2010), 'Identification of a primary target of thalidomide teratogenicity', *Science,* 327 (5971), 1345-50.

61. Jackson, A. P., et al. (2002), 'Identification of microcephalin, a protein implicated in determining the size of the human brain', *Am J Hum Genet,* 71 (1), 136-42.

62. Jin, P. and Warren, S. T. (2000), 'Understanding the molecular basis of fragile X syndrome', *Hum Mol Genet,* 9 (6), 901-8.

63. Johnson, N., et al. (2003), 'Actin-filled nuclear invaginations indicate degree of cell de-differentiation', *Differentiation,* 71 (7), 414-24.

64. Jorgensen, P., et al. (2007), 'The size of the nucleus increases as yeast cells grow', *Mol Biol Cell,* 18 (9), 3523-32.

65. Kaindl, A. M., Passemard, S., and Gressens, P. (2009), 'Autosomal recessive primary microcephalies (MCPH)', *Eur J Paediatr Neurol,* 13 (5), 458.

66. Kang, Y. H., et al. (2006), 'Self-regulated Plk1 recruitment to kinetochores by the Plk1-PBIP1 interaction is critical for proper chromosome segregation', *Mol Cell,* 24 (3), 409-22.

67. Kawashima, S. A., et al. (2007), 'Shugoshin enables tension-generating attachment of kinetochores by loading Aurora to centromeres', *Genes Dev,* 21 (4), 420-35.

68. Kitajima, T. S., Kawashima, S. A., and Watanabe, Y. (2004), 'The conserved kinetochore protein shugoshin protects centromeric cohesion during meiosis', *Nature,* 427 (6974), 510-7.

69. Kitajima, T. S., et al. (2005), 'Human Bub1 defines the persistent cohesion site along the mitotic chromosome by affecting Shugoshin localization', *Curr Biol,* 15 (4), 353-9.

70. Kosugi, S., et al. (2009a), 'Systematic identification of cell cycle-dependent yeast nucleocytoplasmic shuttling proteins by prediction of composite motifs', *Proc Natl Acad Sci U S A,* 106 (25), 10171-6.

71. --- (2008), 'Design of peptide inhibitors for the importin alpha/beta nuclear import pathway by activity-based profiling', *Chem Biol,* 15 (9), 940-9.

72. --- (2009b), 'Six classes of nuclear localization signals specific to different binding grooves of importin alpha', *J Biol Chem,* 284 (1), 478-85.

73. Kruglyak, L., et al. (1996), 'Parametric and nonparametric linkage analysis: a unified multipoint approach', *Am J Hum Genet,* 58 (6), 1347-63.

74. Laemmli, U. K. (1970), 'Cleavage of structural proteins during the assembly of the head of bacteriophage T4', *Nature,* 227 (5259), 680-5.

75. Laml, T., et al. (2002), 'Genetic disorders in premature ovarian failure', *Hum Reprod Update,* 8 (5), 483-91.

76. Lampson, M. A., et al. (2004), 'Correcting improper chromosome-spindle attachments during cell division', *Nat Cell Biol,* 6 (3), 232-7.

77. Lander, E. S. and Botstein, D. (1987), 'Homozygosity mapping: a way to map human recessive traits with the DNA of inbred children', *Science,* 236 (4808), 1567-70.

78. Laumonnier, F., Cuthbert, P. C., and Grant, S. G. (2007), 'The role of neuronal complexes in human X-linked brain diseases', *Am J Hum Genet,* 80 (2), 205-20.

79. Le Hir, H., et al. (2000), 'The spliceosome deposits multiple proteins 20-24 nucleotides upstream of mRNA exon-exon junctions', *EMBO J,* 19 (24), 6860-9.

80. Lenart, P., et al. (2007), 'The small-molecule inhibitor BI 2536 reveals novel insights into mitotic roles of polo-like kinase 1', *Curr Biol,* 17 (4), 304-15.

81. Leonard, H. and Wen, X. (2002), 'The epidemiology of mental retardation: challenges and opportunities in the new millennium', *Ment Retard Dev Disabil Res Rev,* 8 (3), 117-34.

82. Levav, I. and Rutz, W. (2002), 'The WHO World Health Report 2001 new understanding--new hope', *Isr J Psychiatry Relat Sci,* 39 (1), 50-6.

83. Liu, D. and Lampson, M. A. (2009), 'Regulation of kinetochore-microtubule attachments by Aurora B kinase', *Biochem Soc Trans,* 37 (Pt 5), 976-80.

84. Loesch, D. Z., et al. (2009), 'Linking the FMR1 alleles with small CGG expansions with neurodevelopmental disorders: preliminary data suggest an involvement of epigenetic mechanisms', *Am J Med Genet A,* 149A (10), 2306-10.

85. Lu, X., et al. (1998), 'A novel human gene, WSTF, is deleted in Williams syndrome', *Genomics,* 54 (2), 241-9.

86. Ma, Y., et al. (2007), 'Lamin B receptor plays a role in stimulating nuclear envelope production and targeting membrane vesicles to chromatin during nuclear envelope assembly through direct interaction with importin beta', *J Cell Sci,* 120 (Pt 3), 520-30.

87. Macy, B., Wang, M., and Yu, H. G. (2009), 'The many faces of shugoshin, the "guardian spirit," in chromosome segregation', *Cell Cycle,* 8 (1), 35-7.

88. Mandel, J. L. and Chelly, J. (2004), 'Monogenic X-linked mental retardation: is it as frequent as currently estimated? The paradox of the ARX (Aristaless X) mutations', *Eur J Hum Genet,* 12 (9), 689-93.

89. Maquat, L. E. and Gong, C. (2009), 'Gene expression networks: competing mRNA decay pathways in mammalian cells', *Biochem Soc Trans,* 37 (Pt 6), 1287-92.

90. Mattout-Drubezki, A. and Gruenbaum, Y. (2003), 'Dynamic interactions of nuclear lamina proteins with chromatin and transcriptional machinery', *Cell Mol Life Sci,* 60 (10), 2053-63.

91. McCroskery, S., et al. (2006), 'Transmembrane agrin regulates filopodia in rat hippocampal neurons in culture', *Mol Cell Neurosci,* 33 (1), 15-28.

92. McKeon, F. D., Kirschner, M. W., and Caput, D. (1986), 'Homologies in both primary and secondary structure between nuclear envelope and intermediate filament proteins', *Nature,* 319 (6053), 463-8.

93. Mikkelsen, T. S., et al. (2008), 'Dissecting direct reprogramming through integrative genomic analysis', *Nature,* 454 (7200), 49-55.

94. Mir, A., et al. (2009), 'Identification of mutations in TRAPPC9, which encodes the NIK- and IKK-beta-binding protein, in nonsyndromic autosomal-recessive mental retardation', *Am J Hum Genet,* 85 (6), 909-15.

95. Miyoshi, D. and Sugimoto, N. (2008), 'Molecular crowding effects on structure and stability of DNA', *Biochimie,* 90 (7), 1040-51.

96. Mochida, G. H., et al. (2009), 'A truncating mutation of TRAPPC9 is associated with autosomal-recessive intellectual disability and postnatal microcephaly', *Am J Hum Genet,* 85 (6), 897-902.

97. Molinari, F., et al. (2002), 'Truncating neurotrypsin mutation in autosomal recessive nonsyndromic mental retardation', *Science,* 298 (5599), 1779-81.

98. --- (2008), 'Oligosaccharyltransferase-subunit mutations in nonsyndromic mental retardation', *Am J Hum Genet,* 82 (5), 1150-7.

99. Montes de Oca, R., et al. (2009), 'Barrier-to-autointegration factor proteome reveals chromatin-regulatory partners', *PLoS One,* 4 (9), e7050.

100. Motazacker, M. M., et al. (2007), 'A defect in the ionotropic glutamate receptor 6 gene (GRIK2) is associated with autosomal recessive mental retardation', *Am J Hum Genet,* 81 (4), 792-8.

101. Moynihan, K. L., et al. (2009), 'Murine CENP-F regulates centrosomal microtubule nucleation and interacts with Hook2 at the centrosome', *Mol Biol Cell,* 20 (22), 4790-803.

102. Muhlemann, O. and Lykke-Andersen, J. (2010), 'How and where are nonsense mRNAs degraded in mammalian cells?', *RNA Biol,* 7 (1).

103. Nachury, M. V., et al. (2007), 'A core complex of BBS proteins cooperates with the GTPase Rab8 to promote ciliary membrane biogenesis', *Cell,* 129 (6), 1201-13.

104. Nagamine, K., et al. (1997), 'Positional cloning of the APECED gene', *Nat Genet,* 17 (4), 393-8.

105. Najmabadi, H., et al. (2007), 'Homozygosity mapping in consanguineous families reveals extreme heterogeneity of non-syndromic autosomal recessive mental retardation and identifies 8 novel gene loci', *Hum Genet,* 121 (1), 43-8.

106. Nakamoto, M., et al. (2007), 'Fragile X mental retardation protein deficiency leads to excessive mGluR5-dependent internalization of AMPA receptors', *Proc Natl Acad Sci U S A,* 104 (39), 15537-42.

107. Nakamura, A., et al. (2008), 'Freud-1/Aki1, a novel PDK1-interacting protein, functions as a scaffold to activate the PDK1/Akt pathway in epidermal growth factor signaling', *Mol Cell Biol,* 28 (19), 5996-6009.

108. Narayanan, U., et al. (2007), 'FMRP phosphorylation reveals an immediate-early signaling pathway triggered by group I mGluR and mediated by PP2A', *J Neurosci,* 27 (52), 14349-57.

109. Neumann, F. R. and Nurse, P. (2007), 'Nuclear size control in fission yeast', *J Cell Biol,* 179 (4), 593-600.

110. Nichols, J. F., et al. (2007), 'Disordered eating and menstrual irregularity in high school athletes in lean-build and nonlean-build sports', *Int J Sport Nutr Exerc Metab,* 17 (4), 364-77.

111. Nigg, E. A. and Raff, J. W. (2009), 'Centrioles, centrosomes, and cilia in health and disease', *Cell,* 139 (4), 663-78.

112. Noor, A., et al. (2008), 'CC2D2A, encoding a coiled-coil and C2 domain protein, causes autosomal-recessive mental retardation with retinitis pigmentosa', *Am J Hum Genet,* 82 (4), 1011-8.

113. Northup, J., et al. (2007), 'Unusual pseudo dicentric, psu dic (1;19)(q10;q13.42), in a female with premature ovarian failure', *Fertil Steril,* 87 (3), 697 e5-8.

114. O'Connell, J. R. and Weeks, D. E. (1998), 'PedCheck: a program for identification of genotype incompatibilities in linkage analysis', *Am J Hum Genet,* 63 (1), 259-66.

115. Oberle, I., et al. (1991), 'Instability of a 550-base pair DNA segment and abnormal methylation in fragile X syndrome', *Science,* 252 (5009), 1097-102.

116. Ou, X. M., et al. (2003), 'Freud-1: A neuronal calcium-regulated repressor of the 5-HT1A receptor gene', *J Neurosci,* 23 (19), 7415-25.

117. Passemard, S., et al. (2009), 'Expanding the clinical and neuroradiologic phenotype of primary microcephaly due to ASPM mutations', *Neurology,* 73 (12), 962-9.

118. Pegoraro, G., et al. (2009), 'Ageing-related chromatin defects through loss of the NURD complex', *Nat Cell Biol,* 11 (10), 1261-7.

119. Peric-Hupkes, D., et al. (2010), 'Molecular maps of the reorganization of genome-nuclear lamina interactions during differentiation', *Mol Cell,* 38 (4), 603-13.

120. Petronczki, M., Lenart, P., and Peters, J. M. (2008), 'Polo on the Rise-from Mitotic Entry to Cytokinesis with Plk1', *Dev Cell,* 14 (5), 646-59.

121. Petronczki, M., et al. (2007), 'Polo-like kinase 1 triggers the initiation of cytokinesis in human cells by promoting recruitment of the RhoGEF Ect2 to the central spindle', *Dev Cell,* 12 (5), 713-25.

122. Pfaffl, M. W. (2001), 'A new mathematical model for relative quantification in real-time RT-PCR', *Nucleic Acids Res,* 29 (9), e45.

123. Philippe, O., et al. (2009), 'Combination of linkage mapping and microarray-expression analysis identifies NF-kappaB signaling defect as a cause of autosomal-recessive mental retardation', *Am J Hum Genet,* 85 (6), 903-8.

124. Porter, I. M., et al. (2007), 'Bod1, a novel kinetochore protein required for chromosome biorientation', *J Cell Biol,* 179 (2), 187-97.

125. Poser, I., et al. (2008), 'BAC TransgeneOmics: a high-throughput method for exploration of protein function in mammals', *Nat Methods,* 5 (5), 409-15.

126. Qi, H. H., et al. (2010), 'Histone H4K20/H3K9 demethylase PHF8 regulates zebrafish brain and craniofacial development', *Nature*.

127. Ramakers, G. J. (2002), 'Rho proteins, mental retardation and the cellular basis of cognition', *Trends Neurosci,* 25 (4), 191-9.

128. Ramos, C. and Robert, B. (2005), 'msh/Msx gene family in neural development', *Trends Genet,* 21 (11), 624-32.

129. Rieder, C. L. and Salmon, E. D. (1998), 'The vertebrate cell kinetochore and its roles during mitosis', *Trends Cell Biol,* 8 (8), 310-8.

130. Ritchie, K., et al. (2008), 'Loss of ATRX leads to chromosome cohesion and congression defects', *J Cell Biol,* 180 (2), 315-24.

131. Ronesi, J. A. and Huber, K. M. (2008a), 'Metabotropic glutamate receptors and fragile x mental retardation protein: partners in translational regulation at the synapse', *Sci Signal,* 1 (5), pe6.

132. --- (2008b), 'Homer interactions are necessary for metabotropic glutamate receptor-induced long-term depression and translational activation', *J Neurosci,* 28 (2), 543-7.

133. Ropers, H. H. (2006), 'X-linked mental retardation: many genes for a complex disorder', *Curr Opin Genet Dev,* 16 (3), 260-9.

134. --- (2007), 'New perspectives for the elucidation of genetic disorders', *Am J Hum Genet,* 81 (2), 199-207.

135. --- (2008), 'Genetics of intellectual disability', *Curr Opin Genet Dev,* 18 (3), 241-50.

136. --- (2010), 'Single gene disorders come into focus--again', *Dialogues Clin Neurosci,* 12 (1), 95-102.

137. Ropers, H. H. and Hamel, B. C. (2005), 'X-linked mental retardation', *Nat Rev Genet,* 6 (1), 46-57.

138. Ropers, H. H., et al. (2003), 'Nonsyndromic X-linked mental retardation: where are the missing mutations?', *Trends Genet,* 19 (6), 316-20.

139. Ross, M. T., et al. (2005), 'The DNA sequence of the human X chromosome', *Nature,* 434 (7031), 325-37.

140. Ruschendorf, F. and Nurnberg, P. (2005), 'ALOHOMORA: a tool for linkage analysis using 10K SNP array data', *Bioinformatics,* 21 (9), 2123-5.

141. Schirmer, E. C. and Foisner, R. (2007), 'Proteins that associate with lamins: many faces, many functions', *Exp Cell Res,* 313 (10), 2167-79.

142. Schmidt, E. E. and Schibler, U. (1995), 'Cell size regulation, a mechanism that controls cellular RNA accumulation: consequences on regulation of the ubiquitous transcription factors Oct1 and NF-Y and the liver-enriched transcription factor DBP', *J Cell Biol,* 128 (4), 467-83.

143. Selbach, M. and Mann, M. (2006), 'Protein interaction screening by quantitative immunoprecipitation combined with knockdown (QUICK)', *Nat Methods,* 3 (12), 981-3.

144. Shabsigh, R. and Rowland, D. (2007), 'The Diagnostic and Statistical Manual of Mental Disorders, fourth edition, text revision as an appropriate diagnostic for premature ejaculation', *J Sex Med,* 4 (5), 1468-78.

145. Sharma, N., Berbari, N. F., and Yoder, B. K. (2008), 'Ciliary dysfunction in developmental abnormalities and diseases', *Curr Top Dev Biol,* 85, 371-427.

146. Shen, J., et al. (2005), 'ASPM mutations identified in patients with primary microcephaly and seizures', *J Med Genet,* 42 (9), 725-9.

147. Shi, Y., et al. (2008), 'Induction of pluripotent stem cells from mouse embryonic fibroblasts by Oct4 and Klf4 with small-molecule compounds', *Cell Stem Cell,* 3 (5), 568-74.

148. Shimada, M. and Komatsu, K. (2009), 'Emerging connection between centrosome and DNA repair machinery', *J Radiat Res (Tokyo),* 50 (4), 295-301.

149. Shumaker, D. K., et al. (1998), 'TPEN, a Zn2+/Fe2+ chelator with low affinity for Ca2+, inhibits lamin assembly, destabilizes nuclear architecture and may independently protect nuclei from apoptosis in vitro', *Cell Calcium,* 23 (2-3), 151-64.

150. Spiechowicz, M., et al. (2006), 'Density of Sgt1-immunopositive neurons is decreased in the cerebral cortex of Alzheimer's disease brain', *Neurochem Int,* 49 (5), 487-93.

151. Sunkel, C. E. and Glover, D. M. (1988), 'polo, a mitotic mutant of Drosophila displaying abnormal spindle poles', *J Cell Sci,* 89 (Pt 1), 25-38.

152. Takaki, T., et al. (2008), 'Polo-like kinase 1 reaches beyond mitosis--cytokinesis, DNA damage response, and development', *Curr Opin Cell Biol,* 20 (6), 650-60.

153. Tanaka, T. U., et al. (2002), 'Evidence that the Ipl1-Sli15 (Aurora kinase-INCENP) complex promotes chromosome bi-orientation by altering kinetochore-spindle pole connections', *Cell,* 108 (3), 317-29.

154. Tang, Z., et al. (2004), 'Human Bub1 protects centromeric sister-chromatid cohesion through Shugoshin during mitosis', *Proc Natl Acad Sci U S A,* 101 (52), 18012-7.

155. --- (2006), 'PP2A is required for centromeric localization of Sgo1 and proper chromosome segregation', *Dev Cell,* 10 (5), 575-85.

156. Thiele, H. and Nurnberg, P. (2005), 'HaploPainter: a tool for drawing pedigrees with complex haplotypes', *Bioinformatics,* 21 (8), 1730-2.

157. Thomas, P. D., et al. (2006), 'Applications for protein sequence-function evolution data: mRNA/protein expression analysis and coding SNP scoring tools', *Nucleic Acids Res,* 34 (Web Server issue), W645-50.

158. --- (2003), 'PANTHER: a library of protein families and subfamilies indexed by function', *Genome Res,* 13 (9), 2129-41.

159. van de Weerdt, B. C. and Medema, R. H. (2006), 'Polo-like kinases: a team in control of the division', *Cell Cycle,* 5 (8), 853-64.

160. van Vlijmen, T., et al. (2008), 'A unique residue in rab3c determines the interaction with novel binding protein Zwint-1', *FEBS Lett,* 582 (19), 2838-42.

161. Vanoosthuyse, V., Prykhozhij, S., and Hardwick, K. G. (2007), 'Shugoshin 2 regulates localization of the chromosomal passenger proteins in fission yeast mitosis', *Mol Biol Cell,* 18 (5), 1657-69.

162. Vassilev, L. T., et al. (2006), 'Selective small-molecule inhibitor reveals critical mitotic functions of human CDK1', *Proc Natl Acad Sci U S A,* 103 (28), 10660-5.

163. Verkerk, A. J., et al. (1991), 'Identification of a gene (FMR-1) containing a CGG repeat coincident with a breakpoint cluster region exhibiting length variation in fragile X syndrome', *Cell,* 65 (5), 905-14.

164. Villard, L. (2007), 'MECP2 mutations in males', *J Med Genet,* 44 (7), 417-23.

165. Wagner, N. and Krohne, G. (2007), 'LEM-Domain proteins: new insights into lamin-interacting proteins', *Int Rev Cytol,* 261, 1-46.

166. Wang, H., et al. (2007), 'Polo inhibits progenitor self-renewal and regulates Numb asymmetry by phosphorylating Pon', *Nature,* 449 (7158), 96-100.

167. Webster, M., Witkin, K. L., and Cohen-Fix, O. (2009), 'Sizing up the nucleus: nuclear shape, size and nuclear-envelope assembly', *J Cell Sci,* 122 (Pt 10), 1477-86.

168. Welstead, G. G., Schorderet, P., and Boyer, L. A. (2008), 'The reprogramming language of pluripotency', *Curr Opin Genet Dev,* 18 (2), 123-9.

169. Wilcock, A. C., Swedlow, J. R., and Storey, K. G. (2007), 'Mitotic spindle orientation distinguishes stem cell and terminal modes of neuron production in the early spinal cord', *Development,* 134 (10), 1943-54.

170. Woods, C. G., et al. (2006), 'Quantification of homozygosity in consanguineous individuals with autosomal recessive disease', *Am J Hum Genet,* 78 (5), 889-96.

171. Yamashita, A., et al. (2009), 'SMG-8 and SMG-9, two novel subunits of the SMG-1 complex, regulate remodeling of the mRNA surveillance complex during nonsense-mediated mRNA decay', *Genes Dev,* 23 (9), 1091-105.

172. Yu, S., et al. (1991), 'Fragile X genotype characterized by an unstable region of DNA', *Science,* 252 (5009), 1179-81.

173. Zalfa, F., et al. (2007), 'A new function for the fragile X mental retardation protein in regulation of PSD-95 mRNA stability', *Nat Neurosci,* 10 (5), 578-87.

174. Zhao, M., Li, X., and Chen, Z. (2010), 'CC2D1A, a DM14 and C2 domain protein, activates NF-{kappa}B through the canonical pathway', *J Biol Chem*.

175. Zhou, H. and Clapham, D. E. (2009), 'Mammalian MagT1 and TUSC3 are required for cellular magnesium uptake and vertebrate embryonic development', *Proc Natl Acad Sci U S A,* 106 (37), 15750-5.

6.Abstract

In the course of systematic clinical and molecular studies to identify intellectual disability (ID) causing defects that follow an autosomal recessive mode of inheritance (ARID), we found a single 4.3 Mbp interval on chromosome 5q with a LOD score of 4.41 by autozygosity mapping in a family with four females affected by mild to moderate ID and oligomenorrhea. By sequencing the coding regions of all 28 genes within this region we discovered a nonsense mutation in exon 2 of the BOD1 gene. This defect co-segregated with the disease and was not found in 720 Iranian and German control chromosomes. All other genes within the interval were not affected by nucleotide changes. BOD1 is expressed in a wide range of tissues, including brain and ovary. By RT-PCR, we identified two previously unknown isoforms of BOD1 in control lymphoblast and fibroblast cells and showed expression of all four transcripts in a variety of brain tissues. qRT-PCR revealed loss of all BOD1 isoforms in patient fibroblasts, including splice variants that did not contain exon 2. For all transcripts except one, this seems to be due to nonsense mediated decay, as defect of this mRNA could be abrogated by cycloheximide treatment of the cells.

Absence of BOD1 protein in cells of the patients was confirmed by Western blotting experiments. BOD1 is required for proper chromosome segregation and correction of synthelic chromosomes during mitosis (Porter et al. 2007). Fibroblasts from two different patients showed several abnormalities in cell division (chromosomal bi-orientation, mitotic index, mitotic timings, increased levels of Plk1 activity, etc.) which are all in line with the findings in the BOD1 depleted HeLa cells (Porter et al. 2007; Porter et al. unpublished) and may also provide an explanation for the oligomenorrhea observed in this family. In patient fibroblasts, confocal indirect immunoflorescence imaging revealed nuclear structural defects.

Subsequent overexpression experiments using BOD1 cDNA in HaCat cells were performed to further investigate the cell biology of this protein in non-dividing cells and provided preliminary evidence for an involvement of BOD1 in nuclear and chromatin organization. This indicated a putative role in the regulation of

gene expression and whole genome expression profiling in patient lymphoblast cells showed deregulation of target genes that are critical for human cognition.

Moreover, in patient cells the formation of primary cilia was found to be defective. Cilia defects have been observed previously in several other disorders involving ID.

Finally, overexpression experiments in murine primary neuronal cells showed co-localization of GFP-tagged BOD1 with presynaptic proteins, suggesting a putative function of BOD1 in neuronal synapses, which could be an explanation for the ID observed in our patients.

In summary, our results provide evidence indicating that BOD1 plays critical roles in cell cycle progression, the formation of primary cilia, chromatin organization and the regulation of transcription. Furthermore our observations suggest that in humans, this protein is required for normal brain function, which may be related to the role of BOD1 in the regulation of PLK1 during brain development. However, further in depth functional investigations are needed to shed more light on the precise role of this protein during brain development and in fully differentiated neuronal tissues.

7.Zusammenfassung

Im Zuge unserer klinischen und molekularen Studien zur Identifizierung der genetischen Ursachen autosomal-rezessiver geistiger Behinderung, untersuchten wir eine iranische Familie mit vier Patientinnen, welche einen milden bis mittelschweren Grad geistiger Behinderung sowie Oligomenorrhoe aufweisen. Mittels Autozygosity Mapping wurde ein 4,3 Mbp Intervall auf Chromosom 5 identifiziert, welches 28 Gene beinhaltet. Die kodierenden Bereiche dieser Gene wurden sequenziert und als einzige Nukleotidänderung wurde eine Nonsense Mutation in Exon 2 des *BOD1* Gens nachgewiesen. Diese Mutation co-seggregiert mit der Krankheit und wurde nicht in 720 iranischen und deutschen Kontroll-Chromosomen gefunden.

BOD1 wird in einer Vielzahl von Geweben exprimiert, einschließlich des Gehirns sowie der Eierstöcke. Durch RT-PCR wurden zwei bislang unbekannte Isoformen *BOD1*s entdeckt, die ebenfalls im Gehirn exprimiert werden. qRT-PCR zeigte den Verlust aller Isoformen in Fibroblasten der Patientinnen. Für alle Isoformen bis auf eine ist hierfür vermutlich nonsense mediated decay verantwortlich, da in dieser mRNA der Defekt durch die Behandlung mit Cycloheximid aufgehoben wurde. Die Abwesenheit von BOD1 in den Zellen der Patientinnen wurde auch mittels Western Blot nachgewiesen.

BOD1 wird für die korrekte Chromosomentrennung und die Korrektur der synthelischen Chromosomen während der Meiose benötigt (Porter *et al.* 2007). In Übereinstimmung mit bereits beschriebenen Anomalien, welche in HeLa Zellen ohne BOD1 auftreten (Porter *et al.* 2007; Porter *et al.* unveröffentlicht), wiesen Fibroblasten der Patientinnen mehrere Abnormitäten während der Zellteilung auf (chromosomale Biorientierung, mitotischer Index, zeitliche Koordinierung der Mitose, erhöhte Plk1 Aktivität, etc.), welche eine Erklärung für die Oligomenorrhoe der Patientinnen bieten.

Die Untersuchung von Interphase Fibroblasten der Patientinnen mittels konfokaler indirekter Immunfloureszenz ergab, dass strukturelle Defekte des Zellkerns vorliegen. Überexpression von *BOD1* in sich nicht teilenden HaCat

Zellen zeigte eine Beteiligung von BOD1 an der Zellkern- und Chromatinorganisation, was eine putative Rolle BOD1s bei der Regulierung der Genexpression nahe legt.

Whole Genome Expression Profiling in Lymphoblasten der Patientinnen zeigte eine Deregulation von Zielgenen, die entscheidend für die humane Kognition sind. Darüber hinaus ist die Formation der primären Zilien in den Zellen der Patientinnen fehlerhaft. Schäden an Zilien wurden in einer Vielzahl von Krankheiten die mit geistiger Behinderung einhergehen beobachtet.

Letztendlich zeigten Überexpressionsstudien in murinen primären neuronalen Zellen Co-Lokalisation von GFP getaggten BOD1 mit Page: 168 präsynaptischen Proteinen, was auf eine putative Funktion von BOD1 in neuronalen Synapsen hinweist, deren Beeinträchtigung zu der in den Patientinnen beobachteten geistigen Behinderung führen könnten.

Unsere Ergebnisse zeigen die kritische Beteiligung BOD1s am Zellzyklus, an der Formation primärer Zilien, der Chromatinorganisation sowie der Regulierung der Transkription. Des Weiteren weisen unsere Beobachtungen darauf hin, dass BOD1 für die normale Gehirnfunktion des Menschen notwendig ist, was im Zusammenhang mit der Rolle BOD1 als Regulator von PLK1 während der Gehirnentwicklung im Zusammenhang stehen kann.

Weiterführende funktionelle Studien sind nötig um die genaue Funktion BOD1s während der Gehirnentwicklung und besonders im differenzierten neuronalen Gewebe aufzuklären.

8. Publications

1- "Bod1 is required for the proper stability, localisation and function of Plk1 kinase, and its loss causes Mental Retardation in Man". ***S.Esmaeeli-Nieh***, *I.M.Porter, M.M.Motazacker, M.Porter, K.Kahrizi, F.Behjati, A.Tzschach, H.Scherthan, M.Sayfati, H.Najmabadi, J.J.Blow, H.H.Ropers, A.W.Kuss and J.R.Swedlow.* Submitted 2010.

2- "BOD1 act as a nuclear protein and is involved in chromatin organization". ***S.Esmaeeli-Nieh*** *et al.* Manuscript in preparation 2010.

3- "Homozygosity mapping of primary microcephaly in 120 Iranian families: novel mutations and phenotypes". ***S.Esmaeeli-Nieh***, *H.Darvish, Gh.Bahrami Monajemi, M. Mohseni, F.Behjati, S.Ghasemi Firouzabadi, P.Jamali, S.Azimi, F.Mojahedi , A.Dehghan, Y.Shafeghati, A.Jankhah, M.Falah, M.J.Soltani Banavandi, I.Bahman, M.Ghani Kakhki, M.Garshasbi, S.S.Abedini, A.Naghavi, A.W.Kuss, H.H.Ropers, H.Neitzel, K.Kahrizi, H.Najmabadi*. Accepted in Journal of Medical Genetics 2010.

4- "Fragile X Syndrome Screening of Families with Consanguineous and Non-consanguineous Parents in the Iranian Population" *A.R. Pouya, S.S.Abedini, N.Mansoorian, F.Behjati, N.Nikzat, M.Mohseni, **S.Esmaeeli-Nieh**, L.Abbasi, H.Darvish, G.B.Monajemi, S.Banihashemi, K.Kahrizi, H.H.Ropers, H.Najmabadi*. Eur J Med Genet. 2009 Apr 7.

5- "A defect in the ionotropic glutamate receptor 6 gene (GLUR6) causes autosomal recessive mental retardation". *M.M.Motazacker, B.Rost, T.Hucho, M.Garshasbi, K.Kahrizi, R.Ullmann, S.S.Abedini, **S.Esmaeeli-Nieh**, S.H.Amini, Ch.Goswami, A.Tzschach, L.R.Jensen, D.Schmitz, H.H.Ropers, H.Najmabadi, A.W.Kuss.* Am J Hum Genet. 2007 Oct;81(4):792-8.

6- "Homozygosity mapping in consanguineous families reveals extreme heterogeneity of non-syndromic autosomal recessive mental retardation and identifies 8 novel gene loci." *H.Najmabadi, M.M.Motazacker, M.Garshasbi,*

K.Kahrizi, A.Tzschach, W.Chen, F.Behjati,Valeh Hadavi, ***S. Esmaeeli-Nieh****, S.S.Abedini, R.Vazifehmand, S.Ghasemi Firouzabadi, P.Jamali, M.Falah, S.M.Seifati, A.Grüters, S.Lenzner, L.R.Jensen, F.Rüschendorf, A.W. Kuss, H.H.Ropers*. Hum Genet. 2006 Nov 21.

7- "SNP array-based homozygosity mapping reveals MCPH1 deletion in family with autosomal recessive MR and microcephaly". *M.Garshasbi, M.M.Motazacker, K.Kahrizi, F.Behjati, S.S.Abedini,* ***S.Esmaeeli-Nieh****, S.Ghasemi Firouzabadi, C.Becker, F.Rueschendorf, P.Nuernberg, A.Tzschach, R.Vazifehmand, F.Erdogan, R.Ullmann, S.Lenzner, A.W.Kuss, H.H.Ropers, H.Najmabadi*. Hum Genet,2005; DOI 10.1007/s00439-005-0104-y

9. Curriculum vitae

For reasons of data protection,
the curriculum vitae is not included in the online version

10. Supplementary data

10.1. Appendix – A

Transformation of B-lymphocytes with Epstein-Barr Virus (EBV) in vitro

To transform the cells, transforming virus obtained from the lymphoblastoid marmoset cell line B95-8. B95-8 is grown in RPMI 1640 with 10% FBS.

Transformation medium

Took 20 ml of B95-8 and centrifuged for 10 min in 1000 rpm, subsequently Filtrated the supernatant twice through 0.45µm filter

Protocol for preparation of the transformation medium:

- 16 ml filtrated B95-8 supernatant
- 16 ml RPMI 1640 "WASH" (including L-glutamine and penicillin-streptomycin)
- 16 µl Cyclosporin A working solution (0.5 mg/ml)
- 8 ml FBS (final concentration 20%)

Storage condition: maximum of 2 - 4 weeks in 4°C.

Isolation of Lymphocytes with Ficoll-Gradient

Protocol:

- Mix 5 ml fresh blood (stored at room temperature, maximum 48 hr old) with 5 ml RPMI "WASH" (37°C warm)
- Pipette 2 x 5 ml Ficoll (d=1.077) into two clear 15 ml-centrifuge tubes
- Carefully add the diluted blood sample on top of the Ficoll, 5 ml in each tube
- Centrifuge at 1000rpm for 30 min at room temperature (without brake)
- Discard the upper layer from both tubes using a sterile 5 ml-pipette, leaving the lymphocyte layer intact at the interface

- Transfer lymphocyte layer with a sterile Pasteur pipette into one new clear 15 ml-centrifuge tube
- Add Wash-medium up to 10 ml
- Centrifuge 10 min at 1000 rpm and room temperature
- Remove supernatant and add 10 ml Wash-medium (don't pipette the pellet up and down)
- Centrifuge 10 min at 1000 rpm and room temperature
- Remove the supernatant

EBV-transformation

Protocol:

- Resuspend the pellet (very carefully) in 1.5 ml transformation-medium and place the suspension in one well of a 12-well-plate
- After 3-4 days add 1ml transformation medium
- Feed the cells twice a week as follow: 1st and 2nd week feed twice "RPMI Spezial" + Cyclosporin. Take out 1 ml old medium and add 1 ml fresh medium. From the third week on use "RPMI Spezial" without Cyclosporin. Feed twice a week till the cells start growing, it takes 2-4 weeks (up to 8-10 weeks)

Note: When the medium turn into yellow, then the "cell clumps" under the microscope are visible. If enough "big clumps" in the first well were observed, then split the culture into two wells.

- Add 1ml fresh "RPMI Spezial" in each well. After 3-4 days when the medium is bright yellow again, pipette the culture from both wells in one 25cm^2-flask and add 1/2 volume fresh "RPMI Spezial". Keep the flask upright in the incubator.
- After 2 - 4 days add again half of the volume.

Note: Always wait with feeding till the medium is yellow again; the only thing that can kill these cells is a high dilution condition.

Cyclosporin-A dilution

An ampoule contains 50 mg Cyclosporin A in 1 ml. The solution is highly viscous, so first warmed it up by keeping in hand, and then opened the ampoule. Removed the content (Gilsonpipette) and washed it twice or more with medium.

Note: Mix it well, kept it cool and used it for maximum of four months.

Stock:

Dilution 1:10: 1 ml Cyclosporin A (ampoule) + 9 ml RPMI "WASH"

Solution (5 mg/ml):

Dilution 1:10: 1 ml stock + 9 ml RPMI "WASH"⇒ working-solution (0.5 mg/ml)

RPMI Spezial

To prepare Total volume of 50 ml:

- 33.5 ml RPMI 1640
- 0.5 ml Glutamax (stable L-Glutamine)
- 0.5 ml Pen/Strep.
- 5.0 ml Amniomed (medium for Amnion cells)
- 0.5 ml Hepes
- 10 ml FCS (final concentration of 20%)

RPMI Spezial + Cyclosporin

- 10 ml RPMI Spezial
- 4 µl Cyclosporin-A (500µg/ml)

10.2. Appendix – B

Table S1. Primers used for amplification and sequencing of *BOD1*

Exons number	Direction	Primers	Product size
3'UTR	Forward	GATGGCCACAGAAAACTTCC	492 bp
3'UTR	Reverse	CAGAGGCCTGGCTAGTTCC	
1	Forward	CCCTTCACCACCTCTACACG	400 bp
1	Reverse	GGCTTTCGAAAATCAAAGCTG	
2	Forward	GAGACTAAGTTCAAAACTTTGGTGC	259 bp
2	Reverse	CCTCAACCTTCTTGTGCATC	
3	Forward	GGGCTGTAGCTTTGAAGGTG	394 bp
3	Reverse	AATTACGGCCTACCCCATTC	
5'UTR-1	Forward	ATGGAGTGTAAAACATTCATTTTAAG	498 bp
5'UTR-1	Reverse	GGCTATGTTCTCACTGTAGCTTCC	
5'UTR-2	Forward	GCTGTGGGATAAACGGAAGC	400 bp
5'UTR-2	Reverse	CCATTTATTGACCATTCACTTTTC	
5'UTR-3	Forward	AGGGGCCAGTGAGTCTTAGG	580 bp
5'UTR-3	Reverse	TCAGATTAGCAGCAATATGCAGTAG	

10.3. Appendix – C

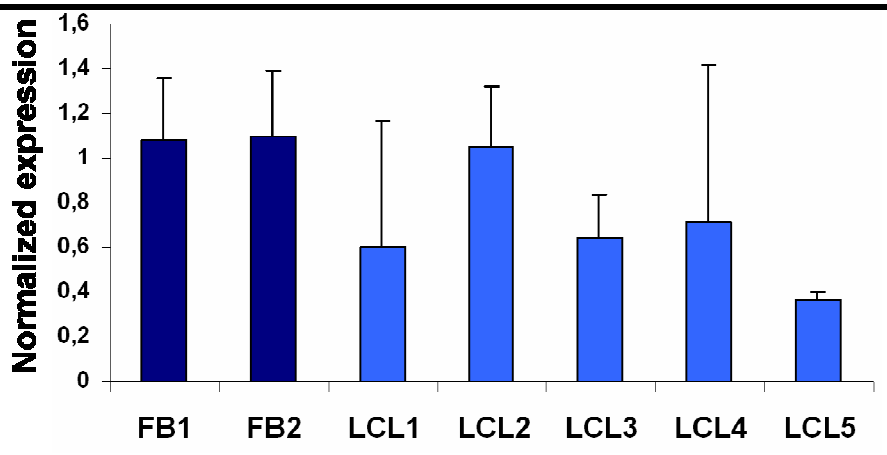

Figure S1. *BOD1* full transcript has variable expression pattern in LCL cells. qRT-PCR was twice performed in triplicates, using isoform specific primers for full transcript. Columns represent *BOD1* expression relative to *GAPDH* expression. *BOD1* has stable and variable pattern of expression in FB cells and LCL cells, respectively. Error bars represent the SD.

10.4. Appendix – D

Visualization of endogenous BOD1 in LCL cells

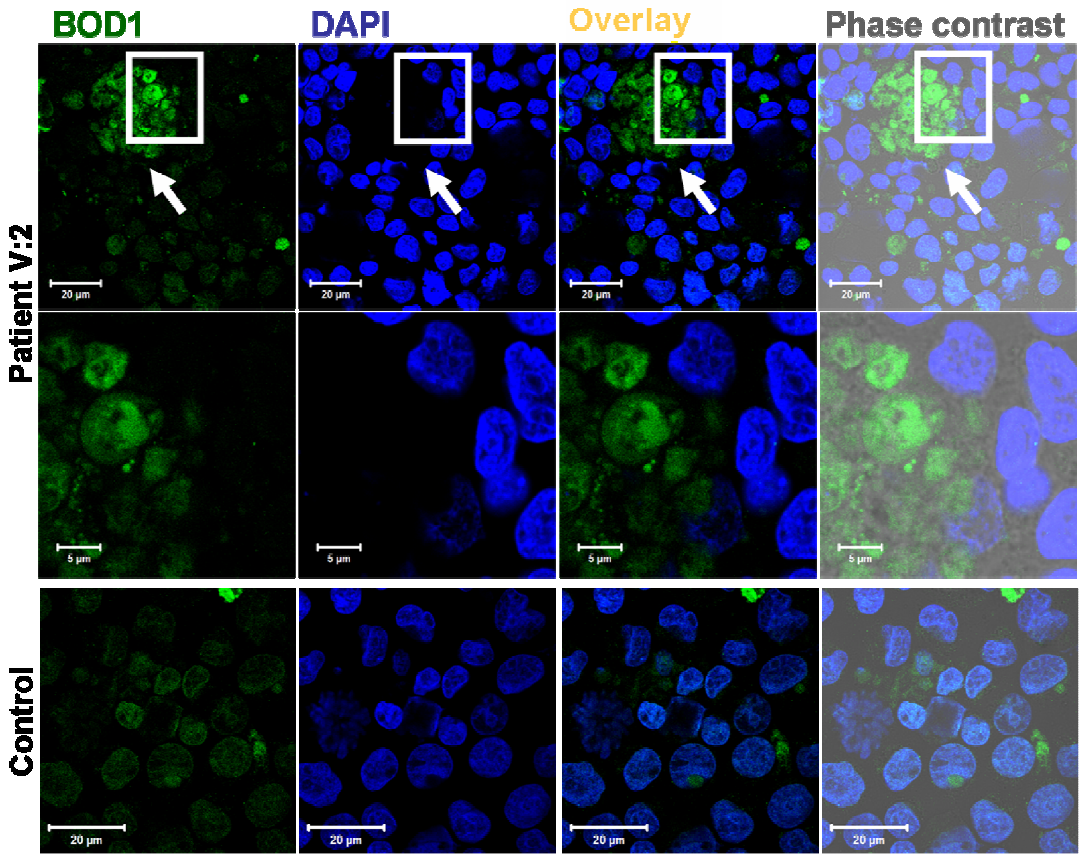

Figure S2: Accumulation of BOD1 staining in patient LCLs. BOD1 was stained with the direct antibody (green) and DNA was stained with DAPI (blue). BOD1 staining is accumulating in some areas where DNA staining is absent (arrow). The middle row images are magnified of the boxed areas from the upper row. Nuclear structural defects can be seen.

10.5. Appendix – E

Table S2. Categorization of FB cells from patients and controls into two subgroups of G1 and G2 by PI staining using FACScan. The cells were harvested in four successive days and each time in triplicate.

	G1					G2				
	1	2	3	SUM_G1	SD_G1	1	2	3	SUM_G2	SD_G2
DAY 1										
Patient V:2		53.87	56.24	55.055	1.67		42.57	40.29	41.43	1.612
Patient V:3	45.11	46.75	45.35	45.736	0.88	46.76	48.01	49.65	48.14	1.449
Control 1	43.83	48.44	46.88	46.383	2.34	50.94	46.57	46.86	48.123	2.443
Control 2	50.02	50.09	48.51	49.54	0.89	47.4	45.85	49.03	47.426	1.590
DAY 2										
Patient V:2	64.02	60.39	62.38	62.263	1.81	33.4	32.03	34.68	33.37	1.325
Patient V:3	58.38	56.63	59.96	58.323	1.66	35.8	35.58	36.44	35.94	0.446
Control 1	57.86	58.58	56.66	57.7	0.96	38.35	37.27	39.63	38.416	1.181
Control 2	68.75	66.39	69.47	68.203	1.61	29.08	31.9	28.76	29.913	1.727
DAY 3										
Patient V:2	68.57	68.57	67.1	68.08	0.84	28.19	29.42	29.37	28.993	0.696
Patient V:3	66.98	65.07	66.69	66.246	1.02	28.38	30.72	30.32	29.806	1.251
Control 1	62.42	61.86	63	62.426	0.57	34.86	35.53	34.57	34.986	0.492
Control 2	65.36	62.83	69.93	66.04	3.59	33.11	35.21	29.3	32.54	2.995
DAY 4										
Patient V:2	69.52	74.31	71.76	71.863	2.39	24.6	22.3	23.76	23.553	1.163
Patient V:3	73.95	72.42	73.08	73.15	0.76	24	24.92	25.11	24.676	0.593
Control 1	70.09	69.68	73.15	70.973	1.89	27.53	27.03	25.1	26.553	1.283
Control 2	85.63	85.76	86.96	86.116	0.73	12.84	13.51	12.57	12.973	0.483

10.6. Appendix – F

Table S3. Nuclear circumference quantification in 150 FB cells from patients and controls.

No.	Control 1	Control 2	Patient V:2	Patient V:2	No.	Control 1	Control 2	Patient V:2	Patient V:2
1	83.19	92.68	69.57	27.21	**48**	137.6	156.79	138.93	183.27
2	94.35	99.74	76.90	81.89	**49**	138.33	157.09	139.76	183.51
3	98.46	107.9	91.97	125.52	**50**	138.94	157.17	140.78	184.43
4	103.38	111.63	94.22	126.19	**51**	139.08	157.32	141.75	184.49
5	107.3	114.79	94.77	129.97	**52**	139.17	157.83	142.01	185.45
6	112.51	115.74	94.97	134.6	**53**	139.44	158.28	142.36	185.67
7	112.8	118.32	95.48	139.47	**54**	139.6	159.64	142.57	185.74
8	113.68	119.65	97.29	140.53	**55**	140.91	159.76	143.90	187.15
9	115.36	120.55	98.47	143.3	**56**	141	160.59	144.63	188.35
10	115.47	121.36	99.37	144.09	**57**	141.01	161.01	145.37	188.88
11	116.42	122.18	99.58	145.66	**58**	142.05	161.85	145.98	189.4
12	116.59	124.04	99.84	145.98	**59**	142.15	161.95	146.34	189.89
13	116.67	124.22	100.69	149.75	**60**	142.38	162.81	146.47	190.61
14	116.73	125.44	100.71	149.85	**61**	142.64	162.92	150.03	191.36
15	118.76	126.06	100.90	151.05	**62**	143.43	163.07	151.35	192.32
16	118.83	128.65	102.03	153.01	**63**	143.46	163.41	151.68	193.2
17	119.99	132.54	102.10	156.31	**64**	143.59	163.83	152.47	194.85
18	120.53	134.09	102.94	157.31	**65**	143.97	163.85	153.28	195.31
19	121.41	134.95	103.28	158.02	**66**	144.06	164.25	159.06	197.88
20	122.22	135.43	103.83	159.49	**67**	144.25	164.28	159.91	198.37
21	122.63	136.97	106.49	159.95	**68**	144.42	165.06	161.46	200.32
22	123.9	138.13	106.65	161.77	**69**	144.68	165.27	161.54	201.16
23	124.27	138.84	107.74	162.22	**70**	145.95	166.06	164.35	201.58
24	124.27	140.08	108.14	162.78	**71**	147.2	166.17	166.94	202.5
25	125.68	142.79	108.70	162.86	**72**	148.42	166.65	167.45	202.93
26	125.9	142.79	109.82	164.65	**73**	148.44	166.87	169.13	203.04
27	126.75	143.35	110.06	164.81	**74**	148.72	167.39	169.26	204.59
28	126.79	143.59	111.62	165.91	**75**	148.84	167.39	171.42	206.12
29	127.16	144.04	111.74	167.58	**76**	149.47	167.49	171.66	206.29
30	127.47	144.22	111.88	167.63	**77**	149.57	170.2	172.71	207.71
31	128.08	145	113.65	168.65	**78**	149.88	171.3	173.76	207.71
32	128.56	145.23	113.74	169.7	**79**	150.41	171.42	174.87	210.01
33	129.37	145.34	114.39	169.98	**80**	151.17	171.58	175.71	210.84
34	129.7	145.37	115.63	170.01	**81**	151.22	171.64	176.02	211.12
35	129.81	145.9	117.98	170.77	**82**	151.53	173.51	177.09	214.14
36	130.07	146.22	118.85	171.76	**83**	152.2	174.99	178.95	215.64
37	130.89	146.73	119.39	173.6	**84**	153.93	175.03	179.44	216.53
38	130.93	146.88	119.85	173.97	**85**	154.79	175.12	181.20	217.18
39	131.01	146.88	121.15	174.31	**86**	155.15	175.31	187.14	219.24
40	131.9	149.64	121.60	174.87	**87**	155.7	175.61	188.55	222.18
41	131.98	150.26	122.86	175.33	**88**	156.44	176.34	188.60	222.86
42	133.78	150.92	124.40	176.12	**89**	156.52	176.52	193.48	228.19
43	134.59	151.66	127.87	177.94	**90**	159.32	176.71	193.51	231.73
44	135.12	152.97	128.24	177.97	**91**	160.32	177.03	193.92	234.09
45	135.23	153.28	130.88	178.82	**92**	161.38	178.73	197.45	238.31
46	135.32	153.52	132.95	179.34	**93**	161.45	179.22	198.10	241.45
47	135.74	154.08	134.45	180.94	**94**	162.71	181.34	198.47	241.56

No.	Control 1	Control 2	Patient V:2	Patient V:2	No.	Control 1	Control 2	Patient V:2	Patient V:2
95	165.83	183.67	207.84	248.56	**123**	164.29	182.53	207.20	246.16
96	166.25	186.4	208.26	248.81	**124**	136.91	156.58	137.85	181.6
97	167.25	186.74	209.14	250.41	**125**	136.5	156.39	137.73	181.46
98	167.66	187.3	209.18	250.53	**126**	163.59	182.45	199.35	245.71
99	167.74	187.92	217.06	250.84	**127**	204.92	210.19	269.68	350.57
100	169.08	188.07	218.02	251.21	**128**	205.75	210.2	278.87	351.86
101	170.06	188.73	218.69	257.92	**129**	206.84	210.23	278.98	355.99
102	171.06	189.31	219.43	261.04	**130**	209.59	210.33	283.05	362.07
103	171.99	189.96	220.99	261.07	**131**	210.16	213.13	284.54	367.62
104	172.81	190.55	222.58	262.42	**132**	213.56	219.65	289.76	368.59
105	172.92	192.84	223.04	262.88	**133**	216.91	222.55	290.98	369.27
106	173.01	194.65	223.24	268.26	**134**	217.38	225.85	291.05	376.02
107	176.47	194.7	236.54	269.82	**135**	218.56	230.65	295.14	376.58
108	178.14	194.74	237.15	271.87	**136**	219.02	238.5	297.76	381.84
109	178.24	195.12	238.18	273.18	**137**	234.2	251.98	301.68	388.42
110	179.48	195.13	239.33	276.06	**138**	249.26	252.76	306.69	392.43
111	180.29	195.45	240.94	281.72	**139**	252.57	258.64	320.76	405.88
112	180.96	199.03	243.12	282.25	**140**	253.05	264.3	345.43	406.46
113	183.48	199.35	245.00	284.28	**141**	258.75	265.72	360.12	437.28
114	183.67	199.58	245.58	286.05	**142**	263.43	301.66	366.98	444.09
115	190.69	200.59	245.72	294.47	**143**	277.94	309.76	367.68	500.92
116	191.5	201.82	247.37	312.57	**144**	280.13	348.41	379.60	551.99
117	193.11	204.86	249.00	321.71	**145**	303.23	359.12	429.50	657.75
118	197.21	205.33	255.76	322.04	**146**	303.48	360.94	467.48	692.65
119	197.95	205.5	258.24	322.76	**147**	310.26	383.75	485.57	788.31
120	198.02	206.71	263.64	336.35	**148**	328.91	414.88	493.15	800.22
121	200.38	209.5	265.13	346.62	**149**	333.43	452.72	741.85	1221.76
122	136.39	156.25	135.04	181.22	**150**	163.43	182.28	199.28	245.61

10.7. Appendix – G

Table S4. Nuclear volume quantification in 150 FB cells from patients and controls.

No.	Control 1	Control 2	Patient V:2	Patient V:2	No.	Control 1	Control 2	Patient V:2	Patient V:2
1	34.44	34.76	30.84	18.17	**48**	41.75	44.51	40.37	48.44
2	35.26	36.46	32.05	20.46	**49**	41.8	44.56	40.56	48.47
3	35.38	36.73	32.22	38.68	**50**	41.81	44.65	40.66	48.57
4	35.43	36.8	32.47	39.41	**51**	41.89	44.84	40.92	48.6
5	35.52	37.44	32.60	39.5	**52**	42.12	44.85	41.04	48.69
6	35.76	37.95	33.28	40.13	**53**	42.18	44.91	41.16	48.77
7	36.4	38.49	33.34	40.76	**54**	42.37	44.94	41.27	48.8
8	37.02	38.62	33.59	40.77	**55**	42.41	45.08	41.44	48.84
9	37.4	39.03	33.67	42.25	**56**	42.47	45.12	41.48	48.96
10	38.08	39.07	33.92	42.3	**57**	42.56	45.16	41.62	49.09
11	38.12	39.58	34.20	42.68	**58**	42.56	45.2	41.75	49.26
12	38.13	39.78	34.39	42.79	**59**	42.62	45.3	41.93	49.26
13	38.32	39.79	34.97	42.81	**60**	42.68	45.48	42.24	49.28
14	38.33	40.01	35.42	43.02	**61**	42.81	45.61	42.39	49.43
15	38.71	40.02	35.86	43.19	**62**	42.81	45.67	42.88	49.44
16	38.71	40.12	35.95	43.23	**63**	42.92	45.84	43.08	49.59
17	38.72	40.69	35.96	43.29	**64**	43.08	45.88	43.15	49.69
18	38.97	40.73	35.97	43.38	**65**	43.09	46.12	43.47	49.81
19	38.99	41.27	36.05	44.09	**66**	43.35	46.26	43.59	49.82
20	39.14	41.66	36.10	44.7	**67**	43.37	46.37	43.75	49.83
21	39.22	41.76	36.17	44.91	**68**	43.56	46.38	43.84	50.02
22	39.31	41.96	36.40	45.28	**69**	43.58	46.41	43.93	50.11
23	39.49	41.96	36.41	45.41	**70**	43.59	46.48	43.94	50.14
24	39.58	42.53	36.42	45.46	**71**	43.61	46.59	44.05	50.15
25	39.68	42.6	36.76	45.75	**72**	43.7	46.66	44.14	50.54
26	39.68	42.66	36.93	45.77	**73**	43.82	46.72	44.22	50.56
27	39.84	42.78	36.99	46.01	**74**	43.83	46.75	44.99	50.57
28	39.87	42.8	37.12	46.15	**75**	43.88	46.77	45.18	50.82
29	39.94	42.86	37.20	46.17	**76**	43.99	46.77	45.77	51.3
30	40.24	42.86	37.32	46.63	**77**	44.07	47.02	45.94	51.56
31	40.25	42.91	37.32	46.8	**78**	44.15	47.1	46.05	52.06
32	40.3	43.17	37.33	46.81	**79**	44.24	47.12	46.14	52.24
33	40.55	43.32	37.45	46.9	**80**	44.26	47.14	46.26	52.38
34	40.57	43.43	37.52	46.91	**81**	44.31	47.25	46.42	52.57
35	40.62	43.64	37.55	47.07	**82**	44.33	47.34	46.57	53.32
36	40.7	43.65	37.59	47.15	**83**	44.39	47.39	47.08	53.56
37	40.75	43.81	38.25	47.2	**84**	44.4	47.39	47.14	53.75
38	40.85	43.88	38.36	47.22	**85**	44.42	47.43	47.31	54.13
39	41.09	43.89	38.59	47.23	**86**	44.61	47.43	47.50	54.13
40	41.13	44.02	38.79	47.46	**87**	44.63	47.45	47.75	54.2
41	41.22	44.04	38.91	47.6	**88**	44.74	47.56	48.31	54.31
42	41.29	44.06	39.33	48.01	**89**	44.8	47.63	48.55	54.45
43	41.3	44.14	39.69	48.05	**90**	44.86	47.67	48.56	54.63
44	41.31	44.15	39.71	48.12	**91**	44.93	47.71	48.67	54.92
45	41.35	44.29	39.83	48.12	**92**	45.08	47.74	49.24	55.39
46	41.39	44.34	39.83	48.17	**93**	45.33	47.91	49.33	55.52
47	41.44	44.34	39.84	48.17	**94**	45.45	47.93	49.36	55.6

No.	Control 1	Control 2	Patient V:2	Patient V:2	No.	Control 1	Control 2	Patient V:2	Patient V:2
95	46.34	48.15	51.16	56.52	**123**	41.64	44.5	40.30	48.44
96	46.38	48.16	51.24	56.71	**124**	46.19	48.14	50.97	56.31
97	46.4	48.26	51.28	57.15	**125**	41.63	44.47	40.27	48.36
98	46.49	48.68	51.46	57.48	**126**	45.52	48.13	50.89	56.22
99	46.52	48.75	51.68	57.5	**127**	50.13	52.31	58.31	66.78
100	46.85	48.78	51.98	57.85	**128**	50.15	52.38	58.41	67.02
101	47.02	48.86	52.02	57.85	**129**	50.42	52.52	58.80	68.57
102	47.09	49.12	52.07	57.87	**130**	51.19	52.75	59.15	68.87
103	47.12	49.19	52.12	58.13	**131**	51.55	52.95	59.48	69.06
104	47.37	49.44	53.07	58.25	**132**	52.28	53.87	59.99	69.39
105	47.49	49.47	53.33	58.3	**133**	52.32	53.99	60.10	69.48
106	47.61	49.5	53.47	58.63	**134**	52.73	54.02	60.67	69.85
107	47.66	49.56	53.76	59.33	**135**	52.74	56.35	61.47	69.91
108	47.69	49.58	53.81	59.53	**136**	52.87	56.56	61.72	70.56
109	47.87	49.7	54.41	59.61	**137**	53.47	57.31	62.34	70.91
110	48.54	49.83	54.68	59.88	**138**	53.62	57.48	63.91	71.14
111	48.55	49.92	55.13	61.03	**139**	54.11	58.35	66.59	72.07
112	48.59	50.09	55.58	61.73	**140**	54.85	58.69	67.41	72.33
113	48.7	50.41	56.05	62.37	**141**	55.7	60.04	68.03	73.86
114	48.79	50.47	56.50	62.95	**142**	56.42	60.48	68.27	76.48
115	48.81	50.8	56.86	63.58	**143**	57.04	61.05	68.45	80.64
116	48.85	50.91	57.17	64.04	**144**	57.86	62.07	69.11	84.69
117	48.86	51.03	57.32	64.74	**145**	60.97	65.19	70.32	90.7
118	49.13	51.15	57.33	64.94	**146**	62.64	69.23	75.42	93.08
119	49.2	51.58	57.49	65.04	**147**	62.72	69.42	77.38	100.43
120	49.7	51.72	58.13	65.66	**148**	64.22	70.42	80.49	111.48
121	50.12	51.81	58.23	66.57	**149**	65.1	75.62	98.31	120.07
122	41.59	44.34	39.99	48.28	**150**	45.49	47.94	49.67	55.64

10.8. Appendix – H

Table S5. Expression intensity of each BOD1-deletion construct in nuclear and cytoplasm.

	Cherry-Bod1	Cytoplasm	Nuclear	NuC/Cyt		Cherry-Bod1	Cytoplasm	Nuclear	Nuc/Cyt
1	ΔN1_1_1	64	231	3.609375	**1**	ΔN3_1_1	42	26	0.61904762
1	ΔN1_1_2	147	76	0.5170068	**1**	ΔN3_1_2	30	40	1.33333333
2	ΔN1_2_1	131	64	0.48854962	**2**	ΔN3_2_1	6	46	7.66666667
2	ΔN1_2_2	47	99	2.10638298	**2**	ΔN3_2_2	101	71	0.7029703
3	ΔN1_3_1	93	253	2.72043011	**3**	ΔN3_3_1	46	116	2.52173913
3	ΔN1_3_2	89	190	2.13483146	**3**	ΔN3_3_2	36	127	3.52777778
4	ΔN1_4_1	86	105	1.22093023	**4**	ΔN3_4_1	81	84	1.03703704
4	ΔN1_4_2	68	108	1.58823529	**4**	ΔN3_4_2	175	211	1.20571429
5	ΔN1_5_1	63	211	3.34920635	**5**	ΔN3_5_1	47	116	2.46808511
5	ΔN1_5_2	59	179	3.03389831	**5**	ΔN3_5_2	59	83	1.40677966
6	ΔN1_6_1	79	186	2.35443038	**6**	ΔN3_6_1	19	93	4.89473684
6	ΔN1_6_2	204	255	1.25	**6**	ΔN3_6_2	16	67	4.1875
7	ΔN1_7_1	167	220	1.31736527	**7**	ΔN3_7_1	152	137	0.90131579
7	ΔN1_7_2	127	179	1.40944882	**7**	ΔN3_7_2	79	107	1.35443038
8	ΔN1_8_1	118	204	1.72881356	**8**	ΔN3_8_1	130	125	0.96153846
8	ΔN1_8_2	67	192	2.86567164	**8**	ΔN3_8_2	108	102	0.94444444
9	ΔN1_9_1	147	255	1.73469388	**9**	ΔN3_9_1	12	152	12.6666667
9	ΔN1_9_2	91	255	2.8021978	**9**	ΔN3_9_2	67	41	0.6119403
10	ΔN1_10_1	93	148	1.59139785	**10**	ΔN3_10_1	89	126	1.41573034
10	ΔN1_10_2	87	73	0.83908046	**10**	ΔN3_10_2	132	21	0.15909091
	ΔN1_MEAN			**1.93309729**		**ΔN3_MEAN**			**2.52932725**
1	ΔN2_1_1	176	199	1.13068182	**1**	ΔN4_1_1	67	76	1.13432836
1	ΔN2_1_2	189	229	1.21164021	**1**	ΔN4_1_2	66	9	0.13636364
2	ΔN2_2_1	48	138	2.875	**2**	ΔN4_2_1	27	55	2.03703704
2	ΔN2_2_2	55	76	1.38181818	**2**	ΔN4_2_2	121	226	1.8677686
3	ΔN2_3_1	14	99	7.07142857	**3**	ΔN4_3_1	84	132	1.57142857
3	ΔN2_3_2	9	37	4.11111111	**3**	ΔN4_3_2	73	92	1.26027397
4	ΔN2_4_1	107	203	1.89719626	**4**	ΔN4_4_1	28	74	2.64285714
4	ΔN2_4_2	113	169	1.49557522	**4**	ΔN4_4_2	29	103	3.55172414
5	ΔN2_5_1	91	156	1.71428571	**5**	ΔN4_5_1	152	208	1.36842105
5	ΔN2_5_2	137	133	0.97080292	**5**	ΔN4_5_2	165	188	1.13939394
6	ΔN2_6_1	23	85	3.69565217	**6**	ΔN4_6_1	18	63	3.5
6	ΔN2_6_2	41	128	3.12195122	**6**	ΔN4_6_2	49	31	0.63265306
7	ΔN2_7_1	74	140	1.89189189	**7**	ΔN4_7_1	155	187	1.20645161
7	ΔN2_7_2	57	203	3.56140351	**7**	ΔN4_7_2	26	89	3.42307692
8	ΔN2_8_1	138	187	1.35507246	**8**	ΔN4_8_1	37	255	6.89189189
8	ΔN2_8_2	109	133	1.22018349	**8**	ΔN4_8_2	170	255	1.5
9	ΔN2_9_1	44	163	3.70454545	**9**	ΔN4_9_1	81	180	2.22222222
9	ΔN2_9_2	160	179	1.11875	**9**	ΔN4_9_2	129	145	1.12403101
10	ΔN2_10_1	12	154	12.8333333	**10**	ΔN4_10_1	76	108	1.42105263
10	ΔN2_10_2	35	129	3.68571429	**10**	ΔN4_10_2	61	166	2.72131148
	ΔN2_MEAN			**3.00240189**		**ΔN4_MEAN**			**2.06761436**

	Cherry-Bod1	Cytoplasm	Nuclear	Nuc/Cyt		Cherry-Bod1	Cytoplasm	Nuclear	Nuc/Cyt
1	ΔC1_1a_1	14	64	4.57142857	**1**	ΔC3_1a_1	64	12	0.1875
1	ΔC1_1a_2	22	62	2.81818182	**2**	ΔC3_1a_2	51	98	1.92156863
2	ΔC1_3a_1	137	59	0.43065693	**2**	ΔC3_1b_1	72	176	2.44444444
2	ΔC1_3a_2	74	87	1.17567568	**3**	ΔC3_1b_2	26	179	6.88461538
3	ΔC1_2a_2	46	87	1.89130435	**3**	ΔC3_2a_1	65	121	1.86153846
3	ΔC1_4a_1	31	30	0.96774194	**4**	ΔC3_2a_2	117	58	0.4957265
4	ΔC1_4a_2	27	5	0.18518519	**4**	ΔC3_2b_1	44	84	1.90909091
4	ΔC1_7a2_2	40	78	1.95	**5**	ΔC3_2b_2	37	56	1.51351351
5	ΔC1_9a_1	151	144	0.95364238	**5**	ΔC3_6a_1	50	67	1.34
5	ΔC1_9a_2	45	76	1.68888889	**6**	ΔC3_6a_2	102	51	0.5
6	ΔC1_10a_1	107	54	0.5046729	**6**	ΔC3_7a_1	57	106	1.85964912
6	ΔC1_10a_2	25	76	3.04	**7**	ΔC3_7a_2	78	113	1.44871795
7	ΔC1_12a_1	62	89	1.43548387	**7**	ΔC3_9a_1	235	187	0.79574468
7	ΔC1_12a_2	127	127	1	**8**	ΔC3_9a_2	132	211	1.59848485
8	ΔC1_14a_1	109	98	0.89908257	**8**	ΔC3_10a_1	115	96	0.83478261
8	ΔC1_14a_2	90	64	0.71111111	**9**	ΔC3_10a_2	76	132	1.73684211
9	ΔC1_2a_1	86	174	2.02325581	**9**	ΔC3_1b_1	16	32	2
9	ΔC1_2a_2	123	128	1.04065041	**10**	ΔC3_1b_1	48	25	0.52083333
10	ΔC1_3a_1	91	79	0.86813187	**10**	ΔC3_4e_1	25	60	2.4
10	ΔC1_3a_2	128	44	0.34375		ΔC3_4e_2	40	17	0.425
	ΔC1_MEAN			**1.42494221**		**ΔC3_MEAN**			**1.63390262**
1	ΔC2_1a_1	13	86	6.61538462	**1**	ΔC4_1C_1	124	221	1.78225806
1	ΔC2_1a_2	27	23	0.85185185	**1**	ΔC4_1C_2	67	207	3.08955224
2	ΔC2_2a_1	127	93	0.73228346	**2**	ΔC4_3b_1	77	134	1.74025974
2	ΔC2_2a_2	142	132	0.92957746	**2**	ΔC4_3b_2	90	176	1.95555556
3	ΔC2_4a_1	76	75	0.98684211	**3**	ΔC4_6a_1	46	51	1.10869565
3	ΔC2_4a_2	69	114	1.65217391	**3**	ΔC4_6a_2	46	107	2.32608696
4	ΔC2_6a_1	147	139	0.94557823	**4**	ΔC4_7a_1	150	203	1.35333333
4	ΔC2_6a_2	88	50	0.56818182	**4**	ΔC4_7a_2	142	234	1.64788732
5	ΔC2_7a_1	60	65	1.08333333	**5**	ΔC4_8a_1	61	86	1.40983607
5	ΔC2_7a_2	19	46	2.42105263	**5**	ΔC4_8a_2	52	84	1.61538462
6	ΔC2_11a_1	82	49	0.59756098	**6**	ΔC4_10a_1	81	148	1.82716049
6	ΔC2_11a_2	77	63	0.81818182	**6**	ΔC4_10a_2	196	120	0.6122449
7	ΔC2_1a_1	110	111	1.00909091	**7**	ΔC4_11b_1	40	75	1.875
7	ΔC2_1a_2	90	101	1.12222222	**7**	ΔC4_11b_2	51	84	1.64705882
8	ΔC2_3_1	23	78	3.39130435	**8**	ΔC4_4d_1	36	41	1.13888889
8	ΔC2_3_2	16	51	3.1875	**8**	ΔC4_4d_2	19	80	4.21052632
9	ΔC2_5a_1	31	14	0.4516129	**9**	ΔC4_7b_1	106	45	0.4245283
9	ΔC2_5a_2	49	34	0.69387755	**9**	ΔC4_7b_2	77	68	0.88311688
10	ΔC2_5C_1	80	59	0.7375	**10**	ΔC4_9_1	52	89	1.71153846
10	ΔC2_5C_2	62	67	1.08064516	**10**	ΔC4_9_2	64	55	0.859375
	ΔC2_MEAN			**1.49378777**		**ΔC4_MEAN**			**1.66091438**

10.9. Appendix – I

Table S6. List of all the genes with differential scores ≤ +13 (corresponding to P-values ≤ 0.05) in LCL cells from one patient against a group of six different controls.

ACCESSION	SYMBOL	Patient diff. Score	ACCESSION	SYMBOL	Patient diff. Score
NM_002707.3	PPM1G	13.06264	NM_198597.1	SEC24C	14.05223
NM_001012643.2	LOC339344	13.06419	NM_012083.2	FRAT2	14.07757
NM_015987.3	HEBP1	13.06716	NM_031434.2	C7orf21	14.10153
NM_199283.4	LOC220686	13.06967	NM_194247.1	HNRPA3	14.10163
NM_139122.1	TAF6	13.12415	NM_003801.2	GPAA1	14.13408
NM_005273.2	GNB2	13.14838	NM_001032279.1	RCE1	14.13408
NM_003858.2	CCNK	13.21667	NM_006312.2	NCOR2	14.17767
CR607514		13.21667	NM_000918.2	P4HB	14.18004
NM_004209.4	SYNGR3	13.22236	NM_017767.1	SLC39A4	14.2095
NM_152563.1	FLJ10661	13.24005	NM_012288.3	TRAM2	14.22626
NM_032641.1	SPSB2	13.24005	NM_001122.2	ADFP	14.2445
AI216576		13.24005	NM_003655.2	CBX4	14.24573
NM_025124.1	FLJ21749	13.24704	NM_181843.1	NUDT8	14.24666
NM_173854.4	SLC41A1	13.27823	NM_005697.3	SCAMP2	14.24666
NM_032910.2	C21orf119	13.30872	NM_153329.2	ALDH16A1	14.25504
NM_006228.2	PNOC	13.30873	NM_017865.2	ZNF692	14.28822
NM_003302.1	TRIP6	13.30873	NM_198489.1	DLNB14	14.30225
XM_938887.1	KLF11	13.39063	NM_138781.2	LOC113386	14.30792
NM_025083.2	LSM16	13.40934	XM_292963.5	LOC643997	14.30792
NM_017723.1	FLJ20245	13.42205	NM_015261.2	hCAP-D3	14.35147
NM_007002.2	ADRM1	13.42708	NM_007244.1	PRR4	14.35147
NM_005013.1	NUCB2	13.47765	NM_133455.2	EMID1	14.35147
NM_005601.3	NKG7	13.49525	NR_001449.1	TRK1	14.41443
NM_018217.1	C20orf31	13.49525	NM_201349.1	DOK2	14.43004
NM_002807.2	PSMD1	13.50402	NM_178238.1	PILRB	14.43004
XM_926814.1	LOC653158	13.50633	NM_006600.2	NUDC	14.44173
NM_013388.4	PREB	13.51233	NM_014282.1	HABP4	14.44776
NM_032797.4	AMID	13.52161	NM_016057.1	COPZ1	14.44776
NM_003056.2	SLC19A1	13.52161	NM_004818.2	DDX23	14.6129
NM_014901.4	RNF44	13.5799	NM_005574.2	LMO2	14.7095
NM_001382.2	DPAGT1	13.67709	AW510851		14.71036
NM_002080.2	GOT2	13.78058	NM_005053.2	RAD23A	14.71645
NM_007022.3	CYB561D2	13.78058	NM_032799.4	ZDHHC12	14.73288
NM_018077.1	RBM28	13.80725	NM_003926.5	MBD3	14.74489
NM_080588.1	PTPN7	13.81569	XM_929420.1	LOC653377	14.75674
NM_030573.2	THAP7	13.81569	NM_015680.3	C2orf24	14.81394
NM_001659.1	ARF3	13.87283	NM_006855.2	KDELR3	14.81966
NM_013265.2	C11orf2	13.88812	XM_927722.1	LOC644608	14.88078
NM_147173.1	NUDT2	13.91514	NM_015305.2	ANGEL1	14.90833
NM_017653.2	DYM	13.91514	NM_153341.1	IBRDC3	14.91797
NM_002096.1	GTF2F1	13.91526	NM_001571.2	IRF3	14.957
NM_005886.1	KATNB1	13.91526	NM_201274.2	M-RIP	14.98093
NM_001002876.1	C22orf18	14.0477	NM_032478.2	MRPL38	14.99119
NM_012145.2	DTYMK	14.0477	NM_022830.1	RBM21	15.01437

NM_002541.2	OGDH	14.0477	NM_005984.1	SLC25A1	15.02357
NM_023007.1	JMJD4	14.0477	NM_153213.2	ARHGEF19	15.04708
NM_016573.1	GMIP	14.04916	NM_007254.2	PNKP	15.062
NM_012191.2	NAT6	15.062	XM_928168.1	LOC645138	16.46285
NM_057089.1	AP1S1	15.062	NM_004104.4	FASN	16.48746
NM_004259.4	RECQL5	15.06926	NM_021934.3	C12orf44	16.56661
XM_928068.1	LOC645001	15.09558	NM_005803.2	FLOT1	16.59285
NM_004565.1	PEX14	15.1151	NM_021095.1	SLC5A6	16.59442
NM_019037.2	EXOSC4	15.1151	NM_004260.1	RECQL4	16.60225
NM_005772.2	RCL1	15.11586	CB047725		16.65457
NM_005563.3	STMN1	15.12792	NM_015259.4	ICOSLG	16.6685
NM_002477.1	MYL5	15.14665	NM_001003684.1	UCRC	16.71217
NM_178502.2	DTX3	15.1674	NM_052925.1	LENG8	16.72709
NM_004383.1	CSK	15.17096	NM_033493.1	CDC2L1	16.74149
NM_021830.3	PEO1	15.188	NM_005892.3	FMNL1	16.74149
NM_001789.2	CDC25A	15.226	NM_199002.1	ARHGEF1	16.77581
NM_021805.1	SIGIRR	15.28605	NM_138801.1	GALM	16.78304
NM_014230.2	SRP68	15.34754	NM_004217.1	AURKB	16.81613
NM_004111.4	FEN1	15.38377	NM_003355.2	UCP2	16.94083
NM_001017956.1	OS9	15.39893	NM_001007468.1	SMARCB1	16.95225
NM_032790.2	FLJ14466	15.43184	NM_003449.3	TRIM26	16.96834
NM_178310.1	SNAI3	15.43933	NM_020230.4	PPAN	17.10019
NM_023948.3	MOSPD3	15.4783	XM_171158.5	MGC27348	17.13264
NM_015399.3	BRMS1	15.5084	NM_001319.5	CSNK1G2	17.16619
NM_018127.4	ELAC2	15.5084	NM_005993.3	TBCD	17.19946
XM_941876.1	BRI3BP	15.52813	NM_175870.3	LOC90925	17.20114
NM_024053.3	C22orf18	15.54004	NM_014886.2	TINP1	17.21931
NM_198284.1	LOC349114	15.54004	NM_014699.2	ZNF646	17.2391
NM_007240.1	DUSP12	15.56066	NM_004935.2	CDK5	17.2391
NM_053050.2	MRPL53	15.58595	NM_003003.1	SEC14L1	17.3358
NM_212552.1	BOLA3	15.68703	NM_004877.1	GMFG	17.40932
NM_003684.3	MKNK1	15.69701	NM_024866.3	ADM2	17.41957
NM_006390.2	IPO8	15.74481	XM_934471.1	LOC399942	17.41957
NR_002157.1	OR2A9P	15.77272	NM_001033561.1	PHF12	17.41957
NM_030973.2	MED25	15.79791	NM_022835.1	PLEKHG2	17.44547
NM_017871.3	CPSF3L	15.89005	NM_183241.1	C9orf142	17.44775
NM_017907.1	FLJ20625	15.91889	NM_016510.3	SCLY	17.47849
NM_016481.2	C9orf156	15.91889	NM_170783.1	ZNRD1	17.51365
NM_005507.2	CFL1	15.92436	NM_032364.4	DNAJC14	17.63119
NM_005873.1	RGS19	15.94771	NM_201554.1	DGKA	17.63842
NM_001552.2	IGFBP4	15.95602	NM_007243.1	NRM	17.64707
NM_138639.1	BCL2L12	15.99676	NM_006234.4	POLR2J	17.64707
NM_182972.1	IRF2BP2	16.0622	NM_014851.2	KLHL21	17.67907
NM_138578.1	BCL2L1	16.06318	NM_144607.2	CYB5D1	17.68097
NM_012474.3	UCK2	16.09187	NM_152285.2	ARRDC1	17.71507
NM_020350.3	AGTRAP	16.09965	NM_022452.1	FBS1	17.71507
NM_004240.2	TRIP10	16.19539	NM_032015.3	RNF26	17.7348
NM_002372.2	MAN2A1	16.21285	NM_175040.1	ST6GALNAC4	17.74122
NM_021602.1	CD79B	16.21285	XR_000904.1	RPL14L	17.76803
NM_004422.2	DVL2	16.21285	NM_152906.2	C22orf25	17.84868
XM_939093.1	FAM89A	16.21285	XM_941155.1	LOC651894	17.92392
XM_938340.1	STX5A	16.23927	NM_002476.2	MYL4	17.98006
NM_020996.1	FGF6	16.24199	XM_944593.1	Sep 01	17.98147

NM_145043.1	NEIL2	16.33093	NM_025182.2	KIAA1539	18.01944
NM_001031707.1	OGFOD1	16.33243	NM_024815.2	NUDT18	18.04197
NM_002097.1	GTF3A	16.35009	NM_006445.2	PRPF8	18.04197
XM_929341.1	LOC653738	16.38951	NM_002018.2	FLII	18.04197
NM_207340.1	ZDHHC24	16.40743	NM_014943.3	ZHX2	18.0745
NM_000858.4	GUK1	16.46285	NM_001031728.1	C9orf100	18.08687
NM_024845.1	FLJ14154	18.1182	NM_001034.1	RRM2	19.64619
NM_012087.1	GTF3C5	18.13288	NM_005861.2	STUB1	19.78477
NM_032319.1	C2orf7	18.15974	NM_006739.2	MCM5	19.80667
NM_031300.2	MXD3	18.18314	NM_006602.2	TCFL5	19.81438
NM_001009944.1	PKD1	18.18545	NM_138476.2	MDP-1	19.81438
NM_206956.1	PRAME	18.21191	NM_015140.2	TTLL12	19.83513
XM_930798.1	LOC642393	18.25399	NM_006510.3	RFP	19.8428
XR_001434.1	AYP1p1	18.26943	NM_000137.1	FAH	19.90529
NM_001005849.1	SUMO2	18.3189	NM_014815.2	THRAP4	19.90529
NM_004494.1	HDGF	18.34133	NM_144732.1	HNRPUL1	19.92972
NM_032889.2	MFSD5	18.34133	NM_004131.3	GZMB	20.004
NM_014771.2	RNF40	18.36078	NM_014877.2	HELZ	20.00694
NM_001013253.1	LSP1	18.39788	NM_139062.1	CSNK1D	20.02597
NM_012329.2	MMD	18.48611	NM_006764.3	IFRD2	20.04654
NM_002800.4	PSMB9	18.51314	NM_152600.1	ZNF579	20.16051
NM_024588.3	FLJ23584	18.54125	NM_030981.1	RAB1B	20.16051
NM_199345.2	LOC375133	18.54807	NM_006808.2	SEC61B	20.18548
NM_005138.1	SCO2	18.58317	NM_005432.2	XRCC3	20.26764
NM_001014839.1	NCDN	18.62538	XM_034819.6	ZNF629	20.31151
NM_001151.2	SLC25A4	18.62538	NM_153813.1	ZFPM1	20.34015
NM_138300.3	PYGO2	18.63872	NM_020182.3	TMEPAI	20.34875
NM_145074.2	HTRA2	18.64585	NM_005085.2	NUP214	20.36246
NM_025082.1	C16orf56	18.64585	NM_030782.2	CRR9	20.44401
NM_002502.2	NFKB2	18.66306	NM_002494.2	NDUFC1	20.45348
XM_942536.1	LOC651143	18.67431	NM_016068.1	FIS1	20.54888
NM_138381.1	MGC15763	18.6769	NM_199485.1	C20orf24	20.55136
NM_001320.5	CSNK2B	18.68142	NM_005119.2	THRAP3	20.57373
NM_012225.1	NUBP2	18.68483	NM_002136.1	HNRPA1	20.65696
NM_014225.3	PPP2R1A	18.68483	NM_177533.2	NUDT14	20.67142
NM_030628.1	KIAA1698	18.71303	NM_001347.2	DGKQ	20.73339
NM_024872.1	DOK3	18.72802	XM_927955.1	LOC644863	20.82055
NM_018182.1	C17orf63	18.74112	NM_006009.2	TUBA3	20.84746
NM_030926.4	ITM2C	18.74615	NM_024635.2	MAK10	20.86742
NM_002417.2	MKI67	18.75108	NM_024544.1	C1orf166	21.06605
AK128384		18.79598	NM_018347.1	C20orf29	21.07222
NM_016525.3	UBAP1	18.84068	NM_002123.2	HLA-DQB1	21.12521
NM_004390.2	CTSH	18.85384	NM_005914.2	MCM4	21.19423
NM_183359.1	BRD8	18.89157	NM_018188.2	ATAD3A	21.25705
NM_006225.1	PLCD1	18.89486	NM_017816.1	LYAR	21.2731
NM_001008566.1	TPST2	18.89499	NM_138940.2	CD200R1	21.33414
NM_004563.2	PCK2	18.90061	NM_005700.2	DPP3	21.36489
NM_018518.3	MCM10	19.03932	NM_016069.8	Magmas	21.40753
NM_014389.1	PELP1	19.10049	BQ420825		21.41187
NM_000837.1	GRINA	19.19281	NM_001687.4	ATP5D	21.50589
NM_182664.1	RASSF5	19.2573	NM_006362.3	NXF1	21.57528
NM_003885.2	CDK5R1	19.26224	NM_006833.4	COPS6	21.5903
NM_030789.2	HM13	19.27351	XM_375456		21.64478

NM_031266.2	HNRPAB	19.36704	NM_014931.2	SAPS1	21.71978
NM_022095.3	ZNF335	19.41197	NM_138334.1	JOSD2	21.76161
NM_139159.3	DPP9	19.42178	NM_001012267.1	RP11-19J3.3	21.76161
NM_021975.2	RELA	19.48535	NM_024828.2	C9orf82	21.79434
NM_031484.1	MARVELD1	19.49324	XM_942035.1	LOC652545	21.84945
NM_201627.1	TRIM41	19.51563	XM_941953.1	LOC652493	21.87105
NM_002918.3	RFX1	19.57909	NM_172004.2	DCAL1	21.88538
NM_018385.1	LSG1	19.58521	NM_000154.1	GALK1	21.89476
NM_025232.2	REEP4	19.63623	NM_007021.2	C10orf10	21.95127
NM_033500.1	HK1	21.98477	NM_030644.1	APOL3	24.34459
NM_012265.1	RHBDD3	22.01277	NM_004091.2	E2F2	24.38452
XM_932044.1	LOC440341	22.01919	NM_198565.1	LRRC33	24.42163
NM_020963.1	MOV10	22.01919	NM_017999.3	RNF31	24.44264
NM_133646.1	ZAK	22.0527	NM_014233.1	UBTF	24.45413
NM_006761.3	YWHAE	22.0527	NM_032907.3	UBL7	24.46969
NM_017838.3	NOLA2	22.07598	NM_006302.1	GCS1	24.46969
NM_003942.2	RPS6KA4	22.07598	NM_144584.1	C1orf59	24.46969
NM_006819.1	STIP1	22.11382	NM_005702.2	ERAL1	24.52922
NM_198969.1	AES	22.1402	NM_001007026.1	ATN1	24.60644
NM_033054.1	MYO1G	22.33667	NM_032442.2	KIAA1787	24.60766
NM_003575.1	ZNF282	22.34672	NM_000421.2	KRT10	24.60766
NM_207393.1	IGFL3	22.41525	NM_003164.2	STX5A	24.78915
NM_002744.4	PRKCZ	22.43419	XM_928425.1	LOC653617	24.92345
NM_138442.2	LOC115098	22.48353	NM_000853.1	GSTT1	24.99117
NM_001394.5	DUSP4	22.50815	NM_080670.2	SLC35A4	24.99151
NM_016941.2	DLL3	22.52249	NM_173537.2	GTF2IRD2	25.07376
NM_012405.2	ICMT	22.56427	NM_001558.2	IL10RA	25.07947
NM_004068.3	AP2M1	22.56427	NM_019896.2	POLE4	25.20437
NM_031917.2	ANGPTL6	22.56427	NM_024321.3	MGC10433	25.2847
NM_199444.1	COPE	22.58247	NM_003190.3	TAPBP	25.32998
NM_173831.2	ZNF707	22.58247	NM_000070.2	CAPN3	25.46356
NM_024718.2	C9orf86	22.70272	NM_014745.1	FAM38A	25.4756
XM_936706.1	KLHL17	22.72538	NM_006367.2	CAP1	25.55494
NM_003959.1	HIP1R	22.73929	NM_016326.2	CKLF	25.65067
NM_201400.1	FAM86A	22.81535	NM_138375.1	CABLES1	25.65682
NM_001031731.1	YIF1B	22.86099	NM_001001975.1	ATP5D	25.67953
DB337747		22.89017	NM_145696.1	BRF1	25.6949
NM_004451.3	ESRRA	23.03684	NM_015696.2	GPX7	25.71739
NM_004953.2	EIF4G1	23.05382	XM_499385.2	LOC650254	25.74381
XM_942595.1	EIF1AX	23.18394	NM_001775.2	CD38	25.95321
NM_022044.2	SDF2L1	23.21507	NM_001986.1	ETV4	25.98127
NM_024571.2	C16orf33	23.22086	NM_003954.1	MAP3K14	26.10574
NM_178044.1	GIYD2	23.23225	NM_002406.2	MGAT1	26.28089
NM_003290.1	TPM4	23.24913	NM_004973.2	JARID2	26.32156
NM_176812.3	CHMP4B	23.28112	NM_004252.1	SLC9A3R1	26.41302
NM_001414.2	EIF2B1	23.28112	NM_174905.2	FAM98C	26.41302
NM_023933.1	C16orf24	23.28578	NM_024608.1	NEIL1	26.41302
NM_012456.1	TIMM10	23.35106	NR_002174.1	CMAH	26.46533
XM_942539.1	ANAPC2	23.38603	NM_014837.3	SMG7	26.55682
NM_178148.1	SLC35B2	23.38603	NM_002114.1	HIVEP1	26.5624
NM_006012.2	CLPP	23.39968	NM_004526.2	MCM2	26.63664
NM_002600.2	PDE4B	23.42643	NM_138493.1	C6orf129	26.69583
NM_004176.3	SREBF1	23.44292	NM_004689.2	MTA1	26.80439

NM_000303.1	PMM2	23.59602	NM_144701.2	IL23R	26.81435
NM_003481.1	USP5	23.64357	NM_004924.3	ACTN4	26.84111
NM_020410.1	ATP13A1	23.79636	NM_006763.2	BTG2	26.84111
NM_006342.1	TACC3	23.83918	NM_145262.2	GLYCTK	26.87793
NM_013336.3	SEC61A1	23.83918	NM_001761.1	CCNF	27.04745
NM_030665.3	RAI1	23.88419	XM_933893.1	LOC389672	27.04745
NM_032809.2	FAM73B	23.8905	NM_024535.1	CORO7	27.14317
NM_006317.3	BASP1	24.00031	NM_020857.2	VPS18	27.17433
NM_000263.3	NAGLU	24.20835	NM_144589.2	COMTD1	27.21404
XM_496943		24.21011	NM_004193.1	GBF1	27.21404
NM_003751.2	EIF3S9	24.24943	NM_004584.2	RAD9A	27.35933
NM_003146.2	SSRP1	24.28708	NM_000067.1	CA2	27.43946
NM_153047.1	FYN	27.6314	NM_020162.2	DHX33	33.34626
NM_015343.3	DULLARD	27.68323	NM_014287.3	NOMO1	33.40644
NM_013284.1	POLM	27.73394	NM_005827.1	SLC35B1	33.40875
NM_021259.1	TMEM8	27.92212	NM_005480.2	TROAP	33.4101
NM_080621.3	SAMD10	28.09725	NM_033161.2	SURF4	33.53239
NM_023018.3	NADK	28.11511	NM_002949.2	MRPL12	33.93333
NM_022156.3	DUS1L	28.13523	NM_152331.2	ACOT4	33.93333
NM_013327.3	PARVB	28.21029	NM_006666.1	RUVBL2	33.93333
NM_007347.3	AP4E1	28.22037	XM_931339.1	INT1	34.07632
NM_016732.1	RALY	28.26883	NM_001109.2	ADAM8	34.10348
NM_006990.2	WASF2	28.34058	NM_015908.4	ARS2	34.13192
NM_005022.2	PFN1	28.58919	NM_032916.3	FAM86B1	34.13772
NM_002413.3	MGST2	28.60189	NM_002540.3	ODF2	34.17337
NM_005701.2	RNUT1	28.98923	NM_002105.2	H2AFX	34.17337
NM_016089.1	ZNF589	29.13493	NM_015950.3	MRPL2	34.3907
NM_198282.1	LOC340061	29.22594	NM_001607.2	ACAA1	34.5216
XM_936750.1	LOC648394	29.57516	NM_052848.1	MGC20255	34.55243
NM_000666.1	ACY1	29.60172	NM_207373.1	C10orf99	34.55797
NM_014508.2	APOBEC3C	29.62311	NM_022089.1	ATP13A2	34.55797
NM_016245.2	DHRS8	29.86736	NM_032309.2	CHCHD5	34.59371
NM_016372.1	GPR175	29.90981	NM_025079.1	ZC3H12A	34.75979
NM_002441.2	MSH5	29.93951	NM_006786.2	UTS2	34.76219
NM_001018059.1	LOC440348	30.16316	NM_014026.3	DCPS	34.89524
NM_002435.1	MPI	30.16316	NM_001006113.1	OATL1	35.0273
NM_001005415.1	MARCH2	30.18944	NM_213720.1	C22orf16	35.0273
NM_002627.3	PFKP	30.23025	XM_946270.1	HIP1R	35.05153
NM_030767.2	AKNA	30.26756	NM_003075.2	SMARCC2	35.08117
NM_031485.2	GRWD1	30.35709	NM_024099.2	C11orf48	35.1242
NM_001224.3	CASP2	30.45598	NM_021971.1	GMPPB	35.37517
NM_178863.2	KCTD13	30.57208	NM_000332.2	ATXN1	35.39105
NM_015533.2	DAK	30.57208	NM_012295.2	CABIN1	35.39543
NM_013399.1	C16orf5	30.72505	NM_001024.3	RPS21	35.57593
NM_005078.1	TLE3	31.16853	NM_006378.2	SEMA4D	35.57593
NM_058195.2	CDKN2A	31.73028	NM_004341.3	CAD	35.60102
NM_015456.2	COBRA1	31.79796	NM_138793.2	CANT1	35.60102
NM_024092.1	TMEM109	31.79796	NM_002419.3	MAP3K11	35.6542
XM_944297.1	EXOSC1	31.90576	NM_153824.1	PYCR1	35.79411
NM_006755.1	TALDO1	31.91012	NM_014147.1	HSPC047	36.04381
NM_017914.2	C19orf24	31.96063	NM_000246.2	CIITA	36.12406
NM_001008219.1	AMY1C	32.04084	XM_939320.1	LOC389816	36.32019
NM_005973.4	PRCC	32.1869	NM_001008540.1	CXCR4	36.58329

NM_004945.2	DNM2	32.1869	NM_138570.1	MGC15523	36.81586
NM_004910.1	PITPNM1	32.30781	NM_080430.2	SELM	36.91498
XM_936496.1	LOC653907	32.30781	NM_007219.2	RNF24	36.93505
NM_005510.3	DOM3Z	32.39904	NM_001771.1	CD22	37.17593
NM_017771.2	PXK	32.39904	NM_017793.1	RPP25	37.2801
NM_006715.2	MAN2C1	32.39904	NM_182556.1	LOC283130	37.2801
NM_019900.1	ABCC1	32.55154	NM_018384.3	GIMAP5	37.45528
NM_001013672.2	LOC400566	32.71653	NM_024068.2	OBFC2B	37.45707
NM_020680.2	SCYL1	32.93648	NM_007260.2	LYPLA2	37.61642
NM_001400.2	EDG1	33.01704	NM_024680.2	E2F8	37.65588
NM_003977.1	AIP	33.02203	NM_017727.3	FLJ20254	37.77266
NM_005439.1	MLF2	33.04014	XM_942691.1	FBXO46	37.91896
NM_199242.1	UNC13D	33.2562	NM_001520.1	GTF3C1	37.93684
NM_024710.1	ISOC2	33.27412	NM_015179.2	KIAA0690	38.12722
NM_003860.2	BANF1	33.30166	BC041923		38.23653
NM_006435.1	IFITM2	38.27549	NM_015125.2	CIC	46.13768
NM_013342.1	TFPT	38.31688	NM_175609.1	ARFGAP1	46.39466
NM_014030.2	GIT1	38.43844	NM_018154.2	ASF1B	46.4159
XM_934176.1	LOC91561	38.66597	NM_015937.2	PIGT	46.79871
NM_173618.1	FLJ90652	38.68525	NM_014712.1	SETD1A	47.39774
NM_002691.1	POLD1	38.71132	NM_032853.2	MUM1	47.40699
NM_004271.3	LY86	39.07639	NM_006010.2	ARMET	47.40699
NM_016368.3	ISYNA1	39.10734	NM_001182.2	ALDH7A1	47.4745
NM_174893.1	C17orf49	39.11211	NM_032484.3	LGP1	47.57341
NM_018056.1	TMEM39B	39.13272	NM_173680.2	MGC33584	47.73707
NM_001628.2	AKR1B1	39.18342	NM_013241.1	FHOD1	47.74468
NM_033363.1	MRPS12	39.25796	NM_015492.3	C15orf39	47.74468
BC040064		39.39124	NM_152270.2	FLJ34922	47.94331
NM_058192.2	RPUSD1	39.39124	NM_198527.1	HDDC3	48.02733
NM_003289.3	TPM2	39.46421	NM_054014.1	FKBP1A	48.11813
NM_031286.2	SH3BGRL3	39.50481	NM_138774.2	C19orf22	48.13585
NM_002695.2	POLR2E	39.50481	NM_006384.2	CIB1	48.35632
NM_003040.2	SLC4A2	39.50481	NM_005632.2	SOLH	48.39693
NM_130443.1	DPP3	40.01443	XM_936150.1	MSH5	48.77211
NM_005375.2	MYB	40.23513	NM_001005376.1	PLAUR	49.45848
NM_016151.2	TAOK2	40.5564	NM_015225.1	KIAA0367	49.5783
NM_133376.1	ITGB1	40.63452	NM_207310.1	CCDC74B	49.5783
NM_006396.1	SSSCA1	40.92992	NM_198576.2	AGRN	49.5783
NM_013282.2	UHRF1	41.11945	NM_003128.1	SPTBN1	49.5783
NM_032344.1	NUDT22	41.57856	NM_014751.2	MTSS1	49.5783
NM_022355.1	DPEP2	41.73436	NM_016565.2	CHCHD8	49.61504
NM_003169.2	SUPT5H	41.74493	NM_002070.2	GNAI2	50.05357
NM_022908.1	NT5DC2	41.79451	NM_016466.4	ANKRD39	50.44118
NM_006116.2	MAP3K7IP1	41.93771	NM_194449.1	PHLPP	51.03521
NM_015914.5	TXNDC11	42.28783	NM_173344.1	ST3GAL1	51.14369
NM_024814.1	CBLL1	42.28783	NM_020145.2	SH3GLB2	51.35444
NM_001024211.1	S100A13	42.36161	NM_006191.1	PA2G4	51.71946
NM_003504.3	CDC45L	42.36161	NM_002626.4	PFKL	52.18495
NM_033557.1	YIF1B	42.36889	NM_017607.1	PPP1R12C	52.72341
NM_001017389.1	SULT1A4	42.62243	NM_001014431.1	AKT1	53.27368
NM_032960.2	MAPKAPK2	42.68404	NM_003938.4	AP3D1	53.55887
NM_031498.1	GNGT2	42.75944	NM_014494.1	TNRC6A	53.733
NM_006433.2	GNLY	42.88941	NM_001009936.1	PHF19	54.07806

XM_942312.1	LOC440990	42.9807	NM_032836.1	FLJ14768	54.21091
NM_173622.2	NBLA10383	43.04367	NM_018337.2	ZNF444	54.37565
NM_001013838.1	RLTPR	43.17508	NM_013335.2	GMPPA	55.55897
NM_024067.2	C7orf26	43.43896	NM_004140.3	LLGL1	55.81142
NM_017647.2	FTSJ3	43.49547	NM_213674.1	TPM2	56.18239
NM_181340.1	WDR21A	43.53491	NM_003863.2	DPM2	56.18239
NM_002103.3	GYS1	43.73319	NM_006618.3	JARID1B	57.0811
NM_006810.1	PDIA5	44.14968	NM_015918.3	POP5	57.35128
NM_004955.1	SLC29A1	44.2804	NM_024602.4	HECTD3	57.53239
NM_004568.4	SERPINB6	44.29851	XM_926231.1	LOC642829	57.6162
NM_003312.4	TST	44.37071	NM_139022.2	TSPAN32	58.0968
NM_005608.2	PTPRCAP	44.4349	NM_003132.2	SRM	59.02153
NM_025195.2	TRIB1	44.92422	NM_022914.1	ACD	59.76162
NM_002199.2	IRF2	45.06002	NM_002015.2	FOXO1A	60.08228
NM_006985.1	NPIP	45.35011	NM_012291.3	ESPL1	60.75972
NM_138392.1	SHKBP1	45.75447	NM_004823.1	KCNK6	60.80425
NM_002082.2	GRK6	45.81319	NM_003467.2	CXCR4	61.16874
NM_001238.1	CCNE1	45.84848	NM_202002.1	FOXM1	61.30812
NM_033200.1	BC002942	62.50231	NM_001010856.1	LOC147804	109.102
NM_013355.3	PKN3	62.64703	NM_014038.1	BZW2	109.102
NM_152931.1	CPNE1	63.14407	AK129956		109.2374
NM_032840.1	SPRYD3	64.27654	NM_001559.2	IL12RB2	110.9676
NM_014516.2	CNOT3	64.35051	XM_928905.1	LOC645937	111.2268
NM_139348.1	BIN1	64.57837	NM_001004358.1	FGFRL1	111.3364
NM_012477.2	WBP1	64.88144	NM_001197.3	BIK	111.9193
NM_003258.1	TK1	65.12166	NM_024693.2	ECHDC3	111.96
NM_021076.2	NEFH	65.20161	NM_003982.2	SLC7A7	116.1936
NM_022141.4	PARVG	66.80949	AK094914		117.3206
NM_004309.3	ARHGDIA	67.59412	NM_003571.2	BFSP2	118.5075
NM_003029.3	SHC1	67.60312	NM_002209.1	ITGAL	118.9557
NM_001031827.1	BOLA2	68.86764	NM_017852.1	NALP2	120.1407
NM_005762.2	TRIM28	70.01176	NM_018665.1	DDX43	123.0857
NM_001010980.2	C1orf130	70.39919	NM_001033046.1	C17orf62	127.7906
NM_145253.1	FAM100A	70.408	NM_033285.2	TP53INP1	127.7906
NM_003127.1	SPTAN1	71.64635	NM_024070.3	MGC2463	127.7906
NM_014977.1	ACIN1	71.66755	XM_936467.1	BEXL1	127.7906
NM_033274.2	ADAM19	71.74365	NM_012483.1	GNLY	172.6615
NM_173636.3	WDR62	71.74365	NM_033301.1	RPL8	173.2514
NM_199074.1	C3orf60	73.20203	NM_001681.2	ATP2A2	173.5356
NM_002227.1	JAK1	73.32023	NM_138410.2	CMTM7	175.1739
NM_130787.2	AP2A1	73.64577	NM_001623.3	AIF1	179.572
NM_024096.1	XTP3TPA	74.08273	NM_014800.8	ELMO1	214.3544
NM_000270.1	NP	74.63692	CR596519		345.3231
NM_005178.2	BCL3	75.26462	NM_017931.1	FLJ20699	345.3231
XM_938297.1	LOC402644	77.64377	NM_024832.3	RIN3	345.3231
NM_006235.1	POU2AF1	78.43597	NM_003038.2	SLC1A4	345.3231
NM_002558.2	P2RX1	78.68965	NM_178507.2	OAF	345.3231
NM_182470.1	PKM2	79.79074	NM_022343.2	C9orf19	345.3231
NM_012261.2	C20orf103	80.33636	NM_002824.4	PTMS	345.3231
NM_017823.3	DUSP23	80.66824	NM_017921.1	NPLOC4	345.3231
NM_080686.1	BAT2	80.71393	XM_937964.1	ALDH7A1	345.3231
NM_015194.1	MYO1D	80.96146	NM_018957.2	SH3BP1	345.3231
NM_000716.3	C4BPB	81.26296	NM_024698.4	SLC25A22	345.3231

NM_002654.3	PKM2	81.42924	NM_014059.1	RGC32	345.3231
NM_004580.3	RAB27A	81.43201	NM_004063.2	CDH17	345.3231
NM_021149.2	COTL1	82.92437	NM_003039.1	SLC2A5	345.3231
NM_014042.1	C11orf51	83.3857	NM_144594.1	FAM112B	345.3231
NM_022720.5	DGCR8	83.47199	NM_000118.1	ENG	345.3231
NM_199169.1	TMEPAI	84.07341	NM_024667.1	VPS37B	345.3231
BX537506		86.81233	NM_004343.2	CALR	345.3231
NM_022092.1	CHTF18	86.87276	NM_006216.2	SERPINE2	345.3231
NM_207346.1	TSEN54	87.09344	NM_014214.1	IMPA2	345.3231
NM_004630.2	SF1	87.39642	NM_170665.2	ATP2A2	345.3231
AL049980		87.95199	NM_022082.2	C20orf59	345.3231
NM_015354.1	NUP188	88.25524	NM_004573.1	PLCB2	345.3231
NM_001321.1	CSRP2	88.94025	NM_001025159.1	CD74	345.3231
NM_182687.1	PKMYT1	93.50898	NM_024536.4	CHPF	345.3231
NM_003139.2	SRPR	94.71024	NM_033120.2	NKD2	345.3231
NM_015254.2	KIF13B	96.6983	NM_015246.1	MGRN1	345.3231
NM_007104.4	RPL10A	97.68945	NM_023930.2	KCTD14	345.3231
NM_018067.2	RPRC1	98.74521	NM_174917.1	LOC197322	345.3231
NM_015559.1	SETBP1	104.7379	NM_206902.1	RTN2	345.3231
NM_006423.1	RABAC1	105.8637	NM_021102.2	SPINT2	345.3231
NM_031934.3	RAB34	107.6602	NM_021995.1	UTS2	345.3231
NM_001009991.1	SYTL3	345.3231	NM_021034.1	IFITM3	345.3231
NM_006799.2	PRSS21	345.3231	NM_018419.2	SOX18	345.3231
XM_940969.1	LOC651751	345.3231	NM_006426.1	DPYSL4	345.3231
NM_015527.2	TBC1D10B	345.3231	NM_206926.1	SEPN1	345.3231
NM_001565.1	CXCL10	345.3231	NM_001002861.1	ARHGEF5	345.3231
NM_001013693.1	LDLRAD2	345.3231	XM_377426.1	LOC401845	345.3231
NM_015187.1	KIAA0746	345.3231	NM_001020820.1	MYADM	345.3231
NM_006389.2	HYOU1	345.3231	NM_003151.2	STAT4	345.3231
NM_003975.2	SH2D2A	345.3231			

10.10. Appendix - J

Table S7. Primers used for qRT-PCR to verify the whole genome expression profiling data.

Gene names	Direction	Primers
ARHGEF5	Forward	ACCTTCCATCTTGCCTGAGG
ARHGEF5	Reverse	CGTCTTGAAAAGCCTCCCATC
AGRN	Forward	CACAAGAACGAGCTGATGCTC
AGRN	Reverse	CATCAGGAGGCGTCGGAG
DPYSL4	Forward	GATCACGAGTGACCGCCTTC
DPYSL4	Reverse	GGACGATGAGGTTTTCTCCG
SETD1A	Forward	GAAGAAGCTCCGATTTGGCC
SETD1A	Reverse	GTAGCGCTTCTCCCGCATG

10.11. Appendix - K

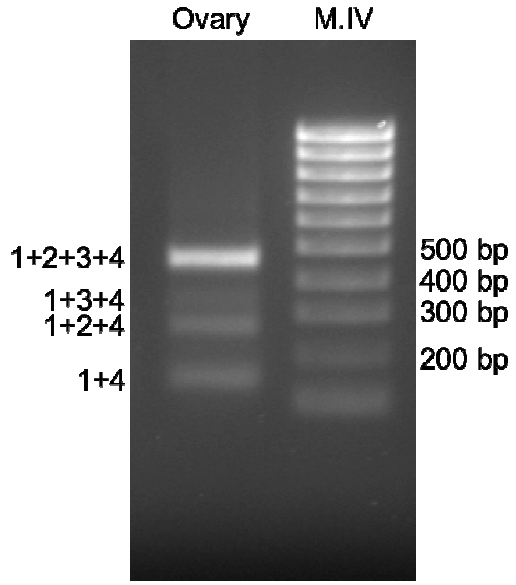

Figure S3: All four splice variants of *BOD1* are expressing in human ovary. The result from RT-PCR on human adult ovaries is shown. RT-PCR with *BOD1* flanking primers shows all four transcripts in human ovary. DNA ladder marker IV (M.IV) were used.